Copyright is owned by the Author of the thesis. Permission is given for a copy to be downloaded by an individual for the purpose of research and private study only. The thesis may not be reproduced elsewhere without the permission of the Author.

MASSEY UNIVERSITY
TE KUNENGA KI PŪREHUROA
UNIVERSITY OF NEW ZEALAND

Modification of MTT colorimetric bacterial assays and investigation of antibacterial compounds from selected *Myrtaceae* plants

A thesis presented in partial fulfilment of the requirements for the

degree of

Doctor of Philosophy

in

Food Technology

At Massey University, Manawatū

New Zealand

Wenliang Xu

2024

Abstract

This thesis presented a pivotal component of a comprehensive bioactivity screening project conducted by our research group, focusing on the improvement and validation of established antibacterial techniques. This investigation aimed to enhance various 3-(4,5-dimethylthiazol-2-yl)-2,5-diphenyl tetrazolium bromide (MTT)-based bacterial assays, resulting in the attainment of several noteworthy accomplishments, which include: (**1**) the development of an equation that establishes a correlation between colony-forming units (CFU) and the quantity of formazan converted by bacteria, enabling accurate calculation of viable bacteria number and precise measurement of the colorimetric microdilution assay; (**2**) a modification to the existing bacterial MTT assay protocol; (**3**) an enhanced direct TLC-bioautography protocol tailored for osmotically vulnerable bacteria; and (**4**) a suggested method for determining the minimum effective dose (MED) using direct TLC-bioautography.

The efficacy of these improved protocols was confirmed through the utilization of feijoa (*Feijoa sellowiana*) fruit peel and steam-distilled mānuka (*Leptospermum scoparium*) leaves and branches, which are two locally available waste materials from the *Myrtaceae* family. The antibacterial components, flavone and grandiflorone, were targeted using direct TLC-bioautography, and subsequently identified using UHPLC-HR-MS in conjunction with Compound Discoverer. These compounds were then purified for NMR verification. To assess their antibacterial properties, the direct TLC-bioautography-based MED determination method, as proposed in this study, was employed, and accompanied by conventional antibacterial assay for comparison. The results have shown that the MED of flavone was 4.2-5.2 μg/cm^2 against the *S. aureus* and 5.2-6.1 μg/cm^2 against the *E. coli*. Similarly, the MED of grandiflorone was observed to be 0.29 - 0.59 μg/cm^2 against *S. aureus* and 2.34 - 4.68 μg/cm^2 against *E. coli*.

Untreated New Zealand and Chinese mānuka samples were also studied for comparison to the steam-distilled samples. A total of **22** compounds were identified through these samples, including five β-triketones, thirteen flavonoids, three phloroglucinol derivatives, and one exotic plant growth retardant only presented in Chinese mānuka. In addition to three volatile β-triketones, there is little difference in the main chemical composition between steam-distilled and untreated New Zealand mānuka. However, most of the compounds identified from New Zealand mānuka, especially β-triketones, were not present in Chinese mānuka.

Keywords: MTT assay; Formazan; HPLC; LC-MS; Viable count; *Staphylococcus aureus*; *Escherichia coli*; TLC-bioautography; Compound Discoverer; NMR; antibacterial activity; *Feijoa sellowiana*; Mānuka; *Leptospermum scoparium*; Flavone; Grandiflorone.

Acknowledgments

I would like to extend my sincere appreciation to my primary supervisor, David Popovich, for affording me the invaluable opportunity to pursue my studies abroad. Throughout the entirety of my doctoral journey, he selflessly provided help and support in all aspects. In my eyes, he has transcended the role of a mere mentor and has become a trusted friend. I would like to express my heartfelt gratitude to my co-supervisors, Gareth Rowlands, Jennifer Tate, and David Harding, who helped me overcome the numerous challenges encountered during the research process. Furthermore, I wish to acknowledge the invaluable contributions of David Lun, Pat Edwards, and Trevor Loo, the technical staff of the Science Tower. Under their diligent help, I have acquired a commendable level of proficiency in diverse analytical instruments and software. Additionally, I express my gratitude towards Paul Hocquard and Panny Abercrombie for their aid in purchasing essential consumables, thereby significantly saving my time.

During my studies at Massey University, I made many friends. I extend my sincerest appreciation to Arka Gupta, Wei Chen, Danxia Shi, and Kent Chen for their companionship throughout my hard time, as well as their collaborative efforts in overcoming experimental challenges. I was fortunate to be a member of Angela Kilford's team and was very happy that I could contribute to the retrieval of ancient Māori botanical knowledge. I am deeply appreciative of her invitation to partake in a pōwhiri, as it afforded me the invaluable chance to acquire knowledge and immerse myself in the captivating Māori culture. I would also extend my gratitude to Dan Carlisle at Massey Venture for his assistance in acquiring funding for my research interests, ultimately enabling me to have the opportunity to obtain patents.

Finally, I express my sincere appreciation to Massey University for bestowing upon me a full scholarship. I am also indebted to New Zealand for its serene and pleasing living environment, and to my family for their unwavering and unspoken encouragement.

Table of Contents

Abstract I
Acknowledgements II
Table of Contents III
Chapter One 1
Introduction, Research framework, Objectives, Thesis structure and Total research outcomes 1
1.1. Introduction 1
1.2. Research Framework 2
1.3. Objectives 3
1.4. Thesis Structure 4
1.5. Total Research Outcomes 5
Chapter Two 7
Bioactive hybrid compounds from *Myrtaceae*: Chemical classification and biological activities – literature review 7
Statement of Contribution 8
Abstract 9
2.1. Introduction 10
2.2. Chemical Constituents 11
2.2.1. Meroterpenoids: 11
2.2.1.1. Phloroglucinol-monoterpene type meroterpenoids (PMMs): 12
2.2.1.2. Phloroglucinol-sesquiterpene type meroterpenoids (PSMs): 12
2.2.1.3. β-Triketone-monoterpene type meroterpenoids (TMMs): 15
2.2.1.4. β-Triketone-sesquiterpene type meroterpenoids (TSMs): 16
2.2.1.5. Trimeric meroterpenoids: 17
2.2.2. Other hybrid compounds: 18
2.3. Biological Activities 24
2.3.1. Antimicrobial activity 25
2.3.1.1. Antibacterial activity 25
2.3.1.2. Antifungal activity 27
2.3.2. Cytotoxicity 30
2.3.3. Anti-inflammatory activity 33
2.3.4. Enzyme inhibitory activity 34
2.4. Conclusion and Future Perspectives 35
2.5. References 36
Chapter Three 44
An improved MTT colorimetric method for rapid viable bacteria counting 44
Statement of Contribution 45
Abstract 46
3.1. Introduction 47
3.2. Materials and Methods 47
3.2.1. Bacterial strains and growth conditions 47
3.2.2. Preparation of MTT and MTT-formazan standard solutions 48

3.2.3. MTT reduction time determination and formazan quantification 48
3.2.4. MTT colorimetric assay on bacteria 49
3.2.5. Enumeration of viable bacteria 49
3.2.6. MTT-formazan peak area-concentration standard curve 49
3.2.7. Statistical analysis 49
3.3. Results and Discussion 49
3.3.1. Establishment of the equation. 49
3.3.2. Optimization of the MTT reduction procedure. 52
3.3.3. Optimization of the dissolution and quantification procedures of formazan. 54
3.3.4. Linear equation of bacteria optical density and formazan peak area 56
3.3.5. Linear equation of bacteria optical density and the number of CFUs 59
3.3.6. Linear equation of formazan peak area and formazan concentration 59
3.3.7. Linear equation of the number of CFUs and the mass of formazan produced. 60
3.4. Conclusion 61
3.5. References 62
Chapter Four 66
TLC-bioautography-guided identification and assessment of the antibacterial compounds from plant extracts 66
Statement of Contribution 67
Abstract 68
4.1. Introduction 69
4.2. Materials and Methods 70
4.2.1. Chemicals and reagents 70
4.2.2. Plant material 70
4.2.3. Extraction of total phytochemicals 70
4.2.4. Bacteria cultivation and MIC test 70
4.2.5. TLC analysis and direct bioautography 71
4.2.6. Rapid identification of target compounds 72
4.2.7. Target compounds purification 72
4.2.8. Nuclear magnetic resonance (NMR) 73
4.2.9. Data acquisition and software analysis 73
4.3. Results and Discussion 73
4.3.1. Direct TLC-bioautography 73
4.3.2. Structure identification 74
4.3.3. Target compound purification and NMR verification 75
4.3.4. Antibacterial activity assessment 77
4.4. Conclusion 79
4.5. References 79
Chapter Five 82
TLC-bioautography guided isolation and assessment of antibacterial compounds from Mānuka (*Leptospermum scoparium*) leaf and branch extracts. 82
Statement of Contribution 83
Abstract 84
5.1. Introduction 85

5.2. Materials and Methods 85
5.2.1. Chemicals and reagents 85
5.2.2. Plant material 86
5.2.3. Extraction of phytochemicals 86
5.2.4. Bacteria cultivation and conventional antibacterial assay 86
5.2.5. TLC analysis and direct bioautography 86
5.2.5.1. TLC analysis 86
5.2.5.2. Conventional direct TLC bioautography 87
5.2.5.3. Direct bioautography-based minimum effective dose determination. 87
5.2.6. Rapid identification of antibacterial compounds 87
5.2.7. Major active compounds purification 88
5.2.8. Nuclear magnetic resonance (NMR) 88
5.2.9. Data acquisition and software analysis 89
5.3. Results and Discussion 89
5.3.1. Analysis of β-triketones 89
5.3.2. Analysis of flavonoids and phloroglucinol derivatives 91
5.3.3. Major active compound purification and NMR verification 93
5.3.4. Minimum effective dose of grandiflorone 94
5.4. Conclusion 96
5.5. References 97
Chapter Six 99
General conclusion, highlights, limitations, and directions for future work. 99
6.1. General conclusions 99
6.2. Highlights of the study 100
6.3. Limitations of the study 101
6.4. Future directions 101
Appendix 1 Supplementary data of Chapter Three. 103
Appendix 2 Supplementary data of Chapter Four. 117
Appendix 3 Supplementary data of Chapter Five. 122
Appendix 4 A correction to the existing bacterial MTT assay protocol 126
Statement of Contribution 127
Appendix 4.1 Letter to the editor: NaOH as a solubilizer in bacterial MTT assay. 128
Appendix 4.2 References 129

Chapter One

Introduction, Research framework, Objectives, Thesis structure and Total research outcomes

1.1. Introduction

This thesis presents a comprehensive optimization of the conventional antibacterial assay. The enhanced assay protocols were rigorously validated by using local *Myrtaceae* plant waste materials and played a crucial role in the entirety of my PhD research. The course of my study encompassed multiple concurrent projects, with the limitation of time preventing the inclusion of many research findings within this thesis. Nevertheless, to enhance readers' comprehension of my research, a concise overview of the entire research framework will be provided in section 1.2, Research Framework.

The objective of my entire research was to investigate the presence of bioactive compounds in waste materials derived from plants. The primary techniques employed in the whole study involved the isolation and identification of phytochemicals and endophytes. The waste materials utilized in this investigation were sourced from the by-products generated by various industries in New Zealand. To assess the bioactivity of the phytochemicals and endophytes, an initial screening was conducted using antibacterial assays. Subsequently, the active compounds or endophytes identified in the screening process underwent further evaluation, including testing against pathogenic fungi, animal parasites, and crop insect pests.

Numerous natural compounds exhibit diverse physical properties, rendering many existing bioassay methods unsuitable for their evaluation. Notably, conventional antibacterial assays encounter difficulties when confronted with natural compounds that possess extreme insolubility or intense darkness in color. Consequently, the modification of existing antibacterial assays and the discovery of novel methods for assessing antibacterial activity emerged as pivotal components of this study.

This thesis concentrated on the enhancement of the traditional antibacterial assay as well as a comprehensive analysis of antibacterial compounds derived from local *Myrtaceae* plant waste materials, such as Feijoa fruit peel and steam-distilled Mānuka leaves and branches. The specifics

of the current thesis will be expounded in section 1.4, Thesis Structure. All scientific research findings, encompassing but not restricted to this thesis, will be addressed in section 1.5, Total Research Outcomes.

1.2. Research Framework

As mentioned above, the waste materials used in this study were collected from local industries. They can be divided into three categories: nutshells and crop husks (**1**) including hazelnut, pistachio, and quinoa, produced by food processing industries; insecticidal garden flowers (**2**) including several artificially cultivated *Delphinium* species, produced by *Delphinium* seed industries; native *Myrtaceae* family plants (**3**) including Mānuka, Kānuka and Feijoa, produced by essential oil or food industries. The fourth category of the samples used were endophytic fungi or bacteria (**4**) isolated from the first three categories. The identification of active phytochemicals or metabolites was achieved by means of antibacterial assays, followed by a series of additional bioassays. The selection of these additional bioassays was informed by the observation of prevailing issues in New Zealand, including crop and livestock diseases caused by microorganisms, parasites, or insect pests.

As depicted in **Fig. 1.1**, the initial step involves the extraction of endophytes and phytochemicals from plant-based by-products. Subsequently, inhibition tests were conducted on the metabolites derived from endophytes and plant extracts. The active constituents identified through this screening process underwent a bioassay-guided isolation to determine the specific active compounds. Detailed descriptions of the isolation and identification of compounds can be found in subsequent chapters.

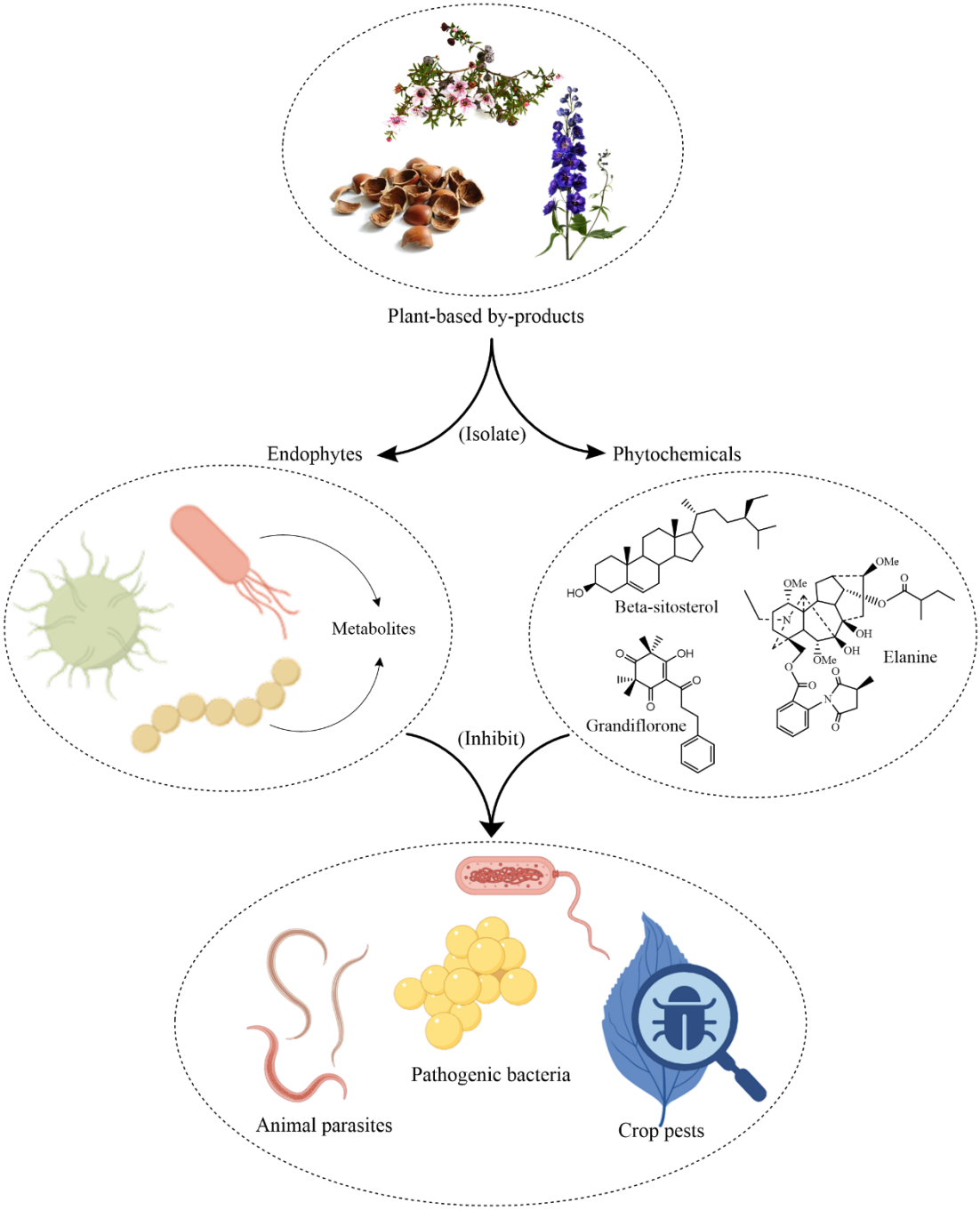

Fig. 1.1 The framework of the entire research.

1.3. Objectives

The broad objectives of this project were to improve the traditional time-consuming bioassay-guided isolation procedures and validate the improved protocols through a few actual experimental works. The achievement of these objectives will not only accelerate the research progress of concurrent projects but also provide valuable references for other researchers in our group.

The specific objectives of this thesis were:

1. Establish a reliable equation for calculating bacterial count based on MTT antibacterial assay.
2. Optimize the existing MTT antibacterial assay procedures to minimize any potential interference caused by insoluble matter and the color of the test compound.
3. Enhance the conventional TLC-bioautography technique to ensure its suitability for osmotically vulnerable bacteria, such as *Escherichia coli*.
4. Verify the optimized methodologies by employing feijoa fruit peel and steam-distilled mānuka leaves and branches as test samples.
5. Construct an expeditious TLC-based methodology for the precise localization, isolation, and characterization of antibacterial compounds derived from selected plant samples.
6. Conduct a comparative analysis of the antibacterial constituents present in Chinese and New Zealand mānuka, encompassing both steam-distilled and untreated samples of the latter.

1.4. Thesis Structure

Chapter One presents a comprehensive framework that served as the foundation for my doctoral research, which involved multiple concurrent research projects. Later chapters of this thesis will incorporate the optimization of the bioassay methodologies and an extensive chemical analysis of the waste materials from *Myrtaceae* plants.

The characteristic components (phloroglucinols, β-triketones and terpenes) in *Myrtaceae* plants have always been a hot research topic. However, the meroterpenoids and other non-terpene-based hybrids derived from these characteristic components, due to the low content, they have not been taken seriously in many studies. Therefore, **Chapter Two** presents an exhaustive literature review of these hybrid compounds, including chemical classification and biological activities.

In **Chapter Three**, an enhanced 3-(4,5-Dimethylthiazol-2-yl)-2,5-Diphenyltetrazolium Bromide (MTT) assay protocol was explicated to mitigate the previously identified interferences, alongside the revelation of a novel limitation discovered in the current study. Additionally, an equation was derived to establish a correlation between colony-forming units (CFU) and the quantity of formazan converted by the bacteria.

Experimental results obtained while optimizing the existing MTT bacterial assay revealed discrepancies with recent reports. Subsequent comparative verification experiments successfully identified errors in these articles. The rectification of these bacterial MTT assay protocols has been published as a letter to the editors in a relevant journal and is detailed in **Appendix Four**.

Chapter Four provides a comprehensive discussion on the rapid targeting, identification, and

purification of antibacterial compounds derived from feijoa fruit peels. Additionally, this chapter elucidates the modification of conventional direct thin-layer chromatography (TLC)-bioautography and introduces a novel direct bioautography-based minimum effective dose (MED) determination method.

Chapter Five provides additional validation for the rapid procedure and innovative MED determination method introduced in Chapter Four. Notably, all discernible antibacterial compounds were successfully isolated and identified. Moreover, a comprehensive comparative analysis was conducted to examine the antibacterial constituents present in steam-distilled and untreated New Zealand mānuka, as well as untreated Chinese mānuka.

Chapter Six summarizes the thesis and points out the highlights, limitations, and future research directions.

1.5. Total Research Outcomes

In this doctoral research, there were four categories of samples studied and the resulting research findings are depicted in **Fig. 1.2**. In addition to the articles included in this thesis, the following research articles or patents are planned to be published in subsequent work:

- A method for rapid crystallization of beta-sitosterol from nut shells or crop husks.
- TLC-bioautography guided isolation and identification of antibacterial long-chain fatty acids from hazelnut shells.
- The antifeedant effect of diterpenoid alkaloids isolated from New Zealand commercial Delphinium spp.
- The antibacterial diterpenoid alkaloids from New Zealand Delphinium spp.
- The potential of using New Zealand native plants as a source of natural dyes for iwi.
- Using grandiflorone as a potential anthelmintic synergist.
- The inhibitors for facial eczema pathogens (*Pseudopithomyces Chartarum*) isolated from the bacterial endophytes in New Zealand
- Using bacterial endophytes from a New Zealand commercial plant for control of sheep intestinal nematodes.

The research findings depicted in **Fig 1.2** but not included in the above list of articles are ongoing works.

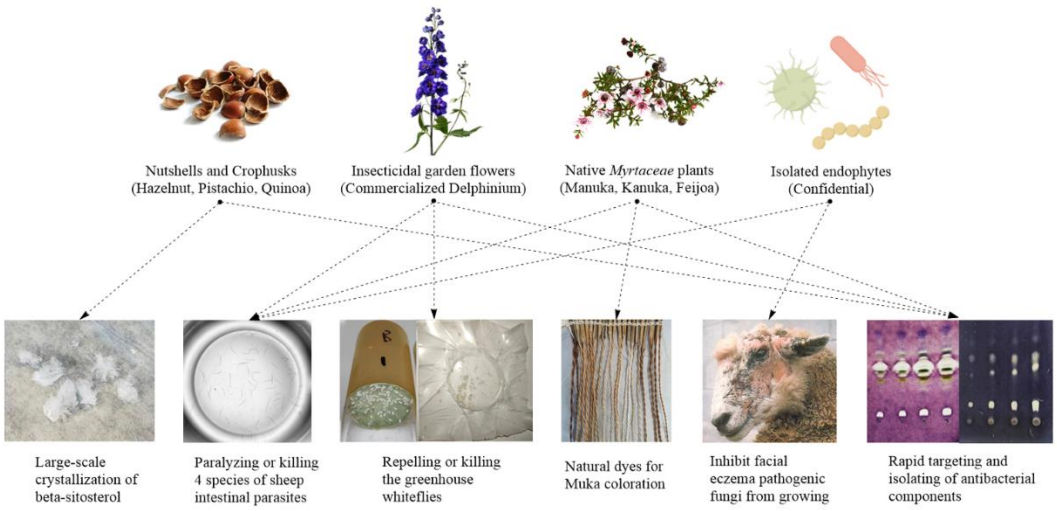

Fig. 1.2. Samples studied and results output throughout the study.

Chapter Two

Bioactive hybrid compounds from *Myrtaceae*: Chemical classification and biological activities – literature review

The objective of this review was to collate the chemical structure of hybrid compounds and related bioactivities from *Myrtaceae* plants, identify gaps in relevant research areas, and serve as a guide for future works.

This chapter has been published in the following peer-reviewed publication:

Xu, W., & Popovich, D. G. (2023). Bioactive hybrid compounds from Myrtaceae: Chemical classification and biological activities. Studies in Natural Products Chemistry, 77, 65-109.

Statement of Contribution

<table>
<tr><td colspan="4">We, the student and the student's main supervisor, certify that all co-authors have consented to their work being included in the thesis and they have accepted the student's contribution as indicated below in the Statement of Originality.</td></tr>
<tr><td colspan="2">Student name:</td><td colspan="2">Wenliang Xu</td></tr>
<tr><td colspan="2">Name and title of main supervisor:</td><td colspan="2">Dr. David Popovich</td></tr>
<tr><td colspan="2">In which chapter is the manuscript/published work?</td><td colspan="2">Chapter Two</td></tr>
<tr><td colspan="2">What percentage of the manuscript/published work was contributed by the student?</td><td colspan="2">85%</td></tr>
<tr><td colspan="4">Describe the contribution that the student has made to the manuscript/published work:
Conceptualization; Data curation; Investigation; Writing - original draft; Writing - review & editing.</td></tr>
<tr><td colspan="4">Please select one of the following three options:</td></tr>
<tr><td>✓</td><td colspan="3">The manuscript/published work is published or in press
Please provide the full reference of the research output:
Xu, W., & Popovich, D. G. (2023). Bioactive hybrid compounds from Myrtaceae: Chemical classification and biological activities. Studies in Natural Products Chemistry, 77, 65-109.</td></tr>
<tr><td></td><td colspan="3">The manuscript is currently under review for publication Please provide the name of the journal:</td></tr>
<tr><td></td><td colspan="3">It is intended that the manuscript will be published, but it has not yet been submitted to a journal</td></tr>
<tr><td>Student's signature:</td><td>Wenliang Xu</td><td>Main supervisor's signature:</td><td> 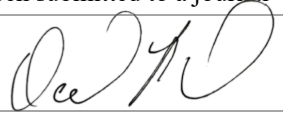 </td></tr>
</table>

Abstract

The Myrtaceae is a flowering plant family that contains around 140 genera and more than 5600 species. Some have significant economic and medicinal value. A series of structurally unique hybrid compounds were discovered from Myrtaceae which includes mono- and sesquiterpene-based meroterpenoids and β-triketone-phloroglucinol. Some of these hybrids exhibit significant antimicrobial, anticancer, anti-inflammatory, and enzyme-inhibitory activities. These hybrids are a special group of phytochemicals that can be considered as a natural "twin drug." Their bioactivities are usually more potent and/or more selective compared to the single moiety, and they possess more predictable pharmacokinetic and pharmacodynamic properties compared with the combination of two individual moieties.

This review is a comprehensive research compilation of the naturally occurring hybrid compounds from the Myrtaceae family published in the past decade. A comprehensive classification of their chemical structures by skeleton type is provided, along with an analysis of their antimicrobial, anticancer, anti-inflammatory, and enzyme-inhibitory activities. The structure-activity relationship is also discussed to provide evidence of the relationship between a certain bioactivity and a specific skeleton or substituent group.

Keywords: Hybrid compound; Mānuka; Meroterpenoid; Myrtaceae; Structure-activity.

2.1. Introduction

The *Myrtaceae* is a huge family of flowering plants that contains around 140 genera and more than 5600 species (Cascaes et al., 2015; Govaerts et al., 2008). Moreover, new species are still being discovered (Fernandes et al., 2020; Valdemarin et al., 2020; Tagane et al., 2018; Santos et al., 2015). *Myrtaceae* are all woody plants and have a predominantly southern hemisphere distribution, with most genera occurring in Australia and South America. They possess leathery evergreen leaves with oil glands and are known for their terpene-rich essential oils (Montalvan et al., 2019; Cao et al., 2018b; Senadeera et al., 2018b; Kubitzki and Klaus, 2011). Previous phytochemical studies have revealed that these plants produce a series of phloroglucinols, β-triketones and terpenes not only in their essential oils but also in their plant tissues (Zou et al., 2006; Reichling et al., 2005; Bloor, 1992; Rotstein et al., 1974). These small molecules are also the main active ingredients in *Myrtaceae* essential oils (Luz et al., 2020; Djebir et al., 2019; Park et al., 2017).

Interestingly, in *Myrtaceae*, these constituents have also been used as "bricks" for building more complex structures, including meroterpenoids and other non-terpene-based hybrids (Shang et al., 2019; Senadeera et al., 2018b; Qin et al., 2018; Liu et al., 2017a; Cao et al., 2016; Liu et al., 2016a; Jeong et al., 2009). These structurally complex phytochemicals have recently received increased attention due to their broad range of significant biological activities such as antimicrobial (Su et al., 2018; Kaneshima et al., 2017; Shang et al., 2016b; Liu et al., 2016e; Agatonovic-Kustrin, 2018), cytotoxicity (Qin et al., 2018; Yang et al., 2018; Shang et al., 2016a), anti-inflammatory (Zhi et al., 2018; Zhang et al., 2018), antiparasitic (Su et al., 2016; Sidana et al., 2011) and multiple enzyme inhibitory activities (Xu et al., 2018; Tang et al., 2017; Khanh et al., 2016; Fu et al., 2010).

These hybrids are a special group of phytochemicals that can be considered as a natural "twin drug", which is a drug containing two covalently bounded pharmacophoric groups. The twin-drug approach is also a strategy for optimizing existing drugs. In this case, most of the hybrids in *Myrtaceae* consist of an association of two different pharmacophores (phloroglucinol, β-triketone or terpene). Their bioactivities are usually more potent and/or more selective compared to the single moiety. They possess more predictable pharmacokinetic and pharmacodynamic properties compared to the combination of two individual moieties (Contreras and Sippl, 2008).

Terpenoids, also known as isoprenoids or terpenes, are the largest class of plant secondary metabolites with a wide variety of skeleton types (Agatonovic-Kustrin, 2018). When hybridized with phloroglucinols or/and β-triketones, they produce a whole new class of natural products. In recent reports, it is often seen that newly discovered hybrid compounds bear a unique skeleton (Qin et al., 2019; Su et al., 2018; Zhang et al., 2016; Liu et al., 2016c; Li et al., 2016).

This paper intends to give an overview of the chemical structures of all newly discovered myrtaceous hybrid compounds from the past decade (2010-2020) and classifies them based on their specific structural characteristics. It also reports their different bioactivities as revealed by various biological and pharmacological tests. Some structure-activity relationships and the perspective and potential direction for future studies on *Myrtaceae* species are discussed.

2.2. Chemical Constituents

Currently, 194 hybrid compounds have been isolated and identified from *Myrtaceae* in the past decade (2010-2020). These kinds of compounds have been frequently described as phloroglucinol or β-triketone derivatives (Jeong et al., 2018; Sun et al., 2015; Har et al., 2012; Zou et al., 2006; Ghisalberti, 1996). Their chemical structures are often not the same. Hybrids are bio-synthesized by two or more different moieties of the following three groups of phytochemicals: phloroglucinols, β-triketones and terpenes. This paper classifies the specific structural characteristics of these hybrid compounds, mainly meroterpenoids; others are phloroglucinols and β-triketones hybrids, and a few special hybrids. The type of structures of reported compounds are classified and displayed in **Figs**. **2.1-2.6**; their names, source of plants, parts and references are listed in **Table 2.1**.

2.2.1. Meroterpenoids:

Meroterpenoids are a group of hybrid natural compounds that are partially derived from terpenoids (Geris and Simpson, 2009). The major characteristic of these unique and complex compounds is the fusion of the structurally diverse terpenoid and non-terpenoid moieties (Matsuda and Abe, 2014). Meroterpenoids discovered in Myrtaceae are predominantly dimers that contain a mono- or sesquiterpenes moiety and a phloroglucinol or β-triketone moiety; less common are trimers, which contain a mono- or sesquiterpenes moiety and two non-terpene moieties. Only one tetramer has been identified so far and it has been classified in the “other hybrids” section.

Based on the specific moiety, the myrtaceous meroterpenoids can be further classified into five categories as shown in **Figs**. **2.1-2.6** below: phloroglucinol-monoterpene type meroterpenoids (**1-21**), phloroglucinol-sesquiterpene type meroterpenoids (**22-82**), β-triketone-monoterpene type meroterpenoids (**83-119**), β-triketone-sesquiterpene type meroterpenoids (**120-154**) and trimeric meroterpenoids (**155-171**). Mono- or sesquiterpenes are often classified according to their basic carbon skeleton types, that is, according to the different arrangement order of isoprene units that make them up. Due to the large number of skeleton types, they can sometimes also be roughly classified into acyclic and various cyclization types (Chizzola, 2013). The detailed classification is discussed in each category below.

2.2.1.1. Phloroglucinol-monoterpene type meroterpenoids (PMMs):

The myrtaceous PMMs contain a phloroglucinol and a monoterpene moiety. Monoterpenes are simple in structure and have four skeleton types: acyclic, monocyclic, bicyclic monoterpene and iridoid. From the structures (**Fig. 2.1**), the type of monoterpene moieties includes but are not limited to bicyclic monoterpenes, which contain pinane-type (**1**-**4**, **19**, **20)**, and thujene-type (**9**, **10**, **18**-**21**) and monocyclic monoterpenes, which contain p-menthane-type (**5**-**8**, **11**-**17**). No acyclic monoterpene and iridoid moiety have been observed in myrtaceous PMMs. This suggests a rule that myrtaceous phloroglucinol may only hybridize with monocyclic and bicyclic monoterpenes in natural conditions. This also indicates that combining phloroglucinol with acyclic monoterpene or iridoid may decrease bioactivity or produce toxicity in plants. It is noteworthy that the isopropyl-cyclopentane ring in compounds **7** and **8** isolated from *Callistemon rigidus* was derived from a rearrangement of a p-menthane-type monoterpene; these meroterpenoids, therefore, feature a unique skeleton (Cao et al., 2018a).

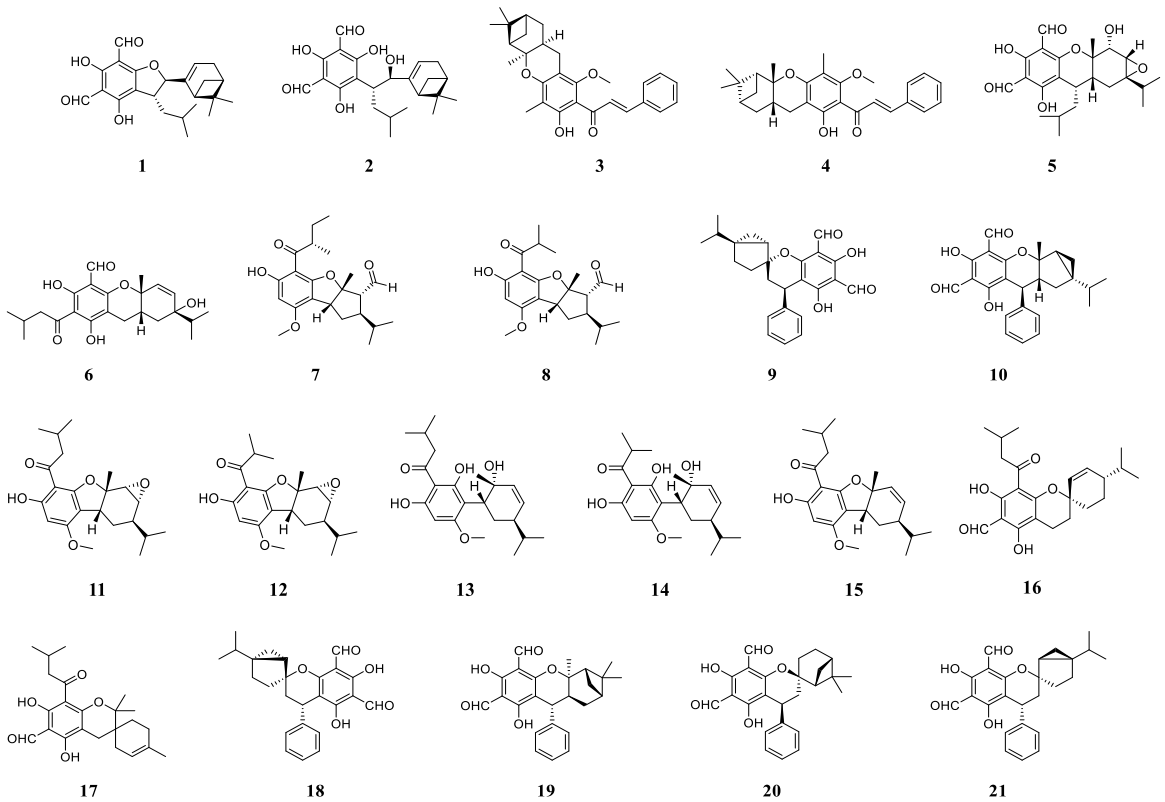

Fig. **2.1**. Structures of PMMs.

2.2.1.2. Phloroglucinol-sesquiterpene type meroterpenoids (PSMs):

Sesquiterpenes include acyclic, lactone and various cyclization types. Unlike monoterpenes, the sesquiterpenes consist of three isoprene units, which allow for many unique combinations and

a greater potential for stereochemical diversity (Sharma et al., 2013; Buckle, 2015). Because of this, the classification based on the number of rings may not be accurate. In this paper, the classification of these compounds was carried out according to their basic skeleton type based on the arrangement order of isoprene units.

The types of sesquiterpene moiety in recently identified myrtaceous PSMs mainly contain cadinene-type (**22**, **23**, **31**, **49**-**51**, **71**), cubebene-type (**24**-**26**, **42** and **43**), aromadendrene-type (**27**-**29**, **32**, **33**, **37**, **39**-**41**, **44**, **52**, **69**, **70**, **73**, **75** and **79**), eudesmane-type (**30**, **36**, **38**, **61**, **65**, **74** and **80**), germacrene-type (**34** and **35**), bicyclogermacrene-type (**46**, **57**, **58**, **62**, **66**-**68**, **77**, **78** and **82**), caryolane-type (**47** and **76**), guaiane-type (**53**), aristolane-type (**54**-**56**, **59**, **60**, **63** and **64**) and caryophyllene-type (**45**, **48**, **72** and **81**). Their chemical structures are listed in **Fig. 2.2**. There is no acyclic sesquiterpene or sesquiterpene lactone observed amongst the collected structures. The authors speculate that *Myrtaceae* plants have no capacity to produce acyclic sesquiterpene- or sesquiterpene lactone-based meroterpenes. In other words, the combination of phloroglucinol with common cyclic sesquiterpene is the result of natural selection for the highest bioactivities.

In the collected structures, some of them bear unusual skeletons. This phenomenon is usually due to certain special reactions occurring when two compounds are binding. The sesquiterpene moiety in compound **30** features an unusual skeleton; according to its proposed biosynthetic pathway, the sesquiterpene portion is formed by a rearrangement of an eudesmane moiety (Qin et al., 2018). As for compounds **32** and **33**, the first example of this type of meroterpenoid is eucalyptone (in *Eucalyptus robusta*), reported in the study of the same plant material (Osawa et al., 1995). However, both studies have no predicted biosynthetic pathways, and the structures of the sesquiterpene part in compounds **32** and **33** do not exist in current natural sesquiterpene collections. However, the authors think the skeleton of the sesquiterpene part in compounds **32** and **33** does not conform to the arrangement law of three isoprene units; the current skeleton should be formed by the ring-opening reaction on the C-1 position of the oxidized aromadendrene moiety.

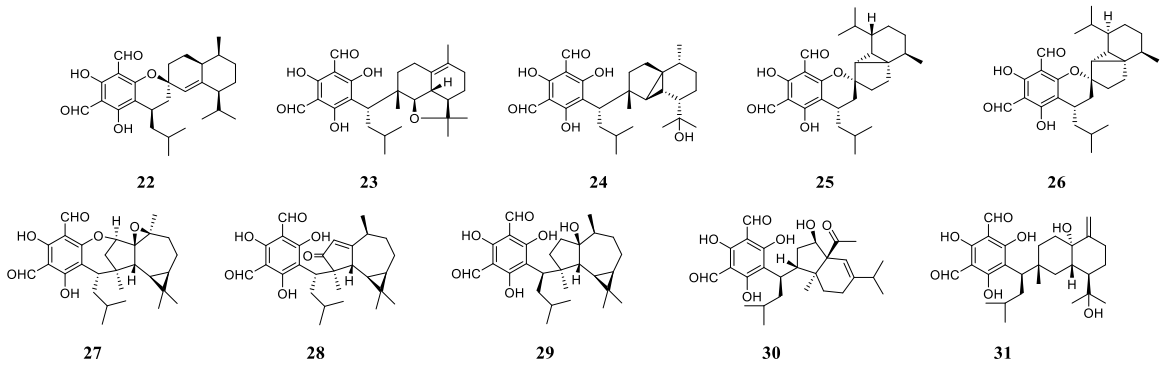

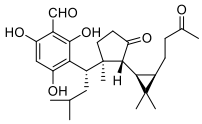

32

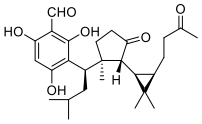

33

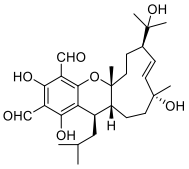

34

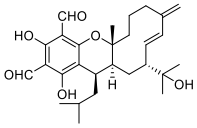

35

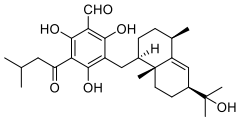

36

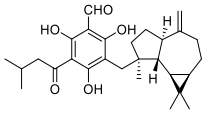

37

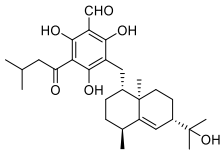

38

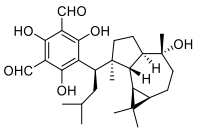

39

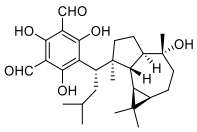

40

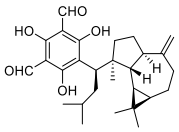

41

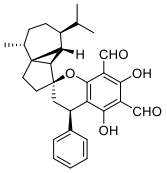

42

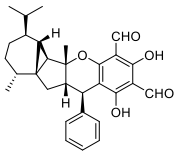

43

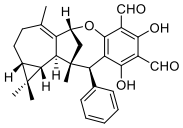

44

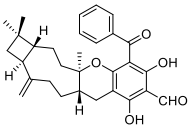

45

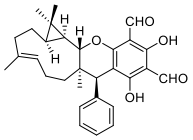

46

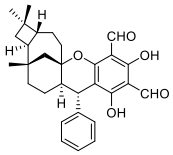

47

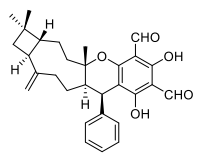

48

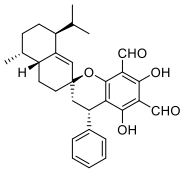

49

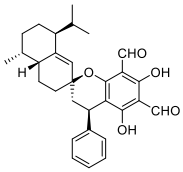

50

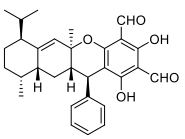

51

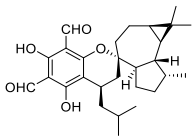

52

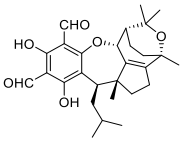

53

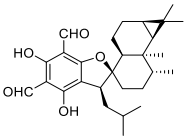

54

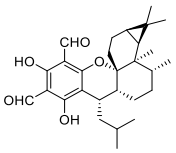

55

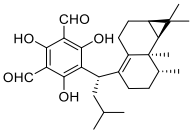

56

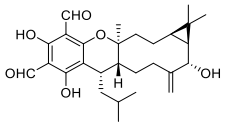

57

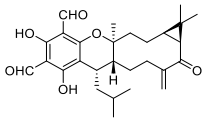

58

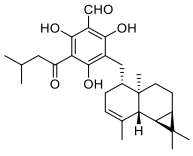

59

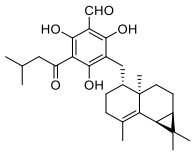

60

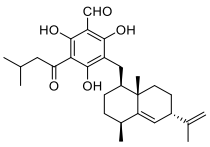

61

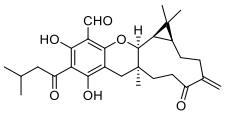

62

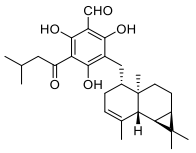

63

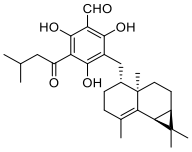

64

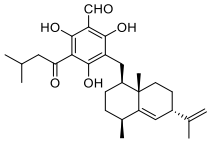

65

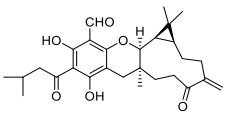

66

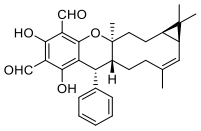

67

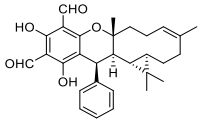

68

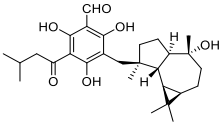

69

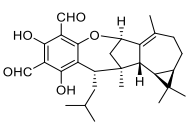

70

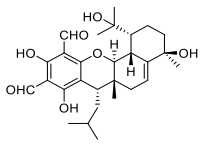

71

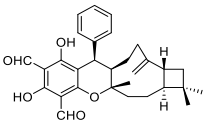

72

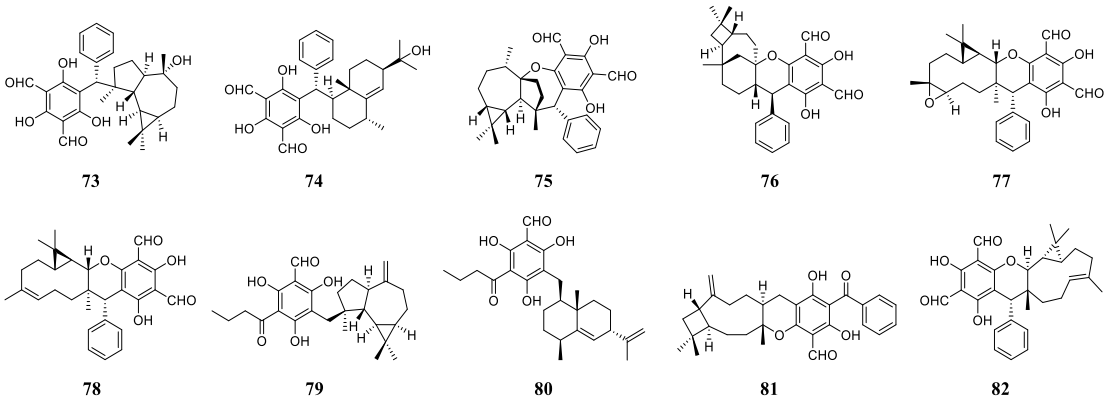

Fig. **2.2.** Structures of PSMs.

2.2.1.3. β-Triketone-monoterpene type meroterpenoids (TMMs):

Compared to PMMs, the types of monoterpene moiety in TMMs are more abundant; the current collection of structures includes both acyclic types and the various cyclization types. According to their basic skeleton types of monoterpene parts, TMMs can be further classified into pinane-type (**83**, **84**, **96-98**, **104-107**, **109-111**, **114** and **119**), thujene-type (**85-90**, **92-95**, **108**, **112** and **113**), p-menthane-type (**99-103**, **117** and **118**) and myrcene-type (**91**, **115** and **116**). Among them, the pinane- and thujene-type are bicyclic compounds, the p-menthane-type are monocyclic compounds and myrcene-type are acyclic compounds. No iridoid-based meroterpenoid has been discovered, which suggests that the iridoid with β-triketone or phloroglucinol may not be able to combine/hybridize in a natural way and that acyclic monoterpene could produce activity only when it is combined with a β-triketone. The chemical structures of TMMs are displayed in **Fig. 2.3**.

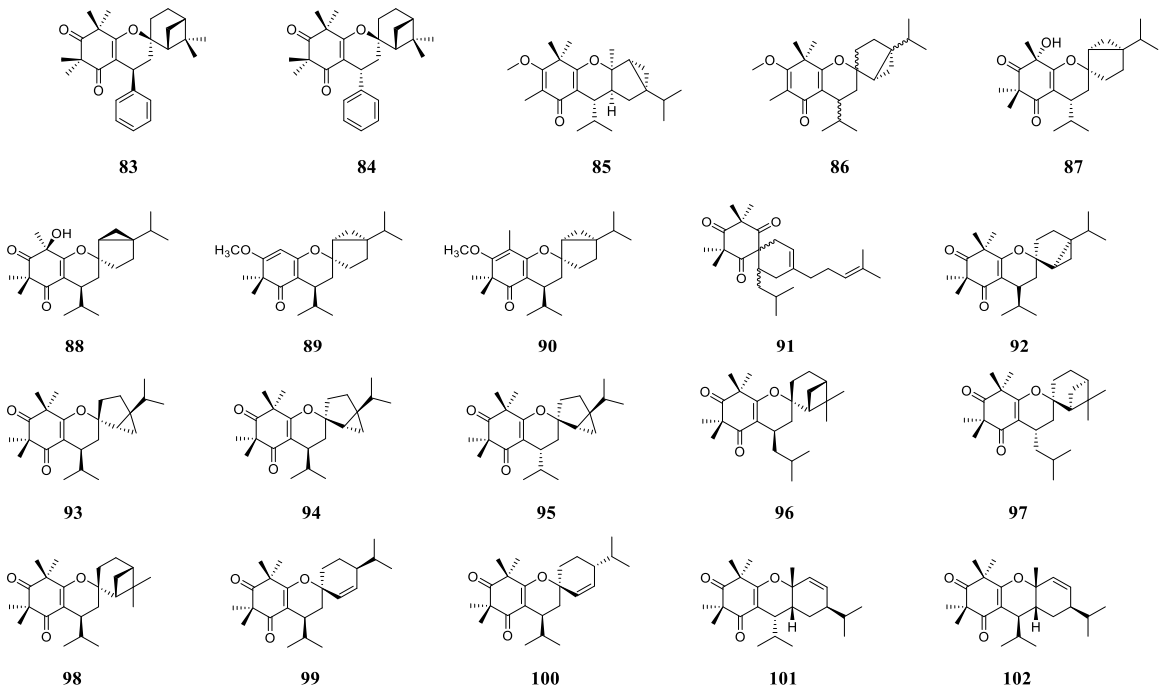

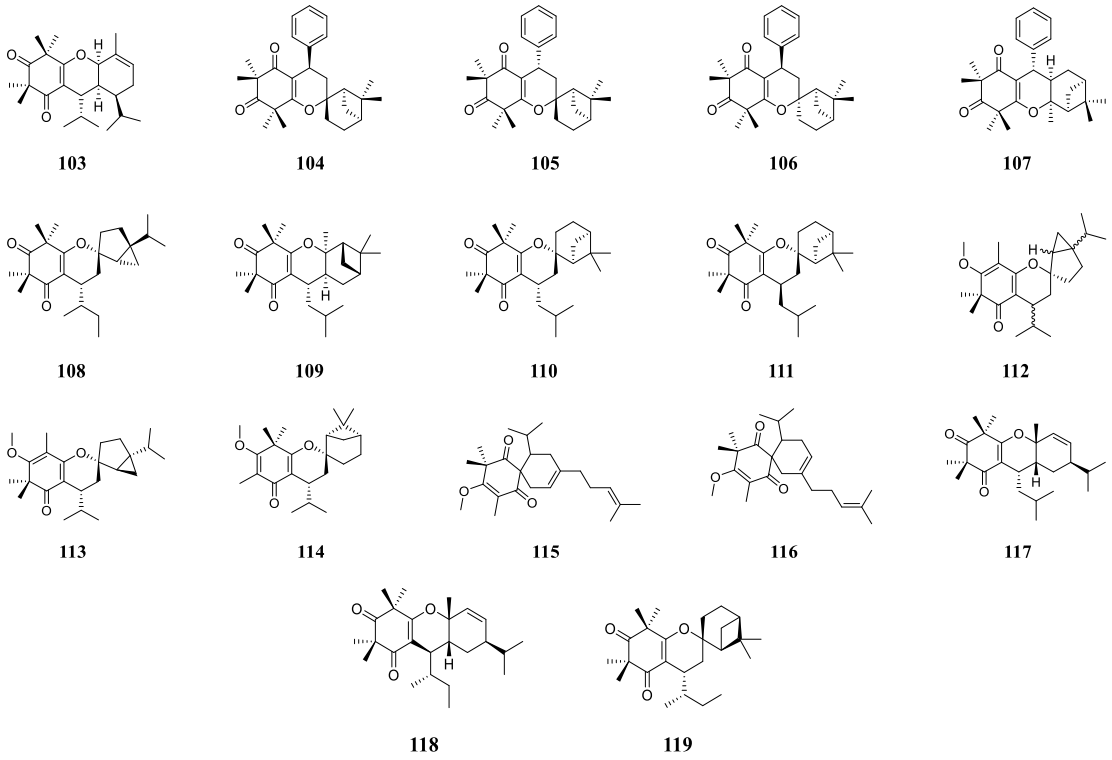

Fig. **2.3**. Structures of TMMs.

2.2.1.4. β-Triketone-sesquiterpene type meroterpenoids (TSMs):

The majority of sesquiterpene moieties in TSMs are caryophyllene-type (**120**-**125**, **131**-**135**, **140**-**145**, **147**, **148** and **152**), followed by cadinene-type (**126**, **127**, and **149**-**151**), α-cadinene-type (**136** and **137**), bicyclogermacrene-type (**128** and **129**), aromadendrene-type (**130** and **138**), humulene-type (**139** and **146**) and cubebene-type (**153** and **154**). Their chemical structures are displayed in **Fig**. **2.4**. As with PSMs, TSMs also have no acyclic sesquiterpene or sesquiterpene lactone type moieties. This result supports the hypothesis in the PSMs section that *Myrtaceae* plants have no corresponding synthase expressions.

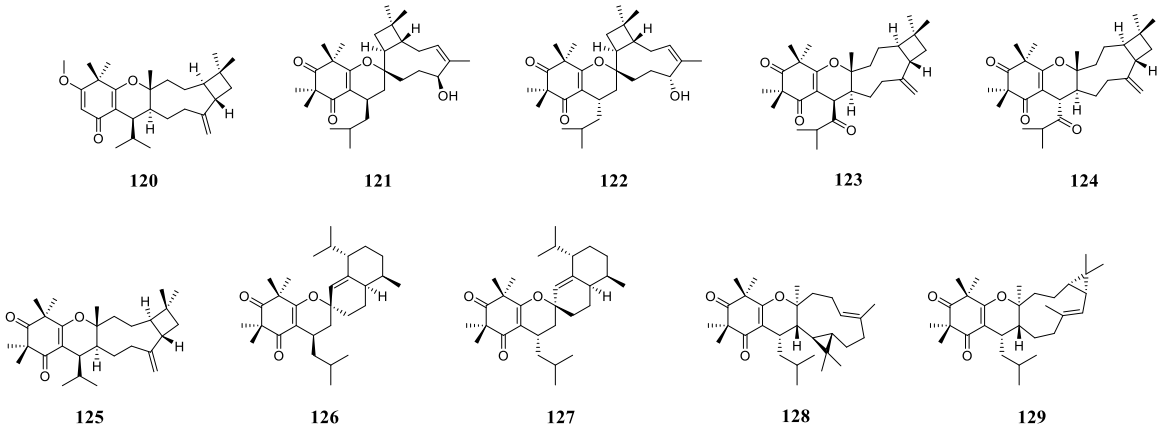

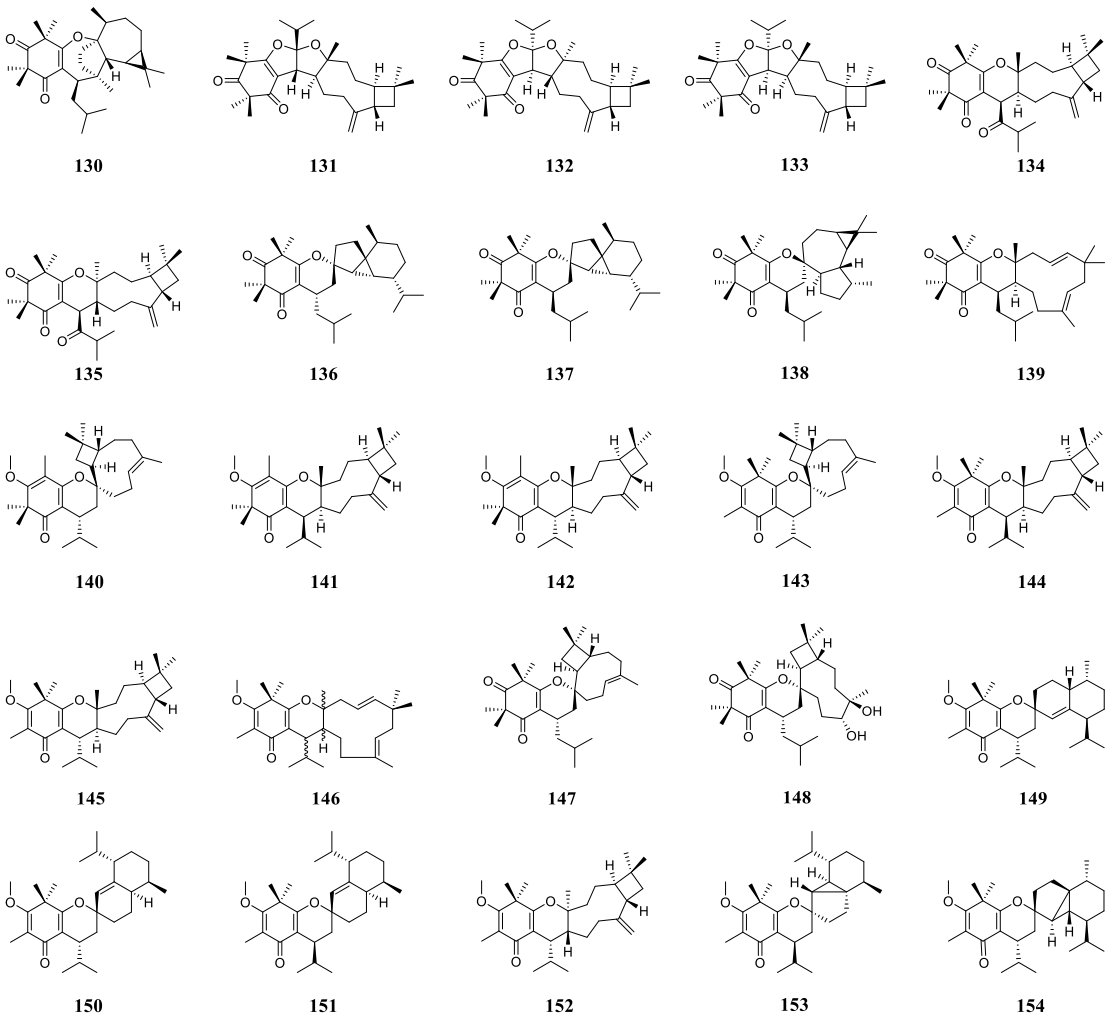

Fig. **2.4**. TMMs.

2.2.1.5. Trimeric meroterpenoids:

The structures of all trimers discovered in the past decade have exhibited obvious regularity. A β-Triketone and a terpene unit combined on different sides of a phloroglucinol unit suggest a regular pattern of biosynthesis, which may help researchers find a key enzyme or synthetic condition to develop a new synthesis route. The terpene parts include p-menthane (**156-164**), thujene (**165-169**) and caryophyllene (**170** and **171**).

Compound **155** discovered from *Myrtus communis* is a special one. It contains a rare terpene-like group; structurally, it should be classified as a nor-sesquiterpenoid. The identification process of another compound in the same article was wrong (Cottiglia et al., 2012), and has been revised to compound **125** by another researcher (Liu et al., 2016a). Due to the terpene part in compound **155** having a structural similarity with its incorrectly identified compound, and then according to all the existing trimer structure features, the authors have some doubts about the authenticity of its

structure. The chemical structures of trimeric meroterpenoids are displayed in **Fig**. **2.5.**

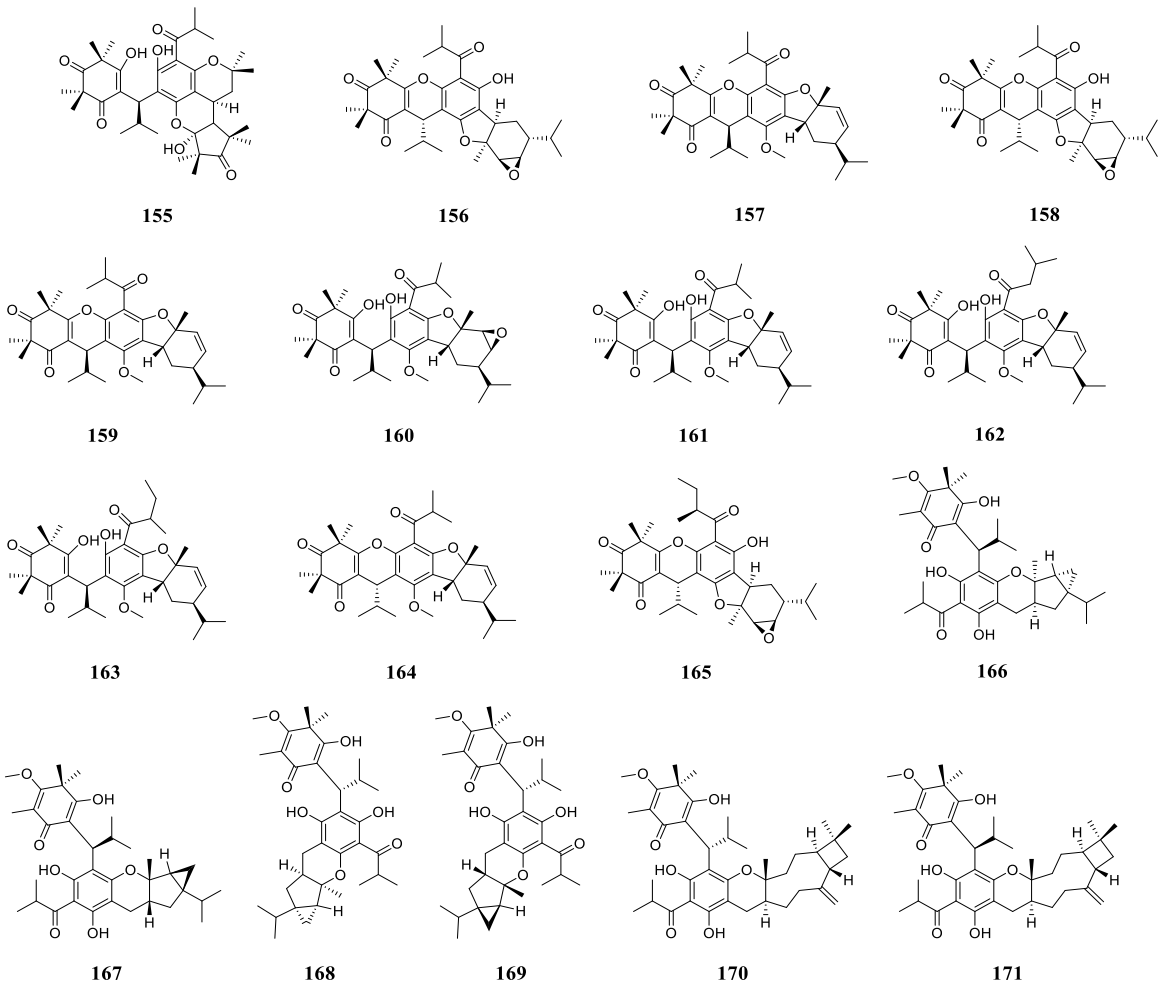

Fig. **2.5.** Structures of Trimeric meroterpenoids.

2.2.2. Other hybrid compounds:

Except for meroterpenoids, the other hybrid compounds are mainly β-triketone-phloroglucinol hybrids (**172**-**188**, **192**). Compounds **183**-**188** are reported as β-triketone-flavanone hybrids (Senadeera et al., 2018a). However, the authors hold different views. Flavanone is a type of flavonoid; its basic structure is a skeleton of diphenylpropane. It is also defined as a C6-C3-C6 structure (Geissman, 1963). The flavanone-like moieties in compounds **183**-**188** do not strictly follow the definition of flavonoids, thus, the present paper has classified them into β-triketone-phloroglucinol hybrids.

Compound **189** is a rare phloroglucinol dimer comprising of two phloroglucinol molecules and featuring a similar skeleton to flavonoids. Some non-terpene based trimeric hybrids have also been found. Compounds **190** and **191** contain a D-glucose unit in the middle of β-triketone-phloroglucinol hybrids; compound **193** has a β-triketone-phloroglucinol-β-triketone

centrosymmetric structure probably because the phloroglucinol in the middle is a bilaterally symmetric structure. Therefore, two groups of β-triketone-phloroglucinol binding reactions were able to take place on both sides at the same time. Only one tetramer, compound **194**, has been discovered so far. It is a phloroglucinol dimer combined with two caryophyllenes on the same phloroglucinol unit that forms an unprecedented skeleton. The chemical structures of the abovementioned hybrid compounds are listed in **Fig**. **2.6**.

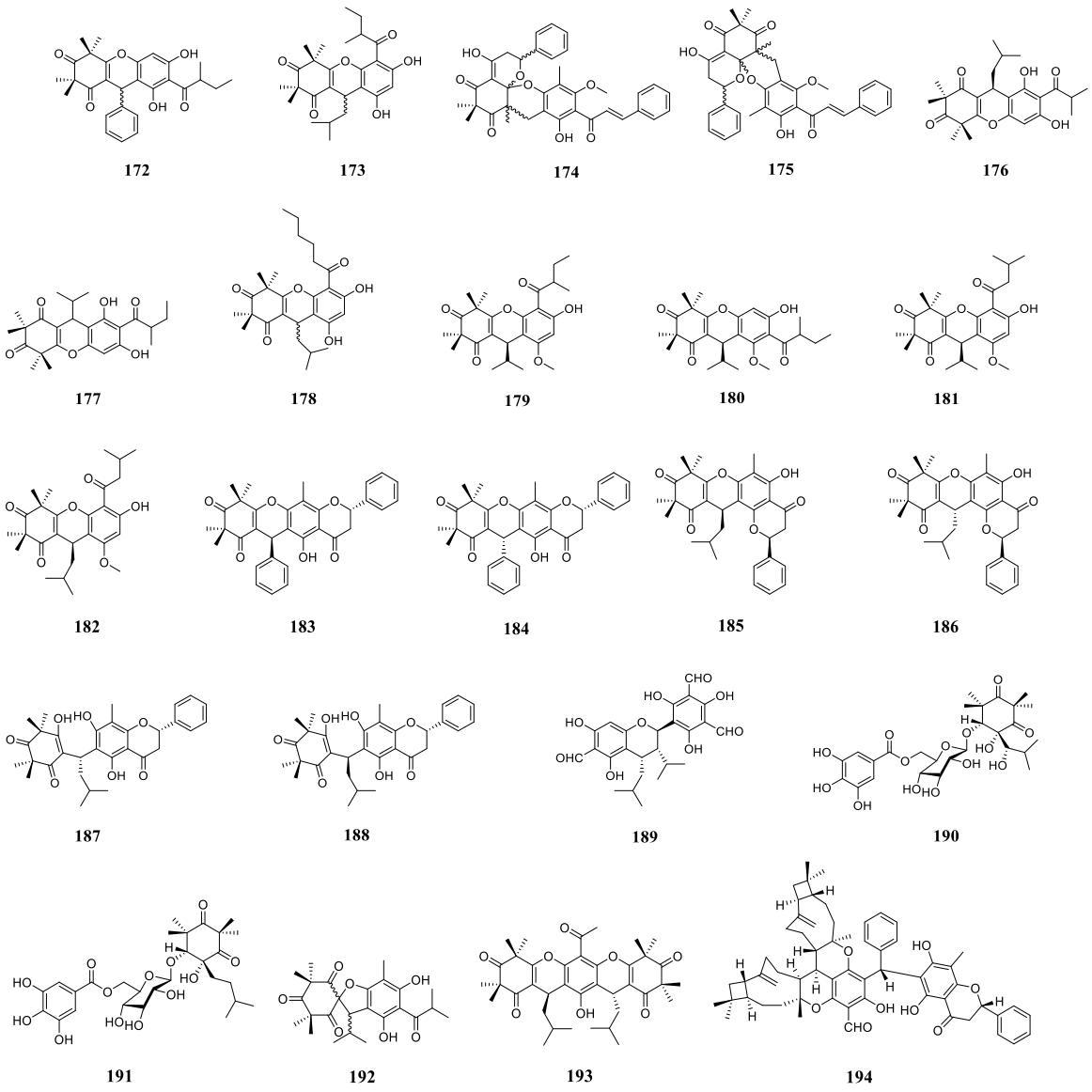

Fig. **2.6.** Structures of other hybrid compounds.

Table 2.1. The hybrid compounds isolated from *Myrtaceae*.

No.	Compound name	**CAS No.**	Plant	Part of plant	References
1	Eucalrobusone Y	2375923-35-4	*Eucalyptus robusta*	Leaf	Shang et al. (2019)
2	Eucalrobusone Z	2375923-36-5	*Eucalyptus robusta*	Leaf	Shang et al. (2019)
3	Operculatol A	2368178-77-0	*Syzygium nervosum*	Leaf	Su et al. (2018)

4	Operculatol B	2368178-78-1	*Syzygium nervosum*	Leaf	Su et al. (2018)
5	Eucalypglobulusal I	2305951-80-6	*Eucalyptus globulus*	Fruit	Qin et al. (2018)
6	Eucalypglobulusal J	2305951-81-7	*Eucalyptus globulus*	Fruit	Qin et al. (2018)
7	Callisretone A	2173210-80-3	*Callistemon rigidus*	Leaf	Cao et al. (2018a)
8	Callisretone B	2173210-81-4	*Callistemon rigidus*	Leaf	Cao et al. (2018a)
9	Psiguajadial K	1402066-93-6	*Psidium guajava*	Leaf	Tang et al. (2017)
10	Guajavadial A	2243235-43-8	*Psidium guajava*	Leaf	Qin et al. (2016)
11	Callviminol A	2091869-42-8	*Callistemon viminalis*	Leaf	Liu et al. (2016b)
12	Callviminol B	2091869-43-9	*Callistemon viminalis*	Leaf	Liu et al. (2016b)
13	Callviminol C	2241246-21-7	*Callistemon viminalis*	Leaf	Liu et al. (2016b)
14	Callviminol D	2241246-22-8	*Callistemon viminalis*	Leaf	Liu et al. (2016b)
15	Callviminol E	2091869-48-4	*Callistemon viminalis*	Leaf	Liu et al. (2016b)
16	Euglobal R1	1449768-69-7	*Eucalyptus robusta*	Leaf	Jian et al. (2012)
17	Euglobal R2	1449768-70-0	*Eucalyptus robusta*	Leaf	Jian et al. (2012)
18	Guadial A	1402066-93-6	*Psidium guajava*	Leaf	Shao et al. (2012)
19	Guadial B	1783802-72-1	*Psidium guajava*	Leaf	Jian et al. (2015)
20	Guadial C	1783802-73-2	*Psidium guajava*	Leaf	Jian et al. (2015)
21	Psiguajavadial A	2108086-50-4	*Psidium guajava*	Fruit	Qin et al. (2017b)
22	Eucalrobusone Q	2375923-25-2	*Eucalyptus robusta*	Leaf	Shang et al. (2019)
23	Eucalrobusone R	2375923-26-3	*Eucalyptus robusta*	Leaf	Shang et al. (2019)
24	Eucalrobusone S	2375923-27-4	*Eucalyptus robusta*	Leaf	Shang et al. (2019)
25	Eucalrobusone T	2375923-28-5	*Eucalyptus robusta*	Leaf	Shang et al. (2019)
26	7R-eucalrobusone T	2375923-29-6	*Eucalyptus robusta*	Leaf	Shang et al. (2019)
27	Eucalrobusone U	2375923-30-9	*Eucalyptus robusta*	Leaf	Shang et al. (2019)
28	Eucalrobusone V	2375923-31-0	*Eucalyptus robusta*	Leaf	Shang et al. (2019)
29	Eucalrobusone W	2375923-32-1	*Eucalyptus robusta*	Fruit	Qin et al. (2018)
30	Eucalypglobulusal A	2226451-51-8	*Eucalyptus globulus*	Fruit	Qin et al. (2018)
31	Eucalypglobulusal B	2305951-73-7	*Eucalyptus globulus*	Fruit	Qin et al. (2018)
32	Eucalypglobulusal C	2305951-74-8	*Eucalyptus globulus*	Fruit	Qin et al. (2018)
33	Eucalypglobulusal D	2305951-75-9	*Eucalyptus globulus*	Fruit	Qin et al. (2018)
34	Eucalypglobulusal E	2305951-76-0	*Eucalyptus globulus*	Fruit	Qin et al. (2018)
35	Eucalypglobulusal F	2305951-77-1	*Eucalyptus globulus*	Fruit	Qin et al. (2018)
36	Eucalypglobulusal G	2305951-78-2	*Eucalyptus globulus*	Fruit	Qin et al. (2018)
37	Eucalypglobulusal H	2305951-79-3	*Eucalyptus globulus*	Fruit	Qin et al. (2018)
38	Eucalyptin B	2232221-79-1	*Eucalyptus globulus*	Fruit	Pham et al. (2018)
39	Macrocarpal A	132951-90-7	*Eucalyptus globulus*	Leaf	Kato et al. (2018)
40	Macrocarpal B	142698-60-0	*Eucalyptus globulus*	Leaf	Kato et al. (2018)
41	Macrocarpal C	142628-53-3	*Eucalyptus globulus*	Leaf	Kato et al. (2018)
42	Psiguajadial A	N/A[#]	*Psidium guajava*	Leaf	Tang et al. (2017)
43	Psiguajadial B	N/A	*Psidium guajava*	Leaf	Tang et al. (2017)
44	Psiguajadial C	1254173-25-5	*Psidium guajava*	Leaf	Tang et al. (2017)
45	Psiguajadial D	2233581-31-0	*Psidium guajava*	Leaf	Tang et al. (2017)
46	Psiguajadial E	N/A	*Psidium guajava*	Leaf	Tang et al. (2017)
47	Psiguajadial F	N/A	*Psidium guajava*	Leaf	Tang et al. (2017)

48	Psiguajadial G	959860-49-2	*Psidium guajava*	Leaf	Tang et al. (2017)
49	Psiguajadial H	1529775-04-9	*Psidium guajava*	Leaf	Tang et al. (2017)
50	Psiguajadial I	1529775-02-7	*Psidium guajava*	Leaf	Tang et al. (2017)
51	Psiguajadial J	1529775-06-1	*Psidium guajava*	Leaf	Tang et al. (2017)
52	Eucalrobusone J	2247645-56-1	*Eucalyptus robusta*	Leaf	Shang et al. (2016b)
53	Eucalrobusone K	2247645-57-2	*Eucalyptus robusta*	Leaf	Shang et al. (2016b)
54	Eucalrobusone L	2247645-58-3	*Eucalyptus robusta*	Leaf	Shang et al. (2016b)
55	Eucalrobusone M	2247645-59-4	*Eucalyptus robusta*	Leaf	Shang et al. (2016b)
56	Eucalrobusone N	2247645-60-7	*Eucalyptus robusta*	Leaf	Shang et al. (2016b)
57	Eucalrobusone O	2247645-61-8	*Eucalyptus robusta*	Leaf	Shang et al. (2016b)
58	Eucalrobusone P	2247645-62-9	*Eucalyptus robusta*	Leaf	Shang et al. (2016b)
59	Eucalrobusone A	1982377-55-8	*Eucalyptus robusta*	Leaf	Shang et al. (2016a)
60	Eucalrobusone B	1982377-56-9	*Eucalyptus robusta*	Leaf	Shang et al. (2016a)
61	Eucalrobusone C	1982377-57-0	*Eucalyptus robusta*	Leaf	Shang et al. (2016a)
62	Eucalrobusone D	1982377-57-0	*Eucalyptus robusta*	Leaf	Shang et al. (2016a)
63	Eucalrobusone E	1982377-59-2	*Eucalyptus robusta*	Leaf	Shang et al. (2016a)
64	Eucalrobusone G	1973479-55-8	*Eucalyptus robusta*	Leaf	Shang et al. (2016a)
65	Eucalrobusone H	1973479-56-9	*Eucalyptus robusta*	Leaf	Shang et al. (2016a)
66	Eucalrobusone I	1973479-57-0	*Eucalyptus robusta*	Leaf	Shang et al. (2016a)
67	Guajavadial B	2243235-45-0	*Psidium guajava*	Leaf	Qin et al. (2016)
68	Guajavadial C	2243235-47-2	*Psidium guajava*	Leaf	Qin et al. (2016)
69	Eucalyptin A	1399065-21-4	*Eucalyptus globulus*	Fruit	Yang et al. (2012)
70	Eucalyptal D	2349306-54-1	*Eucalyptus globulus*	Fruit	Wang et al. (2012)
71	Eucalyptal E	2349306-56-3	*Eucalyptus globulus*	Fruit	Wang et al. (2012)
72	Psidial A	1207181-35-8	*Psidium guajava*	Leaf	Fu et al. (2010)
73	Psidial B	1207181-36-9	*Psidium guajava*	Leaf	Fu et al. (2010)
74	Psidial C	1207181-37-0	*Psidium guajava*	Leaf	Fu et al. (2010)
75	Psiguadial A	1254173-25-5	*Psidium guajava*	Leaf	Shao et al. (2010)
76	Psiguadial B	1254173-26-6	*Psidium guajava*	Leaf	Shao et al. (2010)
77	Psiguadial C	1402066-94-7	*Psidium guajava*	Leaf	Shao et al. (2012)
78	Psiguadial D	1402066-95-8	*Psidium guajava*	Leaf	Shao et al. (2012)
79	Eugenial C	1809524-15-9	*Eugenia umbelliflora*	Fruit	Faqueti et al. (2015)
80	Eugenial D	1809524-16-0	*Eugenia umbelliflora*	Fruit	Faqueti et al. (2015)
81	Guapsidial A	1783802-71-0	*Psidium guajava*	Leaf	Jian et al. (2015)
82	Psiguajavadial B	2108086-51-5	*Psidium guajava*	Fruit	Qin et al. (2017b)
83	Brachyanin A	N/A	*Leptospermum brachyandrum*	Leaf	Zou et al. (2018)
84	Brachyanin B	N/A	*Leptospermum brachyandrum*	Leaf	Zou et al. (2018)
85	Baeckfrutone M	N/A	*Baeckea frutescens*	Twig & Leaf	Zhi et al. (2018)
86	(±)-Baeckfrutone N	N/A	*Baeckea frutescens*	Twig & Leaf	Zhi et al. (2018)
87	Baeckfrutone O	N/A	*Baeckea frutescens*	Twig & Leaf	Zhi et al. (2018)
88	Baeckfrutone P	N/A	*Baeckea frutescens*	Twig & Leaf	Zhi et al. (2018)
89	Baeckfrutone Q	N/A	*Baeckea frutescens*	Twig & Leaf	Zhi et al. (2018)
90	Baeckfrutone R	N/A	*Baeckea frutescens*	Twig & Leaf	Zhi et al. (2018)
91	(±)-Calliviminone C	1928778-29-3	*Syncarpia glomulifera*	Stem bark	Su et al. (2016)

92	Myrtucommulone L	1357149-74-6	*Myrtus communis*	Leaf	Cottiglia et al. (2012)
93	Callistiviminene F	2059134-87-9	*Callistemon viminalis*	Fruit	Wu et al. (2016)
94	Callistiviminene G	2059134-88-0	*Callistemon viminalis*	Fruit	Wu et al. (2016)
95	Callistiviminene H	2059134-89-1	*Callistemon viminalis*	Fruit	Wu et al. (2016)
96	(+)-Callistiviminene I	2059134-90-4	*Callistemon viminalis*	Fruit	Wu et al. (2016)
97	(−)-Callistiviminene I	2059134-97-1	*Callistemon viminalis*	Fruit	Wu et al. (2016)
98	Callistiviminene J	2059134-91-5	*Callistemon viminalis*	Fruit	Wu et al. (2016)
99	Callistiviminene K	2059134-92-6	*Callistemon viminalis*	Fruit	Wu et al. (2016)
100	Callistiviminene L	2059134-93-7	*Callistemon viminalis*	Fruit	Wu et al. (2016)
101	Callistiviminene M	2059134-94-8	*Callistemon viminalis*	Fruit	Wu et al. (2016)
102	Callistiviminene N	2059134-95-9	*Callistemon viminalis*	Fruit	Wu et al. (2016)
103	Callistiviminene O	2059134-96-0	*Callistemon viminalis*	Fruit	Wu et al. (2016)
104	Intermedione A	2279931-41-6	*Corymbia torelliana*	Flower	Senadeera et al. (2018a)
105	Intermedione B	2279931-42-7	*Corymbia torelliana*	Flower	Senadeera et al. (2018a)
106	Intermedione C	2279931-43-8	*Corymbia torelliana*	Flower	Senadeera et al. (2018a)
107	Intermedione D	2279931-44-9	*Corymbia torelliana*	Flower	(Senadeera et al., 2018a)
108	Rtomentone E	N/A	*Rhodomyrtus tomentosa*	Leaf	Deng et al. (2020)
109	Rtomentone F	N/A	*Rhodomyrtus tomentosa*	Leaf	Deng et al. (2020)
110	Rtomentone G	2540666-61-1	*Rhodomyrtus tomentosa*	Leaf	Deng et al. (2020)
111	Rtomentone H	2540665-65-2	*Rhodomyrtus tomentosa*	Leaf	Deng et al. (2020)
112	(±)-Frutescone N	2126805-26-1	*Baeckea frutescens*	Aerial part	Hou et al. (2017)
113	Frutescone O	2126805-22-7	*Baeckea frutescens*	Aerial part	Hou et al. (2017)
114	Frutescone P	2126807-04-1	*Baeckea frutescens*	Aerial part	Hou et al. (2017)
115	(±)-Frutescone Q	2126805-30-7	*Baeckea frutescens*	Aerial part	Hou et al. (2017)
116	(±)-Frutescone R	2126805-28-3	*Baeckea frutescens*	Aerial part	Hou et al. (2017)
117	Callisalignene G	N/A	*Callistemon salignus*	Twig & Leaf	Qin et al. (2017a)
118	Callisalignene H	N/A	*Callistemon salignus*	Twig & Leaf	Qin et al. (2017a)
119	Callisalignene I	N/A	*Callistemon salignus*	Twig & Leaf	Qin et al. (2017a)
120	Baeckfrutone S	N/A	*Baeckea frutescens*	Twig & Leaf	Zhi et al. (2018)
121	Tomentodione O	2241542-73-2	*Rhodomyrtus tomentosa*	Leaf	Zhang et al. (2018)
122	Tomentodione P	2241542-74-3	*Rhodomyrtus tomentosa*	Leaf	Zhang et al. (2018)
123	Tomentodione Q	2241542-75-4	*Rhodomyrtus tomentosa*	Leaf	Zhang et al. (2018)
124	Tomentodione R	2241542-76-5	*Rhodomyrtus tomentosa*	Leaf	Zhang et al. (2018)
125	Myrtucommulone K*	1357149-73-5	*Myrtus communis*	Leaf	Cottiglia et al. (2012)
126	Callistiviminene A	2059134-82-4	*Callistemon viminalis*	Fruit	Wu et al. (2016)
127	Callistiviminene B	2059134-83-5	*Callistemon viminalis*	Fruit	Wu et al. (2016)
128	Callistiviminene C	2059134-84-6	*Callistemon viminalis*	Fruit	Wu et al. (2016)
129	Callistiviminene D	2059134-85-7	*Callistemon viminalis*	Fruit	Wu et al. (2016)
130	Callistiviminene E	2059134-86-8	*Callistemon viminalis*	Fruit	Wu et al. (2016)
131	Rhodomyrtusial A	2376112-07-9	*Rhodomyrtus tomentosa*	Leaf & Stem	Qin et al. (2019)
132	Rhodomyrtusial B	2376112-08-0	*Rhodomyrtus tomentosa*	Leaf & Stem	Qin et al. (2019)
133	Rhodomyrtusial C	2376112-09-1	*Rhodomyrtus tomentosa*	Leaf & Stem	Qin et al. (2019)
134	Rhotomentodione A	2241542-75-4	*Rhodomyrtus tomentosa*	Leaf & Stem	Qin et al. (2019)
135	Rhotomentodione B	2376112-10-4	*Rhodomyrtus tomentosa*	Leaf & Stem	Qin et al. (2019)

136	Rtomentone A	N/A	*Rhodomyrtus tomentosa*	Leaf	Deng et al. (2020)
137	Rtomentone B	N/A	*Rhodomyrtus tomentosa*	Leaf	Deng et al. (2020)
138	Rtomentone C	2540666-60-0	*Rhodomyrtus tomentosa*	Leaf	Deng et al. (2020)
139	Rtomentone D	2540665-09-4	*Rhodomyrtus tomentosa*	Leaf	Deng et al. (2020)
140	Frutescone A	2089049-28-3	*Baeckea frutescens*	Aerial part	Hou et al. (2016)
141	Frutescone B	2089049-29-4	*Baeckea frutescens*	Aerial part	Hou et al. (2016)
142	Frutescone C	2089049-30-7	*Baeckea frutescens*	Aerial part	Hou et al. (2016)
143	Frutescone D	2089049-31-8	*Baeckea frutescens*	Aerial part	Hou et al. (2016)
144	Frutescone E	2089049-32-9	*Baeckea frutescens*	Aerial part	Hou et al. (2016)
145	Frutescone F	2089049-33-0	*Baeckea frutescens*	Aerial part	Hou et al. (2016)
146	(±)-Frutescone G	2089049-34-1	*Baeckea frutescens*	Aerial part	Hou et al. (2016)
147	Rhodomentone A	1982377-64-9	*Rhodomyrtus tomentosa*	Leaf	Liu et al. (2016c)
148	Rhodomentone B	1982377-66-1	*Rhodomyrtus tomentosa*	Leaf	Liu et al. (2016c)
149	Frutescone H	2126805-16-9	*Baeckea frutescens*	Aerial part	Hou et al. (2017)
150	Frutescone I	2126805-15-8	*Baeckea frutescens*	Aerial part	Hou et al. (2017)
151	Frutescone J	2126805-17-0	*Baeckea frutescens*	Aerial part	Hou et al. (2017)
152	Frutescone K	2126805-18-1	*Baeckea frutescens*	Aerial part	Hou et al. (2017)
153	Frutescone L	2126805-19-2	*Baeckea frutescens*	Aerial part	Hou et al. (2017)
154	Frutescone M	2126805-20-5	*Baeckea frutescens*	Aerial part	Hou et al. (2017)
155	Myrtucommulone J	1357149-72-4	*Myrtus communis*	Leaf	Cottiglia et al. (2012)
156	Callistrilone A	1844870-81-0	*Callistemon rigidus*	Leaf	Cao et al. (2016)
157	Callistrilone B	1844870-83-2	*Callistemon rigidus*	Leaf	Cao et al. (2016)
158	Rhodomyrtial A	1983191-56-5	*Rhodomyrtus tomentosa*	Leaf	Zhang et al. (2016)
159	Rhodomyrtial B	1983191-57-6	*Rhodomyrtus tomentosa*	Leaf	Zhang et al. (2016)
160	Callistrilone F	2244987-87-7	*Callistemon rigidus*	Twig & Leaf	Cao et al. (2018b)
161	Callistrilone G	2244987-88-8	*Callistemon rigidus*	Twig & Leaf	Cao et al. (2018b)
162	Callistrilone H	2244987-89-9	*Callistemon rigidus*	Twig & Leaf	Cao et al. (2018b)
163	Callistrilone I	2244987-90-2	*Callistemon rigidus*	Twig & Leaf	Cao et al. (2018b)
164	Callistrilone J	2244987-91-3	*Callistemon rigidus*	Twig & Leaf	Cao et al. (2018b)
165	Callistrilone K	2241225-39-6	*Callistemon rigidus*	Twig & Leaf	Cao et al. (2018b)
166	Baefrutone A	2291323-62-9	*Baeckea frutescens*	Aerial part	Hou et al. (2018)
167	Baefrutone B	2291323-63-0	*Baeckea frutescens*	Aerial part	Hou et al. (2018)
168	Baefrutone C	2291323-64-1	*Baeckea frutescens*	Aerial part	Hou et al. (2018)
169	Baefrutone D	2291323-65-2	*Baeckea frutescens*	Aerial part	Hou et al. (2018)
170	Baefrutone E	2291323-66-3	*Baeckea frutescens*	Aerial part	Hou et al. (2018)
171	Baefrutone F	2291323-67-4	*Baeckea frutescens*	Aerial part	Hou et al. (2018)
172	(±)-Tomentodione S	2241542-77-6	*Rhodomyrtus tomentosa*	Leaf	Zhang et al. (2018)
173	(±)-Tomentodione T	2241542-78-7	*Rhodomyrtus tomentosa*	Leaf	Zhang et al. (2018)
174	(±)-Cleistoperlone A	2368178-80-5	*Syzygium nervosum*	Leaf	Su et al. (2018)
175	(±)-Cleistoperlone B	2368178-82-7	*Syzygium nervosum*	Leaf	Su et al. (2018)
176	Myrciarone A	2253106-93-1	*Myrciaria dubia*	Fruit	Kaneshima et al. (2017)
177	Myrciarone B	2253106-94-2	*Myrciaria dubia*	Seed	Kaneshima et al. (2017)
178	(±)-Rhodomyrtosone F	1928778-28-2	*Syncarpia glomulifera*	Stem bark	Su et al. (2016)
179	Callistenone F	2131269-55-9	*Callistemon viminalis*	Leaf	Liu et al. (2016d)

180	Callistenone G	2131269-56-0	*Callistemon viminalis*	Leaf	Liu et al. (2016d)
181	Callistenone H	2097088-91-8	*Callistemon viminalis*	Leaf	Liu et al. (2016d)
182	Callistenone I	2131269-58-2	*Callistemon viminalis*	Leaf	Liu et al. (2016d)
183	Torellianone A	2583136-09-6	*Corymbia torelliana*	Flower	Senadeera et al. (2018a)
184	Torellianone B	2583136-10-9	*Corymbia torelliana*	Flower	Senadeera et al. (2018a)
185	Torellianone C	2583136-11-0	*Corymbia torelliana*	Flower	Senadeera et al. (2018a)
186	Torellianone D	2583136-12-1	*Corymbia torelliana*	Flower	Senadeera et al. (2018a)
187	Torellianone E	2583136-13-2	*Corymbia torelliana*	Flower	Senadeera et al. (2018a)
188	Torellianone F	2583136-14-3	*Corymbia torelliana*	Flower	Senadeera et al. (2018a)
189	Loxophlebal A	1309273-23-1	*Eucalyptus loxophleba*	Leaf	Sidana et al. (2010)
190	Gallomyrtucommulone E	2070913-10-7	*Callistemon citrinus*	Leaf & Stem	Khanh et al. (2016)
191	Gallomyrtucommulone F	2068807-13-4	*Callistemon citrinus*	Leaf & Stem	Khanh et al. (2016)
192	(±)-Myrtuspirone A	2342579-14-8	*Myrtus communis*	Leaf	Cheng et al. (2019)
193	Tomentosone C	1801847-62-0	*Rhodomyrtus tomentosa*	Leaf	Liu et al. (2016e)
194	Guajavadimer A	1844866-90-5	*Psidium guajava*	Leaf	Li et al. (2016)

* The structure of Myrtucommulone K (**125**) has been revised in another article (Liu et al., 2016a)

N/A: Not Available.

2.3. Biological Activities

Myrtaceae family plants are known for their essential oils; the volatile small molecule in the oil presents many biological activities. For example, antimicrobial effects against *Staphylococcus aureus*, *S. mutans* and *Candida Albicans* (Silva et al., 2019; Dias et al., 2019; Marchese et al., 2017; Silva et al., 2013; Low et al., 1974), cytotoxicity on the human colon (HCT-116), gastric (AGP-01) and lung (Hep-G2) cancer cell lines (Figueiredo et al., 2019; da Silva et al., 2017; Schnitzler et al., 2008; Chaieb et al., 2007) and antiprotozoal activity on Schistosoma and leishmania (Dias et al., 2013; Rodrigues et al., 2013). They also play an important role in inhibiting inflammatory diseases by inhibiting eosinophil, neutrophil and mononuclear cell migration (Siani et al., 2013) and inhibiting acetylcholinesterase as competitive inhibitors (Lima et al., 2012; Souza et al., 2010).

These studies show that these small molecules are promising lead compounds and that hybrid compounds or the “twin drugs” bio-synthesized from them have a high chance of performing well on the abovementioned pharmacological actions. Twin drugs possess initial pharmacological activities and this could be an advantage when the two targeted enzymes or receptors are involved in the same disease (Contreras and Sippl, 2008). For example, inflammation is a basic biological response related to many diseases such as cancer and bacteria/parasite infection (Wu et al., 2020; Candido and Hagemann, 2013; Dalgleish, 2005). The compound, when hybridized by an antimicrobial moiety and an anti-inflammatory moiety, could be a potent twin drug for bacteria-induced inflammation. Various bioactivities of newly discovered myrtaceous hybrid compounds are discussed below.

2.3.1. Antimicrobial activity

In Australia and South America, where *Myrtaceae* are most widely distributed, *Myrtaceae* plant tissues, juices and extracts have a long history of medicinal uses by indigenous people, especially for antimicrobial purposes such as wound healing and relieving diarrhea (de Souza et al., 2018; Sharifi-Rad et al., 2017; Brooker et al., 1989). Modern studies have also revealed the antimicrobial effects of myrtaceous extracts and researchers have isolated compounds such as flavonoids, phloroglucinols, terpenes and meroterpenoids (de Veras et al., 2019; Cascaes et al., 2019; Marchese et al., 2017; Cardoso et al., 2010; Lis-Balchin et al., 2000; Djipa et al., 2000). Among those isolated compounds, meroterpenoids are the most interesting due to their skeletal diversity. Some newly discovered meroterpenoids have been investigated for their antimicrobial activities.

2.3.1.1. Antibacterial activity

A total of 12 newly discovered hybrid compounds have been researched for their activities against gram-positive and gram-negative bacteria. All studies followed the macrodilution or microdilution method. The results are displayed as minimum inhibitory concentration (MIC) values. The MIC values are classified as having significant inhibitory potential (less than 5 μg/mL), moderate inhibitory potential (5-32 μg/mL), weak inhibitory potential (32-100 μg/mL) and inactive (above 100 μg/mL) (Liu et al., 2016d; Cao et al., 2016; Faqueti et al., 2015). The name of compounds, bacteria tested, positive control used, MIC and references are described in **Table 2.2**.

Table 2.2. Antibacterial activities of hybrid compounds.

Compounds (No.)	Type*	Strain	Positive control	MIC(μg/mL)	Reference
Myrciarone A (**176**)	G^+	*Bacillus subtilis*	Kanamycin	1.56	Kaneshima et al. (2017)
	G^+	*Bacillus cereus*		1.56	
	G^+	*Micrococcus luteus*		1.56	
	G^+	*Staphylococcus aureus*		1.56	
	G^+	*Staphylococcus epidermidis*		3.13	
	G^+	*Streptococcus mutans*		3.13	
Myrciarone B (**177**)	G^+	*Bacillus subtilis*	Kanamycin	1.56	Kaneshima et al. (2017)
	G^+	*Bacillus cereus*		1.56	
	G^+	*Staphylococcus aureus*		1.56	
	G^+	*Staphylococcus epidermidis*		3.13	
	G^+	*Streptococcus mutans*		1.56	
Tomentosone C (**193**)	G^+	*Staphylococcus aureus*	Erythromycin	3.66	Liu et al. (2016e)
Callistenones F (**179**)	G^+	*Staphylococcus aureus*	Vancomycin	>100	Liu et al. (2016d)
	G^-	*Escherichia coli*		>100	
Callistenones G (**180**)	G^+	*Staphylococcus aureus*	Vancomycin	>100	Liu et al. (2016d)
	G^-	*Escherichia coli*		>100	

Callistenones H (**181**)	G^+	*Staphylococcus aureus*	Vancomycin	>100	Liu et al. (2016d)
	G^-	*Escherichia coli*		>100	
Callistenones I (**182**)	G^+	*Staphylococcus aureus*	Vancomycin	>100	Liu et al. (2016d)
	G^-	*Escherichia coli*		>100	
Myrtucommulone J (**155**)	G^+	*Staphylococcus aureus*	Chloramphenicol	0.38	Cottiglia et al. (2012)
Callistrilone A (**156**)	G^+	*Staphylococcus aureus*	Oxacillin	16	Cao et al. (2016)
	G^+	*Enterococcus faecalis*		32	
	G^+	MRSA		16	
	G^+	*Staphylococcus aureus* [1]		16	
	G^+	*Enterococcus faecium* [2]		32	
	G^-	*Escherichia coli*		>128	
	G^-	*Acinetobacter baumanni*		>128	
	G^-	*Klebsiella pneumoniae*		>128	
	G^-	*Pseudomonas aeruginosa*		>128	
Callistrilone B (**157**)	G^+	*Staphylococcus aureus*	Oxacillin	>128	Cao et al. (2016)
	G^+	*Enterococcus faecalis*		64	
	G^+	MRSA		>128	
	G^+	*Staphylococcus aureus* [1]		>128	
	G^+	*Enterococcus faecium* [2]		>128	
	G^-	*Escherichia coli*		>128	
	G^-	*Acinetobacter baumanni*		>128	
	G^-	*Klebsiella pneumoniae*		>128	
	G^-	*Pseudomonas aeruginosa*		>128	
Eugenial C (**79**)	G^+	*Bacillus subtilis*	Vancomycin	0.78	Faqueti et al. (2015)
	G^+	*Staphylococcus aureus*		3.12	
	G^+	MRSAs[3]		0.39-1.56	
	G^-	*Escherichia coli*		>1000	
Eugenial D (**80**)	G^+	*Bacillus subtilis*	Vancomycin	0.78	Faqueti et al. (2015)
	G^+	*Staphylococcus aureus*		1.56	
	G^+	MRSAs[3]		0.39-3.12	
	G^-	*Escherichia coli*		>1000	

* Classified by gram staining.

1. Multiresistant strain *Staphylococcus aureus* Mu50, MRSA/VISA.

2. Multiresistant strain *Enterococcus faecium* ATCC29212 13-01.

3. A series of methicillin-resistant *Staphylococcus aureus*.

According to this established profile, the myrtaceous hybrid compounds seem more sensitive to gram-positive bacteria; tested compounds showed as inactive to all the abovementioned gram-negative bacteria. These results are largely consistent with numerous studies of crude extracts from *Myrtaceae*, especially in the inhibition of *Staphylococcus* species, including drug-resistant strains (Batiha et al., 2020; Silva et al., 2019; Famuyide et al., 2019; Dias et al., 2019; Larayetan et al., 2017; Carneiro et al., 2017; Borges et al., 2014; Alipour et al., 2014; de Paula et al., 2012; Zanetti et al., 2010; Alem et al., 2008). This indicates that the myrtaceous hybrid compounds target the

cell walls of gram-positive bacteria but have different mechanisms with methicillin and vancomycin. They have similar inhibition effects on drug-resistant and non-drug-resistant bacteria. This may be due to their teichoic acid inhibition effect, which means the drug resistance of bacteria is thereby reduced (Lee et al., 2016).

Among the tested compounds, **79** and **80** are PSMs, **156** and **157** are trimeric meroterpenoids, **193** is a special β-triketone-phloroglucinol-β-triketone structure and **179**-**182**, **176** and **177** are β-triketone-phloroglucinol hybrids. Analysis of their structure-activity relationship found that the hydroxyl group on the phloroglucinol moiety at a specific position might be a key factor that affects the antibacterial activity. This is the C-6 position in compounds **79** and **80** and the C-8 position in others. As the red highlights in **Fig**. **2.7** show, compounds with significant inhibitory potential must possess a hydroxyl group on the C-6 or C-8 position. Moreover, the methoxy group in the same position may hugely reduce antibacterial activity, and when combined with a monoterpene, the methoxy group converted to the cyclic ether and the antibacterial activity increased to have a moderate inhibitory potential. This phenomenon may be due to the disappearance of the methoxy group or the compensating action of monoterpenes.

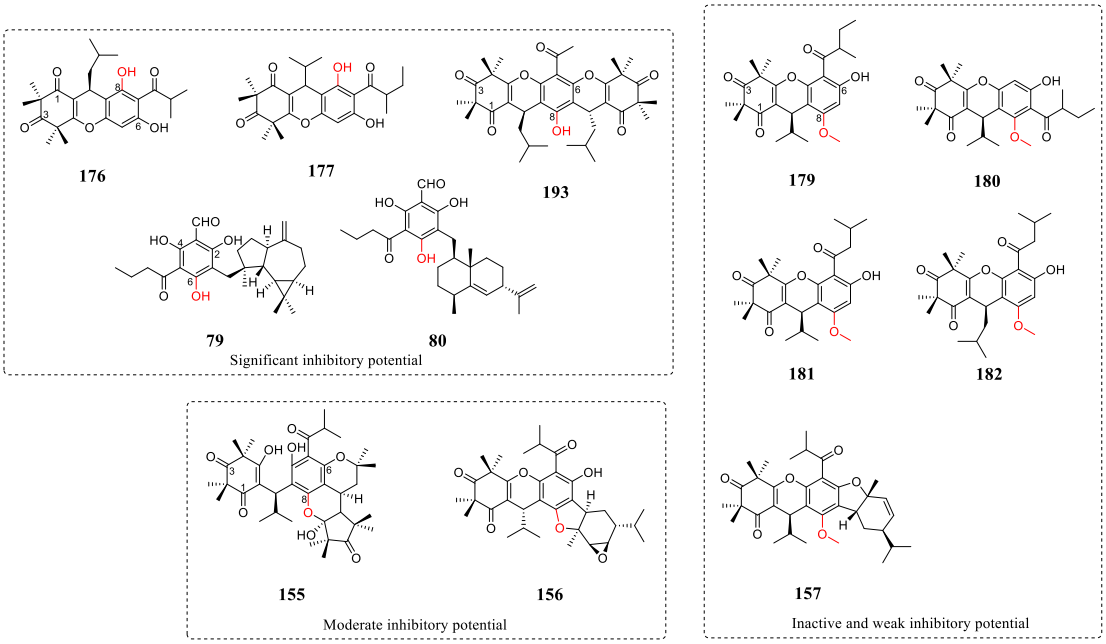

Fig. **2.7.** Possible structure-activity of the antibacterial relationship of all tested compounds.

2.3.1.2. Antifungal activity

Existing data suggest that fungi may not be susceptible to these hybrid compounds compared with bacteria. Many promising antibacterial extracts from *Myrtaceae* showed merely weak inhibitory effects on tested fungi, especially on the commonly used *Candida* species (Bouzabata et al., 2016; Berka-Zougali et al., 2012; Auricchio et al., 2007; Souza et al., 2004; Lis-Balchin et

al., 2000).

Nevertheless, there are some promising compounds. The present paper lists the antifungal activities of 17 hybrid compounds against two *Candida* species. They belong to PMMs (**1** and **2**) and PSMs (**22**-**29** and **52**-**58**). The results of microdilution experiments are shown in **Table 2.3**. *Candida glabrata* seems more susceptible to these compounds. Among tested compounds, Eucalrobusone U (**27**), Eucalrobusone J (**52**) and Eucalrobusone O (**57**) exhibited significant antifungal activities; their structures are displayed in **Fig**. **2.8**.

Table 2.3. Antifungal activities of hybrid compounds.

Compounds (No.)	*Candida albicans*[1]	*Candida glabrata*[1]	Reference
Eucalrobusone Y (**1**)	> 50	15.70 ± 3.59	
Eucalrobusone Z (**2**)	> 50	25.15 ± 4.70	
Eucalrobusone Q (**22**)	> 50	> 50	
Eucalrobusone R (**23**)	39.60 ± 9.35	> 50	
Eucalrobusone S (**24**)	> 50	> 50	
Eucalrobusone T (**25**)	46.87 ± 8.75	7.40 ± 1.05	Shang et al. (2019)
7R-eucalrobusone T (**26**)	35.80 ± 9.10	15.35 ± 2.15	
Eucalrobusone U (**27**)	30.49 ± 9.96	1.53 ± 0.47	
Eucalrobusone V (**28**)	> 50	> 50	
Eucalrobusone W (**29**)	> 50	> 50	
Fluconazole [2]	0.28 ± 0.14	0.27 ± 0.11	
Eucalrobusone J (**52**)	> 50	2.57 ± 0.06	
Eucalrobusone K (**53**)	> 50	> 50	
Eucalrobusone L (**54**)	49.29 ± 4.78	> 50	
Eucalrobusone M (**55**)	47.24 ± 5.60	15.40 ± 3.17	
Eucalrobusone N (**56**)	> 50	> 50	Shang et al. (2016b)
Eucalrobusone O (**57**)	12.54 ± 2.14	1.95 ± 0.68	
Eucalrobusone P (**58**)	> 50	30.56 ± 3.67	
Fluconazole [2]	0.25±0.12		
Amphotericin B [2]		0.26±0.07	

1. MIC_{50} values (μg/mL). MIC_{50}: the minimum concentration of compound at which the growth of the microorganism was half inhibited. Data represented as the mean value ± SD.

2. Positive control.

A recent study revealed a hybrid compound, Eucarobustol E, exerted a strong inhibitory effect against *Candida albicans* at a concentration of 16 μg/mL; its mechanism is to inhibit the carbon flow to ergosterol and eventually led to biofilm inhibition (Liu et al., 2017b). Another structurally similar hybrid compound, Macrocarpal C, exhibited strong inhibitory effects against *Trichophyton rubrum* and *Paecilomyces variotii* at 2.16 μg/mL MIC_{50} (Lau et al., 2010) and against *Candida glabrata* with MIC_{50} value of 2.49 μg/mL (Shang et al., 2016b). According to the classification method described in the foregoing paragraphs, both compounds are analogues of the above-listed compounds in **Table 2.3.** The chemical structures of Macrocarpal C and Eucarobustol E are

displayed in **Fig**. **2.8.**

Structurally speaking, the phloroglucinol moieties in all tested compounds are identical, therefore, their antifungal activities are affected by the structure of terpene moieties, including pinane (**1** and **2**), cadinane (**22** and **23**), cubebane (**24-26**), aromadendrane (**27-29**, **52**), guaiane-type (**53**), aristolane-type (**54-56**), and bicyclogermacrene-type (**57**, **58**). According to the data displayed in **Table 2.3**, aromadendrane or bicyclogermacrene might be the key terpene moieties for inhibitory activities (red color in **Fig**. **2.8**). In addition, the substituent groups on C-10 in aromadendrane and C-5 in bicyclogermacrene also play an important role. As shown in **Fig**. **2.8**, all the active aromadendrane based hybrids (**27**, **52**, Eucarobustol E and Macrocarpal C) were oxidized at the C-10 site (blue marked) compared to inactive compounds **28** and **29**, while the active bicyclogermacrene-based hybrid **57** is reduced from compound **58** at the C-5 site (blue color), this small difference in structure makes a great difference in its antifungal activity.

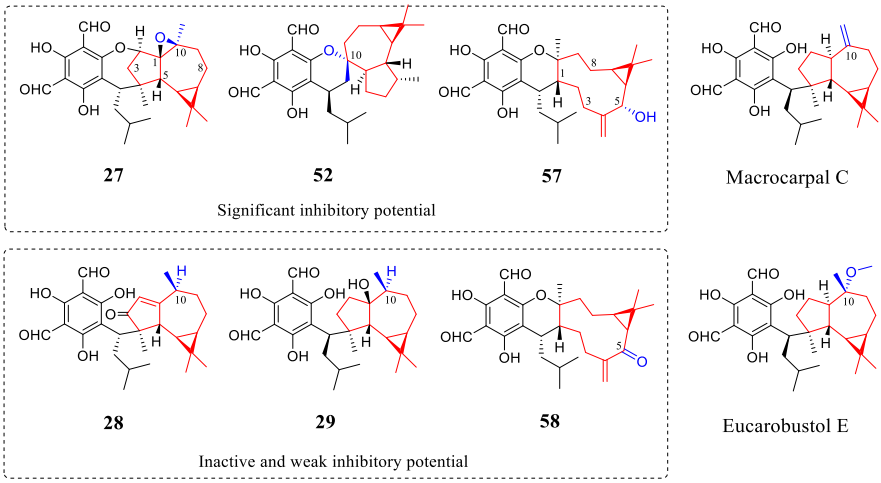

Fig. **2.8.** Possible structure-activity of the antifungal relationship of aromadendrane- and bicyclogermacrene-based hybrids.

The antifungal potential of some aromadendranes has been studied by Moreira et al. (2003) using direct bioautography. Compounds A and B showed antifungal activity against *C. cladosporioides*, the minimum amount required on the TLC plate was at 5 µg; however, compounds C and D were inactive even at 100 µg. This result supports the hypothesis that aromadendrane might be one of the key terpene moieties for the antifungal activities of these hybrid compounds, and that the oxidation of the C-10 site is necessary. However, the oxidation of the C-15 site will inactivate the compounds (**Fig**. **2.9**).

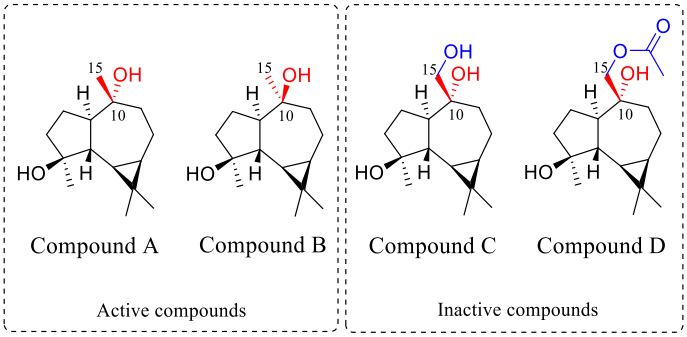

Fig. 2.9. Effects of oxidation at different sites on the antifungal activity of aromadendranes.

2.3.2. Cytotoxicity

Since the discovery of the anticancer potential of myrtaceous essential oils, the phytochemicals produced by *Myrtaceae* have attracted much attention (Joyce et al., 2017; Schnitzler et al., 2008; Sailer et al., 1998; Hayes et al., 1997). Structurally complex hybrid compounds are a major part of these phytochemicals. Except for those inactive compounds, all reported cytotoxic effects of newly discovered hybrid compounds on cancer cells are listed in **Table 2.4**. The 33 compounds listed cover all the types described above. The IC_{50} values were obtained by MTT (3-[4,5-dimethylthiazol-2-yl]-2,5 diphenyl tetrazolium bromide) assay and classified as significant cytotoxicity (less than 5 μM), moderate cytotoxicity (5-40 μM) and weak cytotoxicity (above 40 μM) (Pham et al., 2018; Liu et al., 2016a; Liu et al., 2016d).

Table 2.4. Cytotoxicity of hybrid compounds on cancer cells.

Compounds (No.)	Cancer type	Cell line	IC_{50} (μM)[1]	Reference
Tomentodione O (**121**)	Cervical cancer	HeLa	9.73 ± 0.41	Zhang et al. (2018)
Tomentodione P (**122**)	Cervical cancer	HeLa	9.82 ± 0.15	Zhang et al. (2018)
Tomentodione Q (**123**)	Cervical cancer	HeLa	14.12 ± 0.20	Zhang et al. (2018)
Tomentodione R (**124**)	Cervical cancer	HeLa	11.90 ± 0.25	Zhang et al. (2018)
(±)-Tomentodione S (**172**)	Cervical cancer	HeLa	1.45 ± 0.04	Zhang et al. (2018)
(±)-Tomentodione T (**173**)	Cervical cancer	HeLa	8.43 ± 0.08	Zhang et al. (2018)
Eucalypglobulusal F (**35**)	Leukemia	CCRF-CEM	3.3 ± 0.7	Qin et al. (2018)
	Colon cancer	HCT116	>10	
	Prostate cancer	DU145	>10	
	Liver cancer	Huh7	>10	
	Lung cancer	A549	>10	
Eucalyptin B (**38**)	Lung cancer	A549	1.51 ± 0.72	Pham et al. (2018)
	Breast cancer	4T1	15.20 ± 2.98	
	Skin cancer	B16F10	5.23 ± 1.08	
Eucalrobusone C (**61**)	Liver cancer	HepG2	7.40	Shang et al. (2016a)
	Breast cancer	MCF7	8.99	
	Osteosarcoma	U2OS	8.50	

Guajavadial A (**21**)	Leukemia	HL60	4.73	Qin et al. (2016)
	Lung cancer	A549	5.62	
	Liver cancer	SMMC7721	4.73	
	Breast cancer	MCF7	22.28	
	Colon cancer	SW480	14.55	
Guajavadial B (**67**)	Leukemia	HL60	6.49	Qin et al. (2016)
	Lung cancer	A549	5.78	
	Liver cancer	SMMC7721	5.05	
	Breast cancer	MCF7	18.02	
	Colon cancer	SW480	13.07	
Guajavadial C (**68**)	Leukemia	HL60	3.38	Qin et al. (2016)
	Lung cancer	A549	5.66	
	Liver cancer	SMMC7721	3.54	
	Breast cancer	MCF7	14.54	
	Colon cancer	SW480	18.97	
Callistenone I (**182**)	Breast cancer	MCF7	40-100	Liu et al. (2016d)
	Lung cancer	NCI-H460	40-100	
	Brain cancer	SF268	40-100	
	Liver cancer	HepG2	40-100	
Psiguajavadial A (**81**)	Colon cancer	HCT116	7.60 ± 1.0	Qin et al. (2017b)
	Leukemia	CCRF-CEM	25.2 ± 4.0	
	Prostate cancer	DU145	20.2 ± 4.7	
	Liver cancer	Huh7	48.8 ± 5.3	
	Lung cancer	A549	2.99 ± 0.1	
Psiguajavadial B (**82**)	Colon cancer	HCT116	21.6 ± 2.8	Qin et al. (2017b)
	Leukemia	CCRF-CEM	9.63 ± 3.4	
	Prostate cancer	DU145	26.3 ± 4.1	
	Liver cancer	Huh7	13.7 ± 1.7	
	Lung cancer	A549	0.90 ± 0.8	
Callisalignene G (**117**)	Colon cancer	HCT116	8.51 ± 1.8	Qin et al. (2017a)
	Liver cancer	Huh7	44.41 ± 3.2	
	Cervical cancer	Hela	36.46 ± 8.4	
	Leukemia	CCRF-CEM	4.52 ± 1.3	
	Prostate cancer	DU145	39.92 ± 6.8	
	Lung cancer	A549	12.85 ± 8.2	
Callisalignene H (**118**)	Colon cancer	HCT116	9.12 ± 0.3	Qin et al. (2017a)
	Liver cancer	Huh7	42.11 ± 3.6	
	Cervical cancer	Hela	46.99 ± 8.7	
	Leukemia	CCRF-CEM	6.20 ± 0.8	
	Prostate cancer	DU145	18.44 ± 9.5	
	Lung cancer	A549	26.61 ± 6.4	
Callisalignene I (**119**)	Colon cancer	HCT116	16.33 ± 3.3	Qin et al. (2017a)
	Liver cancer	Huh7	56.13 ± 7.3	
	Cervical cancer	Hela	62.27 ± 5.1	

	Leukemia	CCRF-CEM	30.66 ± 4.6	
	Prostate cancer	DU145	36.24 ± 7.0	
	Lung cancer	A549	10.03 ± 8.2	
Frutescone A (**140**)	Colon cancer	Caco2	8.08 ± 2.79	Hou et al. (2016)
	Lung cancer	A549	20.07 ± 5.77	
	Liver cancer	HepG2	> 50	
Frutescone B (**141**)	Colon cancer	Caco2	23.25 ± 3.91	Hou et al. (2016)
	Lung cancer	A549	41.33 ± 4.42	
	Liver cancer	HepG2	> 50	
Frutescone C (**142**)	Colon cancer	Caco2	14.83 ± 5.97	Hou et al. (2016)
	Lung cancer	A549	27.74 ± 4.76	
	Liver cancer	HepG2	> 50	
Frutescone D (**143**)	Colon cancer	Caco2	10.20 ± 3.44	Hou et al. (2016)
	Lung cancer	A549	26.25 ± 6.10	
	Liver cancer	HepG2	> 50	
Frutescone E (**144**)	Colon cancer	Caco2	7.96 ± 2.56	Hou et al. (2016)
	Lung cancer	A549	12.14 ± 5.55	
	Liver cancer	HepG2	> 50	
Frutescone F (**145**)	Colon cancer	Caco2	16.51 ± 2.52	Hou et al. (2016)
	Lung cancer	A549	39.02 ± 6.02	
	Liver cancer	HepG2	> 50	
(±)-Frutescone G (**146**)	Colon cancer	Caco2	14.31 ± 4.07	Hou et al. (2016)
	Lung cancer	A549	25.71 ± 5.89	
	Liver cancer	HepG2	> 50	
Guadial C (**20**)	Liver cancer	HepG2/ADM	36.70 ± 2.37	Jian et al. (2015)
Psiguadial A (**75**)	Liver cancer	HepG2	61.07 ± 1.77 nM	Shao et al. (2010)
	Liver cancer	HepG2/ADM	17.94 ± 0.21	
Psiguadial B (**76**)	Liver cancer	HepG2	61.07 ± 1.77 nM	Shao et al. (2010)
	Liver cancer	HepG2/ADM	25.09 ± 0.21	
Psiguadial C (**77**)	Liver cancer	HepG2	104.5 ± 13.71 nM	Shao et al. (2012)
	Liver cancer	HepG2/ADM	21.06 ± 1.25	
Psiguadial D (**78**)	Liver cancer	HepG2	128.3 ± 18.2 nM	Shao et al. (2012)
	Liver cancer	HepG2/ADM	23.65 ± 1.71	
Myrtucommulone J (**155**)	Leukemia	MT4	2.1	Cottiglia et al. (2012)
	Liver cancer	HepG2	4.0	
	Prostate cancer	DU145	3.0	
Eucalyptal D (**70**)	Gastric cancer	KE97	5.20 ± 1.16	Wang et al. (2012)
	Leukemia	Jurkat	7.16 ± 2.84	
	Gastric cancer	BGC823	6.65 ± 1.36	
	Liver cancer	Huh7	11.73 ± 1.81	
Eucalyptal E (**71**)	Gastric cancer	KE97	7.22 ± 2.06	Wang et al. (2012)
	Leukemia	Jurkat	10.71 ± 4.21	
	Gastric cancer	BGC823	10.16 ± 0.89	
	Liver cancer	Huh7	24.57 ± 4.45	

1. Data represented as the mean value ± SD or effective concentration.

The highly active compounds (IC_{50} < 5 μM), except compound **21**, belongs to PMMs. **117** belongs to TMMs. **172** is a β-triketone-phloroglucinol hybrid and **155** is a trimeric meroterpenoid; all other compounds are PSMs (**35**, **38**, **68**, **75-78**, **81** and **82**). In addition, the other PSMs in **Table 2.4** are also active (**61**, **67**, **70** and **71** with IC_{50} 5~10 μM). They mainly exhibit toxicity to lung cancer, liver cancer and leukemic cells. From the available data, the PSMs are toxic to multiple cancer cells and the structures of these classes of compounds are very variable. It is hard to deduce further structure-activity relationships.

2.3.3. Anti-inflammatory activity

Many species of *Myrtaceae* are used in folk medicine for the treatment of various inflammatory ailments such as rheumatism, snakebites, arthritis, dermitis, influenza and common cold (Siebert et al., 2017; Donatini et al., 2013; Paula et al., 2012; Chan and Chen, 2010; Silva et al., 2003). Phytochemicals have been shown to play an important role in the anti-inflammatory activity of *Myrtaceae* and they are listed in **Table 2.5**. Their IC_{50} values were obtained by the Griess assay, which measures the nitric oxide (NO) production of tested cells.

Table 2.5. Inhibitory effects of hybrid compounds on LPS[1]-induced NO production.

Compounds (No.)	IC_{50} (μM)[2]	Reference
(+)-Baeckfrutone N (**86**)	20.86 ± 0.60	
Baeckfrutone S (**120**)	36.21 ± 1.18	Zhi et al. (2018)
L-NMMA[3]	54.07 ± 1.05	
Tomentodione O (**121**)	NE[4]	
Tomentodione P (**122**)	26.40 ± 1.15	
Tomentodione Q (**123**)	20.05 ± 0.99	
Tomentodione R (**124**)	NE	Zhang et al. (2018)
(±)-Tomentodione S (**172**)	NE	
(±)-Tomentodione T (**173**)	34.37 ± 1.52	
Indometacin[3]	126.25 ± 1.26	
Baefrutone A (**166**)	9.15 ± 0.82	
Baefrutone B (**167**)	17.73 ± 2.54	
Baefrutone C (**168**)	11.62 ± 2.93	
Baefrutone D (**169**)	18.04 ± 3.14	Hou et al. (2018)
Baefrutone E (**170**)	>50	
Baefrutone F (**171**)	>50	
L-NMMA	30.92 ± 4.12	
Frutescone H (**149**)	>50	
Frutescone I (**150**)	18.75 ± 3.84	
Frutescone J (**151**)	>50	
Frutescone K (**152**)	>50	

Frutescone L (**153**)	30.54 ± 2.30	
Frutescone M (**154**)	15.17 ± 1.45	Hou et al. (2017)
(±)-Frutescone N (**112**)	1.80 ± 0.29	
Frutescone O (**113**)	0.36 ± 0.16	
Frutescone P (**114**)	3.70 ± 1.25	
(±)-Frutescone Q (**115**)	2.07 ± 0.84	
(±)-Frutescone R (**116**)	6.50 ± 0.96	
L-NMMA	30.92 ± 4.12	
Callisretone A (**7**)	15.3 ± 1.0	
Callisretone B (**8**)	17.7 ± 1.1	Cao et al. (2018a)
Indomethacin	21.1 ± 1.4	

1. Lipopolysaccharide.
2. Data represented as the mean value ± SD or effective concentration.
3. Positive control. L-NMMA: N-Monomethyl-L-arginine.
4. NE means no antiinflammatory effect under maximal nontoxic concentration.

In terms of classification, the active compounds are TMMs (**86**, **112-116**), TSMs (**120**, **122**, **123**, **150**, **153** and **154**), trimeric meroterpenoids (**166-169**), followed by two PMMs (**7** and **8**) and compound **173**, a β-triketone-phloroglucinol hybrid. Structurally speaking, except for compounds **7** and **8**, all other 16 compounds contain a β-triketone unit, which might be a key factor to their anti-inflammatory properties.

Compound **113** exhibited the most potent anti-inflammatory effects with a 0.36 ± 0.16 μM IC_{50} value. A mechanistic study demonstrated that its anti-inflammatory activity was derived from the suppression of the NF-κB p65 nuclear translocation and the decrease of pro-inflammatory cytokines TNF-α (Hou et al., 2017).

2.3.4. Enzyme inhibitory activity

DNA topoisomerase I (Top1) is an essential human enzyme responsible for DNA replication, transcription, and recombination; it is, therefore, a potential target for anticancer drug discovery (Lafayette et al., 2013). Eucalypglobulusal A (**30**, **Fig**. **2.10**), a potential Top1 inhibitor isolated recently, has exhibited high Top1 inhibitory effects, and it did not show significant cytotoxicity (IC_{50} > 10 μM). It acts as a Top1 catalytic inhibitor. Eucalypglobulusal A inhibits the cleavage of DNA and delays the Top1 poison-caused DNA double-strand damage (Qin et al., 2018).

Dipeptidyl peptidase 4 (DPP-4) is the enzyme responsible for the degradation of glucagon-like peptide-1 (GLP-1). The inhibition of DPP-4 allows GLP-1 to restore insulin secretion in type-2 diabetes mellitus patients. The natural DPP-4 inhibitors are usually small molecules and therefore can be developed as oral antidiabetic drugs (Nauck, 2016; Vilsbll et al., 2003). An activity-guided fractionation accomplished by Kato et al. (2018) led to the isolation of Macrocarpal C (**41**, **Fig**.

2.10), a potent DPP-4 inhibitor with 90% inhibition at 50 μM. Its inhibition curve is characterized by a dramatic rise within a narrow concentration range; this might result from the self-aggregation of the compound.

Acetylcholinesterase (AChE) acts in the final step of the nervous impulse transmission by hydrolyzing the neurotransmitter acetylcholine (ACh). Acetylcholinesterase inhibitor (AChEI) inhibits AChE from breaking down ACh, is used for the symptomatic management of neurodegenerative disorder-related diseases such as Alzheimer's (Muhammad et al., 2017; Webster, 2012). Qin et al. (2019) discovered two meroterpenoids: Rhodomyrtusial A and B (**131** and **132**, **Fig. 2.10**), featuring a unique skeleton and displaying significant AChE inhibitory activities with IC_{50} values of 8.8 and 6.0 μM, respectively.

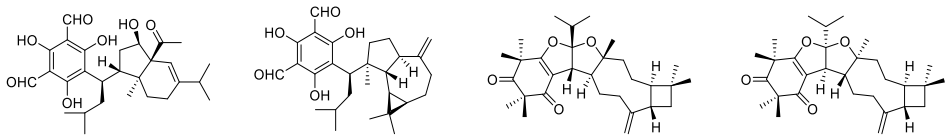

Fig. **2.10**. Chemical structures of compounds **30**, **41**, **131** and **132**.

2.4. Conclusion and Future Perspectives

Myrtaceae is a diverse family; its plants have been used in folk medicine around the world for centuries. Of the *Myrtaceae* species known, only a limited number have been investigated for their chemical composition and biological activity. Characterization of their potential medicinal usage is needed. Interestingly, most of the pharmacological studies have been carried out using crude extracts or essential oils; studies on specific phytochemicals are lacking.

Interest in myrtaceous hybrid compounds is just in their infancy. In the past decade, a total of 194 hybrid compounds have been isolated and identified. But nearly all the compounds have been isolated from the fruits or leaves of the plant. Further phytochemical studies should focus more on other parts of the plant, such as the roots, flowers, or stems.

Several isolated compounds featuring unique skeletons and significant pharmacological effects have been shown to possess great potential as lead compounds for new antimicrobial, anticancer, anti-inflammatory and enzyme inhibitory agent discovery. Hopefully, the collection of their structures and the discussion of their bioactivities in this paper can provide clues for further researchers.

2.5. References

Agatonovic-Kustrin, S. 2018. The Current and Potential Therapeutic Uses of Parthenolide. *Studies in Natural Products Chemistry*, 61-91.

Alem, G., Mekonnen, Y., Tiruneh, M. & Mulu, A. 2008. Invitro antibacterial activity of crude preparation of myrtle (Myrtus communis) on common human pathogens. *Ethiop Med J*, 46, 63-9.

Alipour, G., Dashti, S. & Hosseinzadeh, H. 2014. Review of pharmacological effects of Myrtus communis L. and its active constituents. *Phytother Res*, 28, 1125-36.

Auricchio, M. T., Bugno, A., Barros, S. B. M. & Bacchi, E. M. 2007. Antimicrobial and antioxidant activities and toxicity of Eugenia uniflora. *Latin American Journal of Pharmacy*, 26, 76-81.

Batiha, G. E., Alkazmi, L. M., Wasef, L. G., Beshbishy, A. M., Nadwa, E. H. & Rashwan, E. K. 2020. Syzygium aromaticum L. (Myrtaceae): Traditional Uses, Bioactive Chemical Constituents, Pharmacological and Toxicological Activities. *Biomolecules*, 10.

Berka-Zougali, B., Ferhat, M. A., Hassani, A., Chemat, F. & Allaf, K. S. 2012. Comparative Study of Essential Oils Extracted from Algerian Myrtus communis L. Leaves Using Microwaves and Hydrodistillation. *International Journal of Molecular Sciences*, 13.

Bloor, S. J. 1992. Antiviral phloroglucinols from New Zealand Kunzea species. *J Nat Prod*, 55, 43-7.

Borges, L. L., Conceicao, E. C. & Silveira, D. 2014. Active compounds and medicinal properties of Myrciaria genus. *Food Chem*, 153, 224-33.

Bouzabata, A., Casanova, J., Bighelli, A., Cavaleiro, C., Salgueiro, L. & Tomi, F. 2016. The Genus Myrtus L. in Algeria: Composition and Biological Aspects of Essential Oils from M. communis and M. nivellei: A Review. *Chem Biodivers*, 13, 672-80.

Brooker, S. G., Cambie, R. C. & Cooper, R. C. 1989. Economic native plants of New Zealand. *Economic Botany*, 43, 79-106.

Buckle, J. 2015. Basic Plant Taxonomy, Basic Essential Oil Chemistry, Extraction, Biosynthesis, and Analysis. *In:* Buckle, J. (ed.) *Clinical Aromatherapy (Third Edition).* St. Louis: Churchill Livingstone.

Candido, J. & Hagemann, T. 2013. Cancer-Related Inflammation. *Journal of Clinical Immunology*, 33, 79-84.

Cao, J. Q., Huang, X. J., Li, Y. T., Wang, Y., Wang, L., Jiang, R. W. & Ye, W. C. 2016. Callistrilones A and B, Triketone-Phloroglucinol-Monoterpene Hybrids with a New Skeleton from Callistemon rigidus. *Org Lett*, 18, 120-3.

Cao, J. Q., Tian, H. Y., Li, M. M., Zhang, W., Wang, Y., Wang, L. & Ye, W. C. 2018a. Rearranged Phloroglucinol-Monoterpenoid Adducts from Callistemon rigidus. *J Nat Prod*, 81, 57-62.

Cao, J. Q., Wu, Y., Zhong, Y. L., Li, N. P., Chen, M., Li, M. M., Ye, W. C. & Wang, L. 2018b. Antiviral Triketone-Phloroglucinol-Monoterpene Adducts from Callistemon rigidus. *Chem Biodivers*, 15, e1800172.

Cardoso, C. A., Salmazzo, G. R., Honda, N. K., Prates, C. B., Vieira Mdo, C. & Coelho, R. G. 2010. Antimicrobial activity of the extracts and fractions of hexanic fruits of Campomanesia species (Myrtaceae). *J Med Food*, 13, 1273-6.

Carneiro, N. S., Alves, C. C. F., Alves, J. M., Egea, M. B., Martins, C. H. G., Silva, T. S., Bretanha, L. C., Balleste, M. P., Micke, G. A., Silveira, E. V. & Miranda, M. L. D. 2017. Chemical composition, antioxidant and antibacterial activities of essential oils from leaves and flowers of Eugenia klotzschiana Berg (Myrtaceae). *An Acad Bras Cienc*, 89, 1907-1915.

Cascaes, M. M., Guilhon, G., Zoghbi, M. D. G., Andrade, E. H. A., Santos, L. S., Kelly, R. d. S. J., Trovatti Uetanabaro, A. P. & Araujo, I. S. 2019. Flavonoids, antioxidant potential and antimicrobial activity of Myrcia rufipila mcvaugh leaves (myrtaceae). *Nat Prod Res*, 1-5.

Cascaes, M. M., Guilhon, G. M., Andrade, E. H., Zoghbi, M. & Santos Lda, S. 2015. Constituents and Pharmacological Activities of Myrcia (Myrtaceae): A Review of an Aromatic and Medicinal Group of Plants. *Int J Mol Sci*, 16, 23881-904.

Chaieb, K., Hajlaoui, H., Zmantar, T., Kahla-Nakbi, A. B., Rouabhia, M., Mahdouani, K. & Bakhrouf, A. 2007. The chemical composition and biological activity of clove essential oil, Eugenia caryophyllata (Syzigium aromaticum L. Myrtaceae): a short review. *Phytother Res*, 21, 501-6.

Chan, W. K. & Chen, K. 2010. Chinese medicinal herbs of Hong Kong. Edited by Cheung Siu-Cheong and Li Ning-Hon. Vols 1–5 Commercial Press, Hong Kong, 1978–1986. No Price Given. *Phytotherapy Research*, 2.

Cheng, M. J., Yang, X. Y., Cao, J. Q., Liu, C., Zhong, L. P., Wang, Y., You, X. F., Li, C. C., Wang, L. & Ye, W. C. 2019. Isolation, Structure Elucidation, and Total Synthesis of Myrtuspirone A from Myrtus communis. *Org Lett*, 21, 1583-1587.

Chizzola, R. 2013. *Natural Products*, Springer New York.

Contreras, J. M. & Sippl, W. 2008. *Homo and Heterodimer Ligands: The Twin Drug Approach*, Elsevier Ltd.

Cottiglia, F., Casu, L., Leonti, M., Caboni, P., Floris, C., Busonera, B., Farci, P., Ouhtit, A. & Sanna, G. 2012. Cytotoxic phloroglucinols from the leaves of Myrtus communis. *J Nat Prod*, 75, 225-9.

da Silva, J. K. R., Andrade, E. H. A., Barreto, L. H., da Silva, N. C. F., Ribeiro, A. F., Montenegro, R. C. & Maia, J. G. S. 2017. Chemical Composition of Four Essential Oils of Eugenia from the Brazilian Amazon and Their Cytotoxic and Antioxidant Activity. *Medicines (Basel)*, 4.

Dalgleish, A. G. 2005. Cancer and Inflammation. *British Journal of Cancer*, 92, 792-793.

de Paula, J. A., Silva Mdo, R., Costa, M. P., Diniz, D. G., Sa, F. A., Alves, S. F., Costa, E. A., Lino, R. C. & de Paula, J. R. 2012. Phytochemical Analysis and Antimicrobial, Antinociceptive, and Anti-Inflammatory Activities of Two Chemotypes of Pimenta pseudocaryophyllus (Myrtaceae). *Evid Based Complement Alternat Med*, 2012, 420715.

de Souza, A. M., de Oliveira, C. F., de Oliveira, V. B., Betim, F. C. M., Miguel, O. G. & Miguel, M. D. 2018. Traditional Uses, Phytochemistry, and Antimicrobial Activities of Eugenia Species - A Review. *Planta Med*, 84, 1232-1248.

de Veras, B. O., Dos Santos, Y. Q., Oliveira, F., Almeida, J., da Silva, A. G., Correia, M., Diniz, K. M., de Oliveira, J. R. S., Lima, V. L. M., Navarro, D., de Aguiar, J., de Oliveira, M. B. M., Lopes, A. C. S. & da Silva, M. V. 2019. Algrizea Minor Sobral, Faria & Proenca (Myrteae, Myrtaceae): chemical composition, antinociceptive, antimicrobial and antioxidant activity of essential oil. *Nat Prod Res*, 1-5.

Deng, X., Wang, X. R. & Wu, L. 2020. Triketone-terpene meroterpenoids from the leaves of Rhodomyrtus tomentosa. *Fitoterapia*, 104585.

Dias, A. L. B., Batista, H. R. F., Estevam, E. B. B., Alves, C. C. F., Forim, M. R., Nicolella, H. D., Furtado, R. A., Tavares, D. C., Silva, T. S., Martins, C. H. G. & Miranda, M. L. D. 2019. Chemical composition and in vitro antibacterial and antiproliferative activities of the essential oil from the leaves of Psidium myrtoides O. Berg (Myrtaceae). *Nat Prod Res*, 33, 2566-2570.

Dias, C. N., Rodrigues, K. A., Carvalho, F. A., Carneiro, S. M., Maia, J. G., Andrade, E. H. & Moraes, D. F. 2013. Molluscicidal and leishmanicidal activity of the leaf essential oil of Syzygium cumini (L.) SKEELS from Brazil. *Chem Biodivers*, 10, 1133-41.

Djebir, S., Ksouri, S., Trigui, M., Tounsi, S., Boumaaza, A., Hadef, Y. & Benakhla, A. 2019. Chemical Composition and Acaricidal Activity of the Essential Oils of Some Plant Species of Lamiaceae and Myrtaceae against the Vector of Tropical Bovine Theileriosis: Hyalomma scupense (syn. Hyalomma detritum). *Biomed Res Int*, 2019, 7805467.

Djipa, C. D., Delmee, M. & Quetin-Leclercq, J. 2000. Antimicrobial activity of bark extracts of Syzygium jambos

(L.) alston (Myrtaceae). *J Ethnopharmacol*, 71, 307-13.

Donatini, R. S., Kato, E. T. M., Ohara, M. T. & Bacchi, E. M. 2013. Morphoanatomy and antimicrobial study of Syzygium jambos (L.) Alston (Myrtaceae) leaves. *Latin American Journal of Pharmacy*, 32, 518-523.

Famuyide, I. M., Aro, A. O., Fasina, F. O., Eloff, J. N. & McGaw, L. J. 2019. Antibacterial and antibiofilm activity of acetone leaf extracts of nine under-investigated south African Eugenia and Syzygium (Myrtaceae) species and their selectivity indices. *BMC Complement Altern Med*, 19, 141.

Faqueti, L. G., Farias, I. V., Sabedot, E. C., Delle Monache, F., San Feliciano, A., Schuquel, I. T., Cechinel-Filho, V., Cruz, A. B. & Meyre-Silva, C. 2015. Macrocarpal-like Compounds from Eugenia umbelliflora Fruits and Their Antibacterial Activity. *J Agric Food Chem*, 63, 8151-5.

Fernandes, T., Lima, D. F. & Braga, J. M. A. 2020. Two new species of Myrcia sect. Reticulosae (Myrtaceae) from the campo rupestre of Minas Gerais, Brazil. *Brittonia*.

Figueiredo, P. L. B., Pinto, L. C., da Costa, J. S., da Silva, A. R. C., Mourão, R. H. V., Montenegro, R. C., da Silva, J. K. R. & Maia, J. G. S. 2019. Composition, antioxidant capacity and cytotoxic activity of Eugenia uniflora L. chemotype-oils from the Amazon. *J Ethnopharmacol*, 232, 30-38.

Fu, H. Z., Luo, Y. M., Li, C. J., Yang, J. Z. & Zhang, D. M. 2010. Psidials A-C, three unusual meroterpenoids from the leaves of Psidium guajava L. *Org Lett*, 12, 656-9.

Geissman, T. 1963. Natural Products Chemistry. (Book Reviews: The Chemistry of Flavonoid Compounds). *Science*, 139.

Geris, R. & Simpson, T. J. 2009. Meroterpenoids produced by fungi. *Natural Product Reports*, 26, 1063-1094.

Ghisalberti, E. L. 1996. Bioactive acylphloroglucinol derivatives from Eucalyptus species. *Phytochemistry*, 41, 7-22.

Govaerts, R., Sobral, M., Ashton, P., Barrie, F., Holst, B., Landrum, L., Matsumoto, K., Mazine, F., Nic Lughadha, E., Proença, C., Soares-Silva, L., Wilson, P. & Lucas, E. 2008. *World Checklist of Myrtaceae*.

Har, L. W., Shaari, K., Boon, L. H., Kamarulzaman, F. A. & Ismail, I. S. 2012. Two new phloroglucinol derivatives and five photosensitizing pheophorbides from Syzygium polyanthum leaves (Salam). *Nat Prod Commun*, 7, 1033-6.

Hayes, A. J., Leach, D. N., Markham, J. L. & Markovic, B. 1997. In vitro Cytotoxicity of Australian Tea Tree Oil using Human Cell Lines. *Journal of Essential Oil Research*, 9, 575-582.

Hou, J. Q., Guo, C., Zhao, J. J., Dong, Y. Y., Hu, X. L., He, Q. W., Zhang, B. B., Yan, M. & Wang, H. 2017. Anti-inflammatory Meroterpenoids from Baeckea frutescens. *J Nat Prod*, 80, 2204-2214.

Hou, J. Q., Guo, C., Zhao, J. J., He, Q. W., Zhang, B. B. & Wang, H. 2016. Frutescone A-G, Tasmanone-Based Meroterpenoids from the aerial parts of Baeckea frutescens. *J Org Chem*, 82, 1448-1457.

Hou, J. Q., Wang, B. L., Han, C., Xu, J., Wang, Z., He, Q. W., Zhang, P. L., Zhao, S. M., Pei, X. & Wang, H. 2018. Atropisomeric meroterpenoids with rare triketone-phloroglucinol-terpene hybrids from Baeckea frutescens. *Org Biomol Chem*, 16, 8513-8524.

Jeong, E. Y., Kim, M. G. & Lee, H. S. 2009. Acaricidal activity of triketone analogues derived from Leptospermum scoparium oil against house-dust and stored-food mites. *Pest Manag Sci*, 65, 327-31.

Jeong, E. Y., Lee, M. J. & Lee, H. S. 2018. Antimicrobial activities of leptospermone isolated from Leptospermum scoparium seeds and structure-activity relationships of its derivatives against foodborne bacteria. *Food Sci Biotechnol*, 27, 1541-1547.

Jian, Y. Q., Huang, X. J., Zhang, D. M., Jiang, R. W., Chen, M. F., Zhao, B. X., Wang, Y. & Ye, W. C. 2015. Guapsidial A and Guadials B and C: Three New Meroterpenoids with Unusual Skeletons from the Leaves of Psidium guajava. *Chemistry*, 21, 9022-7.

Jian, Y. Q., Wang, Y., Huang, X. J., Li, G. Q., Zhao, B. X., Guo, Q. Y. & Ye, W. C. 2012. Two new euglobals from

the leaves of Eucalyptus robusta. *J Asian Nat Prod Res*, 14, 831-7.

Joyce, D. S., Eloisa, A., Leilane, B., Nádia, d. S., Alcy, R., Raquel, M. & José, M. 2017. Chemical Composition of Four Essential Oils of Eugenia from the Brazilian Amazon and Their Cytotoxic and Antioxidant Activity. *Medicines*, 4, 51.

Kaneshima, T., Myoda, T., Toeda, K., Fujimori, T. & Nishizawa, M. 2017. Antimicrobial constituents of peel and seeds of camu-camu (Myrciaria dubia). *Biosci Biotechnol Biochem*, 81, 1461-1465.

Kato, E., Kawakami, K. & Kawabata, J. 2018. Macrocarpal C isolated from Eucalyptus globulus inhibits dipeptidyl peptidase 4 in an aggregated form. *J Enzyme Inhib Med Chem*, 33, 106-109.

Khanh, P. N., Duc, H. V., Huong, T. T., Son, N. T., Ha, V. T., Van, D. T., Tai, B. H., Kim, J. E., Jo, A. R., Kim, Y. H. & Cuong, N. M. 2016. Alkylphloroglucinol derivatives and triterpenoids with soluble epoxide hydrolase inhibitory activity from Callistemon citrinus. *Fitoterapia*, 109, 39-44.

Kubitzki & Klaus 2011. Flowering Plants. Eudicots. *Families & Genera of Vascular Plants*, 12.

Lafayette, E. A., Vitalino de Almeida, S. M., Pitta, M. G., Carneiro Beltrão, E. I., da Silva, T. G., Olímpio de Moura, R., Pitta Ida, R., de Carvalho, L. B., Jr. & de Lima Mdo, C. 2013. Synthesis, DNA binding and topoisomerase I inhibition activity of thiazacridine and imidazacridine derivatives. *Molecules*, 18, 15035-50.

Larayetan, R. A., Okoh, O. O., Sadimenko, A. & Okoh, A. I. 2017. Terpene constituents of the aerial parts, phenolic content, antibacterial potential, free radical scavenging and antioxidant activity of Callistemon citrinus (Curtis) Skeels (Myrtaceae) from Eastern Cape Province of South Africa. *BMC Complement Altern Med*, 17, 292.

Lau, K. M., Fu, L. H., Cheng, L., Wong, C. W., Wong, Y. L., Lau, C. P., Han, S. Q., Chan, P. K., Fung, K. P., Lau, C. B., Hui, M. & Leung, P. C. 2010. Two antifungal components isolated from Fructus Psoraleae and Folium Eucalypti Globuli by bioassay-guided purification. *Am J Chin Med*, 38, 1005-14.

Lee, S. H., Wang, H., Labroli, M., Koseoglu, S., Zuck, P., Mayhood, T., Gill, C., Mann, P., Sher, X., Ha, S., Yang, S. W., Mandal, M., Yang, C., Liang, L., Tan, Z., Tawa, P., Hou, Y., Kuvelkar, R., DeVito, K., Wen, X., Xiao, J., Batchlett, M., Balibar, C. J., Liu, J., Xiao, J., Murgolo, N., Garlisi, C. G., Sheth, P. R., Flattery, A., Su, J., Tan, C. & Roemer, T. 2016. TarO-specific inhibitors of wall teichoic acid biosynthesis restore β-lactam efficacy against methicillin-resistant staphylococci. *Sci Transl Med*, 8, 329ra32.

Li, C. J., Ma, J., Sun, H., Zhang, D. & Zhang, D. M. 2016. Guajavadimer A, a Dimeric Caryophyllene-Derived Meroterpenoid with a New Carbon Skeleton from the Leaves of Psidium guajava. *Org Lett*, 18, 168-71.

Lima, B. G., Tietbohl, L. A. C., Fernandes, C. P., Cruz, R. A. S. & Rocha, L. 2012. Chemical composition of essential oils and anticholinesterasic activity of Eugenia sulcata Spring ex Mart. *Latin American Journal of Pharmacy*, 31, 152-155.

Lis-Balchin, M., Hart, S. L. & Deans, S. G. 2000. Pharmacological and antimicrobial studies on different tea-tree oils (Melaleuca alternifolia, Leptospermum scoparium or Mānuka and Kunzea ericoides or Kānuka), originating in Australia and New Zealand. *Phytother Res*, 14, 623-9.

Liu, C., Ang, S., Huang, X. J., Tian, H. Y., Deng, Y. Y., Zhang, D. M., Wang, Y., Ye, W. C. & Wang, L. 2016a. Meroterpenoids with New Skeletons from Myrtus communis and Structure Revision of Myrtucommulone K. *Org Lett*, 18, 4004-7.

Liu, F., Yuan, T., Liu, W., Ma, H., Seeram, N. P., Li, Y., Xu, L., Mu, Y., Huang, X. & Li, L. 2017a. Phloroglucinol Derivatives with Protein Tyrosine Phosphatase 1B Inhibitory Activities from Eugenia jambolana Seeds. *J Nat Prod*, 80, 544-550.

Liu, H. X., Chen, K., Liu, Y., Li, C., Wu, J. W., Xu, Z. F., Tan, H. B. & Qiu, S. X. 2016b. Callviminols A-E, new terpenoid-conjugated phloroglucinols from the leaves of Callistemon viminalis. *Fitoterapia*, 115, 142-147.

Liu, H. X., Chen, K., Yuan, Y., Xu, Z. F., Tan, H. B. & Qiu, S. X. 2016c. Rhodomentones A and B, novel meroterpenoids with unique NMR characteristics from Rhodomyrtus tomentosa. *Org Biomol Chem*, 14, 7354-60.

Liu, H. X., Chen, Y. C., Liu, Y., Zhang, W. M., Wu, J. W., Tan, H. B. & Qiu, S. X. 2016d. Acylphloroglucinols from the leaves of Callistemon viminalis. *Fitoterapia*, 114, 40-44.

Liu, H. X., Tan, H. B. & Qiu, S. X. 2016e. Antimicrobial acylphloroglucinols from the leaves of Rhodomyrtus tomentosa. *J Asian Nat Prod Res*, 18, 535-41.

Liu, R. H., Shang, Z. C., Li, T. X., Yang, M. H. & Kong, L. Y. 2017b. In Vitro Antibiofilm Activity of Eucarobustol E against Candida albicans. *Antimicrob Agents Chemother*, 61.

Low, D., Rawal, B. D. & Griffin, W. J. 1974. Antibacterial action of the essential oils of some Australian Myrtaceae with special references to the activity of chromatographic fractions of oil of Eucalyptus citriodora. *Planta Med*, 26, 184-5.

Luz, T., de Mesquita, L. S. S., do Amaral, F. M. M. & Coutinho, D. F. 2020. Essential oils and their chemical constituents against Aedes aegypti L. (Diptera: Culicidae) larvae. *Acta Trop*, 105705.

Marchese, A., Barbieri, R., Coppo, E., Orhan, I. E., Daglia, M., Nabavi, S. F., Izadi, M., Abdollahi, M., Nabavi, S. M. & Ajami, M. 2017. Antimicrobial activity of eugenol and essential oils containing eugenol: A mechanistic viewpoint. *Crit Rev Microbiol*, 43, 668-689.

Matsuda, Y. & Abe, I. 2014. *Meroterpenoids*, Springer New York.

Montalvan, M., Penafiel, M. A., Ramirez, J., Cumbicus, N., Bec, N., Larroque, C., Bicchi, C. & Gilardoni, G. 2019. Chemical Composition, Enantiomeric Distribution, and Sensory Evaluation of the Essential Oils Distilled from the Ecuadorian Species Myrcianthes myrsinoides (Kunth) Grifo and Myrcia mollis (Kunth) DC. (Myrtaceae). *Plants (Basel)*, 8.

Moreira, I. C., Lago, J. o. H. G., M., Y. M. C. & F., R. N. 2003. Antifungal aromadendrane sesquiterpenoids from the leaves of Xylopia brasiliensis. *Journal of the Brazilian Chemical Society*, 14, 828-831.

Muhammad, A., Abdul, S., Muhammad, J., Farhat, U., Fazal, S. & Jawad, A. 2017. Neuroprotective and Anti-Aging Potentials of Essential Oils from Aromatic and Medicinal Plants. *Frontiers in Aging Neuroscience*, 9.

Nauck, M. 2016. Incretin therapies: highlighting common features and differences in the modes of action of glucagon-like peptide-1 receptor agonists and dipeptidyl peptidase-4 inhibitors. *Diabetes Obesity & Metabolism*, 18.

Osawa, K., Yasuda, H., Morita, H., Takeya, K. & Itokawa, H. 1995. Eucalyptone from Eucalyptus globulus. *Phytochemistry*, 40, 183-184.

Park, C. G., Jang, M., Shin, E. & Kim, J. 2017. Myrtaceae Plant Essential Oils and their beta-Triketone Components as Insecticides against Drosophila suzukii. *Molecules*, 22.

Paula, J. A. M. D., Silva, M. d. R. R., Costa, M. P., Diniz, D. G. A. & Paula, J. R. d. 2012. Phytochemical Analysis and Antimicrobial, Antinociceptive, and Anti-Inflammatory Activities of Two Chemotypes of Pimenta pseudocaryophyllus (Myrtaceae). *Evidence-Based Complementray and Alternative Medicine,2012,(2012-8-27)*, 2012, 420715.

Pham, T. A., Shair Mohammad, I., Vu, V. T., Hu, X. L., Birendra, C., Ulah, A., Guo, C., Lu, X. Y., Ye, W. C. & Wang, H. 2018. Phloroglucinol Derivatives from the Fruits of Eucalyptus globulus and Their Cytotoxic Activities. *Chem Biodivers*, 15, e1800052.

Qin, X. J., Jin, L. Y., Yu, Q., Liu, H., Khan, A., Yan, H., Hao, X. J., An, L. K. & Liu, H. Y. 2018. Eucalypglobulusals A-J, Formyl-Phloroglucinol-Terpene Meroterpenoids from Eucalyptus globulus Fruits. *J Nat Prod*, 81, 2638-2646.

Qin, X. J., Rauwolf, T. J., Li, P. P., Liu, H., McNeely, J., Hua, Y., Liu, H. Y. & Porco, J. A., Jr. 2019. Isolation and

Synthesis of Novel Meroterpenoids from Rhodomyrtus tomentosa: Investigation of a Reactive Enetrione Intermediate. *Angew Chem Int Ed Engl*, 58, 4291-4296.

Qin, X. J., Shu, T., Yu, Q., Yan, H., Ni, W., An, L. K., Li, P. P., Zhi, Y. E., Khan, A. & Liu, H. Y. 2017a. Cytotoxic Acylphloroglucinol Derivatives from Callistemon salignus. *Nat Prod Bioprospect*, 7, 315-321.

Qin, X. J., Yan, H., Ni, W., Yu, M. Y., Khan, A., Liu, H., Zhang, H. X., He, L., Hao, X. J., Di, Y. T. & Liu, H. Y. 2016. Cytotoxic Meroterpenoids with Rare Skeletons from Psidium guajava Cultivated in Temperate Zone. *Sci Rep*, 6, 32748.

Qin, X. J., Yu, Q., Yan, H., Khan, A., Feng, M. Y., Li, P. P., Hao, X. J., An, L. K. & Liu, H. Y. 2017b. Meroterpenoids with Antitumor Activities from Guava (Psidium guajava). *J Agric Food Chem*, 65, 4993-4999.

Reichling, J., Koch, C., Stahl-Biskup, E., Sojka, C. & Schnitzler, P. 2005. Virucidal activity of a beta-triketone-rich essential oil of Leptospermum scoparium (mānuka oil) against HSV-1 and HSV-2 in cell culture. *Planta Med*, 71, 1123-7.

Rodrigues, K. A., Amorim, L. V., de Oliveira, J. M., Dias, C. N., Moraes, D. F., Andrade, E. H., Maia, J. G., Carneiro, S. M. & Carvalho, F. A. 2013. Eugenia uniflora L. Essential Oil as a Potential Anti-Leishmania Agent: Effects on Leishmania amazonensis and Possible Mechanisms of Action. *Evid Based Complement Alternat Med*, 2013, 279726.

Rotstein, A., Lifshitz, A. & Kashman, Y. 1974. Isolation and antibacterial activity of acylphloroglucinols from Myrtus communis. *Antimicrob Agents Chemother*, 6, 539-42.

Sailer, R., Berger, T., Reichling, J. & Harkenthal, M. 1998. Pharmaceutical and medicinal aspects of Australian tea tree oil. *Phytomedicine International Journal of Phytotherapy & Phytopharmacology*, 5, 489-95.

Santos, M., Lucas, E. & Sano, P. 2015. Five new South American species of Myrcia s.l. (Myrtaceae). *Phytotaxa*, 234, 159.

Schnitzler, P., Wiesenhofer, K. & Reichling, J. 2008. Comparative study on the cytotoxicity of different Myrtaceae essential oils on cultured vero and RC-37 cells. *Pharmazie*, 63, 830-5.

Senadeera, S. P. D., Lucantoni, L., Duffy, S., Avery, V. M. & Carroll, A. R. 2018a. Antiplasmodial beta-Triketone-Flavanone Hybrids from the Flowers of the Australian Tree Corymbia torelliana. *J Nat Prod*, 81, 1588-1597.

Senadeera, S. P. D., Robertson, L. P., Duffy, S., Wang, Y., Avery, V. M. & Carroll, A. R. 2018b. beta-Triketone-Monoterpene Hybrids from the Flowers of the Australian Tree Corymbia intermedia. *J Nat Prod*, 81, 2455-2461.

Shang, Z. C., Han, C., Xu, J. L., Liu, R. H., Yin, Y., Wang, X. B., Yang, M. H. & Kong, L. Y. 2019. Twelve formyl phloroglucinol meroterpenoids from the leaves of Eucalyptus robusta. *Phytochemistry*, 163, 111-117.

Shang, Z. C., Yang, M. H., Jian, K. L., Wang, X. B. & Kong, L. Y. 2016a. (1) H NMR-Guided Isolation of Formyl-Phloroglucinol Meroterpenoids from the Leaves of Eucalyptus robusta. *Chemistry*, 22, 11778-84.

Shang, Z. C., Yang, M. H., Liu, R. H., Wang, X. B. & Kong, L. Y. 2016b. New Formyl Phloroglucinol Meroterpenoids from the Leaves of Eucalyptus robusta. *Sci Rep*, 6, 39815.

Shao, M., Wang, Y., Jian, Y. Q., Huang, X. J., Zhang, D. M., Tang, Q. F., Jiang, R. W., Sun, X. G., Lv, Z. P., Zhang, X. Q. & Ye, W. C. 2012. Guadial A and psiguadials C and D, three unusual meroterpenoids from Psidium guajava. *Org Lett*, 14, 5262-5.

Shao, M., Wang, Y., Liu, Z., Zhang, D. M. & Ye, W. C. 2010. Psiguadials A and B, two novel meroterpenoids with unusual skeletons from the leaves of Psidium guajava. *Organic Letters*, 12, 5040-5043.

Sharifi-Rad, J., Salehi, B., Varoni, E. M., Sharopov, F., Yousaf, Z., Ayatollahi, S. A., Kobarfard, F., Sharifi-Rad, M., Afdjei, M. H., Sharifi-Rad, M. & Iriti, M. 2017. Plants of the Melaleuca Genus as Antimicrobial Agents: From Farm to Pharmacy. *Phytother Res*, 31, 1475-1494.

Sharma, A., Bajpai, V. K. & Shukla, S. 2013. Sesquiterpenes and Cytotoxicity. 3515-3550.

Siani, A. C., Souza, M. C., Henriques, M. G. M. O. & Ramos, M. F. S. 2013. Anti-inflammatory activity of essential oils from Syzygium cumini and Psidium guajava. *Pharmaceutical Biology*, 51, 881-887.

Sidana, J., Rohilla, R. K., Roy, N., Barrow, R. A., Foley, W. J. & Singh, I. P. 2010. Antibacterial sideroxylonals and loxophlebal A from Eucalyptus loxophleba foliage. *Fitoterapia*, 81, 878-83.

Sidana, J., Singh, S., Arora, S. K., Foley, W. J. & Singh, I. P. 2011. Formylated phloroglucinols from Eucalyptus loxophleba foliage. *Fitoterapia*, 82, 1118-22.

Siebert, D. A., Bastos, J., Spudeit, D. A., Micke, G. A. & Alberton, M. D. 2017. Determination of phenolic profile by HPLC-ESI-MS/MS and anti-inflammatory activity of crude hydroalcoholic extract and ethyl acetate fraction from leaves of Eugenia brasiliensis. *Revista Brasilra de Farmacognosia*, 27.

Silva, A. N., Uetanabaro, A. P. & Lucchese, A. M. 2013. Chemical composition and antibacterial activity of essential oils from Myrcia alagoensis (Myrtaceae). *Nat Prod Commun*, 8, 269-71.

Silva, E. A. J., Estevam, E. B. B., Silva, T. S., Nicolella, H. D., Furtado, R. A., Alves, C. C. F., Souchie, E. L., Martins, C. H. G., Tavares, D. C., Barbosa, L. C. A. & Miranda, M. L. D. 2019. Antibacterial and antiproliferative activities of the fresh leaf essential oil of Psidium guajava L. (Myrtaceae). *Braz J Biol*, 79, 697-702.

Silva, J., Abebe, W., Sousa, S. M., Duarte, V. G., Machado, M. I. L. & Matos, F. J. A. 2003. Analgesic and anti-inflammatory effects of essential oils of Eucalyptus. *Journal of Ethnopharmacology*, 89, 277-283.

Souza, A. D., Lopes, E. M. C., Silva, M. C. D., Cordeiro, I., Young, M. C. M., Sobral, M. E. G. & Moreno, P. R. H. 2010. Chemical composition and acetylcholinesterase inhibitory activity of essential oils of Myrceugenia myrcioides(Cambess.) O. Berg and Eugenia riedelianaO. Berg, Myrtaceae. *Revista Brasilra De Farmacognosia*, 20, 175-179.

Souza, G. C. D., Haas, A. P. S., Poser, G. L. V., Schapoval, E. E. S. & Elisabetsky, E. 2004. Ethnopharmacological studies of antimicrobial remedies in the south of Brazil. *Journal of Ethnopharmacology*, 90, 135-143.

Su, J. C., Wang, S., Cheng, W., Huang, X. J., Li, M. M., Jiang, R. W., Li, Y. L., Wang, L., Ye, W. C. & Wang, Y. 2018. Phloroglucinol Derivatives with Unusual Skeletons from Cleistocalyx operculatus and Their in Vitro Antiviral Activity. *J Org Chem*, 83, 8522-8532.

Su, Q., Dalal, S., Goetz, M., Cassera, M. B. & Kingston, D. G. 2016. Antiplasmodial phloroglucinol derivatives from Syncarpia glomulifera. *Bioorg Med Chem*, 24, 2544-8.

Sun, M., Gobu, F. R., Pan, D., Li, Y. & Gao, K. 2015. Acylphloroglucinol derivatives from Decaspermum gracilentum and their antiradical and cytotoxic activities. *J Asian Nat Prod Res*, 18, 13-9.

Tagane, S., Dang, V. S., Souladeth, P., Nagamasu, H., Toyama, H., Naiki, A., Fuse, K., Tran, H., Yang, C. J. & Prajaksood, A. 2018. Five new species of Syzygium (Myrtaceae) from Indochina and Thailand. *Phytotaxa*, 375.

Tang, G. H., Dong, Z., Guo, Y. Q., Cheng, Z. B., Zhou, C. J. & Yin, S. 2017. Psiguajadials A-K: Unusual Psidium Meroterpenoids as Phosphodiesterase-4 Inhibitors from the Leaves of Psidium guajava. *Sci Rep*, 7, 1047.

Valdemarin, K. S., Faria, J. E. Q., Mazine, F. F. & Souza, V. C. 2020. A New Species of Eugenia subg. Pseudeugenia (Myrtaceae, Myrteae) from Brazilian Atlantic Forest. *Systematic Botany*, 45, 537-543.

Vilsbll, T., Agers, H., Krarup, T. & Holst, J. J. 2003. Similar Elimination Rates of Glucagon-Like Peptide-1 in Obese Type 2 Diabetic Patients and Healthy Subjects. *J Clin Endocrinol Metab*, 220-224.

Wang, J., Zhai, W. Z., Zou, Y., Zhu, J. J., Xiong, J., Zhao, Y., Yang, G. X., Fan, H., Hamann, M. T., Xia, G. & Hu, J. F. 2012. Eucalyptals D and E, new cytotoxic phloroglucinols from the fruits of Eucalyptus globulus and assignment of absolute configuration. *Tetrahedron Lett*, 53, 2654-2658.

Webster, A. A. 2012. *Chapter 132 - Acetylcholinesterase and its Inhibitors*, Elsevier Inc.

Wu, C., Chen, W., He, J., Jin, S., Liu, Y., Yi, Y., Gao, Z., Yang, J., Yang, J., Cui, J. & Zhao, W. 2020. Interplay of

m^{6}A and H3K27 trimethylation restrains inflammation during bacterial infection. *Science Advances*, 6, eaba0647.

Wu, L., Wang, X. B., Li, R. J., Zhang, Y. L., Yang, M. H., Luo, J. & Kong, L. Y. 2016. Callistiviminenes A-O: Diverse adducts of beta-triketone and sesqui- or monoterpene from the fruits of Callistemon viminalis. *Phytochemistry*, 131, 140-149.

Xu, S. H., Xu, W., Wang, L., Hu, Y. K., Liu, J. P., Zhao, Y., Li, M. J., Li, F., Huang, S. X. & Zhao, Y. 2018. New phloroglucinol derivatives with protein tyrosine phosphatase 1B (PTP1B) inhibitory activities from Syzygium austroyunnanense. *Fitoterapia*, 131, 141-145.

Yang, J., Su, J. C., Lei, X. P., Huang, X. J., Zhang, D. M., Ye, W. C. & Wang, Y. 2018. Acylphloroglucinol derivatives from the leaves of Syzygium samarangense and their cytotoxic activities. *Fitoterapia*, 129, 1-6.

Yang, S. P., Zhang, X. W., Ai, J., Gan, L. S., Xu, J. B., Wang, Y., Su, Z. S., Wang, L., Ding, J., Geng, M. Y. & Yue, J. M. 2012. Potent HGF/c-Met axis inhibitors from Eucalyptus globulus: the coupling of phloroglucinol and sesquiterpenoid is essential for the activity. *J Med Chem*, 55, 8183-7.

Zanetti, S., Cannas, S., Molicotti, P., Bua, A., Cubeddu, M., Porcedda, S., Marongiu, B. & Sechi, L. A. 2010. Evaluation of the Antimicrobial Properties of the Essential Oil of Myrtus communis L. against Clinical Strains of Mycobacterium spp. *Interdisciplinary Perspectives on Infectious Diseases*, 2010, 931530.

Zhang, Y. B., Li, W., Jiang, L., Yang, L., Chen, N. H., Wu, Z. N., Li, Y. L. & Wang, G. C. 2018. Cytotoxic and anti-inflammatory active phloroglucinol derivatives from Rhodomyrtus tomentosa. *Phytochemistry*, 153, 111-119.

Zhang, Y. L., Chen, C., Wang, X. B., Wu, L., Yang, M. H., Luo, J., Zhang, C., Sun, H. B., Luo, J. G. & Kong, L. Y. 2016. Rhodomyrtials A and B, Two Meroterpenoids with a Triketone-Sesquiterpene-Triketone Skeleton from Rhodomyrtus tomentosa: Structural Elucidation and Biomimetic Synthesis. *Org Lett*, 18, 4068-71.

Zhi, Y. E., Qi, X. J., Liu, H., Zeng, Y., Ni, W., He, L., Wang, Z. D. & Liu, H. Y. 2018. Structurally Diverse Polymethylated Phloroglucinol Meroterpenoids from Baeckea frutescens. *Nat Prod Bioprospect*, 8, 431-439.

Zou, J., Mi, Y., Chen, W., Liu, Q., Wang, J., Lou, L. & Zhao, W. 2006. Alkyl phloroglucinol derivatives from Syzygium levinei and their differentiation-inducing activity. *Planta Med*, 72, 533-8.

Zou, Z. X., Tan, G. S., Huang, Q., Sun, H. H., Huo, L. Q., Zhong, W. Q., Zhao, L. Y., Liu, H. X. & Tan, H. B. 2018. Brachyanins A-C, pinene-derived meroterpenoids and phloroglucinol derivative from Leptospermum brachyandrum. *Fitoterapia*, 130, 184-189.

Chapter Three

An improved MTT colorimetric method for rapid viable bacteria counting.

Traditional methods for enumerating live bacteria necessitate considerable repetitive manual labor. Consequently, the development of a live bacteria calculation formula tailored to a fixed experimental environment represents a significant advancement in reducing manpower and time requirements for the whole study.

This chapter has been published in the following peer-reviewed publication:

Xu, W., Shi, D., Chen, K., Palmer, J., & Popovich, D. G. (2023). An improved MTT colorimetric method for rapid viable bacteria counting. *Journal of Microbiological Methods*, *214*, 106830.

Statement of Contribution

<table>
<tr><td colspan="4">We, the student and the student's main supervisor, certify that all co-authors have consented to their work being included in the thesis and they have accepted the student's contribution as indicated below in the Statement of Originality.</td></tr>
<tr><td colspan="2">Student name:</td><td colspan="2">Wenliang Xu</td></tr>
<tr><td colspan="2">Name and title of main supervisor:</td><td colspan="2">Dr. David Popovich</td></tr>
<tr><td colspan="2">In which chapter is the manuscript/published work?</td><td colspan="2">Chapter Three</td></tr>
<tr><td colspan="2">What percentage of the manuscript/published work was contributed by the student?</td><td colspan="2">70%</td></tr>
<tr><td colspan="4">Describe the contribution that the student has made to the manuscript/published work:
Conceptualization; Data curation; Formal analysis; Visualization; Investigation; Methodology; Validation; Writing - original draft; Writing - review & editing.</td></tr>
<tr><td colspan="4">Please select one of the following three options:</td></tr>
<tr><td>✓</td><td colspan="3">The manuscript/published work is published or in press
Please provide the full reference of the research output:
Xu, W., Shi, D., Chen, K., Palmer, J., & Popovich, D. G. (2023). An improved MTT colorimetric method for rapid viable bacteria counting. Journal of Microbiological Methods, 214, 106830.</td></tr>
<tr><td></td><td colspan="3">The manuscript is currently under review for publication Please provide the name of the journal:</td></tr>
<tr><td></td><td colspan="3">It is intended that the manuscript will be published, but it has not yet been submitted to a journal</td></tr>
<tr><td>Student's signature:</td><td>Wenliang Xu</td><td>Main supervisor's signature:</td><td> 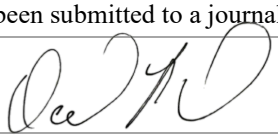 </td></tr>
</table>

Abstract

The 3-(4,5-dimethylthiazol-2-yl)-2,5-diphenyl tetrazolium bromide (MTT) assay has been employed in the analysis of bacterial growth. In comparison to experiments conducted on mammalian cells, the MTT bacterial assay encounters a greater number of interfering factors and obstacles that impact the accuracy of results. In this study, we have elucidated an improved MTT assay protocol and put forth an equation that establishes a correlation between colony-forming units (CFU) and the amount of formazan converted by the bacteria, drawing upon the fundamental principle of the MTT assay. This equation is represented as $\mathrm{CFU} = k\mathrm{F}$. Furthermore, we have explicated a methodology to determine the scale factor "k" by employing *S. aureus* and *E. coli* as illustrative examples. The findings indicate that *S. aureus* and *E. coli* reduce MTT by a cyclic process, from which the optimal reduction time at room temperature was determined to be approximately 30 mins. Furthermore, individual *E. coli* exhibits an MTT reduction capacity approximately four times greater than that of *S. aureus*. HPLC analysis proves to be the most accurate method for mitigating interferences during the dissolution and quantification of formazan. Additionally, this study has identified a new constraint related to the narrow linear range (0~125 μg/mL) of formazan concentration-absorbance and has presented strategies to circumvent this limitation.

Keywords: MTT bacterial assay; Formazan; HPLC; Viable count; *Staphylococcus aureus*; *Escherichia coli*.

3.1. Introduction

Rapid enzymatic tetrazolium salts reduction has been widely used to assess microbial viability and estimate growth. This method offers great advantages over conventional methods such as the time-consuming steps of counting colony-forming units (CFU) (Tunney et al., 2004; Rahman et al., 2004; Gabrielson et al., 2002; Wang et al., 2010). The 3-(4,5-dimethylthiazol-2-yl)-2,5-diphenyl tetrazolium bromide (MTT) is the most used compound (Oh and Hong, 2022; Benov, 2021; Hut et al., 2021; Houdkova et al., 2017; Hundie et al., 2016; Grela et al., 2015; Wang et al., 2010; Li and Song, 2007; Foongladda et al., 2002; Bernas and Dobrucki, 2000). The MTT assay is based on the enzymatic reduction of water-soluble yellow dye to a water-insoluble purple crystal called formazan. The amount of formazan is therefore positively correlated with cell viability (Morgan, 1998; Carmichael et al., 1987; Mosmann, 1983). The whole assay can be divided into two stages: the reduction of MTT into formazan and the measurement of the amount of formazan. Tested bacteria are often many in number and have quite high MTT reduction efficiency and suspension characteristics which can block light and reduce the efficiency of spectrometer readings. Moreover, each stage in the process has some technical limitations. These limitations include uncertain reaction times of MTT, incomplete dissolution of formazan, high turbidity of bacterial suspension, and the effect of pH on the conversion of formazan (Grela et al., 2018; Grela et al., 2015; Wang et al., 2012; Wang et al., 2010). However, several modified protocols are available, but they only focus on improving the dissolution of formazan and neglect the other interfering factors. Furthermore, there is interference caused by the choice of solubilizer used (Oh and Hong, 2022; Benov, 2021; Wang et al., 2012; Wang et al., 2010).

The objective of this study was to enhance the MTT bacterial assay protocol to eliminate interference and achieve precise quantification of formazan. Additionally, the study aimed to establish a correlation equation between colony-forming units and formazan production for selected bacteria, thereby offering an alternative approach to the conventional colony plate counting method. *Staphylococcus aureus* and *Escherichia coli*, representative species of gram-positive and gram-negative bacteria, were chosen for the MTT assay and subsequent creation of equations.

3.2. Materials and Methods

3.2.1. Bacterial strains and growth conditions

Gram-positive *Staphylococcus aureus* (ATCC 25923) and Gram-negative *Escherichia coli* (ATCC 25922) strains were used as illustrative examples in this study. The strains used were obtained from the Microbiology Department of Massey University, and stored in brain heart

infusion (BHI, Difco) agar slants at 4 °C. For each experiment, a single colony of each strain was picked and cultured in BHI broth at 37 °C for 24 h. The current experiment refers to this culture condition as the standard condition.

3.2.2. Preparation of MTT and MTT-formazan standard solutions

A concentration of 5 mg/mL MTT (99% HPLC grade, AK Scientific, USA) was prepared in sterile water and stored at 4°C in the dark. MTT-formazan (99% HPLC grade, Sigma-Aldrich, USA) with a concentration of 1000 μg/mL was prepared in dimethyl sulfoxide (DMSO, AR grade, Merck) and stored at room temperature (22 °C) in the dark.

3.2.3. MTT reduction time determination and formazan quantification

The MTT reduction time was determined by a continuous time-yield study. The volume of 1 mL (V1) of *S. aureus* and *E. coli* suspensions were accurately taken and centrifuged (2400*g, 2 min) to remove the supernatant. Twenty-four samples were prepared for each bacterium and divided into 8 groups. Then all samples were resuspended in 1 mL of sterile water or phosphate buffered saline PBS (it has been found in multiple replicate experiments that changing PBS to sterile water did not affect the bacterial ability to reduce MTT, data not shown), mixed with 100 μL 0.5% MTT (V: V = 10:1) and stirred. Groups 1-8 were left to stand for 5, 15, 30, 45, 60, 75, 90, and 105 minutes, respectively, at room temperature (22 °C). After each MTT reduction time point, the samples were centrifuged (11337*g, 2 mins), the supernatant was removed, and 1 mL (V2) of isopropanol (AR grade, Merck) was added for *S. aureus* and 2 mL (V2) of isopropanol for *E. coli* to dissolve the formazan. The volume V2 is variable depending on the type of bacteria tested and will be described in detail in 3.3.4. Ultrasonic equipment (Bandelin DT 52) was used to accelerate the dissolution.

The obtained formazan solution was centrifuged (11337*g, 10 mins) and filtered through a 0.22 μm syringe filter (13 mm diameter, Whatman Uniflo) to remove bacteria and precipitates, and then measured by high-performance liquid chromatography (HPLC, Thermofisher Ultimate 3000) with a diode array detector (DAD, Dionex Ultimate 3000) at 570 nm under the following conditions: Thermofisher Hypersil GOLD C18 Column 100 × 2.1 mm, particle size 1.9 μm and column guard Accucore C18 10 × 2.1 mm were used. Running method: Eluent A-MilliQ water, eluent B-Acetonitrile; 0-2 min 5% B, 2-3 min 5%-100% B, 3-10 min 100% B, 10-10.5 min 100%-5% B, 10.5-15 min 5% B. Column oven temperature: 25 °C; inject volume: 10 μL; flow rate: 0.3 mL/min. Each sample was repeated two-fold, followed by a blank run for washing accumulated various inorganic salts off the column. The column was washed using the following running method: 0-15 min 5% B. Column oven temperature: 25 °C; flow rate: 0.2 mL/min.

3.2.4. MTT colorimetric assay on bacteria

Newly cultured *S. aureus* and *E. coli* suspensions (BHI broth, 37 °C, 24 h) were serially diluted into seven concentration gradients (10%, 25%, 40%, 55%, 70%, 85% and 100% of the initial concentration) with BHI broth respectively, and the optical density (OD) at 600 nm (OD_{600}, referred to as y_1) of each concentration was measured using a microplate reader (96 well plate, 200 μL /well, Thermofisher Varioskan LUX). For both bacteria, 1 mL (V1) of each concentration gradient was accurately taken and an MTT assay with a reduction time determined in 3.2.3 was performed. The peak area (x) of formazan was measured by HPLC as described in section 3.2.3. The values of y_1 and 'x' were used to calculate key equation 1 mentioned in 3.3.1.

3.2.5. Enumeration of viable bacteria

The dilution plate-counting method was used to obtain the concentration of colony-forming units (referred to as y_2 CFU/mL) of each gradient. Each bacterial suspension was diluted 10^6 or 10^7 times with sterile water, and 400 μL was put into the plate and mixed well with liquefied BHI agar (45°C) and repeated 4 times. All plates were incubated at 37 °C for 24 h–72 h. The values of y_2 and y_1 (measured in 3.2.4) were used to calculate the key equation 2 described in section 3.3.1.

3.2.6. MTT-formazan peak area-concentration standard curve

The formazan standard solution with the initial concentration of 1000 μg/mL was serial two-fold diluted seven times and used to test linear intervals and derive a standard curve using the same HPLC conditions mentioned in 3.2.3. Each concentration was repeated 6 times. Key equation 3 mentioned in 3.3.1 was derived from formazan concentration (y_3) and peak areas (x) to calculate the amount of formazan produced by bacteria.

3.2.7. Statistical analysis

Chameleon 7.2.7 (Thermofisher) was used for HPLC results analysis. Linear equations were calculated by GraphPad Prism 9.3.1, and linear regression analysis and linear correlation coefficients were calculated. Each data point was averaged from two to six replicates and expressed as mean ± standard deviation.

3.3. Results and Discussion

3.3.1. Establishment of the equation.

Based on the principle of the MTT assay, within a certain range of time and number of viable

bacteria, the number of bacteria is linearly related to the amount of formazan transformed by them (Wang et al., 2010; Oh and Hong, 2022).

Therefore, we proposed the following equation:

$$\mathrm{CFU} = k\mathrm{F}$$

CFU is the number of colony-forming units, "k" is a constant scale factor, and F is the mass of formazan produced by bacteria.

This study introduced a method to find "k" in this equation so that a relatively accurate number of viable bacteria can be quickly calculated by detecting the amount of formazan produced.

It is known that within a certain range, the concentration of bacteria is linearly related to their optical density, and that the concentration of formazan is also linearly related to its absorbance (Stevens and Olsen, 1993). Showing the linear relationship between the optical density of bacterial suspension and the absorbance of formazan produced by bacteria is the key step to calculating "k".

"k" was calculated using three key equations:

(1) The equation between the OD_{600} of bacterial suspension (referred to as "y_1") and the peak area of the formazan solution (referred to as "x"), is displayed as follows:

$y_1 = ax$ (Key Equation 1)

"a" is the value of the scale factor.

Tested bacteria were liquid-cultured under a standard condition described in 3.2.1. The OD_{600} of bacterial suspension (y_1) was measured by a microplate reader. To initiate formazan production, 1 mL (V1) of the bacterial suspension was utilized in a 30-minute MTT assay. Subsequently, the supernatant was replaced with either 1 or 2 mL (V2) of isopropanol, depending on the specific type of bacteria used. Isopropanol serves two functions: it inactivates bacteria and dissolves formazan. The formazan isopropanol solution was measured by HPLC, and the peak area "x" was then calculated. The whole process was conducted on 7 different concentrations of bacterial suspension to obtain the value of the scale factor (a).

(2) The equation between the concentration of bacteria (y_2, CFU/mL) and the OD_{600} of the bacterial suspension (y_1), is shown below:

$y_2 = by_1$ (Key Equation 2)

"b" is the value of the scale factor.

The traditional plate count method was applied for enumerating bacteria. The newly cultured bacterial suspension was mixed with different amounts of broth to prepare multiple concentrations. Subsequently, immediate plate counts were conducted to determine the bacteria concentration (y_2, CFU/mL) and the OD_{600} of the bacterial suspension (y_1) under each concentration gradient was measured. The linear relationship equation was therefore obtained.

(3) The equation between the concentration of MTT-formazan standard (y_3) and its peak area (x):

$y_3 = cx$ (Key Equation 3)

"c" is the value of the scale factor.

The MTT-formazan standard was accurately prepared at 1000 μg/mL, the peak area was measured by HPLC after multiple two-fold dilutions.

Combine the above equations:

$$\begin{cases} y_1 = ax \\ y_2 = by_1 \\ y_3 = cx \end{cases} \rightarrow y_2 = \frac{ab}{c} y_3$$

∵ y_2 is the bacteria concentration.

∴ $y_2 = \frac{CFU}{V1}$, CFU is the number of colony-forming units, and V1 is the volume of bacteria suspension used for formazan production.

∵ y_3 is formazan concentration.

∴ $y_3 = \frac{F}{V2}$, F is the mass of formazan produced by bacteria, and V2 is the volume of solvent used to dissolve formazan.

∴ $\frac{CFU}{V1} = \frac{ab}{c} \cdot \frac{F}{V2}$

∴ $CFU = \frac{abV1}{cV2} \cdot F$

∴ $k = \frac{abV1}{cV2}$

For a single species, this equation describes the relationship between a certain number of CFUs and the mass of formazan produced by them at room temperature for 30 minutes.

3.3.2. Optimization of the MTT reduction procedure.

MTT reduction time of 2-4 hours is commonly used in most protocols and is likely selected by following the protocols used for mammalian cells (Brambilla et al., 2014; Wu et al., 2010; Walencka et al., 2008; Shi et al., 2007; Wang et al., 2007; Li and Song, 2007; Corrado and Rodrigues, 2004; Foongladda et al., 2002; Mshana et al., 1998). Continuous MTT assays at 37 °C have already been done on several kinds of bacteria, such as Gram-negative bacteria *E. coli* (Oh and Hong, 2022; Wang et al., 2010) and *P. mirabilis* (Grela et al., 2015), and Gram-positive bacteria *L. mesenteroides* (Oh and Hong, 2022) and *S. aureus* (Stevens et al., 1991). For all the bacteria we tested, MTT quickly reduced in the first 10-20 mins, and then the reduction rate decreased rapidly over the next 40-100 mins. This phenomenon may be caused by limited space in the bacteria for formazan to accumulate and the high efficiency of bacterial transformation of MTT. Cell injury caused by the transportation and accumulation of MTT and formazan crystals may also have affected the MTT reducing efficiency (Lü et al., 2012). Unlike mammalian cells, bacterial formazan tends to form cell-bound complexes. Some researchers also suggest that formazan can form complexes with biofilms, rather than forming needle-like crystals on the surface (Wang et al., 2010; Liu et al., 1997). To optimize the MTT reduction time at room temperature and to observe the time point of possible cell damage, we performed a continuous MTT assay, and took microscopic observations.

In the current study, to simplify the process and to avoid potential interference caused by changing temperature, as well as to slow down the efficiency of bacterial transformation of MTT, experiments were performed at room temperature after bacteria were cultured overnight. Bacteria have a high conversion efficiency of MTT; we found that at 37 °C, the bacteria produced formazan quantities beyond the linear range in a short period of time, thus performing the MTT assay at 37 °C is likely to lead to inaccurate results. **Fig. 3.1** shows the results of this continuous MTT assay for 105 mins at room temperature. Compared with the production efficiency of formazan at 37 °C reported in articles (Oh and Hong, 2022; Grela et al., 2015; Wang et al., 2010), at room temperature, the efficiency slowed down and peaked at 30–40 mins, and then showed a significant downward trend.

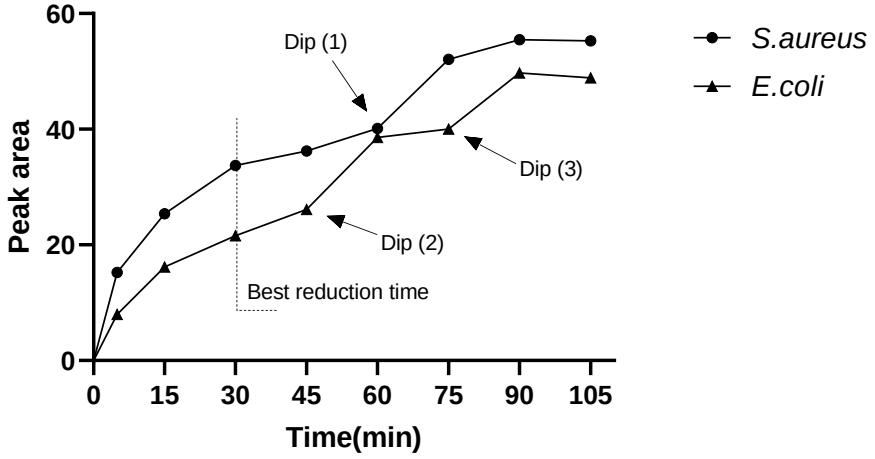

Fig. 3.1. Time-course profiles of formazan yield by *S. aureus* and *E. coli*. Tested bacteria were cultured in fresh BHI broth for 24 hours and their capacity to reduce MTT at 5, 15, 30, 45, 60, 75, 90, and 105 mins were measured respectively. The formazan produced was dissolved with isopropanol and measured by HPLC at 570 nm.

It is worth noting that in many parallel experiments, we found that both curves formed dips at specific reduction time points: 60 min for *S. aureus*, and 45 min and 75 min for *E. coli*, respectively. We compared the state and behavior of bacteria across time periods by microscopic observation and found that during 0-40 minutes, both tested bacteria began to rapidly form formazan in the cells and excreted formazan complexes at a specific time so that free formazan began to appear in the medium. This phenomenon has also been found in *P. mirabilis* (Grela et al., 2015). As shown in **Figs. 3.2-1** and **3.2-3**, formazan complexes can be observed inside the cell, and in **Figs. 3.2-2** and **3.2-4**, free formazan complexes can be found in the medium. To fully dissolve the formazan in the cells, the medium was removed prior to the formazan measurement. Thus, formazan excretion is an explanation for the dips formed on the curves since formazan excreted via exocytosis was not measured in this experiment. It can also be seen from the curve that after the first exocytosis, the bacteria continued to accumulate formazan in the cells, but the production efficiency dropped significantly, which we think is affected by the cell damage caused by the exocytosis of formazan (Lü et al., 2012).

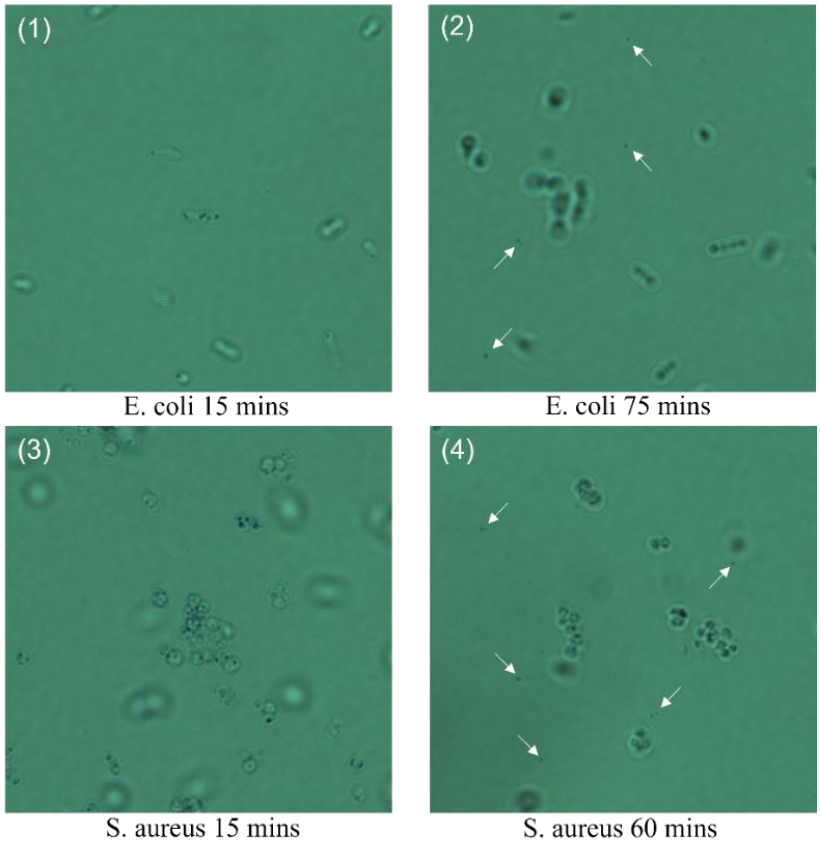

Fig. 3.2. Oil immersion microscope observation of *E. coli* and *S. aureus* during the MTT assay. In pictures **1** and **3**, the presence of formazan is exclusively observed within the bacterial cells. The identification of free formazan complexes is denoted by arrows in pictures **2** and **4**, corresponding to dip **3** and dip **1** in **Fig. 3.1**, respectively.

Overall, in continuous MTT assays, the bacteria exhibit recurring patterns of MTT reduction and formazan excretion, as evidenced by the current findings indicating a cycle duration of approximately one hour, and this cyclic process potentially leads to continuous cellular impairment.

To ensure a more accurate representation of cell viability, it is recommended to measure the amount of formazan prior to the initiation of the first exocytosis phase, before cellular damage occurs. Consequently, a reduction time of 30 minutes at room temperature was selected as the optimal duration for MTT reduction in *S. aureus* and *E. coli*.

3.3.3. Optimization of the dissolution and quantification procedures of formazan.

To measure the formazan accurately, adequate dissolution of formazan and suppression of interferences is essential. Some protocols advise removing the culture medium prior to adding the organic solvent, to ensure full dissolution of the formazan crystals and to avoid errors lead by the medium, such as unreduced MTT and chemical components that can disturb the formazan

dissolution or the absorbance of formazan (Wang et al., 2010; Shi et al., 2007; Li and Song, 2007; Young et al., 2005). Removing the culture medium requires an additional step, and different amounts of culture medium residues also cause errors. Other researchers aim to avoid this step by using potent solubilizers such as ammonia and NaOH (Oh and Hong, 2022; Benov, 2021; Perri et al., 2016; Wang et al., 2012; Niks, 1990). However, we observed the following tetrazolium ring-opening reaction through color transformation under room and higher temperatures in 30 mins, shown in **Fig. 3.3.** This property of MTT has been suggested for antioxidant ability testing (Liu and Nair, 2010). But in cell viability testing, it will give false positive results, leading to a read higher than the actual value.

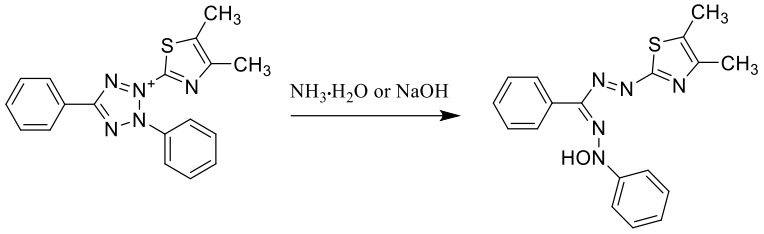

Fig. 3.3. The spontaneous conversion of MTT to formazan in $NH_3 \cdot H_2O$ (1-10 M) and NaOH (0.1-1 M) solution.

It is also worth noting that the commonly used absorption wavelengths of formazan (490–630 nm) (Deb and Vimala, 2018; Wang et al., 2012; Shi et al., 2007; Wang et al., 2007; Stowe et al., 1995; Stevens and Olsen, 1993; Mosmann, 1983; Broughton and Jahans, 1997) overlaps with the wavelength range used for most microorganisms (400-770 nm) (Wang et al., 2011), which means neither method mentioned above can avoid the error caused by the bacteria itself; a clarified solution is difficult to obtain even with potent solubilizers. In addition, some other interferences cannot be ignored. Prolonged reduction time possibly causes the conversion of formazan to colorless derivatives (Stowe et al., 1995). Using a low pH buffer or acidic organic solvent causes absorbance to shift, leading to a lower reading (Wang et al., 2012; Plumb et al., 1989).

To eliminate all the above interferences, we suggest that the best path is to isolate formazan from the cell suspension and measure it individually. Structurally speaking, MTT formazan is a non-polar lipophilic compound; it will accumulate inside the cells before being actively transported out of the cell by bacteria. In this experiment, we optimized the MTT reduction time (30 mins); we then completed the MTT assay (taking advantage of the property that MTT formazan is insoluble in water and is deposited inside the cells), separated the bacteria from aqueous solution by centrifugation, followed by pure organic solvent immersion and ultrasound-assisted dissolution. Next, the formazan was isolated by HPLC to achieve precise quantification. In this step, the solution loss during HPLC sample preparation did not affect the results because the concentration and injection volume of formazan solution was constant. Besides, during the analysis, a column

guard was used to filter possible cell debris, and blank runs were applied after each sample for washing accumulated salt and monitoring the column pressure. The present study did not observe an obvious pressure increase after hundreds of runs, indicating that the HPLC sample preparation steps described in section 3.2.3 were effective to remove debris. For the smooth entry of organic solvents into cells and subsequent reversed-phase HPLC analysis, we recommend acetone, isopropanol and DMSO, which are less polar (≤ 50% water polarity) and miscible with water. In this experiment, the low-cost solvent isopropanol was used.

3.3.4. Linear equation of bacteria optical density and formazan peak area

The disadvantage of the microplate reader is that there is no selectivity for the target compound. That is, components that interfere with absorption will be read as well. HPLC results are shown in **Fig. 3.4.** Compared with the blank sample (1) and formazan standard (2), the impurity detected in the high-yield group (3) caused an error of around 10%, and the impurity detected in the low yield group (4) caused an error of over 30%. This result indicates that despite removing the bacteria and precipitates during sample preparation, there are still non-negligible impurities that can be read.

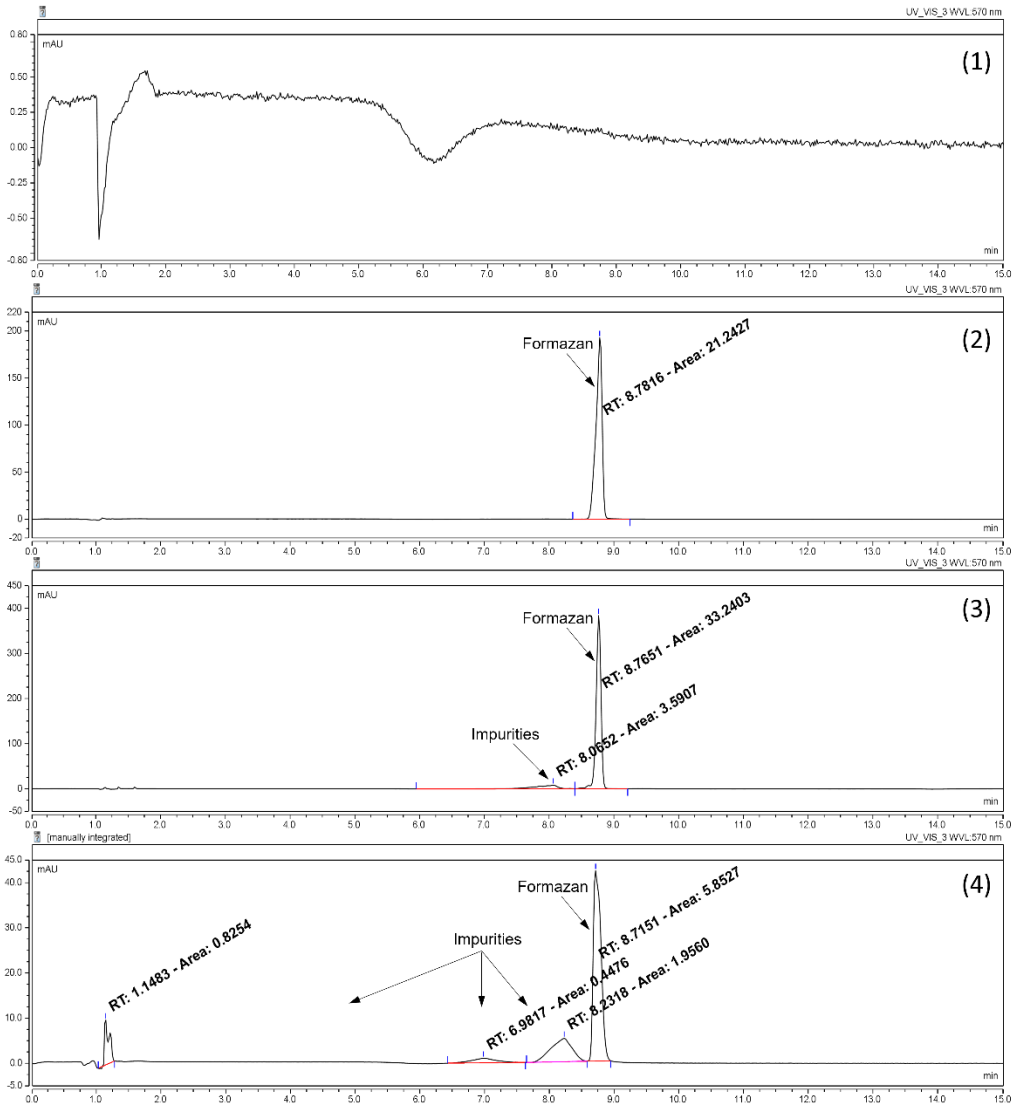

Fig. 3.4. Examples of HPLC measurement of formazan at 570 nm. 1) Pure water (Blank); 2) Formazan standard. No significant impurity signal peaks were observed; 3) Formazan produced by a high concentration of bacteria. The peak area of formazan accounts for 90% of the total peak area; 4) Formazan produced by the low concentration of bacteria. The peak area of formazan accounts for 64% of the total peak area.

Therefore, in this experiment, HPLC was chosen as the best formazan measurement method for eliminating errors to the greatest extent. The peak area of formazan can be selectively and accurately obtained, demonstrating strong reproducibility in experiments.

To compare the reducing ability of the two tested bacteria, we first prepared *S. aureus* and *E. coli* suspensions into seven concentration gradients respectively and measured the OD_{600} with a microplate reader before the MTT assay. Thus, the OD_{600} of each concentration gradient was *S. aureus*: 0.0795, 0.1448, 0.2212, 0.3089, 0.4612, 0.6387, and 0.7709; *E. coli*: 0.0813, 0.1465, 0.2266, 0.3131, 0.5061, 0.6393, and 0.7640.

During the assay, we noticed that under culture conditions, the amount of formazan (peak area) produced by *S. aureus* had a good linear relationship with the concentration of the selected bacterial suspension, while *E. coli* lost the linear relationship when the OD_{600} of the bacterial suspension exceeded 0.5 and the measured value was lower than the theoretical value. At first, we thought that the increase in bacterial density reduced the overall viability of *E. coli*. However, when we double-diluted the formazan produced by *E. coli* and measured it again, a good linear equation was obtained. This result shows that for *E. coli*, when the OD_{600} of the bacterial solution is greater than 0.5, the amount of formazan produced at room temperature for 30 mins still can exceed the linear range of the formazan absorbance, resulting in a lower reading than the actual value.

In the current protocol, for the *S. aureus* assay, we replaced the medium with the same volume of organic solvent to dissolve the formazan (V2=V1=1 mL) and used twice the volume of organic solvent for the *E. coli* assay (V2=2V1=2 mL) to ensure that subsequent testing results were all within the linear interval. The regression curves of bacterial OD_{600} and formazan peak area are shown in **Fig. 3.5.**

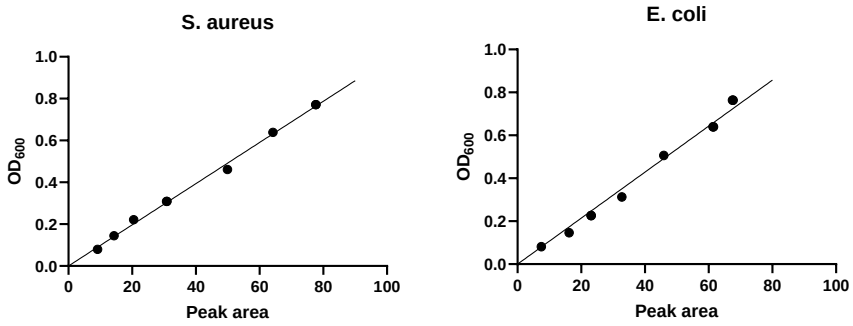

Fig. 3.5. The linear relationship between the optical density (OD) of bacterial suspension measured by microplate reader at 600 nm and the amount of formazan yield during MTT assay measured by HPLC at 570 nm.

This step measured the scale factor "a" of both selected bacterium in key equation 1: $y_1(\mathrm{OD}_{600}) = ax(\text{Peak area})$

S. aureus: $y_1 = 0.009840x$ (Intercept set to 0, $R^2 = 0.9962$, 1/slope = 101.6, $P < 0.0001$).

E. coli: $y_1 = 0.01071x$ (Intercept set to 0, $R^2 = 0.9918$, 1/slope = 93.33, $P < 0.0001$).

Interestingly, we obtained two similar equations after a double dilution of the formazan produced by *E. coli*. This result suggests that at the same volume and OD_{600}, the capacity of *E. coli* to reduce MTT is roughly twice that of *S. aureus.*

3.3.5. Linear equation of bacteria optical density and the number of CFUs

The pour plate technique was used in this experiment to reduce cell aggregation and cell adhesion caused by using the spreader. In our comparative pre-experiments, the higher CFU counting results were obtained by the pour plate technique, which agreed with the results in Pyar and Peh (2014).

Like the bacterial suspension preparation process mentioned in section 3.2.4, the OD_{600} of each bacterial suspension was measured using a microplate reader before 10-fold dilution. We repeated the whole viable counting experiment three times, and each plate was counted twice after 24 hours and 72 h, respectively. The linear relationship, with outliers removed, is shown in **Fig. 3.6.**

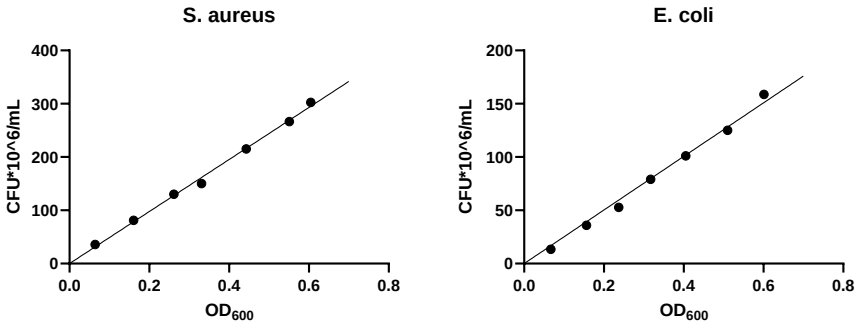

Fig. 3.6. The linear relationship between the optical density (OD) of bacterial suspension measured by microplate reader at 600 nm and CFU number obtained by the pour plate counting method.

This step measured the scale factor "b" of both selected bacterium in key equation 2: $y_2(\text{CFU/mL}) = by_1(\text{OD}_{600})$

S. aureus: $y_2 = 488.3\times10^6 y_1$ (Intercept set to 0, $R^2 = 0.9961$, 1/slope = 0.002048, $P < 0.0001$).

E. coli: $y_2 = 251.3\times10^6 y_1$ (Intercept set to 0, $R^2 = 0.9959$, 1/slope = 0.003979. $P < 0.0001$).

The equations suggest that, under the current culture conditions, at the same volume and OD_{600}, the CFUs of *S. aureus* are roughly twice that of *E. coli*. In section 3.3.4 we concluded that the capacity of *E. coli* to reduce MTT at the same volume and OD_{600} was twice that of *S. aureus.* Therefore, under the present culture conditions, individual *E. coli* demonstrate approximately four times greater capacity for MTT reduction compared to *S. aureus*.

3.3.6. Linear equation of formazan peak area and formazan concentration

Formazan has a long history as a dye compound (Aljamali et al., 2019). According to the

color wheel, a dye normally absorbs light that is complementary to the reflected light; the deeper the color, the stronger the absorption (Parkhurst and Feller, 1982; Kumar et al., 2021). Due to this property, the absorbance-concentration linear interval of dyes tends to be much narrower than colorless substances since they may have stronger light absorption properties at very low concentrations.

In the linear interval measuring experiment, the real deviation was observed at a formazan concentration higher than 125 μg/mL, as shown in **Fig. 3.7.** This result indicates that the linear range of the formazan dye as an indicator is indeed very narrow. It also further supports our inference in section 3.3.4 that bacterium could produce formazan beyond the linear range in a short period of time. Moreover, the MTT reduction time should be controlled in a short period of time or the applicable concentration of MTT should be prepared much lower than that commonly used for mammalian cell experiments.

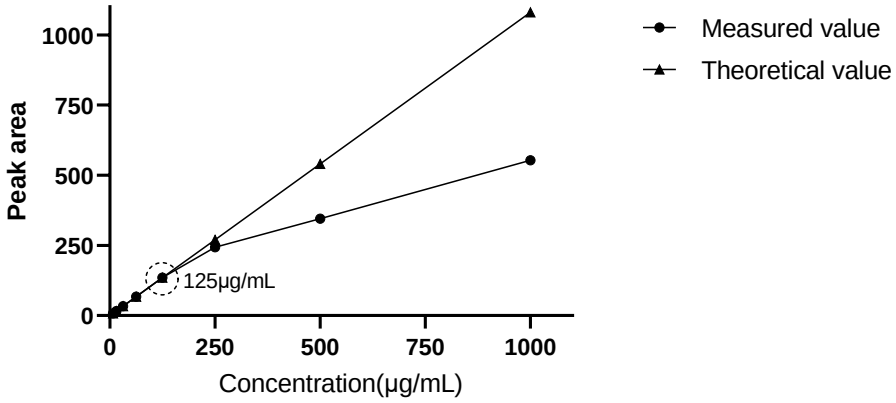

Fig. 3.7. Concentration-absorbance relationship curve of formazan standard measured by HPLC at 570 nm. The real deviation was observed at concentrations above 125 μg/mL.

The linear equation within the linear interval of **Fig. 3.7** was calculated. This step measured the scale factor "c" in key equation 3: y_3(μg/mL) = cx(Peak area)

$y_3 = 0.9278x$ (Intercept set to 0, $R^2 = 1.0$, 1/slope = 1.078, $P < 0.0001$).

3.3.7. Linear equation of the number of CFUs and the mass of formazan produced.

Back to the proposed equation $CFU = kF = \frac{abV1}{cV2} \cdot F$

'CFU' is the number of colony-forming units, and 'F' is the mass of formazan produced by bacteria. 'V1' is the volume of bacterial suspension to be tested, and 'V2' is the volume of organic solvent used to dissolve formazan. Both are artificially chosen constants. 'a', 'b' and 'c' are the

constants associated with the bacterial culture conditions that have been calculated in the three key equations described above.

Therefore, the CFU number and the amount of formazan relationship equations are:

S. aureus: $CFU = \frac{abV1}{cV2} \cdot F = \frac{0.00984 \cdot 488.3 \times 10^6 \cdot 1}{0.9278 \cdot 1} \cdot F = 5.1788 \times 10^6 \cdot F$

E. coli: $CFU = \frac{abV1}{cV2} \cdot F = \frac{0.01071 \cdot 251.3 \times 10^6 \cdot 1}{0.9278 \cdot 2} \cdot F = 1.4504 \times 10^6 \cdot F$

Using these equations, the number of CFUs in the bacterial suspension (cultured under standard conditions) can be calculated directly by measuring the amount of formazan produced at room temperature for 30 mins. Moreover, the CFU calculated by these equations can also be used as a unit for the overall viability of bacteria, representing the equivalent of bacteria cultured under other conditions relative to standard conditions.

This method also has the potential to improve the current evaluation methods such as minimum inhibition concentration (MIC) testing. For the conventional broth dilution method, by performing an MTT assay, the inhibition rate at each concentration of tested compound can be evaluated by calculating the initial and final CFU number, thereby obtaining the growth inhibition curve to evaluate the amount-effect relationship. Furthermore, this method greatly reduces the errors caused by colored compounds (colored solution) as well as non-water-soluble compounds (turbid liquid).

3.4. Conclusion

The present study provided an improved protocol that aims to eliminate interferences in both the reduction and measurement stages of the bacterial MTT assay, achieving an accurate quantification of formazan. We described a method to establish an equation for a given bacterium to calculate its CFUs by measuring the amount of formazan. Providing a possible alternative method for microplate counting greatly saves time for subsequent experiments. This equation is based on the fundamental principle of the MTT assay. Theoretically, the establishment method of the equation is applicable to most microorganisms. In the current study, *S. aureus* and *E. coli* were used, and the reduction time was determined according to their cycle of production and excretion of formazan. It may be necessary to re-determine the reduction time by using the continuous MTT assay described in section 3.2.3 when it is applied to other strains.

Our experiment also identified a new limitation of using the MTT assay on bacteria, which is the narrow linear interval of formazan concentration-absorbance and provided the strategies to solve it. The experiment was conducted under controlled conditions at room temperature to reduce

formazan production. Additionally, the concentration of the resulting formazan solution was regulated within the linear range using solvent dilution. The current findings provide evidence that *S. aureus* and *E. coli* reduce MTT by a cyclic process of formazan accumulation, exocytosis, and re-accumulation. The first cycle takes about 40-60 mins and causes cell damage and formazan leakage. The optimal reduction time for both bacterial strains tested is 30 mins. The capacity of individual *E. coli* to reduce MTT is roughly four times greater than that of *S. aureus*. To avoid interferences in the dissolution and quantification of formazan, HPLC was employed to separate the formazan from the mixture, enabling precise measurement of the peak area. This method is different from conventional MTT assay protocols for bacteria and achieved a significant improvement.

In summary, this enhanced MTT bacterial assay serves as a means of data standardization through HPLC analysis. The precise quantification of formazan facilitates the accurate determination of CFUs, potentially obviating the necessity for protracted and repetitive plate-counting procedures in extended experiments. Furthermore, the refinement of this methodology may yield valuable insights for other assays associated with MTT.

3.5. References

Aljamali, N. M., Kadhim, A. J., Mohammed, J. H. & Ghafil, R. A. A. 2019. Review on Preparation and Applications of Formazan Compounds. *International Journal of Thermodynamics and Chemical Kinetics*, 5, 23-33p.

Benov, L. 2021. Improved Formazan Dissolution for Bacterial MTT Assay. *Microbiology Spectrum*, 9, e01637-21.

Bernas, T. & Dobrucki, J. W. 2000. The role of plasma membrane in bioreduction of two tetrazolium salts, MTT, and CTC. *Archives of Biochemistry and Biophysics*, 380, 108-116.

Brambilla, E., Ionescu, A., Cazzaniga, G., Edefonti, V. & Gagliani, M. 2014. The influence of antibacterial toothpastes on in vitro Streptococcus mutans biofilm formation: a continuous culture study. *Am J Dent*, 27, 160-6.

Broughton, E. & Jahans, K. 1997. The differentiation of Brucella species by substrate specific tetrazolium reduction. *Veterinary Microbiology*, 57, 253-271.

Carmichael, J., DeGraff, W. G., Gazdar, A. F., Minna, J. D. & Mitchell, J. B. 1987. Evaluation of a tetrazolium-based semiautomated colorimetric assay: assessment of chemosensitivity testing. *Cancer Research*, 47, 936-942.

Corrado, M. & Rodrigues, K. F. 2004. Antimicrobial evaluation of fungal extracts produced by endophytic strains of Phomopsis sp. *Journal of Basic Microbiology: An International Journal on Biochemistry, Physiology, Genetics, Morphology, and Ecology of Microorganisms*, 44, 157-160.

Deb, A. & Vimala, R. 2018. Biofilm Formation by Pseudomonas Species Onto Graphene Oxide–TiO2 Nanocomposite-Coated Catheters: In vitro Analysis. *International Journal of Nanoscience*, 17, 1760014.

Foongladda, S., Roengsanthia, D., Arjrattanakool, W., Chuchottaworn, C., Chaiprasert, A. & Franzblau, S. 2002. Rapid and simple MTT method for rifampicin and isoniazid susceptibility testing of Mycobacterium tuberculosis. *The International Journal of Tuberculosis and Lung Disease*, 6, 1118-1122.

Gabrielson, J., Hart, M., Jarelöv, A., Kühn, I., McKenzie, D. & Möllby, R. 2002. Evaluation of redox indicators and the use of digital scanners and spectrophotometer for quantification of microbial growth in microplates. *Journal of Microbiological Methods*, 50, 63-73.

Grela, E., Kozłowska, J. & Grabowiecka, A. 2018. Current methodology of MTT assay in bacteria–A review. *Acta Histochemica*, 120, 303-311.

Grela, E., Ząbek, A. & Grabowiecka, A. 2015. Interferences in the optimization of the MTT assay for viability estimation of Proteus mirabilis. *Avicenna Journal of Medical Biotechnology*, 7, 159.

Houdkova, M., Rondevaldova, J., Doskocil, I. & Kokoska, L. 2017. Evaluation of antibacterial potential and toxicity of plant volatile compounds using new broth microdilution volatilization method and modified MTT assay. *Fitoterapia*, 118, 56-62.

Hundie, G. B., Woldemeskel, D. & Gessesse, A. 2016. Evaluation of direct colorimetric MTT assay for rapid detection of rifampicin and isoniazid resistance in mycobacterium tuberculosis. *PLoS One*, 11, e0169188.

Hut, E.-F., Radulescu, M., Pilut, N., Macasoi, I., Berceanu, D., Coricovac, D., Pinzaru, I., Cretu, O. & Dehelean, C. 2021. Two antibiotics, ampicillin and tetracycline, exert different effects in HT-29 colorectal adenocarcinoma cells in terms of cell viability and migration capacity. *Current Oncology*, 28, 2466-2480.

Kumar, A., Dixit, U., Singh, K., Gupta, S. P. & Beg, M. S. J. 2021. Structure and Properties of Dyes and Pigments. *Dyes and Pigments-Novel Applications and Waste Treatment.* IntechOpen.

Li, J. & Song, L. 2007. Applicability of the MTT assay for measuring viability of cyanobacteria and algae, specifically for Microcystis aeruginosa (Chroococcales, Cyanobacteria). *Phycologia*, 46, 593-599.

Liu, Y. & Nair, M. G. 2010. An efficient and economical MTT assay for determining the antioxidant activity of plant natural product extracts and pure compounds. *Journal of Natural Products*, 73, 1193-1195.

Liu, Y., Peterson, D. A., Kimura, H. & Schubert, D. 1997. Mechanism of cellular 3-(4, 5-dimethylthiazol-2-yl)-2, 5-diphenyltetrazolium bromide (MTT) reduction. *Journal of Neurochemistry*, 69, 581-593.

Lü, L., Zhang, L., Wai, M. S. M., Yew, D. T. W. & Xu, J. 2012. Exocytosis of MTT formazan could exacerbate cell injury. *Toxicology in Vitro*, 26, 636-644.

Morgan, D. M. 1998. Tetrazolium (MTT) assay for cellular viability and activity. *Polyamine Protocols.* Springer.

Mosmann, T. 1983. Rapid colorimetric assay for cellular growth and survival: application to proliferation and cytotoxicity assays. *Journal of Immunological Methods*, 65, 55-63.

Mshana, R. N., Tadesse, G., Abate, G. & Miörner, H. 1998. Use of 3-(4, 5-dimethylthiazol-2-yl)-2, 5-diphenyl tetrazolium bromide for rapid detection of rifampin-resistant Mycobacterium tuberculosis. *Journal of Clinical Microbiology*, 36, 1214-1219.

Niks, M. 1990. Towards an optimized MTT assay. *J. Immunol. Methods*, 130, 149-151.

Oh, Y. J. & Hong, J. 2022. Application of the MTT-based colorimetric method for evaluating bacterial growth using different solvent systems. *LWT*, 153, 112565.

Parkhurst, C. & Feller, R. L. 1982. Who invented the color wheel? *Color Research & Application*, 7, 217-230.

Perri, M., Caroleo, M. C. & Cione, E. 2016. Basic condition to formazan improve sensitivity of the MTT colorimetric assay dye. *J Biochem Anal Stud*.

Plumb, J. A., Milroy, R. & Kaye, S. 1989. Effects of the pH dependence of 3-(4, 5-dimethylthiazol-2-yl)-2, 5-diphenyltetrazolium bromide-formazan absorption on chemosensitivity determined by a novel tetrazolium-based assay. *Cancer Research*, 49, 4435-4440.

Pyar, H. & Peh, K. 2014. Characterization and identification of Lactobacillus acidophilus using biolog rapid identification system. *International Journal of Pharmacy and Pharmaceutical Sciences*, 6, 189-193.

Rahman, M., Kühn, I., Rahman, M., Olsson-Liljequist, B. & Möllby, R. 2004. Evaluation of a scanner-assisted colorimetric MIC method for susceptibility testing of gram-negative fermentative bacteria. *Applied and Environmental Microbiology*, 70, 2398-2403.

Shi, L., Ge, H.-M., Tan, S.-H., Li, H.-Q., Song, Y.-C., Zhu, H.-L. & Tan, R.-X. 2007. Synthesis and antimicrobial activities of Schiff bases derived from 5-chloro-salicylaldehyde. *European Journal of Medicinal*

Chemistry, 42, 558-564.

Stevens, M. G., Kehrli Jr, M. E. & Canning, P. C. 1991. A colorimetric assay for quantitating bovine neutrophil bactericidal activity. *Veterinary Immunology and Immunopathology*, 28, 45-56.

Stevens, M. G. & Olsen, S. C. 1993. Comparative analysis of using MTT and XTT in colorimetric assays for quantitating bovine neutrophil bactericidal activity. *Journal of immunological methods*, 157, 225-231.

Stowe, R. P., Koenig, D. W., Mishra, S. & Pierson, D. L. 1995. Nondestructive and continuous spectrophotometric measurement of cell respiration using a tetrazolium-formazan microemulsion. *Journal of Microbiological Methods*, 22, 283-292.

Tunney, M. M., Ramage, G., Field, T. R., Moriarty, T. F. & Storey, D. G. 2004. Rapid colorimetric assay for antimicrobial susceptibility testing of Pseudomonas aeruginosa. *Antimicrobial Agents and Chemotherapy*, 48, 1879-1881.

Walencka, E., Różalska, S., Sadowska, B. & Różalska, B. 2008. The influence of Lactobacillus acidophilus-derived surfactants on staphylococcal adhesion and biofilm formation. *Folia Microbiologica*, 53, 61-66.

Wang, F., Cao, L.-t. & Hu, S.-h. 2007. A rapid and accurate 3-(4, 5-dimethyl thiazol-2-yl)-2, 5-diphenyl tetrazolium bromide colorimetric assay for quantification of bacteriocins with nisin as an example. *Journal of Zhejiang University SCIENCE B*, 8, 549-554.

Wang, H., Cheng, H., Wang, F., Wei, D. & Wang, X. 2010. An improved 3-(4, 5-dimethylthiazol-2-yl)-2, 5-diphenyl tetrazolium bromide (MTT) reduction assay for evaluating the viability of Escherichia coli cells. *Journal of Microbiological Methods*, 82, 330-333.

Wang, H., Wang, F., Tao, X. & Cheng, H. 2012. Ammonia-containing dimethyl sulfoxide: An improved solvent for the dissolution of formazan crystals in the 3-(4, 5-dimethylthiazol-2-yl)-2, 5-diphenyl tetrazolium bromide (MTT) assay. *Analytical Biochemistry*, 421, 324-326.

Wang, W., Peng, Y., Huang, H. & Wu, J. 2011. Application of hyper-spectral imaging technique for the detection of total viable bacteria count in pork. *Sensor Letters*, 9, 1024-1030.

Wu, Y. T., Zhu, H., Willcox, M. & Stapleton, F. 2010. Removal of biofilm from contact lens storage cases. *Investigative Ophthalmology & Visual Science*, 51, 6329-6333.

Young, F. M., Phungtamdet, W. & Sanderson, B. J. 2005. Modification of MTT assay conditions to examine the cytotoxic effects of amitraz on the human lymphoblastoid cell line, WIL2NS. *Toxicology in Vitro*, 19, 1051-1059.

Chapter Four

TLC-bioautography-guided identification and assessment of the antibacterial compounds from plant extracts

This chapter presents a refined approach for bioassay-guided isolation and identification from plant extracts and was demonstrated using *Feijoa sellowiana* fruit peels as an example. Moreover, it is noted that the conventional direct TLC-bioautography method is not appropriate for osmotically susceptible bacteria, such as *Escherichia coli*. To address this limitation, a straightforward technique is introduced in this research to overcome this challenge, enabling the establishment of a universal TLC-based antibacterial assay for both *Staphylococcus aureus* and *Escherichia coli*.

This chapter has been published in the following peer-reviewed publication:

Xu, W., Shi, D., Chen, K., & Popovich, D. G. (2024). TLC-bioautography-guided identification and assessment of the antibacterial compounds from *Feijoa sellowiana*. Phytochemical Analysis.

Statement of Contribution

<table>
<tr><td colspan="4">We, the student and the student's main supervisor, certify that all co-authors have consented to their work being included in the thesis and they have accepted the student's contribution as indicated below in the Statement of Originality.</td></tr>
<tr><td>Student name:</td><td colspan="3">Wenliang Xu</td></tr>
<tr><td>Name and title of main supervisor:</td><td colspan="3">Dr. David Popovich</td></tr>
<tr><td colspan="2">In which chapter is the manuscript/published work?</td><td colspan="2">Chapter Four</td></tr>
<tr><td colspan="2">What percentage of the manuscript/published work was contributed by the student?</td><td colspan="2">75%</td></tr>
<tr><td colspan="4">Describe the contribution that the student has made to the manuscript/published work:
Conceptualization; Data curation; Formal analysis; Visualization; Investigation; Methodology; Validation; Writing - original draft; Writing - review & editing.</td></tr>
<tr><td colspan="4">Please select one of the following three options:</td></tr>
<tr><td>✓</td><td colspan="3">The manuscript/published work is published or in press
Please provide the full reference of the research output:
Xu, W., Shi, D., Chen, K., & Popovich, D. G. (2024). TLC-bioautography-guided identification and assessment of the antibacterial compounds from Feijoa sellowiana. Phytochemical Analysis.</td></tr>
<tr><td></td><td colspan="3">The manuscript is currently under review for publication Please provide the name of the journal:</td></tr>
<tr><td></td><td colspan="3">It is intended that the manuscript will be published, but it has not yet been submitted to a journal</td></tr>
<tr><td>Student's signature:</td><td>Wenliang Xu</td><td>Main supervisor's signature:</td><td> 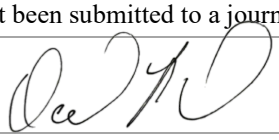 </td></tr>
</table>

Abstract

A rapid method was developed for the targeted isolation and assessment of antibacterial compounds from plant-based materials. The effectiveness of this method was demonstrated using *Feijoa sellowiana* fruit peels as an example. Active compounds were targeted using TLC-bioautography against *S. aureus*, and their identification was achieved through HR-ESI-MS and -MS/MS combined with Compound Discoverer 3.3. Purification was carried out using a customized separation method. The main antibacterial compound identified was flavone. A total of 29 mg of flavone with a purity of approximately 96% was isolated from 102 g of dried *Feijoa sellowiana* fruit peels. The structure of flavone was confirmed using Nuclear Magnetic Resonance (NMR) spectroscopy. Two enhanced antibacterial assays were described, specifically the Minimum Effective Dose (MED) determination based on direct Thin Layer Chromatography (TLC)-bioautography, and the colorimetric broth microdilution assisted by High Performance Liquid Chromatography (HPLC). These methods were refined to mitigate the interference arising from compounds exhibiting intense coloration in solution or extreme insolubility in the aqueous matrix. The results indicate that the MED (on the TLC plate), Minimum Inhibitory Concentration (MIC), and Minimum Bactericidal Concentration (MBC) of flavone against *S. aureus* were found to be 4.2-5.2 μg/cm^2, 225-275 μg/mL, and 550-650 μg/mL, respectively. Similarly, the MED, MIC, and MBC against *E. coli* were determined to be 5.2-6.1 μg/cm^2, 325-375 μg/mL, and 375-425 μg/mL, respectively.

Keywords: *Feijoa sellowiana*; TLC-bioautography; Compound Discoverer; NMR; antibacterial activity; colorimetric broth dilution.

4.1. Introduction

Antibiotic resistance is a growing global concern (Westh et al., 2004). The excessive and improper utilization of antibiotics has been recognized as the primary factor for the swift emergence of antibiotic-resistant bacteria (Blaskovich et al., 2017; Chandra et al., 2017). Although the capacity to alter their chemical structure allows for the development of new antibiotics, these ostensibly novel antibiotics continue to fall within the chemical classifications identified since the 1960s. In other words, the genuine novel antibiotics have not been successfully developed in recent decades (Lewis, 2013; Prasad et al., 2019). Clinical investigations have revealed that resistance developed against one antibiotic often extends to other antibiotics within the same class (Cheesman et al., 2017; Chandra et al., 2017). Consequently, our capacity to combat microbial infections has remained stagnant for an extended period.

In order to address the escalating issue of antibiotic resistance, phytochemicals may offer a promising avenue for resolution. Over the course of 350 million years, plants and their associated microorganisms have undergone co-evolution, resulting in the development of secondary metabolites that serve as integral components of plant defense mechanisms against pathogens (Magallón and Hilu, 2009; Clarke et al., 2011; Chassagne et al., 2021). Recent statistical analyses have unveiled that the estimated count of known plant species stands at approximately 374,000 (Christenhusz and Byng, 2016), implying that a considerable number of bioactive compounds remain undiscovered.

Conventional bacterial susceptibility tests can be categorized into dilution methods that determine Minimum Inhibitory Concentration (MIC) and diffusion methods that generate zone diameter as results (Jorgensen and Turnidge, 2015). There exist numerous phytochemicals that pose challenges in conducting conventional bacteriostatic activity assays, primarily due to their physical characteristics. For instance, terpenes and certain alkaloids exhibit poor water solubility, impeding their diffusion and dissolution even with the aid of solubilizers. Additionally, compounds like tannins possess intense coloration, which can potentially result in erroneous absorbance readings. (Shi et al., 2023).

Consequently, the objective of this study was to develop an efficient procedure utilizing direct TLC-bioautography to facilitate the targeting, identification, and purification of pure antibacterial compounds from plant extracts. Moreover, to enhance the precision of assessing the antibacterial efficacy of phytochemicals, this investigation delineated a method based on TLC-bioautography to determine the Minimum Effective Dose (MED), alongside a colorimetric broth microdilution aided by HPLC for evaluating the isolated active compounds. The choice of Feijoa (*Feijoa sellowiana*) fruit peel as the plant material under examination was primarily motivated by the

scarcity of research related to the identification and purification of its active constituents.

4.2. Materials and Methods

4.2.1. Chemicals and reagents

Methanol, n-hexane, acetone, absolute ethanol, and ethyl acetate for extraction and non-instrumental analysis were analytical research grade, acetonitrile, methanol, and formic acid used for instrumental analysis were LC-MS-grade (Merck, Germany). Normal phase thin-layer chromatography (TLC, silica gel F_{254}, 0.2 mm in thickness, aluminum sheets), silica gel used for column chromatography (particle size 40 μm) and aluminum oxide used for column chromatography (activated, neutral, particle size 60 μm) were purchased from Sigma-Aldrich, USA. The TLC chromogenic reagent used (Vanillin-H_2SO_4 reagent) was a mixture of two stock solutions: solution A contained 2 g of vanillin (99%, Sigma-Aldrich, USA) and 50 mL absolute ethanol, solution B contained 10 mL sulfuric acid (98%, Sigma-Aldrich, USA) and 40 mL absolute ethanol, stored at room temperature (22 °C) in the dark. 3-(4,5-Dimethylthiazol-2-yl)-2,5-Diphenyltetrazolium Bromide (MTT, 99%, AK Scientific, USA) stock solution, 5 mg/mL, and tetracycline, ampicillin (98%, Sigma-Aldrich, USA) stock solution, 0.1 mg/mL, were prepared in sterile water and stored at 4 °C in the dark. Chloroform-d (99.9%, Sigma-Aldrich, USA) was used for nuclear magnetic resonance (NMR).

4.2.2. Plant material

Feijoa fruits were locally collected in Palmerston North, New Zealand (June 2021). The plant was identified as *Feijoa sellowiana* at the School of Natural Science, Massey University. After the flesh was removed, the peels were air dried in an oven at 40 °C and ground into a fine powder (60-80 mesh) by a grinding mill (HC-2000Y, Wuyi Haina Electric Appliance Co., Ltd, China), 102 g of total dry matter was obtained.

4.2.3. Extraction of total phytochemicals

The powder of feijoa fruit peel (102 g) was extracted by 500 mL of methanol in a Soxhlet extractor for 12 hours. The temperature in the thimble during extraction is about 60 °C. Extracts obtained were concentrated on a rotary evaporator at 35 °C to yield approximately 10 g of gum-like crude extracts.

4.2.4. Bacteria cultivation and MIC test

Staphylococcus aureus (ATCC 25923) and *Escherichia coli* (ATCC 25922) strains were used

in this study. The strain was obtained from the Microbiology Department, Massey University, and stored in brain heart infusion (BHI, Difco) agar slants at 4 °C. For each experiment, a single colony was picked and cultured in BHI broth at 37 °C for 24 h. A bacterial suspension with an optical density of 1.2 measured by a spectrophotometer (ThermoFisher GENESYSTM 180) at 600 nm was prepared for direct TLC-bioautographic detection.

The broth microdilution method was employed to assess the MIC of purified compounds. The assay was performed on a 96-well plate, bacterial suspensions were 100 times diluted after overnight culture, and tested samples were prepared in 950, 850, 750, 650, 550, 450, 350, 250, 150, and 50 μg/mL, 100 μL of bacterial suspension and 100 μL of sample solution were mixed during the test. Tetracycline and ampicillin (100 μg/mL) were used as a positive control, DMSO was used as a solubilizer, and the final concentration was controlled to less than 2%. The results were read directly by a microplate reader (Thermofisher Varioskan LUX) and again read by HPLC after the addition of MTT (30 mins, 22 °C). This improved colorimetric method was detailed in our previous research (Xu et al., 2023).

4.2.5. TLC analysis and direct bioautography

Feijoa sellowiana fruit peels crude methanol extract was dissolved in methanol at a concentration of 1 mg/mL and used for following TLC analysis. A mixture of n-hexane and acetone (7:3, v:v) was used as the developing agent. Plates were developed in a rectangular TLC developing chamber. The chamber was shaken with the developing agent and sealed with parafilm before each experiment. The plates were removed when the solvent front had moved to 90% of the total plate length (10 cm) and subsequently allowed to dry. The separated compounds were visualized under 254 nm UV light (Dark Box UV lamp, Qiwei ZF-1, China) followed by vanillin-H_2SO_4 reagent sprayed and heated for color reaction.

Direct bioautography was performed by the procedure described in the recent articles (Wang et al., 2021; Dewanjee et al., 2015). TLC plates with separated compounds were dried in a fume hood overnight, sterilized with UV light for 20 minutes, and immersed for 10 seconds in the bacterial suspension. The plates were kept in a glass container and wrapped with aluminum foil. For TLC with *S. aureus*, the wrapped containers were directly incubated at 37 °C for 16 hours. For TLC with *E. coli*, the inner walls of the container were sprayed with a layer of water mist, and water-saturated absorbent cotton (10 mL) was placed in the corner of the container before wrapping, then incubated at 37 °C for 16 hours in total. For visualization of microbial growth, MTT was sprayed onto the plates and re-incubated at 37 °C for 3 hours. Clear white zones against a bluish-violet background on the TLC plate indicate the anti-microbial activity of the compounds (Choma and Grzelak, 2011; Das et al., 2010; Dewanjee et al., 2015). The white zone is referred to as the inhibition zone in this study.

The MED of tested chemicals was determined by continuously reducing the amount of sample spotted. The minimum dose that maintains a clear inhibition zone on the plate after 16-20 hours was defined as the MED. The spotting volume throughout the study was unified to 3 μL to ensure the sample area on the TLC plate was consistent, and a pipette was used to complete the spotting. The tested sample solutions were first diluted into several concentration gradients (475, 425, 375, 325, 275, 225, 175, 125, 75, and 25 μg/mL), then cultured and stained following common TLC-bioautography procedures after spotting.

4.2.6. Rapid identification of target compounds

The main compound related to the major inhibition zone was selected as the target compound in this study. For rapid identification, the target compound to be tested was located by retention factor (R_f) value and the color response of vanillin-H_2SO_4 staining and was collected by scraping the silica gel from the TLC plates directly and flushing with acetone. The crude methanol extracts (1 mg/mL) and the collected target compound were analyzed by UHPLC-HR-MS (Thermofisher Dionex Ultimate 3000 High-Performance Liquid Chromatography and Q Executive Focus High-Resolution Mass Spectrometer) and identified through online database matching performed by Compound Discoverer 3.3. The separation was performed by a Thermofisher Hypersil GOLD C18 Column, 100 × 2.1 mm, particle size 1.9 μm. Running method: solvent A water/0.1% formic acid, solvent B acetonitrile/0.1% formic acid. 0-3 min 5% B, 3-20 min 5%-60% B, 20-22 min 60%-95% B, 22-25 min 95% B, 25-28 min 95%-5% B, 28-30 min 5% B, 0.2 mL/min flow rate. The inject volume was set to 5 μL and the column oven was maintained at 25 °C. Mass spectra were acquired under an electrospray ionization (ESI) source in both positive and negative ionization modes through full MS and data-dependent MS/MS analysis. The optimal MS parameters were set as follows: spray voltage, 2.5 kV; capillary temperature, 350 °C; sheath gas, 35 units; auxiliary gas, 10 units; auxiliary gas heater temperature, 200 °C; sweep gas, 5 units; collision energy, 30 eV. The mass range was set from 100 to 800 m/z at a resolution of 70,000.

4.2.7. Target compounds purification

Based on the physical properties (molecular weight, polarity, adsorbability, etc.) of the identified compound, a targeted gradient elution column chromatography method was designed. To fully dissolve the target compounds and minimize impurities, different proportions (10:0, 9:1, 8:2, 7:3, 6:4, 5:5) of the n-hexane: acetone mixtures were tested to dissolve the crude extract (first dissolution). The insoluble residue was then filtered and fully dissolved in a mixture of acetone and methanol (second dissolution). To test for the complete dissolution of the target compounds, TLC detection was performed on both solutions obtained from the two dissolutions. The present study discovered that when the ratio was 7 to 3, the n-hexane: acetone mixture could fully dissolve the target compounds in the crude methanol extract.

The crude methanol extracts 10 g were suspended in a 200 mL mixture of n-hexane and acetone (7:3, v:v) to fully dissolve the target compound and undissolved high polar non-target compounds were removed by filtration. The resultant solution was concentrated into 10 ml and separated by silica gel column chromatography (n-hexane: acetone, 9.5:0.5 to 8.5:1.5 to 7:3, v:v) and the target compound was found in the second fraction by TLC testing. The second fraction was further separated by aluminum oxide column chromatography (n-hexane: acetone, 9:1, v:v). The purity of the isolated compound was determined by the HPLC area normalization method on triplicate experiments, the detection was with a DAD (diode array detector, Dionex, Ultimate 3000) at 210 nm and 255 nm respectively, performed in the same column described in section 4.2.6. The running method included pure methanol, 15 mins, 5 μL inject volume, 0.2 mL/min flow rate, and column oven maintained at 25 °C.

4.2.8. Nuclear magnetic resonance (NMR)

The ^{1}H, ^{13}C and Distortionless Enhancement by Polarization Transfer (DEPT 135°) NMR (Bruker AV 500 spectrometer) were used to verify the identification results of Compound Discoverer as well as for detecting any other non-UV-active organic compounds (impurities) derived from the extract. The tested sample was prepared in chloroform-d. The chemical shifts were reported in parts per million (ppm) downfield from Tetramethylsilane (TMS).

4.2.9. Data acquisition and software analysis

Images of the plates were processed by ImageJ (National Institutes of Health, USA, version 1.53t). The structure diagram of compounds was edited using ChemBioDraw (CambridgeSoft, USA, version 14.0). The mass data acquisition and analysis were performed by Xcalibur (Thermofisher, USA, version 4.4). The compound identification was performed by Compound Discoverer (Thermofisher, USA, version 3.3). The NMR spectrum was processed by MestReNova (Mestrelab Research, Spain, version 6.1.0).

4.3. Results and Discussion

4.3.1. Direct TLC-bioautography

The first step of the investigation was to develop a method to separate the main compounds on normal phase TLC and then measure the bacterial growth inhibitory activity of each separated compound. The target compound should exhibit a strong color response, regular shape, and obvious inhibition zone on the TLC plate. As shown in **Fig. 4.1**, four inhibition zones can be observed in the four parallel incremental spotting bioautography tests (**Fig. 4.1A**), the zones of inhibition did not show a trend of shrinking until the spotting volume was as low as 2.5 μL,

equivalent to 2.5 µg of the crude extract, which indicates the high amount of the active compounds in the total extracts. Three of the zones exhibited fuzzy boundaries and irregular shapes. This phenomenon indicates that the anti-bacterial ingredient is losing its effect after 24 hours of culture, and the surrounding bacteria has begun to grow and cover the original inhibition zone, suggesting a poorly sustained bacteriostatic effect of the related compounds.

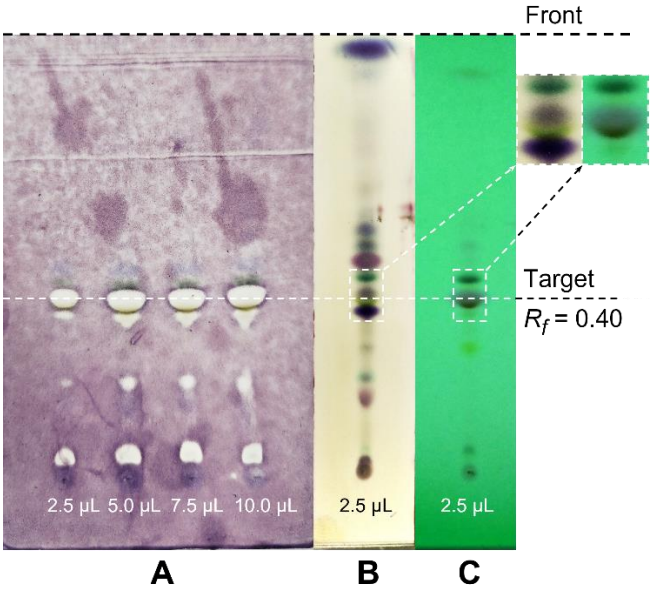

Fig. 4.1. A) Bioautography assay of 1 mg/mL *Feijoa sellowiana* fruit peels crude extract under incremental spotting method against *Staphylococcus aureus* at 37 °C, 24 h. **B**) Vanillin-H_2SO_4 staining result. **C**) 254 nm UV absorption result.

In the Vanillin-H_2SO_4 staining test (**Fig. 4.1B**), the clear zone corresponded with two major color responses, purple and chartreuse. The chartreuse spot assumed a crescent shape underneath the purple oval spot, indicating a competitive adsorption effect. Both compounds have strong UV absorption (**Fig. 4.1C**), showing the same results under a 254 nm UV lamp that can be easily traced and distinguished. Besides, the chartreuse compound can also be observed underneath the clear zones in **Fig. 4.1A**, therefore, the purple-colored compound with the same shape as the zone of inhibition is most likely its active ingredient. Combining the above factors, the compound at 0.40 R_f value that can be purple-colored by Vanillin-H_2SO_4 reagent was chosen as the target in this study.

4.3.2. Structure identification

After the target was selected, the multiple TLC separations were repeated. The target compound was collected from plates and analyzed by UHPLC-HR-MS, and Compound Discoverer 3.3 was used for spectra matching to the mzCloud MS^n spectral library, ChemSpider structure database and Mass List (Piovesana et al., 2020; Figueroa et al., 2021; Oulkar et al., 2022). The Fragment Ion Search (FISh) was applied to further identify the fragments under 30 eV

collision energy (Wank et al., 2016). The identification results are listed in **Fig. 4.2.** Other details of software settings, the database included in Mass List, and workflows are provided in supplementary data (Appendix 2).

Name	Flavone
Formula	$C_{15}H_{10}O_2$
m/z	223.0750
RT [min]*	10.638
Calc. MW*	222.0677
Match Score	97.4
Match Confidence	95.6
Tree Match	95.6
Reference Ion	[M+H]+1

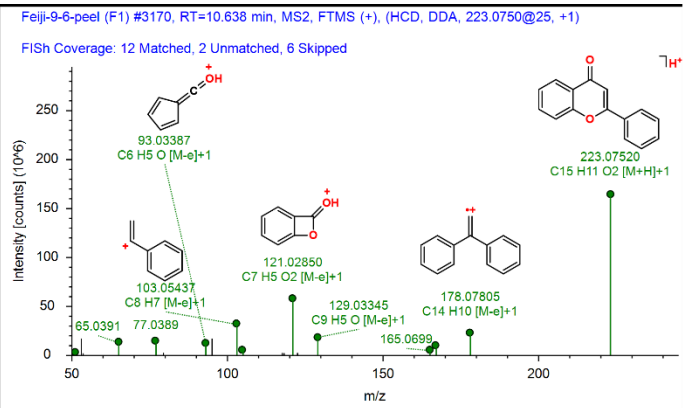

Fig. 4.2. The chemical information and identified MS^2 fragments of the compound matched with the inhibition zone. *RT: retention time; Calc. MW: calculated molecule weight.

This result largely agreed with a previous activity-guided fractionation study, where flavone was identified as the active compound of feijoa fruit that showed high anti-bacterial activity against multiple bacterial strains tested (Basile et al., 2010). However, compared to the conventional column chromatography fractionation-activity determination cyclic process, the procedures in the present study can target and identify the active compound more rapidly so that the purification process can be designed according to the physical properties of the target compound, which greatly saves time and consumables costs.

4.3.3. Target compound purification and NMR verification

According to the identification results, the target compound is flavone or 2-phenylchromen-4-one, the backbone of all flavonoids (Das, 1994). Compared with most other flavonoids, the absence of hydroxyl groups greatly increases its lipid solubility. Therefore, to find a suitable elution gradient, we dissolved a small amount of the methanol extract in n-hexane: acetone mixed in different proportions as described in section 4.2.7 and the undissolved precipitates were filtered and dissolved in an acetone methanol mixture, followed by TLC detection. It was found that the flavone in the methanol extract could be completely dissolved when the ratio of n-hexane to acetone was 7:3.

After dissolving the methanol extract using a mixture of n-hexane and acetone (7:3, v:v), we performed normal-phase silica gel column chromatography on the dissolved compounds. Then, using its lack of phenolic hydroxyl groups and its poor adsorption properties to aluminum oxide, the obtained crude flavone was further purified by aluminum oxide column chromatography, and

29 mg of pure product was obtained. The final yield of flavone in this study is approximately 2.9 mg/g (crude extracts, wet weight) and 280 mg/kg (original plant, dry weight). Compared with another related study, the yield of flavone was 7.3 mg, approximately 23.6 mg/kg (original plant, dry weight) (Aoyama et al., 2018). The purity of flavone in the final product is 96.06%, calculated by HPLC using the area normalization method (**Fig. 4.3**).

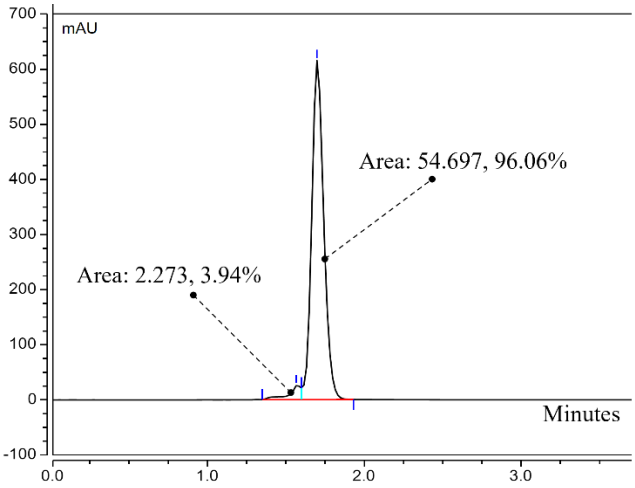

Fig. 4.3. HPLC chromatogram of flavone isolated from *Feijoa sellowiana* fruit peel. Due to partial overlap between peaks, this experiment calculated the peak area after segmentation (Light blue line).

To further validate the accuracy of the software identification results and to eliminate the possibility of non-ultraviolet absorbing impurities in the product, a Nuclear Magnetic Resonance (NMR) analysis was conducted on the obtained product. The ^{13}C spectrum is shown in **Fig. 4.4**, and the full ^{1}H, ^{13}C and DEPT spectra were given in the supplementary data. Chemical shifts are given in δ (ppm), marked on the corresponding positions in the structure. All chemical shifts matched previously reported data (Aksnes et al., 1996). No obvious impurity signal can be observed in the present spectra, indicating that the target compound has been successfully purified from other phytochemicals in the extract and the purity calculated with the HPLC was relatively accurate, and the accuracy of the Compound Discoverer identification result was also verified.

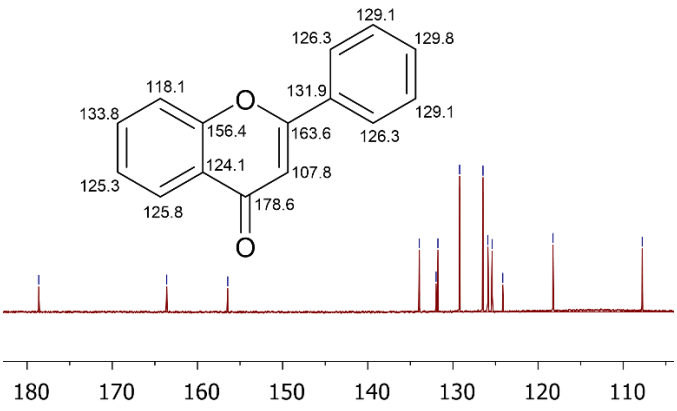

Fig. 4.4. ^{13}C NMR Spectrum (1D, 125 MHz, $CDCl_3$) of flavone isolated from *Feijoa sellowiana* fruit peel.

4.3.4. Antibacterial activity assessment

The antibacterial activity of isolated flavone was assessed by both TLC-bioautography and improved colorimetric broth dilution method. As shown in **Fig. 4.5**, flavone solutions were prepared in ten concentrations (475, 425, 375, 325, 275, 225, 175, 125, 75 and 25 μg/mL), and each concentration of the solutions was evenly spotted on the TLC plate (spot 1-10). The adsorption area of the sample on the TLC plate was fixed at approximately 0.16 cm^2 (example labelled in **Fig. 4.5A**) by controlling the spotting volume at a constant 3 μL in one shot. The MED of the tested sample was defined as the lowest amount that could maintain a clear inhibition zone after the direct bioautography assay described in section 4.2.5.

The inhibition effect of flavone against *S. aureus* (**Fig. 4.5B**) and *E. coli* (**Fig. 4.5C**) at 37 °C after 16 hours can be directly observed from the plates, namely the spot 5 in **Fig 4.5B** and spot 4 in **Fig 4.5C.** The solution concentrations corresponding to these two spots were 275 μg/mL against the *S. aureus* and 325 μg/mL against the *E. coli*, respectively. According to the spotted volume and adsorption area of the chemicals, the MED of flavone can be calculated, that is 4.2-5.2 μg/cm^2 against the *S. aureus* and 5.2-6.1 μg/cm^2 against the *E. coli*.

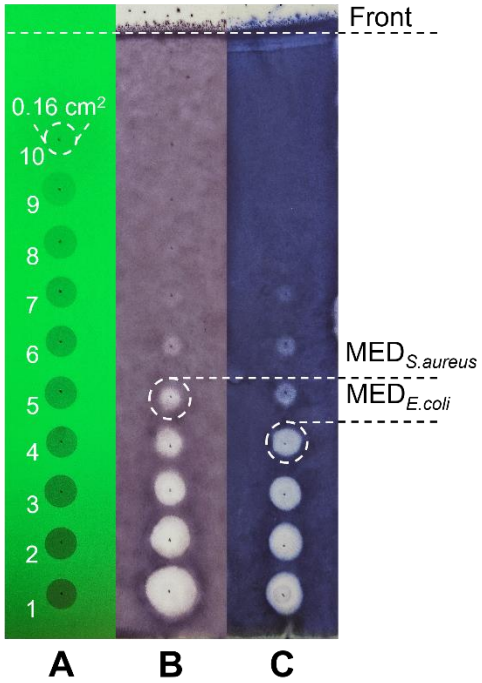

Fig. 4.5. Direct bioautography-based minimum effective dose (MED) determination. Spot 1-10 on each plate were serial diluted Flavone samples, constant 3 μL spotting to control an approximately 0.16 cm^2 sample area. The three pictures were: visualized under 254 nm UV light (**A**), inhibition effect

against *S. aureus* (**B**) and *E. coli* (**C**), 37 °C, 16 h.

The MIC testing of isolated flavone was initially followed by the conventional micro broth dilution method, the results were assessed via the employment of the microplate reader and HPLC. Two different types of results were therefore obtained, **Fig. 4.6A** was the inhibition curve read directly by a microplate reader after an overnight incubation, and the curve in **Fig. 4.6B** was obtained by an MTT assay (30 mins, 22 °C) performed immediately after the overnight incubation. The viable count was expressed as peak area measured through HPLC.

Due to the non-water solubility of flavone, even when using a solubilizer, turbidity can still be observed at concentrations higher than 175 μg/mL. Therefore, the MIC of flavone was obtained through the trend of the inhibition curve, that is 225-275 μg/mL against *S. aureus* and 325-375 μg/mL against *E. coli* (**Fig. 4.6A**). The function of the additional MTT assay was to eliminate the interference caused by sample turbidity. As shown in **Fig. 4.6B**, the MIC of flavone was further confirmed to be 225-275 μg/mL against *S. aureus* and 325-375 μg/mL against *E. coli.* Additionally, the Minimum Bactericidal Concentration (MBC, peak area close to zero) can also be found to be approximately 550-650 μg/mL against *S. aureus* (estimated by downward trend) and 375-425 μg/mL against *E. coli.*

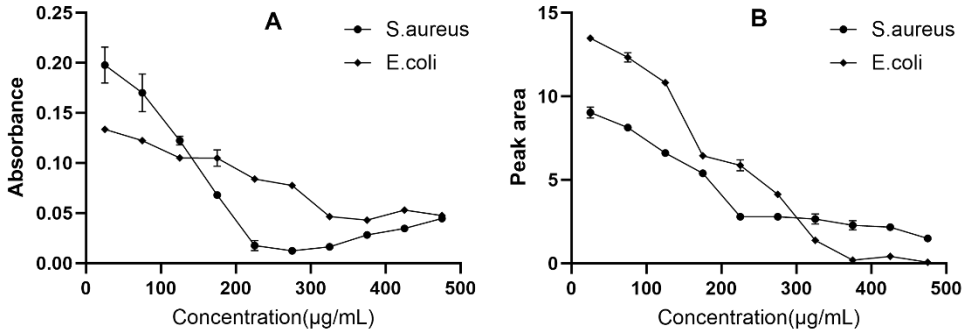

Fig. 4.6. Inhibition curves of flavone against *S. aureus* and *E. coli.* Diagram **A**: using broth microdilution method read by microplate reader; Diagram **B**: using colorimetric broth microdilution method read by HPLC (MTT assay, 30 mins, 22 °C).

The current study did not follow the colorimetric broth microdilution method described in other studies, with the outcomes being assessed through visual observation or via the employment of a microplate reader (Knezevic et al., 2018; Gattringer et al., 2002). According to the data presented in **Fig. 4.6B**, *S. aureus* curve, the tested sample demonstrated a strong inhibitory effect when compared to concentrations below 225 μg/mL. However, bacterial growth was still detectable using the MTT assay, the results were visually read as no inhibitory activity. On the other hand, the presence of turbidity caused by the limited water solubility of the flavone resulted in inaccurate readings when using a microplate reader. These issues and the HPLC-assist colorimetric antibacterial assay were discussed in our previous research (Xu et al., 2023).

4.4. Conclusion

The present study established a procedure to rapidly target, identify and isolate a pure bioactive component from the plant extract, and was employed to the waste part of feijoa (*Feijoa sellowiana*) fruit. The major antibacterial compound, flavone, from feijoa fruit peel extracts was targeted by direct TLC-bioautography, followed by UHPLC-HR-MS combined with Compound Discoverer 3.3 for the identification of the chemical structure, and lastly, a purification process was designed specifically for the physical properties of the identified compound. A total of 29 mg flavone with purity at around 96% was produced from 102 g of dried peels. The accuracy of the software identification and the purity of the isolated flavone was further verified by the NMR.

The antibacterial activity of flavone was assessed in this study by two improved methods. Namely, the TLC-bioautography-based MED determination and HPLC-assist colorimetric broth microdilution assay. The results have shown that the MED of flavone was 4.2-5.2 μg/cm^2 against the *S. aureus* and 5.2-6.1 μg/cm^2 against the *E. coli*; the MIC of flavone against the *S. aureus* and *E. coli* was 225-275 μg/mL and 325-375 μg/mL, respectively; the MBC were approximately 550-650 μg/mL against *S. aureus* and 375-425 μg/mL against *E. coli*.

In conclusion, this study proposed an enhanced bioassay-guided separation technique for the isolation of antibacterial compounds from plants, along with two improved methods for assessing the antibacterial efficacy of insoluble or colored compounds.

4.5. References

Aksnes, D. W., Standnes, A. & Andersen, Ø. M. 1996. Complete assignment of the 1H and 13C NMR spectra of flavone and its A-ring hydroxyl derivatives. *Magnetic Resonance in Chemistry*, 34, 820-823.

Aoyama, H., Sakagami, H. & Hatano, T. 2018. Three new flavonoids, proanthocyanidin, and accompanying phenolic constituents from Feijoa sellowiana. *Bioscience, Biotechnology, and Biochemistry*, 82, 31-41.

Basile, A., Conte, B., Rigano, D., Senatore, F. & Sorbo, S. 2010. Antibacterial and antifungal properties of acetonic extract of Feijoa sellowiana fruits and its effect on Helicobacter pylori growth. *Journal of Medicinal Food*, 13, 189-195.

Blaskovich, M. A., Butler, M. S. & Cooper, M. A. 2017. Polishing the tarnished silver bullet: the quest for new antibiotics. *Essays in biochemistry*, 61, 103-114.

Chandra, H., Bishnoi, P., Yadav, A., Patni, B., Mishra, A. P. & Nautiyal, A. R. 2017. Antimicrobial resistance and the alternative resources with special emphasis on plant-based antimicrobials—a review. *Plants*, 6, 16.

Chassagne, F., Samarakoon, T., Porras, G., Lyles, J. T., Dettweiler, M., Marquez, L., Salam, A. M., Shabih, S., Farrokhi, D. R. & Quave, C. L. 2021. A systematic review of plants with antibacterial activities: A taxonomic and phylogenetic perspective. *Frontiers in pharmacology*, 11, 2069.

Cheesman, M. J., Ilanko, A., Blonk, B. & Cock, I. E. 2017. Developing new antimicrobial therapies: are synergistic combinations of plant extracts/compounds with conventional antibiotics the solution? *Pharmacognosy reviews*, 11, 57.

Choma, I. M. & Grzelak, E. M. 2011. Bioautography detection in thin-layer chromatography. *Journal of Chromatography A*, 1218, 2684-2691.

Christenhusz, M. J. & Byng, J. W. 2016. The number of known plants species in the world and its annual increase. *Phytotaxa*, 261, 201–217-201–217.

Clarke, J. T., Warnock, R. C. & Donoghue, P. C. 2011. Establishing a time-scale for plant evolution. *New Phytologist*, 192, 266-301.

Das, D. K. 1994. Naturally occurring flavonoids: Structure, chemistry, and high-performance liquid chromatography methods for separation and characterization. *Methods in Enzymology.* Elsevier.

Das, K., Tiwari, R. & Shrivastava, D. 2010. Techniques for evaluation of medicinal plant products as antimicrobial agent: Current methods and future trends. *Journal of Medicinal Plants Research*, 4, 104-111.

Dewanjee, S., Gangopadhyay, M., Bhattacharya, N., Khanra, R. & Dua, T. K. 2015. Bioautography and its scope in the field of natural product chemistry. *Journal of Pharmaceutical Analysis*, 5, 75-84.

Figueroa, J. G., Borrás-Linares, I., Del Pino-García, R., Curiel, J. A., Lozano-Sánchez, J. & Segura-Carretero, A. 2021. Functional ingredient from avocado peel: Microwave-assisted extraction, characterization and potential applications for the food industry. *Food Chemistry*, 352, 129300.

Gattringer, R., Nikš, M., Ostertág, R., Schwarz, K., Medvedovic, H., Graninger, W. & Georgopoulos, A. 2002. Evaluation of MIDITECH automated colorimetric MIC reading for antimicrobial susceptibility testing. *Journal of antimicrobial chemotherapy*, 49, 651-659.

Jorgensen, J. H. & Turnidge, J. D. 2015. Susceptibility test methods: dilution and disk diffusion methods. *Manual of clinical microbiology*, 1253-1273.

Knezevic, P., Sabo, V. A., Simin, N., Lesjak, M. & Mimica-Dukic, N. 2018. A colorimetric broth microdilution method for assessment of Helicobacter pylori sensitivity to antimicrobial agents. *Journal of pharmaceutical and biomedical analysis*, 152, 271-278.

Lewis, K. 2013. Platforms for antibiotic discovery. *Nature reviews Drug discovery*, 12, 371-387.

Magallón, S. & Hilu, K. 2009. Land plants (embryophyta). *The timetree of life*, 133-137.

Oulkar, D., Singh, K. & Narayan, B. 2022. Characterization of different parts of litchi fruit using UHPLC-QExactive Orbitrap. *Journal of Food Science and Technology*, 59, 4889-4906.

Piovesana, S., Cavaliere, C., Cerrato, A., Montone, C. M., Laganà, A. & Capriotti, A. L. 2020. Developments and pitfalls in the characterization of phenolic compounds in food: From targeted analysis to metabolomics-based approaches. *TrAC Trends in Analytical Chemistry*, 133, 116083.

Prasad, M. A., Zolnik, C. P. & Molina, J. 2019. Leveraging phytochemicals: the plant phylogeny predicts sources of novel antibacterial compounds. *Future Science OA*, 5, FSO407.

Shi, D., Xu, W., Wong, M. & Popovich, D. G. 2023. An Improved Purification Method for Removing Colour Interference from 3-(4,5-Dimethylthiazol-2-yl)-2,5-diphenyl Tetrazolium Bromide (MTT) Antibacterial Assays. *Applied Sciences*, 13, 5067.

Wang, M., Zhang, Y., Wang, R., Wang, Z., Yang, B. & Kuang, H. 2021. An evolving technology that integrates classical methods with continuous technological developments: Thin-layer chromatography bioautography. *Molecules*, 26, 4647.

Wank, J., Wagner-Redeker, W., Taylor, A., Herbold, R. & Lassahn, P.-G. 2016. High-Resolution, Accurate Mass Measurements and Metabolite Identification: An Automated Approach Using Fragment Prediction in Combination with Fragment Ion Search (FISh). *Mass Spectrometry*, 28, 10.

Westh, H., Zinn, C. S., Rosdahl, V. T. & Group, S. S. 2004. An international multicenter study of antimicrobial consumption and resistance in Staphylococcus aureus isolates from 15 hospitals in 14 countries. *Microbial drug resistance*, 10, 169-176.

Xu, W., Shi, D., Chen, K., Palmer, J. & Popovich, D. G. 2023. An improved MTT colorimetric method for rapid viable bacteria counting. *Journal of Microbiological Methods*, 214, 106830.

Chapter Five

TLC-bioautography guided isolation and assessment of antibacterial compounds from Mānuka (*Leptospermum scoparium*) leaf and branch extracts.

The advanced methodologies introduced in Chapter 4, along with the novel thin-layer chromatography-based antimicrobial detection technique, were further validated in this chapter. Mānuka (*Leptospermum scoparium*) leaves and branches from various sources were studied, including an examination of their antibacterial capacity and the variations in antibacterial compounds.

This chapter has been published in the following peer-reviewed publication:

Xu, W., Shi, D., Chen, K., & Popovich, D. G. (2024). TLC-Bioautography-Guided isolation and assessment of antibacterial compounds from Mānuka (*Leptospermum scoparium*) leaf and branch extracts. *Molecules*, *29*(3), 717.

Statement of Contribution

<table>
<tr><td colspan="4">We, the student and the student's main supervisor, certify that all co-authors have consented to their work being included in the thesis and they have accepted the student's contribution as indicated below in the Statement of Originality.</td></tr>
<tr><td colspan="2">Student name:</td><td colspan="2">Wenliang Xu</td></tr>
<tr><td colspan="2">Name and title of main supervisor:</td><td colspan="2">Dr. David Popovich</td></tr>
<tr><td colspan="2">In which chapter is the manuscript/published work?</td><td colspan="2">Chapter Five</td></tr>
<tr><td colspan="2">What percentage of the manuscript/published work was contributed by the student?</td><td colspan="2">75%</td></tr>
<tr><td colspan="4">Describe the contribution that the student has made to the manuscript/published work:
Conceptualization; Data curation; Formal analysis; Visualization; Investigation; Methodology; Validation; Writing - original draft; Writing - review & editing.</td></tr>
<tr><td colspan="4">Please select one of the following three options:</td></tr>
<tr><td>✓</td><td colspan="3">The manuscript/published work is published or in press
Please provide the full reference of the research output:
Xu, W., Shi, D., Chen, K., & Popovich, D. G. (2024). TLC-Bioautography-Guided isolation and assessment of antibacterial compounds from Mānuka (Leptospermum scoparium) leaf and branch extracts. Molecules, 29(3), 717.</td></tr>
<tr><td></td><td colspan="3">The manuscript is currently under review for publication Please provide the name of the journal:</td></tr>
<tr><td></td><td colspan="3">It is intended that the manuscript will be published, but it has not yet been submitted to a journal</td></tr>
<tr><td colspan="2">Student's signature:</td><td>Wenliang Xu</td><td>Main supervisor's signature:</td></tr>
</table>

Abstract

A rapid procedure for the targeted isolation of antibacterial compounds from Mānuka (*Leptospermum scoparium*) leaf and branch extracts is described in this paper. Antibacterial compounds from three different Mānuka samples collected from New Zealand and China were compared. The active compounds were targeted by TLC-bioautography against *S. aureus* and were identified by HR-ESI-MS, and -MS/MS analysis in conjunction with Compound Discoverer 3.3 (ThermoFisher Scientific). The major antibacterial component, grandiflorone, was identified, along with 20 β-triketones, flavonoids, phloroglucinol derivatives. To verify the software identification, grandiflorone underwent purification via column chromatography, and its structure was elucidated through NMR analysis, ultimately confirming its identity as grandiflorone. This study successfully demonstrated that the leaves and branches remaining after Mānuka essential oil distillation serve as excellent sources for extracting grandiflorone. Additionally, we proposed an improved TLC-bioautography protocol for evaluating the antibacterial efficacy on solid surfaces, which is suitable for both *S. aureus* and *E. coli*. The minimum effective dose (MED) of grandiflorone was observed to be 0.29-0.59 μg/cm^2 against *S. aureus* and 2.34-4.68 μg/cm^2 against *E. coli*, respectively. Furthermore, the synthetic plant growth retardant, paclobutrazol, was isolated from the samples obtained in China. It is hypothesized that this compound may disrupt the synthesis pathway of triketones, consequently diminishing the antibacterial efficacy of Chinese Mānuka extract in comparison to that of New Zealand.

Keywords: Mānuka; *Leptospermum scoparium*; TLC-bioautography; LC-MS; Compound Discoverer; Grandiflorone; NMR; antibacterial activity.

5.1. Introduction

Leptospermum scoparium J.R. et G. Forst, also known as Mānuka, is a member of the family *Myrtaceae* which all species are woody and produce essential oils (Old, 2013). The Mānuka tree was originally growing throughout New Zealand (Stephens et al., 2005) and in eastern Australia (Thompson, 1989), and was used as herbal medicine by Māori people for hundreds of years (Dip and Kinesiology, 2013). This plant is well known as the source of essential oil and the nectar source for Mānuka honey. High concentrations of volatile triketones are characteristic compounds and the main antibacterial component in its essential oils (Porter and Wilkins, 1999; van Klink et al., 2005). The essential oil from the East Cape region of New Zealand's North Island is the most well-known (Perry et al., 1997; Douglas et al., 2004).

β-triketone, specifically grandiflorone (van Klink et al., 2005) is both antimicrobial and herbicidal (Dayan et al., 2007; Dayan et al., 2009). It only occurs in essential oils and is difficult to extract by steam distillation due to its low volatility (Porter and Wilkins, 1999; Perry et al., 1997; Douglas et al., 2004; Killeen et al., 2016). We speculated that the by-product left over after Mānuka essential oil production (steam-distilled Mānuka leaves and branches) could contain bioactive molecules, especially grandiflorone.

Mānuka is also widely cultured in southern and eastern China with a trade name 'Song Hongmei' or 'Australian Tea Tree' (An, 2015) as an ornamental shrub. The objective of this study was to rapidly identify and isolate antibacterial components in Mānuka leaves and branches that were surplus after essential oil extraction. At the same time, a comparative analysis of the antibacterial compounds in steam-distilled, untreated New Zealand Mānuka and untreated Chinese Mānuka was conducted. This study also aimed to establish a TLC-bioautography-based method to assess the antibacterial ability of tested compounds on the plate surface.

5.2. Materials and Methods

5.2.1. Chemicals and reagents

Methanol, n-hexane, dichloromethane, and acetone for extraction and chromatography were analytical research grade; acetonitrile, methanol, and formic acid used for instrumental analysis were LC-MS-grade (Merck, Germany). Chloroform-d (99.9%, Sigma-Aldrich, USA) was used for nuclear magnetic resonance (NMR). Normal phase thin-layer chromatography (TLC, silica gel F_{254}, 0.2 mm in thickness, aluminum sheets), silica gel for column chromatography (40 μm, Sigma-Aldrich, USA). 3-(4,5-Dimethylthiazol-2-yl)-2,5-Diphenyltetrazolium Bromide (MTT, 99%, AK Scientific, USA) stock solution, 5 mg/mL, and tetracycline (98%, Sigma-Aldrich, USA) stock

solution, 0.1 mg/mL, were prepared in sterile water and stored at 4 °C in the dark.

5.2.2. Plant material

Leptospermum scoparium samples were collected from New Zealand and China. New Zealand (NZ) Mānuka was harvested from the East Cape area of New Zealand provided by Mānuka Biologicals company, including untreated and steam-distilled samples (Essential oil distillation by-products). Chinese (CN) Mānuka was purchased from China Fujian province Longyan City and was untreated. The present study focused on the leaves and branches. Mānuka samples were air-dried and ground into a fine powder (60-80 mesh) by a grinding mill (HC-2000Y, Wuyi Haina Electric Appliance Co., Ltd, China). The dry weight of each sample was 200 g.

5.2.3. Extraction of phytochemicals

The powders of three Mānuka samples (untreated NZ Mānuka, steam-distilled NZ Mānuka, and untreated CN Mānuka) were extracted by 1000 mL of methanol in a Soxhlet extractor for 12 h, respectively. The temperature in the thimble during extraction was approximately 60 °C. Methanol extracts obtained from each sample were concentrated on a rotary evaporator at 35 °C to yield gum-like crude extracts. Then, the crude extracts were suspended in water, and liquid-liquid extracted by hexane and dichloromethane respectively, to separate compounds based on polarity.

5.2.4. Bacteria cultivation and conventional antibacterial assay

Gram-positive *Staphylococcus aureus* (ATCC 25923) and Gram-negative *Escherichia coli* (ATCC 25922) strains were used in this study. The strains were obtained from the Microbiology Department, Massey University, and stored in brain heart infusion (BHI, Difco) agar slants at 4 °C. For each experiment, a single colony was freshly picked and cultured in BHI broth at 37 °C for 24 hours.

The broth microdilution method was employed to assess the minimum inhibition concentration (MIC) of purified compounds. The assay was performed on a 96-well plate, bacterial suspensions were 100 times diluted after overnight culture, tested samples were 2-fold diluted from 500 μg/mL, and tetracycline (100 μg/mL) was used as positive control. The lowest concentration that remained clear after overnight incubation was determined as the MIC.

5.2.5. TLC analysis and direct bioautography

5.2.5.1. TLC analysis

The hexane and dichloromethane extracts were dissolved at a concentration of 1 mg/mL for TLC analysis. A mixture of n-hexane and acetone (7:3, v:v) was used as the developing agent. The analysis was performed in a rectangular TLC developing chamber. The chamber was shaken with the developing agent and sealed with parafilm while developing. The plates were removed when the solvent front had moved to 90% of the total plate length (10 cm) and subsequently allowed to dry. The results were visualized under 254 nm UV light (Dark Box UV lamp, Qiwei ZF-1, China) followed by UV sterilization and bioautography experiments.

5.2.5.2. Conventional direct TLC bioautography

Direct bioautography was performed by the procedure described in the published articles (Wang et al., 2021; Dewanjee et al., 2015). A bacterial suspension with an optical density of 1.2 was newly prepared before each test. TLC plates with separated compounds were dried in a fume hood overnight, sterilized with UV light for 20 minutes and immersed in the bacterial suspension for 10 seconds and stored in a glass container, wrapped with aluminum foil. For TLC with *S. aureus*, the wrapped containers were directly incubated at 37 °C for 16 hours. For TLC with *E. coli*, the inner walls of the container were sprayed with a layer of water mist, and water-saturated absorbent cotton (10 mL) was placed in the corner of the container before wrapping, then incubated at 37 °C for 16 hours in total. It was discovered that this treatment method can best ensure the effective duration of the experiment and the best survival of bacteria. For visualization of microbial growth, MTT solution was sprayed onto the plates and re-incubated at 37 °C for 3 h. Clear white zones against a bluish-violet background on the TLC plate indicate the anti-microbial activity of the compounds (Choma and Grzelak, 2011; Das et al., 2010; Dewanjee et al., 2015), the white zone is referred to as the inhibition zone in this study.

5.2.5.3. Direct bioautography-based minimum effective dose determination.

This experiment determined the minimum effective dose (MED) of tested chemicals by continuously reducing the amount of sample spotted. The minimum dose that maintains a clear inhibition zone on the plate after 16-20 hours was defined as the MED. To ensure that the sample area on the TLC plate is consistent, the spotting volume throughout the study was unified to 3 μL, and a pipette was used to complete the spotting. The tested sample solutions were first diluted into several concentration gradients, then cultured and stained as described in the above-mentioned procedures after spotting.

5.2.6. Rapid identification of antibacterial compounds

The main compound(s) related to an inhibition zone were selected as the target compounds in this study. For rapid identification, each target compound to be analyzed was located by retention

factor (R_f) value and was collected by scraping the silica gel from other newly developed TLC plates without bacteria and flushed with acetone. The hexane and dichloromethane extracts (1 mg/mL) and each collected target compound were analyzed by UHPLC-HR-MS (Thermofisher Dionex Ultimate 3000 High-Performance Liquid Chromatography and Q Executive Focus High-Resolution Mass Spectrometer) and identified through online database matching performed by Compound Discoverer 3.3. The results obtained were further revised with reference to the reported chemical composition of Mānuka accomplished by other researchers (Chan et al., 2013; Häberlein and Tschiersch, 1998; Mayer, 1990; Häberlein and Tschiersch, 1994). The separation was performed using a Thermofisher Hypersil GOLD C18 Column, 100 × 2.1 mm, particle size 1.9 μm. Solvent A water/0.1% formic acid, solvent B acetonitrile/0.1% formic acid. Running method for hexane extracts: 0-4 min 5%-45% B, 4-8 min 45% B, 8-16 min 45%-95% B, 16-25 min 95% B, 25-26 min 95%-5% B, 26-30 min 5% B, 0.2 mL/min flow rate. Running method for dichloromethane extracts: 0-3 min 5% B, 3-15 min 5%-95% B, 15-18 min 95% B, 18-23 min 95%-5% B, 0.3 mL/min flow rate. The inject volume was set to 5 μL, column oven was maintained at 25 °C. Mass spectra were acquired under an electrospray ionization (ESI) source in both positive and negative ionization modes through full MS and data-dependent MS/MS analysis. The optimal MS parameters were set as follows: spray voltage, 2.5 kV; capillary temperature, 350 °C; sheath gas, 35 units; auxiliary gas, 10 units; auxiliary gas heater temperature, 200 °C; sweep gas, 5 units; collision energy, 30 eV. The mass range was set from 120 to 1500 m/z at a resolution of 70,000.

5.2.7. Major active compounds purification

Normal phase silica gel column chromatography was used to isolate the major active compounds related to the maximal inhibition zone. The hexane extracts ~3 g were loaded on a manually packed column (4 cm diameter, 50g silica gel), with eluent n-hexane: dichloromethane (10:0 to 9.5:0.5 to 8.5:1.5, v:v). Semi-purified compounds were subjected to another column (1 cm diameter, 10 g silica gel), with eluent n-hexane: dichloromethane (9.5:0.5 to 9.4:0.6 to 9.3:0.7, v:v). The purity of the isolated compound was measured by HPLC using the area normalization method on triplicate experiments, the detection was with a DAD (diode array detector, Dionex, Ultimate 3000) at 220 nm and 254 nm respectively, performed in the same column described in section 5.2.6. Running method: linear increases acetonitrile from 45% to 95% in water, 10 mins, 5 μL inject volume, 0.2 mL/min flow rate at 25 °C.

5.2.8. Nuclear magnetic resonance (NMR)

To confirm the structure of key active compounds identified by Compound Discoverer and detect non-UV-active organic impurities from the extract, ^{1}H (500 MHz), ^{13}C (125 MHz), and DEPT 135° NMR analyses were conducted using a Bruker AV 500 spectrometer. The analyte was prepared in chloroform-d. The chemical shifts were reported in parts per million (ppm) downfield

from Tetramethylsilane (TMS).

5.2.9. Data acquisition and software analysis

Images of TLC plates were processed by ImageJ (National Institutes of Health, USA, version 1.53t). The chemical structure diagrams were edited using ChemBioDraw (CambridgeSoft, USA, version 14.0). The Mass data acquisition and analysis were performed by Xcalibur (Thermofisher, USA, version 4.4). The compound identification was performed by Compound Discoverer (Thermofisher, USA, version 3.3), through ChemSpider, mzCloud, mzVault and Mass List library matching. The NMR spectrum was analyzed by MestReNova (Mestrelab Research, Spain, version 6.1.0).

5.3. Results and Discussion

5.3.1. Analysis of β-triketones

This experiment simultaneously analyzed and compared the antibacterial compounds in hexane extracts of three different Mānuka samples. The hexane extract of untreated CN Mānuka (**Fig. 5.1-I**), untreated NZ Mānuka (**Fig. 5.1-II**) and steam-distilled NZ Mānuka (**Fig. 5.1-III**) exhibited different antibacterial effects. Under the same concentration (1 mg/mL) and the same spotting volume (3 μL), no clear inhibition zone can be observed from the CN untreated Mānuka sample. Therefore, we analyzed the corresponding compounds in the inhibition zone displayed by two NZ Mānuka samples. The identical TLC separation was repeated five times, and the compounds in the center of each inhibitory zone were collected based on the R_f value. Through LC-MS and Compound Discoverer analysis, we discovered that there are 4 inhibition zones that were formed by a single main compound, the other inhibition zones were caused by complex mixtures. The position collected and the structure of major active compounds (**1**-**4**) are displayed in **Fig. 5.1.**

The four major antibacterial compounds are leptospermone (**1a**) and isoleptospermone (**1b**), a pair of isomers, that were unable to be separated by current TLC and HPLC method; flavesone (**2**), grandiflorone (**3**) and myrigalone A (**4**). These compounds belong to β-triketones and are the main antibacterial ingredients in Mānuka (van Klink et al., 1999; Killeen et al., 2016). Among them, **1a**, **1b** and **2** are also characteristic components in Mānuka essential oils (Porter and Wilkins, 1999; van Klink et al., 2005).

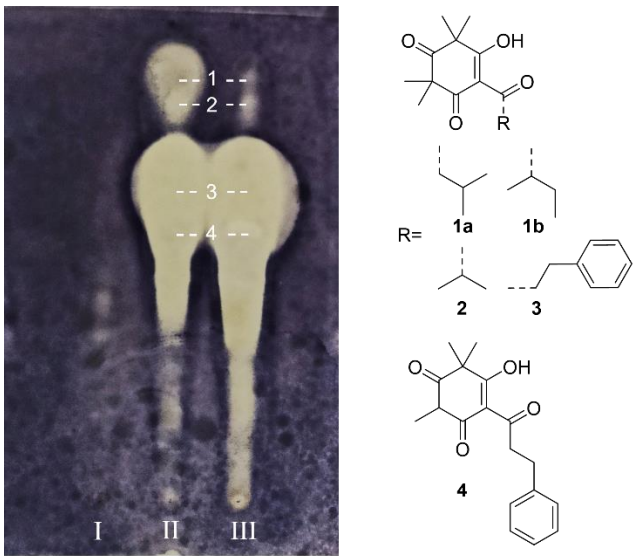

Fig. 5.1. Bioautography assay of Mānuka hexane extract (1 mg/mL, 3 µL spotting) against *S. aureus* at 37 °C, 16 hours. Sample **I**: untreated CN Mānuka; Sample **II**: untreated NZ Mānuka; Sample **III**: steam-distilled NZ Mānuka. Compounds **1**-**4** are β-triketones detected from the corresponding inhibition zones, including: a pair of isomers leptospermone (**1a**) and isoleptospermone (**1b**); flavesone (**2**); grandiflorone (**3**); myrigalone A (**4**).

Mass spectrometry analysis of two NZ Mānuka hexane extracts (**Fig. 5.2**) also revealed that the untreated sample contained high concentrations of five β-triketones (**Fig. 5.2A**), while only (**3**) and (**4**) could be detected in significant amounts in the steam-distilled sample (**Fig. 5.2B**). The extraction of grandiflorone (**3**) and myrigalone A (**4**) through steam distillation is challenging due to the presence of benzene-containing substituents in their structure, which elevate their boiling point. Consequently, a significant quantity of these compounds persists in the leaves and branches after Mānuka essential oil extraction.

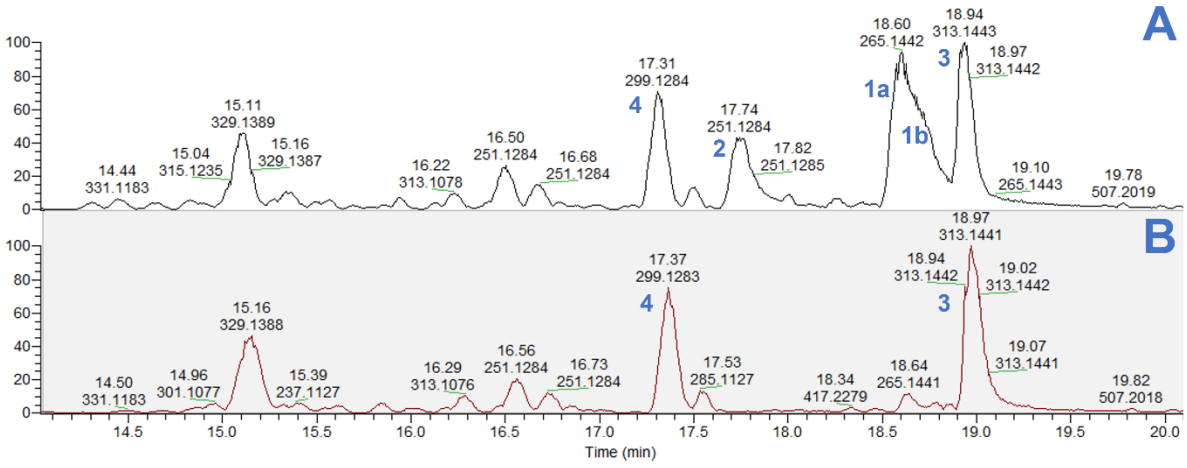

Fig. 5.2. Negative mode base peak chromatogram of untreated (**A**) and steam-distilled (**B**) NZ Mānuka hexane extract. Compound (**1**): a pair of isomers, leptospermone (**a**) and isoleptospermone (**b**); Compound **2**-**4**: flavesone (**2**); grandiflorone (**3**); myrigalone A (**4**).

Interestingly, in the R_f 0-0.5 area of the TLC plate in **Fig. 5.1**, steam-distilled Mānuka contains significantly more antibacterial compounds than untreated Mānuka. Due to the complex components, the present study has not conducted a detailed analysis of its chemical structure conversion. However, this result still demonstrated that heating may be an effective way to enhance the antibacterial ability of Mānuka products.

5.3.2. Analysis of flavonoids and phloroglucinol derivatives

It was noted that when the sample spotting amounts were the same (1 mg/mL, 3 µL spotting), the content of antibacterial ingredients in CN Mānuka was almost unobservable, while the inhibition zones displayed by the two NZ Mānuka extracts were significantly greater than CN sample and showed obvious overlap. In LC-MS analysis, we found that the dichloromethane-extracted compounds of two Mānuka samples were almost identical. In this section, we selected the steam-distilled NZ Mānuka samples (0.5 mg/mL, 3 µL spotting) to compare with CN Mānuka samples (1 mg/mL, 3×3 µL spotting). The spotting volume was adjusted to allow all samples to present clearer inhibition zones, as shown in **Fig. 5.3.** Despite this, we still did not isolate more active compounds from the hexane extract of NZ Mānuka (**Fig. 5.3A-I**), and like the previous analysis, no clear inhibition zone can be observed from the hexane extract of CN Mānuka (**Fig. 5.3B-I**).

Six antibacterial flavonoids were identified from the dichloromethane extract of NZ Mānuka (**Fig. 5.3A-II**). The antibacterial compounds isolated from the dichloromethane extract of CN Mānuka (**Fig. 5.3B-II**) were largely the same as those in NZ Mānuka and include two additional active compounds (**7**) and (**10**) that are different from NZ Mānuka. The structures of isolated compounds and their positions on TLC are displayed in **Fig. 5.3.**

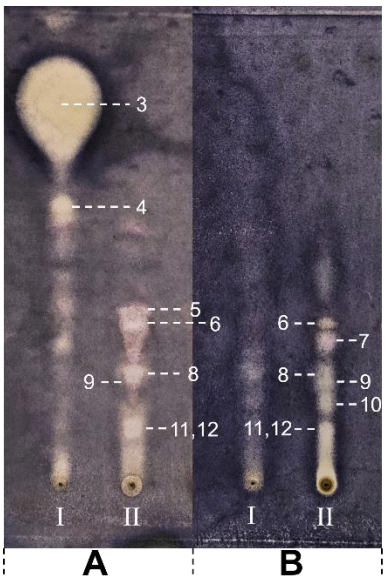

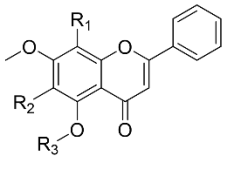

	R_1	R_2	R_3
5	H	Me	Me
6	H	H	Me
9	Me	Me	H
12	H	Me	H

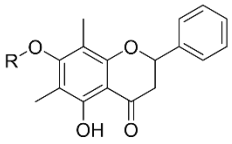

	R
8	Me
11	H

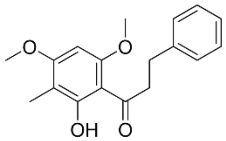

7

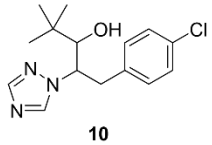

10

Fig. 5.3. Bioautography assay of steam-distilled NZ Mānuka (**A**, 0.5 mg/mL, 3 µL spotting) and untreated CN Mānuka (**B**, 1 mg/mL, 3×3 µL spotting) extract against *Staphylococcus aureus* at 37 °C, 24 hours. Sample **I**: hexane extract; Sample **II**: untreated NZ Mānuka. Compounds **3**-**12** are chemicals detected from the corresponding inhibition zones including: β-triketones (**3**) and (**4**); phloroglucinol derivative (**7**); synthetic plant growth retardant, paclobutrazol (**10**); flavonoids (**5**, **6**, **8**, **9**, **11** and **12**).

The LC-MS analysis revealed that the NZ Mānuka (**Fig. 5.4A**) contains significantly more types of flavonoids compared with CN Mānuka (**Fig. 5.4B**). Compound (**7**) is a phloroglucinol derivative and was only present in CN Mānuka. However, compound (**10**) was identified as paclobutrazol, a synthetic chemical used as a plant growth retardant and fungicide (Tesfahun, 2018). The CN Mānuka utilized in this study was cultivated as an ornamental plant in China; thus, the discovery of paclobutrazol was not unexpected. It is worth noting that this study did not find β-triketones, the characteristic components of Mānuka, from CN Mānuka. The flavonoid content was also much less than NZ Mānuka. This result is probably caused by the use of paclobutrazol.

The other flavonoids and phloroglucinol derivatives (**13**-**21**) with low content or not collected from the inhibition zone are identified and displayed in **Fig. 5.5.**

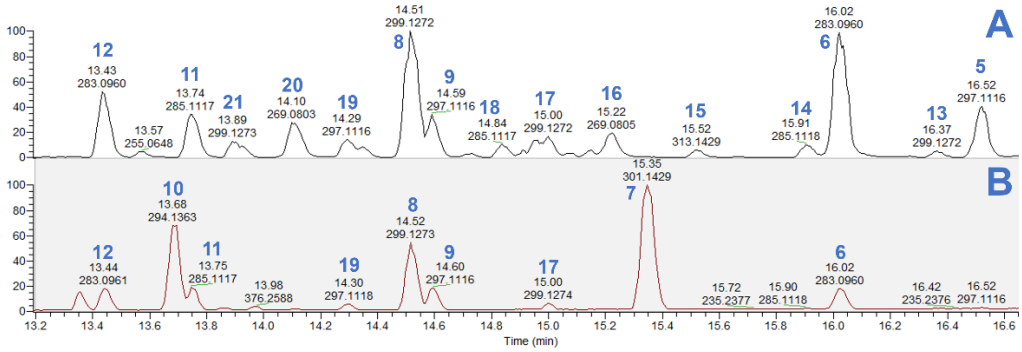

Fig. 5.4. Positive mode base peak chromatogram of NZ (**A**) and CN (**B**) Mānuka dichloromethane extract. Compounds **5**-**12**: chemicals detected from the corresponding inhibition zones shown in **Fig. 5.3.** Compounds **13**-**21**: flavonoids and phloroglucinol derivatives identified that have not been collected from bioautography assay, structures shown in **Fig. 5.5.**

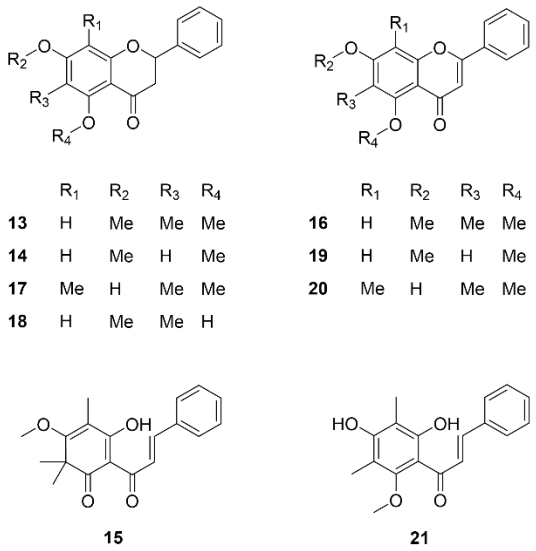

Fig. 5.5. Chemical structures of low-content or inactive flavonoids (**13**,**14**, **16**-**20**) and phloroglucinol derivatives (**15** and **21**) identified from NZ Mānuka dichloromethane extract.

5.3.3. Major active compound purification and NMR verification

The bioautography assay (above) and matching of fragmentation patterns have determined that grandiflorone (**3**) was the primary antibacterial compound present in steam-distilled Mānuka. Consequently, this section aims to validate the identification results and investigate the potential for rapid purification of grandiflorone by employing the most straightforward and expeditious method, followed by structural verification using NMR.

Two steps of normal phase silica gel column chromatography yielded around 30 mg of grandiflorone (**3)** from steam-distilled NZ Mānuka and an NMR analysis was carried on the obtained product, the ^{13}C spectrum is shown in **Fig. 5.6**, and the full ^{1}H, ^{13}C and DEPT spectra are given in the supplementary data. Chemical shifts are given in δ (ppm). Compound **3** was confirmed to be grandiflorone. All chemical shifts matched previously reported data (van Klink et al., 1999). No obvious impurity signal can be observed in both the present spectra and HPLC detection, indicating that the target compound has been successfully purified from other phytochemicals.

The identical purification procedures were applied to untreated Mānuka as well, however, the purity of the resulting grandiflorone was significantly lower compared to the utilization of steam-distilled Mānuka. This outcome suggests that the process of extracting essential oil played a crucial role in concentrating the non-volatile β-triketones in plant materials, such as grandiflorone. Steam distillation rendered the by-product of Mānuka essential oil extraction a valuable source for extracting grandiflorone.

No.	δ (ppm)	No.	δ (ppm)
1	109.4	7	203.7
2	198.8	8	41.1
3	51.9	9	31.0
3-CH_3	24.5	10	140.6
4	210.0	11,(15)	128.6
5	57.0	12,(14)	128.6
5-CH_3	23.9	13	126.4
6	196.8		

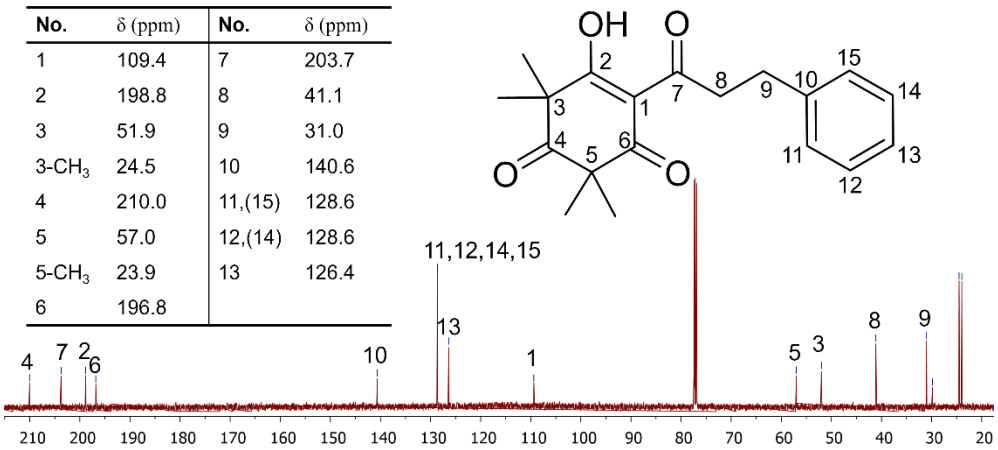

Fig. 5.6. ^{13}C NMR Spectrum (1D, 125 MHz, $CDCl_3$) of grandiflorone isolated from steam-distilled NZ Mānuka leaves and branches.

5.3.4. Minimum effective dose of grandiflorone

Different from conventional MIC testing, the minimum effective dose (MED) was defined in this study by the lowest amount of the tested sample to maintain an inhibition zone on the plate surface after 16-20 hours. As shown in **Fig. 5.7**, after eight consecutive twofold diluted of the grandiflorone (1 mg/mL), the solution of each concentration was evenly spotted on the TLC plate (**Fig. 5.7**, Sample **I**). The adsorption area of the sample on the TLC plate is fixed at approximately 0.16 cm^2 (example labelled in **Fig. 5.7A**) by controlling the spotting volume at a constant 3 µL in one shot. This procedure is subsequently followed by the conventional direct bioautography method, as detailed in Section 5.2.5. Tetracycline (0.1 mg/mL, **Fig. 5.7**, Sample **II**), was used as positive control and was subjected to the same treatment as grandiflorone.

The inhibition effect of grandiflorone against *S. aureus* (**Fig. 5.7A-I**) and *E. coli* (**Fig. 5.7B-I**) at 37°C after 16 hours can be directly observed from the plates. The spotted solution concentrations corresponding to the last clear inhibition zone are 31.25 µg/mL to the *S. aureus* and 250 µg/mL to the *E. coli*, respectively. According to the spotted volume and adsorption area of the chemicals, the MED of grandiflorone can be calculated, as 0.29 - 0.59 µg/cm^2 against *S. aureus* and 2.34 - 4.68 µg/cm^2 against *E. coli*.

As a comparison, the minimum inhibitory concentration (MIC) of isolated grandiflorone was measured by conventional micro broth dilution method, the MIC value against *S. aureus* and *E. coli* was 15.63 - 31.25 µg/mL and 250 - 500 µg/mL, respectively, as expected from previous reports (Killeen et al., 2016; van Klink et al., 2005). The results of the two experiments were close, grandiflorone showed a potent inhibition effect against *S. aureus* while requiring about 10 times the dose against *E. coli.* From our existing data, TLC-MED determination requires much less sample amount than conventional MIC testing, and the results were clear. The present study

discovered that it is very suitable for non-water-soluble compound testing and solved the interference caused by certain compounds having a strong color in liquid which can interfere with the absorbance reading.

The sustained antibacterial effect of grandiflorone was also recorded. **Fig. 5.7D** and **5.7E** exhibited the inhibition zones after 40 hours of incubation, even at the highest dose, the effect against *E. coli* was completely disappeared (**Fig. 5.7E-I**), while the effect against *S. aureus* just started dissipating (**Fig. 5.7D-I**), until the TLC plate dried out (greater than 48 hours). It can be inferred that bacteria will progressively occupy the inhibition zones over a certain period. Consequently, in forthcoming research, we intend to investigate the time necessary for the inhibition zone to be colonized by bacteria at a specific molar dosage. This parameter will serve as an evaluative measure of the compound's susceptibility.

Like the disk diffusion method, the TLC-MED determination is also an observation of the inhibition zone, but we do not think that the diffusion diameter of the zones has a strong correlation with the antibacterial ability of the compound tested. Both experiments share a common shortcoming: the size of the zones is also affected by the diffusion ability of the sample on the attached matrix. As shown in **Fig. 5.7B** and **5.7C**, either against *S. aureus* or *E. coli*, there is a significant difference in the diameter of the inhibition zone of sample **I** (grandiflorone) from high dose to low dose. However, the difference in the diameter of the inhibition zone presented by sample **II** (tetracycline) within the effective dose range was not obvious. This finding contradicts the observations made in previous experiments conducted with the disk diffusion method. In the case of conventional water-based semisolid media, the non-polar compound grandiflorone exhibited insolubility, impeding its diffusion, whereas tetracycline demonstrated efficient diffusion. Conversely, on the TLC plate, the silica gel became saturated with the liquid culture medium, facilitating the desorption and diffusion of non-polar compounds. Therefore, the size of the inhibition zone was not employed as a parameter to assess antibacterial efficacy in this study.

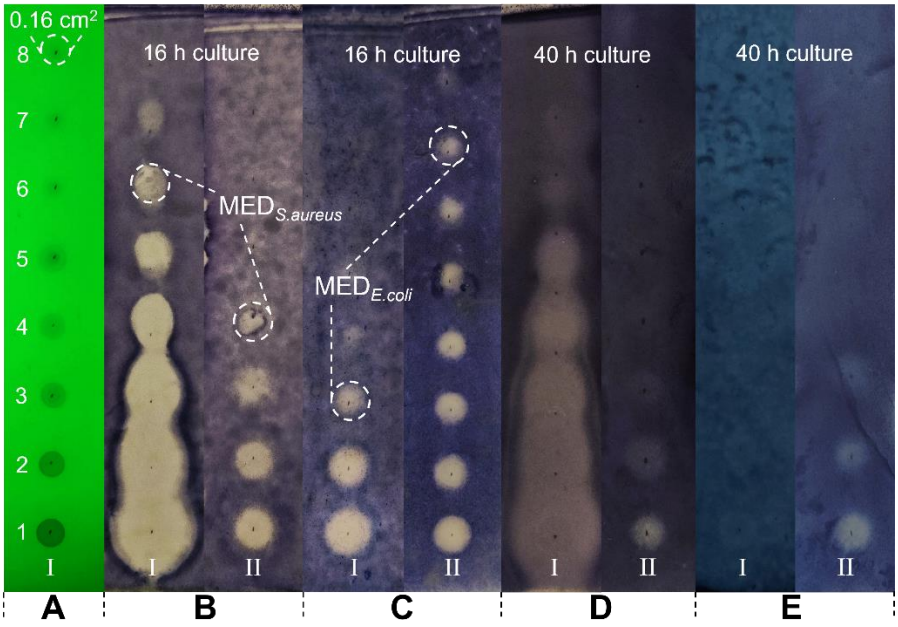

Fig. 5.7. Direct bioautography-based minimum effective dose (MED) determination. Spot 1-8 on each plate were twofold diluted samples, constant 3 μL spotting to control an approximately 0.16 cm^2 sample area. Visualized under 254 nm UV light (**A**), inhibition effect against *S. aureus* (**B**, 37 °C, 16 h; **D**, 37 °C, 40 h) and *E. coli* (**C**, 37 °C, 16 h; **E**, 37 °C, 40 h). Sample **I**: grandiflorone, initial concentration 1 mg/mL; Sample **II**: tetracycline, initial concentration 0.1 mg/mL.

5.4. Conclusion

The present study rapidly targeted and identified the antibacterial compounds presented in untreated, steam-distilled NZ Mānuka and untreated CN Mānuka respectively. A total of **22** compounds were identified through LC-MS analysis and by matching with Compound Discoverer library, included β-triketones (**1a**, **1b** and **2-4**), flavonoids (**5**, **6**, **8**, **9**, **11-14** and **16-20**), phloroglucinol derivatives (**7**, **15** and **21**), and a synthetical plant growth retardant (**10**). Compounds **1-12** were the major antibacterial compounds isolated through direct TLC-bioautography-guided separation. Among them, five β-triketones were only detectable in two NZ Mānuka samples, compounds (**7** and **10**) were only present in CN Mānuka and the types of flavonoids detected in CN Mānuka were also much less than those in NZ Mānuka. The reason for this phenomenon may be that a large amount of growth retardant (**10**) was applied to CN Mānuka which was cultured as ornamental plants. Compounds **13-21** were low-content or inactive flavonoids and phloroglucinol derivatives identified through LC-MS analysis directly.

The comparative TLC and LC-MS analysis between untreated and steam-distilled NZ Mānuka revealed that a large amount of grandiflorone (**3**) and myrigalone A (**4**) remained in the leaves and branches after Mānuka essential oil extraction, due to their low volatility. The column chromatography was conducted to purify grandiflorone (**3**) identified by LC-MS analysis, from both untreated and steam-distilled NZ Mānuka. Subsequently, NMR analysis confirmed that

compound **3** was indeed grandiflorone. Notably, the results of this purification process demonstrated that steam distillation treatment significantly alleviated the challenges associated with purifying grandiflorone. Consequently, Mānuka leaves and branches, which are retained after essential oil production, emerged as a more favorable source for extracting grandiflorone compared to fresh Mānuka.

An improved TLC-bioautography protocol was described for assessing the antibacterial ability of grandiflorone. The minimum effective dose (MED) was observed to be 0.29 - 0.59 μg/cm^2 against *S. aureus* and 2.34 - 4.68 μg/cm^2 against *E. coli*. The enhanced protocol demonstrated suitability for both *S. aureus* and *E. coli.* The obtained results were unambiguous and intuitive, and remained unaffected by the solubility, diffusion capacity, or color of the test compounds, in contrast to the conventional antibacterial assay.

5.5. References

An, F. 2015. *Characteristics and uses of common ornamental shrubs*, Yunnan University Press.

Chan, C. W., Deadman, B. J., Manley-Harris, M., Wilkins, A. L., Alber, D. G. & Harry, E. 2013. Analysis of the flavonoid component of bioactive New Zealand mānuka (Leptospermum scoparium) honey and the isolation, characterisation and synthesis of an unusual pyrrole. *Food Chem*, 141, 1772-81.

Choma, I. M. & Grzelak, E. M. 2011. Bioautography detection in thin-layer chromatography. *Journal of Chromatography A*, 1218, 2684-2691.

Das, K., Tiwari, R. & Shrivastava, D. 2010. Techniques for evaluation of medicinal plant products as antimicrobial agent: Current methods and future trends. *Journal of Medicinal Plants Research*, 4, 104-111.

Dayan, F. E., Duke, S. O., Sauldubois, A., Singh, N., McCurdy, C. & Cantrell, C. 2007. p-Hydroxyphenylpyruvate dioxygenase is a herbicidal target site for beta-triketones from Leptospermum scoparium. *Phytochemistry*, 68, 2004-14.

Dayan, F. E., Singh, N., McCurdy, C. R., Godfrey, C. A., Larsen, L., Weavers, R. T., Van Klink, J. W. & Perry, N. B. 2009. β-triketone inhibitors of plant p-hydroxyphenylpyruvate dioxygenase: Modeling and comparative molecular field analysis of their interactions. *Journal of agricultural and food chemistry*, 57, 5194-5200.

Dewanjee, S., Gangopadhyay, M., Bhattacharya, N., Khanra, R. & Dua, T. K. 2015. Bioautography and its scope in the field of natural product chemistry. *Journal of Pharmaceutical Analysis*, 5, 75-84.

Dip, H. & Kinesiology, C. I. 2013. The Medicine of the Mānuka.

Douglas, M. H., van Klink, J. W., Smallfield, B. M., Perry, N. B., Anderson, R. E., Johnstone, P. & Weavers, R. T. 2004. Essential oils from New Zealand mānuka: triketone and other chemotypes of Leptospermum scoparium. *Phytochemistry*, 65, 1255-64.

Häberlein, H. & Tschiersch, K.-P. 1994. Triterpenoids and flavonoids from Leptospermum scoparium. *Phytochemistry*, 35, 765-768.

Häberlein, H. & Tschiersch, K.-P. 1998. On the occurrence of methylated and methoxylated flavonoids in Leptospermum scoparium. *Biochemical Systematics and Ecology*, 26, 97-103.

Killeen, D. P., Larsen, L., Dayan, F. E., Gordon, K. C., Perry, N. B. & van Klink, J. W. 2016. Nortriketones: Antimicrobial Trimethylated Acylphloroglucinols from Mānuka (Leptospermum scoparium). *J Nat Prod*, 79, 564-9.

Mayer, R. 1990. Flavonoids from Leptospermum scoparium. *Phytochemistry*, 29, 1340-1342.

Old, N. 2013. The Medicine of the Mānuka: an investigation of the usages and methods for utilization of honey derived from the pollen of leptospermum scoparium in holistic nursing practice. *Journal of Holistic Nursing*, 31, 200-203.

Perry, N. B., Brennan, N. J., Van Klink, J. W., Harris, W., Douglas, M. H., McGimpsey, J. A., Smallfield, B. M. & Anderson, R. E. 1997. Essential oils from New Zealand mānuka and kānuka: chemotaxonomy of Leptospermum. *Phytochemistry*, 44, 1485-1494.

Porter, N. G. & Wilkins, A. L. 1999. Chemical, physical and antimicrobial properties of essential oils of Leptospermum scoparium and Kunzea ericoides. *Phytochemistry*, 50, 407-15.

Stephens, J. M., Molan, P. C. & Clarkson, B. D. 2005. A review of Leptospermum scoparium (Myrtaceae) in New Zealand. *New Zealand Journal of Botany*, 43, 431-449.

Tesfahun, W. 2018. A review on: Response of crops to paclobutrazol application. *Cogent Food & Agriculture*, 4, 1525169.

Thompson, J. 1989. A revision of the genus Leptospermum (Myrtaceae). *Telopea*, 3, 301-448.

van Klink, J. W., Brophy, J. J., Perry, N. B. & Weavers, R. T. 1999. beta-triketones from myrtaceae: isoleptospermone from leptospermum scoparium and papuanone from corymbia dallachiana. *J Nat Prod*, 62, 487-9.

van Klink, J. W., Larsen, L., Perry, N. B., Weavers, R. T., Cook, G. M., Bremer, P. J., MacKenzie, A. D. & Kirikae, T. 2005. Triketones active against antibiotic-resistant bacteria: Synthesis, structure–activity relationships, and mode of action. *Bioorganic & medicinal chemistry*, 13, 6651-6662.

Wang, M., Zhang, Y., Wang, R., Wang, Z., Yang, B. & Kuang, H. 2021. An evolving technology that integrates classical methods with continuous technological developments: Thin-layer chromatography bioautography. *Molecules*, 26, 4647.

Chapter Six

General conclusion, highlights, limitations, and directions for future work.

6.1. General conclusions

In this thesis, a comprehensive research compilation of the naturally occurring hybrid compounds from the *Myrtaceae* family was accomplished. It included a detailed classification of their chemical structures and an in-depth discussion on their reported bioactivities. The structure-activity relationship based on existing research was also discussed.

In the experimental section, the existing bacterial assay methods were optimized in order to accurately evaluate compounds isolated from selected samples, with the aim of minimizing any potential interference arising from insoluble matter and the color of the test compounds. Firstly, an improved MTT assay protocol and an equation that establishes the correlation between colony-forming units (CFU) and the amount of formazan converted by the bacteria, were elaborated. This protocol was developed following an extensive review of numerous published protocols. It comprehensively enumerates all currently identified factors that may cause interference and provides detailed guidance on how to mitigate them, thereby facilitating the accurate quantification of formazan. Taking advantage of HPLC analysis, the precise quantification of formazan facilitates the accurate determination of CFUs, potentially obviating the necessity for protracted and repetitive plate-counting procedures in extended experiments. Secondly, an improved direct TLC-bioautography-guided isolation and identification of antibacterial compounds were conducted on two selected waste products from *Myrtaceae* plants, namely feijoa fruit peels and steam-distilled/untreated mānuka leaves and branches. The antibacterial compounds, flavone, from feijoa fruit peel, and a total of **22** compounds from mānuka were identified by UHPLC-HR-MS combined with Compound Discoverer 3.3. Namely, this experiment facilitates the separation and activity determination of compounds via a straightforward and expeditious TLC method, followed by structural identification through mass spectrometry and database comparison. This approach significantly reduces the time required compared to traditional methods, and the expanding online databases enhance the practicality and reliability of software-based compound identification. The flavone in the feijoa sample and grandiflorone, the lead antibacterial compound in the mānuka sample, were purified and further verified by NMR. Finally, the innovative TLC-bioautography-based MED determination was conducted on both isolates. This method offers an innovative

alternative to conventional antibacterial assays, specifically tailored for evaluating the antibacterial activity of water-insoluble and colored compounds. It addresses the challenge posed by the insolubility of numerous natural products, which persists despite the use of substantial quantities of solubilizers. Furthermore, this method can be integrated with the aforementioned HPLC formazan quantitative technique to facilitate the precise analysis of parameters such as bacterial sensitivity and resistance to the compounds under investigation. The results have shown that the MED of flavone was 4.2-5.2 μg/cm^2 against the *S. aureus* and 5.2-6.1 μg/cm^2 against the *E. coli*. Similarly, the MED of grandiflorone was observed to be 0.29 - 0.59 μg/cm^2 against *S. aureus* and 2.34 - 4.68 μg/cm^2 against *E. coli*.

In summary, this study focuses on the advancement of novel experimental methodologies for natural product research, as well as the optimization of existing techniques. The strength of the work is its significant reduction in the duration of experimental procedures and enhancement of data measurement accuracy, thereby offering a valuable reference for subsequent screening of antibacterial compounds and the evaluation of their antibacterial activity.

6.2. Highlights of the study

- Systematically reviewed the chemical classification and biological activities of the hybrid compounds from *Myrtaceae*. (**Chapter Two**)
- An equation relating colony-forming units to the amount of formazan converted by the bacteria was developed. (**Chapter Three**)
- The best MTT reduction time was found to be 30 mins, longer reduction times will produce obvious errors. (**Chapter Three**)
- HPLC analysis proves to be the best way for formazan quantification. (**Chapter Three**)
- Formazan concentration and absorbance are linear only up to 125 ug/mL, further dilution may be needed before measurement. (**Chapter Three**)
- The flaws in the recently reported bacterial MTT assay protocol were rectified. (**Appendix Four**)
- Successfully employed a TLC-based approach combined with software-assisted identification to target and identify antibacterial compounds derived from plants. (**Chapters Four and Five**)
- Flavone was identified as the main antibacterial compound in feijoa fruit peel. (**Chapter Four**)
- Two 29 mg of flavone was produced per kg (dry weight) through a customized isolation process, at ~96% purity. (**Chapter Four**)
- Rapidly targeted and identified the antibacterial compounds presented in untreated, steam-distilled NZ Mānuka and untreated CN Mānuka respectively. A total of **22** compounds were identified. (**Chapter Five**)
- Grandiflorone was identified as the primary antibacterial compound present in both steam-distilled and untreated mānuka samples. (**Chapter Five**)

- Discovered that steam distillation treatment significantly alleviated the challenges associated with purifying grandiflorone. Make mānuka essential oil production by-products an excellent source for extracting grandiflorone. (**Chapter Five**)
- A novel TLC-based method was introduced to assess the antibacterial efficacy of specific chemicals on solid surfaces. (**Chapters Four and Five**)
- The chemical structure and purity of flavone and grandiflorone were further verified by NMR. (**Chapters Four and Five**)

6.3. Limitations of the study

The bioactive compounds in this investigation were specifically targeted and isolated using TLC-bioautography. Consequently, the examination of phytochemical constituents was similarly constrained by the limitations inherent in common TLC techniques. For instance, plant extract compositions are intricate, and TLC methods are only capable of detecting a limited number of predominant components with relatively high concentrations. It is noteworthy that none of the hybrid compounds discussed in Chapter 2 were detected through TLC-bioautography, primarily due to their low content.

It is widely acknowledged that the biological efficacy of numerous natural products stems from the synergistic action of multiple compounds. Regrettably, the methodology employed in this study solely permits the identification and isolation of an individual active substance. Moreover, as previously mentioned, the initial screening was carried out utilizing antibacterial assays. This testing approach is deemed highly convenient and expeditious, enabling the identification of numerous active substances within a limited timeframe. Nevertheless, this method's drawback lies in its disregard for compounds lacking antibacterial properties yet possessing other biological activities. Consequently, the bioassay-guided isolation procedures presented in this study still need to be further optimized.

6.4. Future directions

Subsequent investigations will be conducted in future studies, building upon the existing research findings:

- Introducing more bioassays into TLC-bioautography, such as antioxidant, ovicidal or embryocidal activities.
- Employing enhanced separation techniques, such as high-performance TLC and preparative HPLC, in conjunction with current bioassays, may facilitate the identification of more bioactive compounds.

- Perform mixed isolates on bioassays or combine active isolates with known bioactive substances, to explore potential synergistic effects.
- Reinforce collaborative research efforts with Māori researchers to further unlock the potential value of New Zealand endemic plants.

Appendix 1 Supplementary data of Chapter Three.

Appendix 1.1. HPLC raw data for time-course profiles of formazan yield by *S. aureus* and *E. coli* (**Fig. 3.1** in the main text).

Table 1.1 Peak area used for Fig.1 in the main text (Mean ± standard deviation).

Species \ Time	5 min	15 min	30 min	45 min	60 min	75 min	90 min	105 min
S. aureus	15.2058±0.0697	25.3586±0.0427	33.7371±0.2280	36.2039±0.0134	40.1410±0.0746	52.0956±0.0111	55.4619±0.3309	55.2677±0.2235
E. coli	7.9609±0.0112	16.1687±0.0419	21.5869±0.1980	26.1170±0.1966	38.5841±0.1006	40.0170±0.3130	49.7014±0.5787	48.8866±0.0791

Fig 1.1-1. Original HPLC data for *S. aureus* (5 mins).

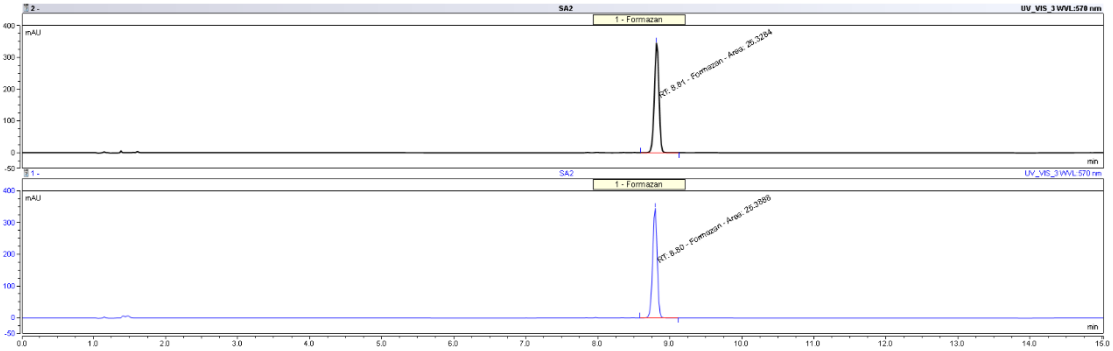

Fig 1.1-2. Original HPLC data for *S. aureus* (15 mins).

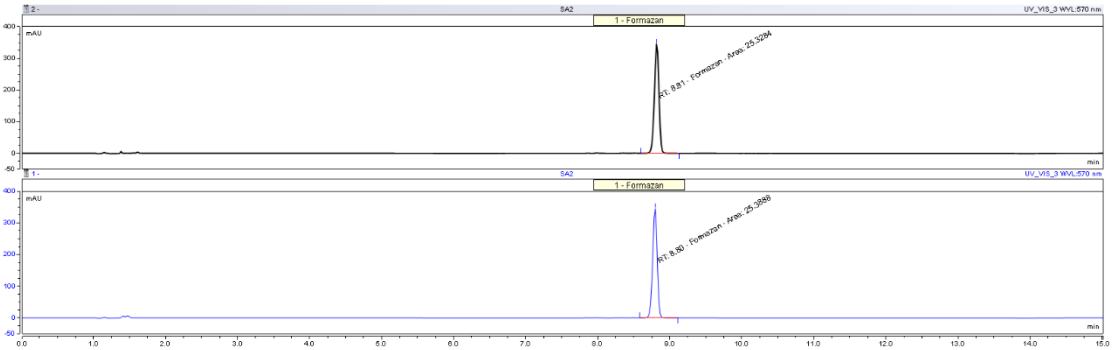

Fig 1.1-3. Original HPLC data for *S. aureus* (30 mins).

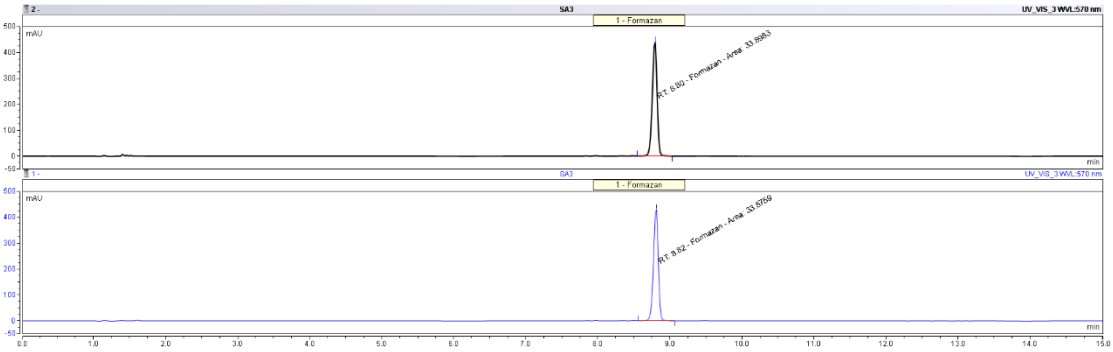

Fig 1.1-4. Original HPLC data for *S. aureus* (45 mins).

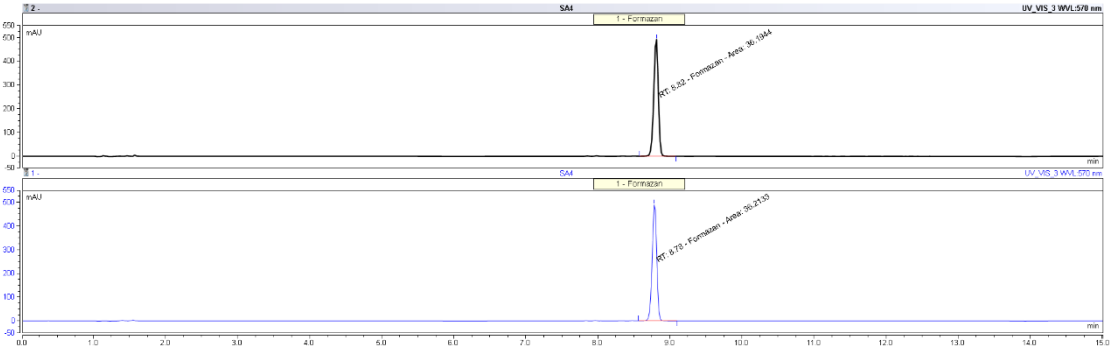

Fig 1.1-5. Original HPLC data for *S. aureus* (60 mins).

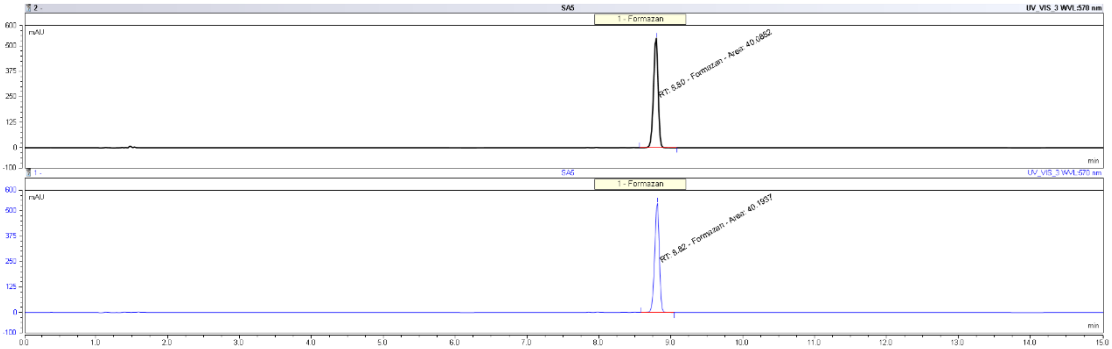

Fig 1.1-6. Original HPLC data for *S. aureus* (75 mins).

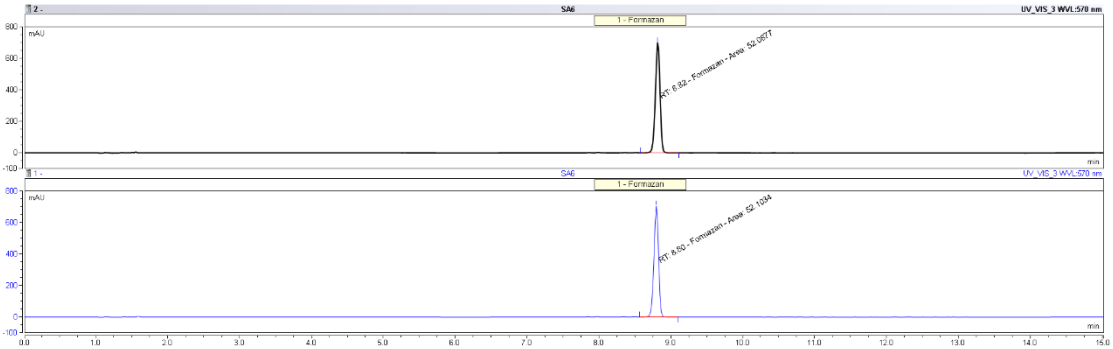

Fig 1.1-7. Original HPLC data for *S. aureus* (90 mins).

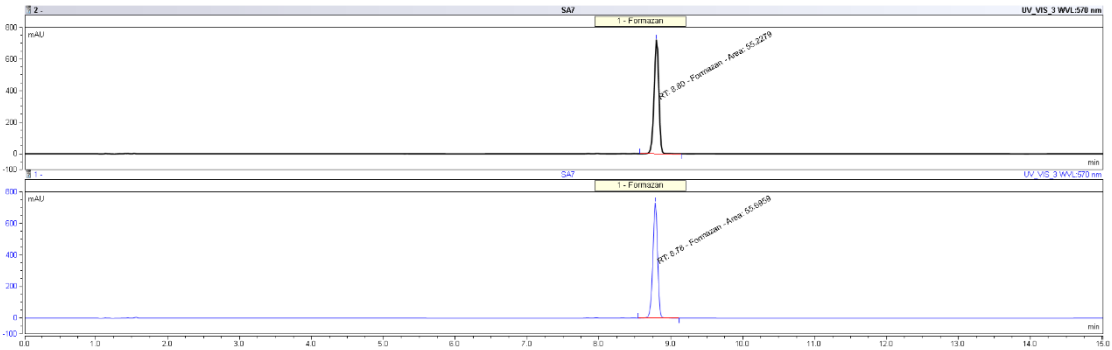

Fig 1.1-8. Original HPLC data for *S. aureus* (105 mins).

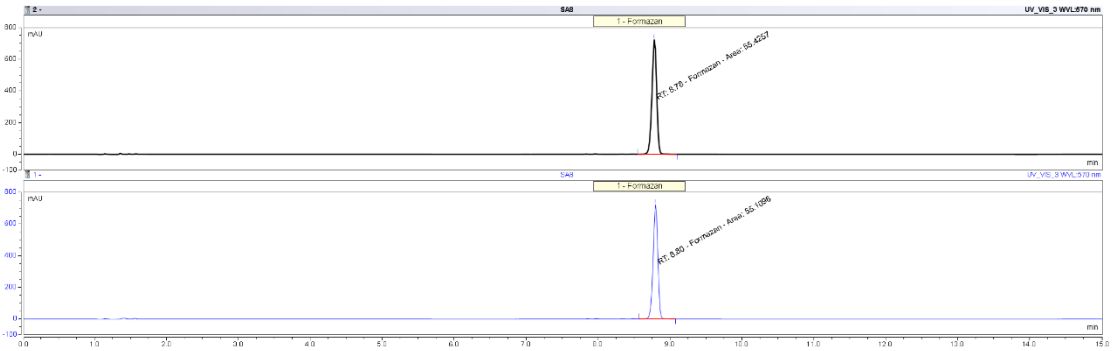

Fig 1.1-9. Original HPLC data for *E. coli* (5 mins).

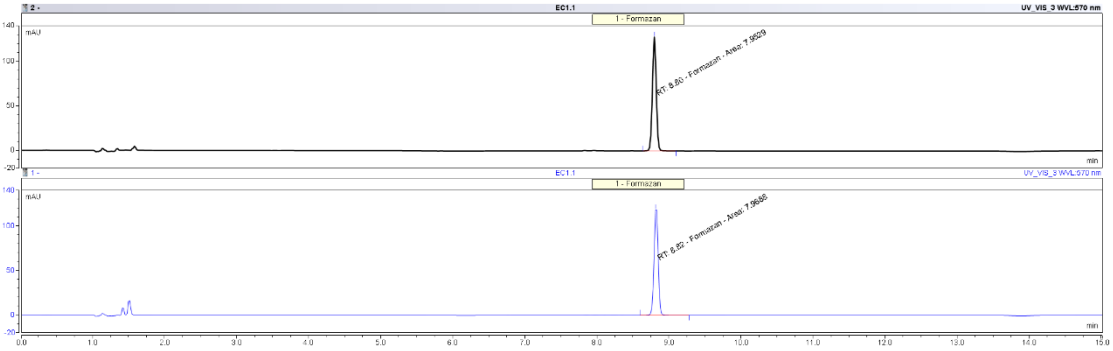

Fig 1.1-10. Original HPLC data for *E. coli* (15 mins).

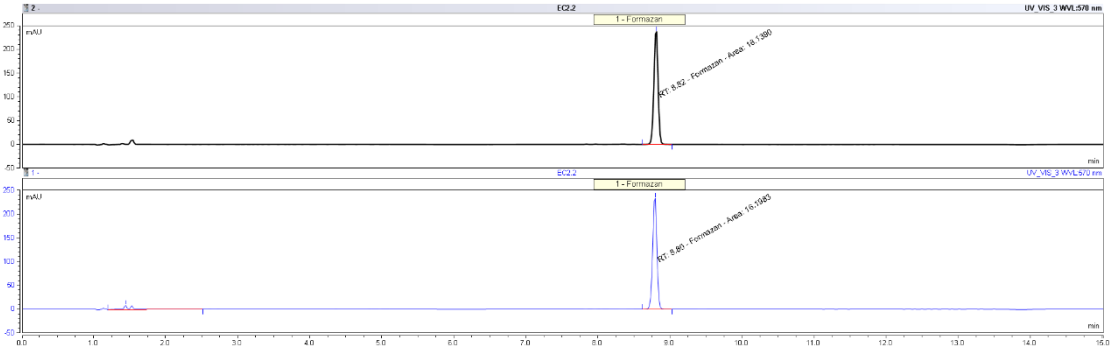

Fig 1.1-11. Original HPLC data for *E. coli* (30 mins).

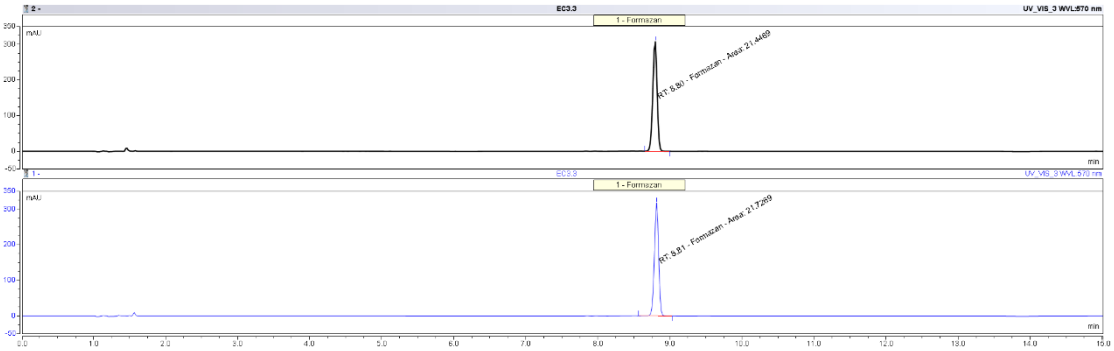

Fig 1.1-12. Original HPLC data for *E. coli* (45 mins).

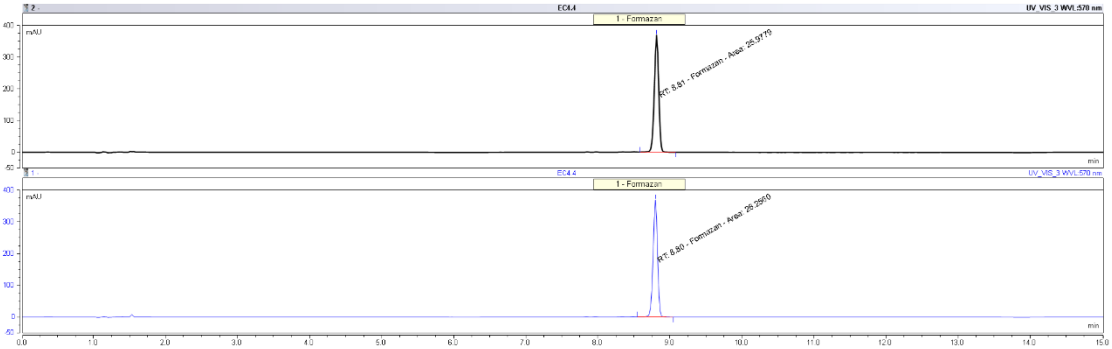

Fig 1.1-13. Original HPLC data for *E. coli* (60 mins).

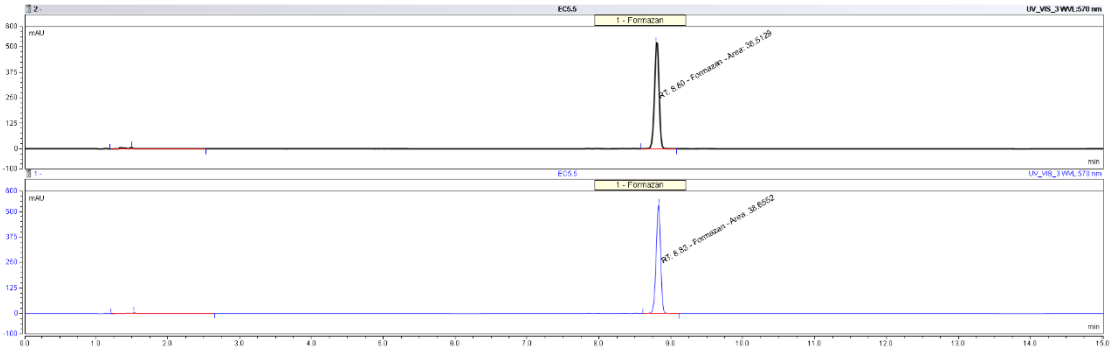

Fig 1.1-14. Original HPLC data for *E. coli* (75 mins).

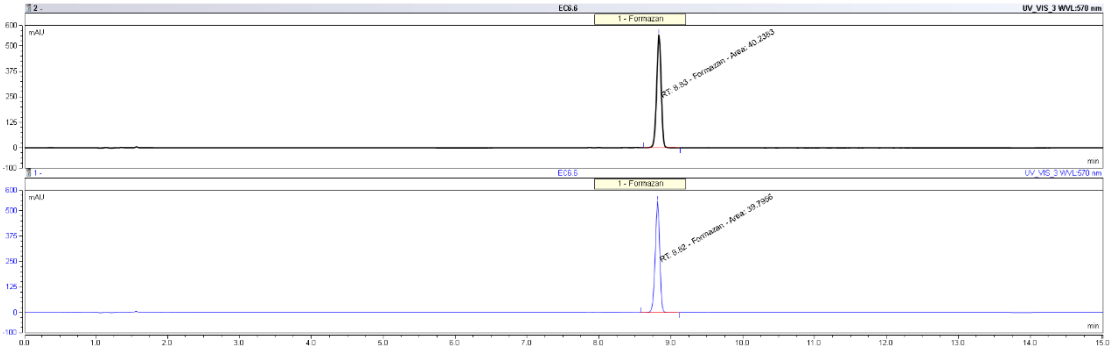

Fig 1.1-15. Original HPLC data for *E. coli* (90 mins).

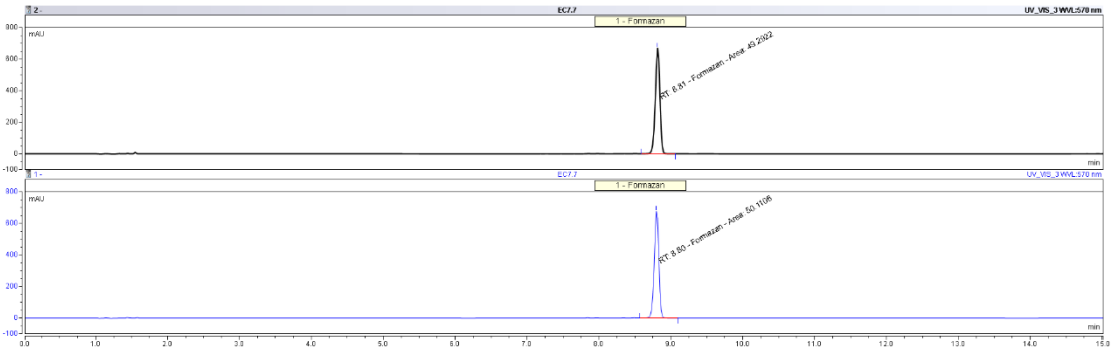

Fig 1.1-16. Original HPLC data for *E. coli* (105 mins).

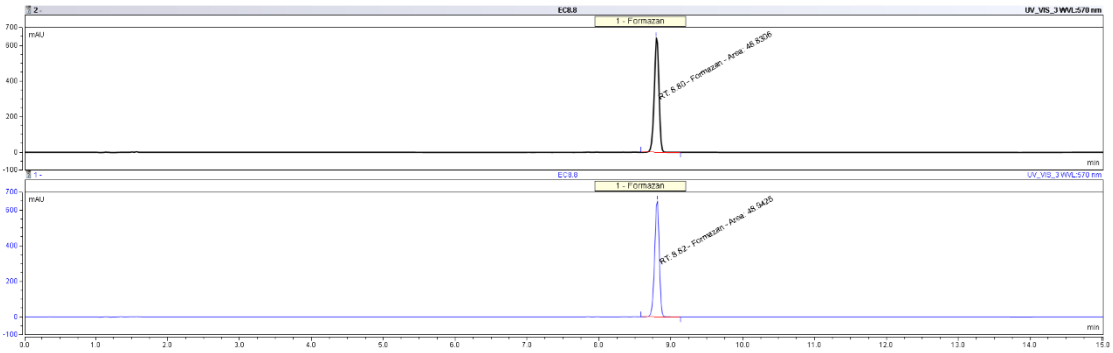

Appendix 1.2. HPLC raw data for the regression curve of tested bacterial absorbance and formazan yield during MTT assay (**Fig. 3.4** in the main text).

Table 1.2. Peak area used for Fig.4 in the main text (Mean ± standard deviation).

Species \ ABs	0.0795	0.1448	0.2212	0.3088	0.4612	0.6387	0.7709
S. aureus	8.9927±0.2046	14.3150±0.0165	20.4363±0.0513	30.8556±0.0583	49.9260±0.0012	64.2081±0.0139	77.6711±0.0397
Species \ ABs	0.0813	0.1465	0.2266	0.3131	0.5061	0.6393	0.7640
E. coli	7.5251±0.0390	16.2399±0.0607	23.10399±0.0107	32.7407±0.0181	45.9852±0.0914	61.4354±0.0958	67.5698±0.1453

Abs: absorbance read by microplate reader.

Fig 1.2-1. Original HPLC data for *S. aureus* (Abs 0.0795).

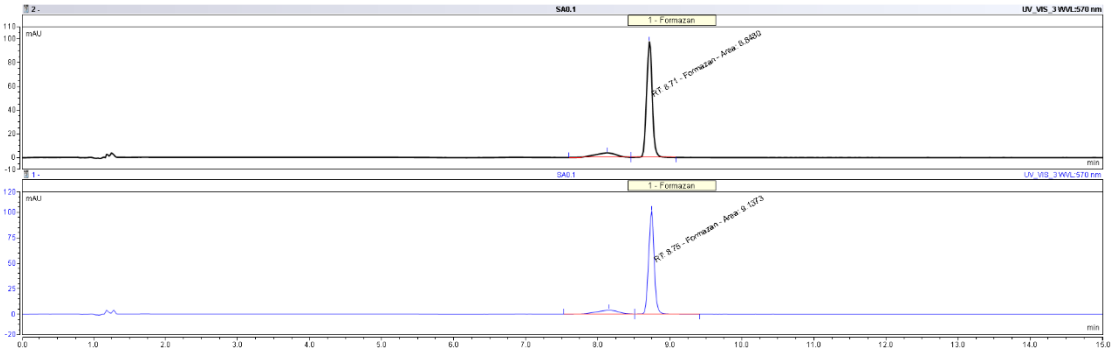

Fig 1.2-2. Original HPLC data for *S. aureus* (Abs 0.1448).

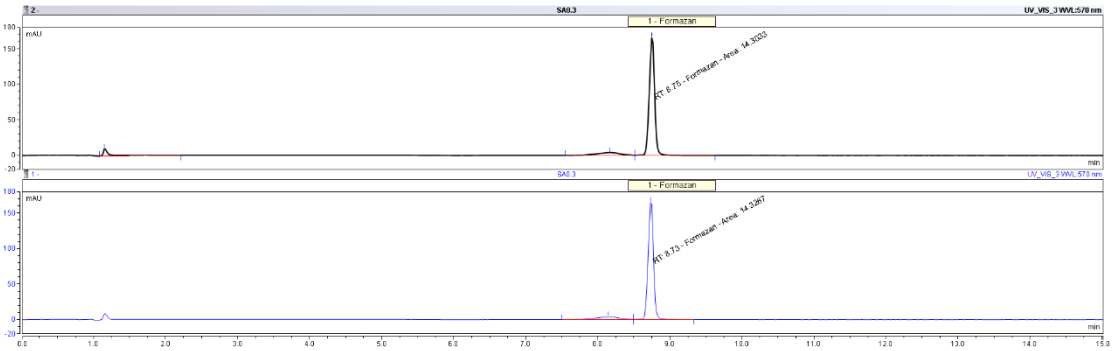

Fig 1.2-3. Original HPLC data for *S. aureus* (Abs 0.2212).

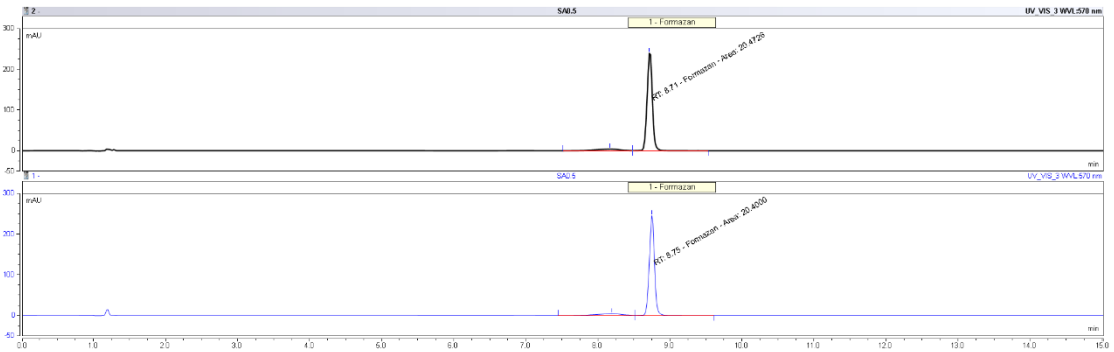

Fig 1.2-4. Original HPLC data for *S. aureus* (Abs 0.3088).

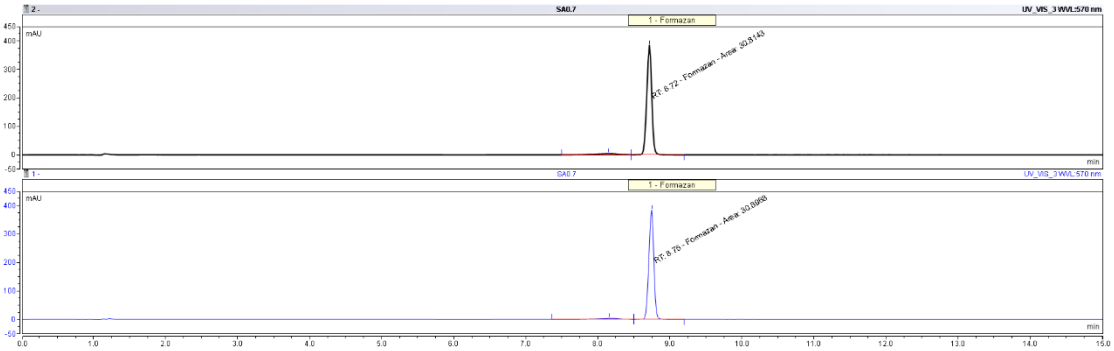

Fig 1.2-5. Original HPLC data for *S. aureus* (Abs 0.4612).

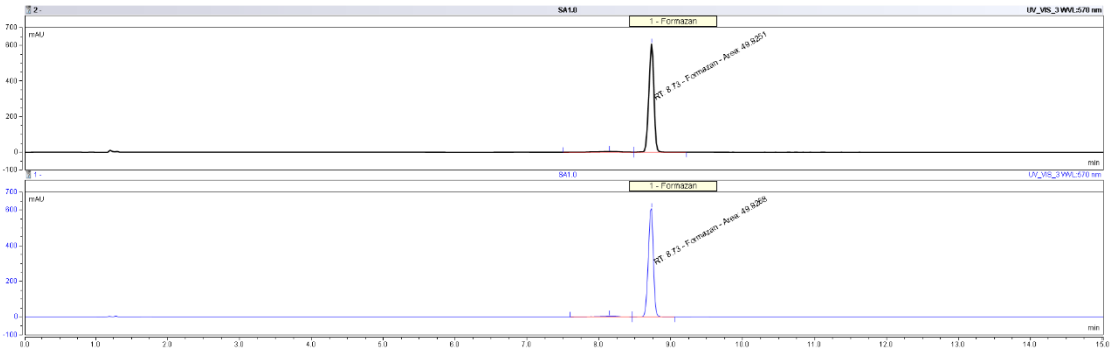

Fig 1.2-6. Original HPLC data for *S. aureus* (Abs 0.6387).

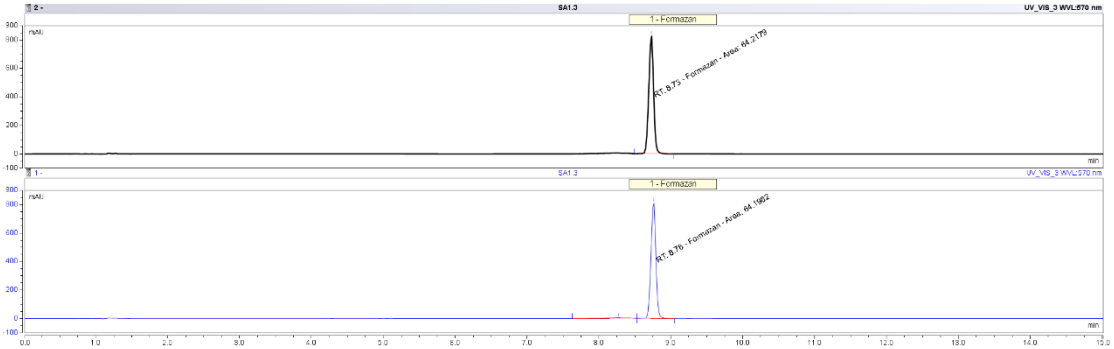

Fig 1.2-7. Original HPLC data for *S. aureus* (Abs 0.7709).

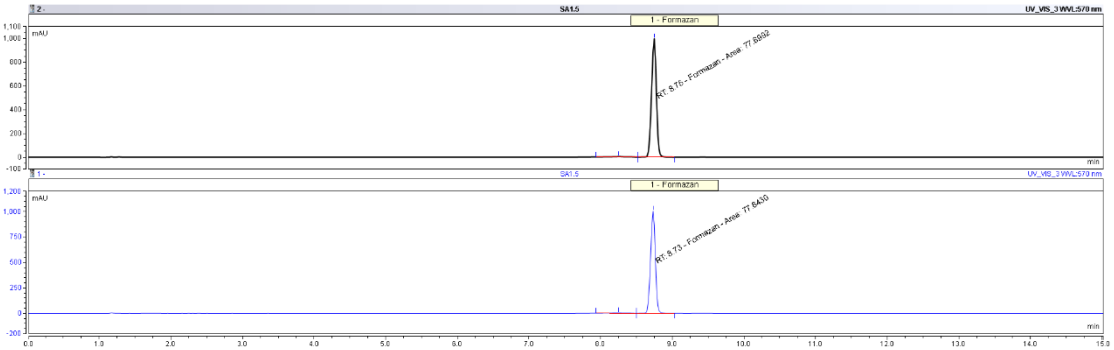

Fig 1.2-8. Original HPLC data for *E. coli* (Abs 0.0813).

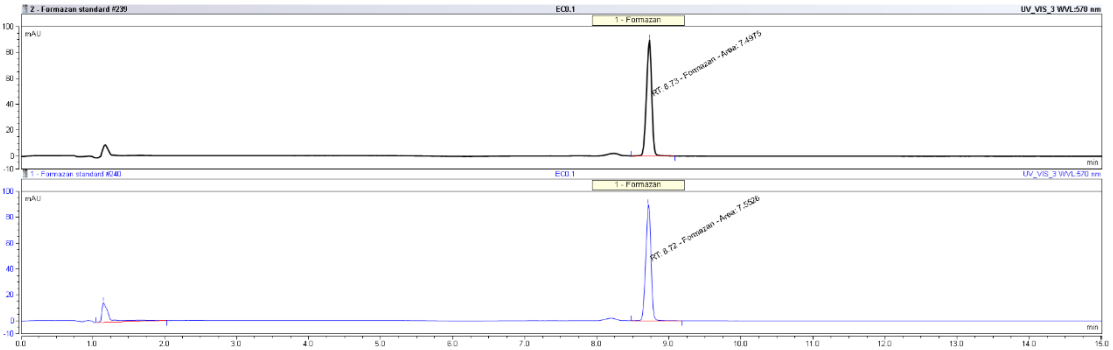

Fig 1.2-9. Original HPLC data for *E. coli* (Abs 0.1465).

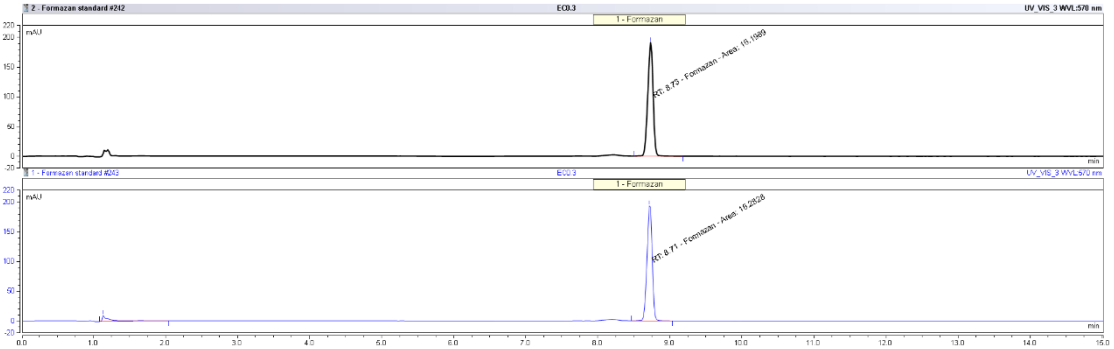

Fig 1.2-10. Original HPLC data for *E. coli* (Abs 0.2266).

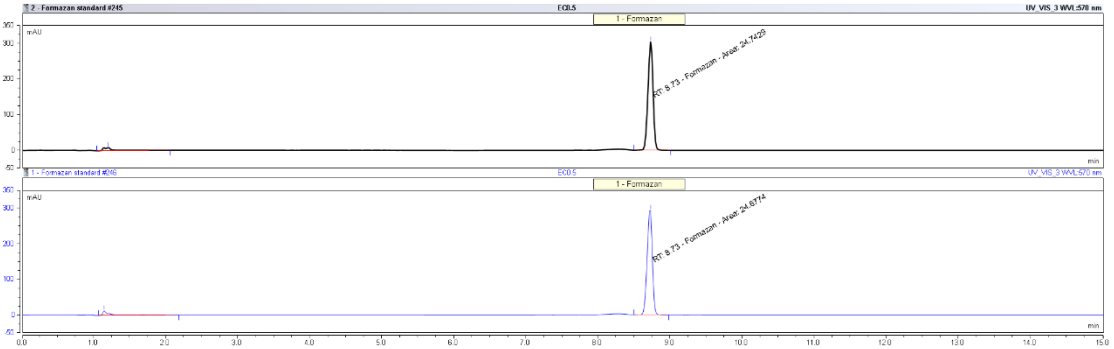

Fig 1.2-11. Original HPLC data for *E. coli* (Abs 0.3131).

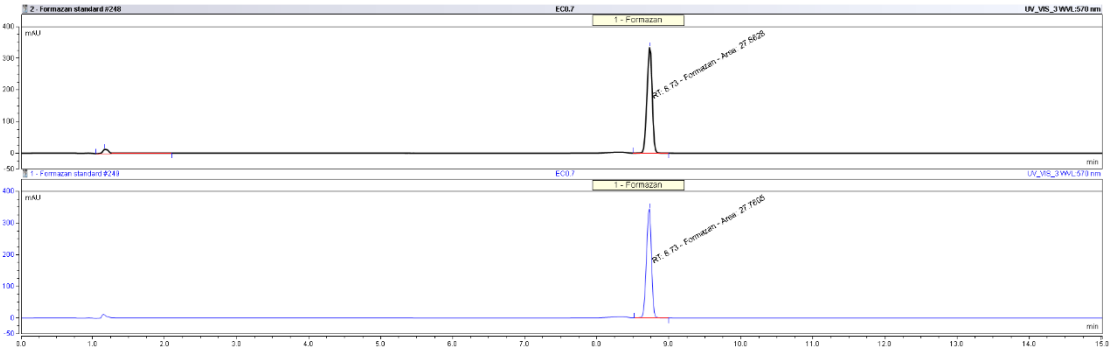

Fig 1.2-12. Original HPLC data for *E. coli* (Abs 0.5061).

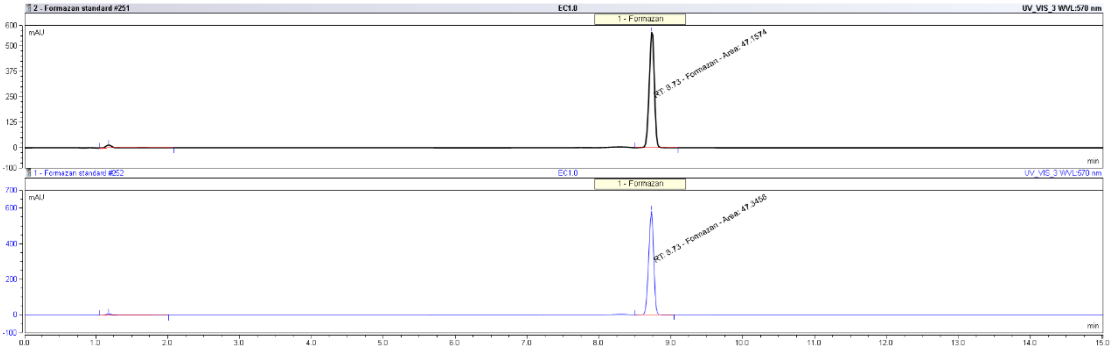

Fig 1.2-13. Original HPLC data for *E. coli* (Abs 0.6393).

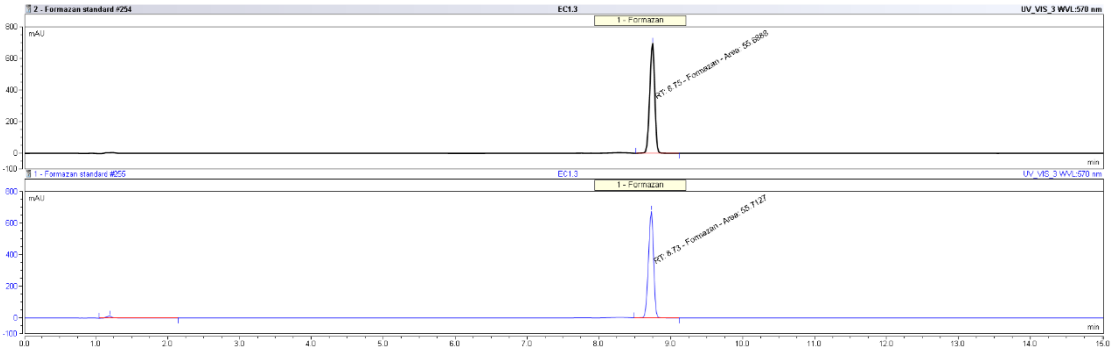

Fig 1.2-14. Original HPLC data for *E. coli* (Abs 0.7640).

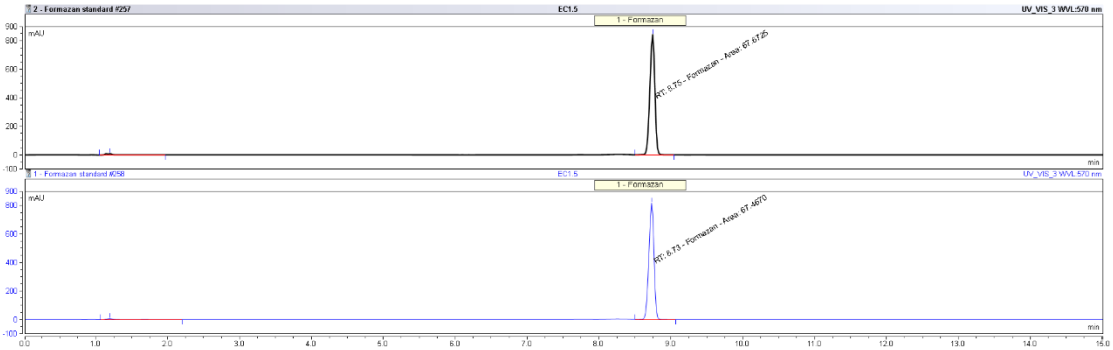

Appendix 1.3. HPLC raw data for Concentration-absorbance relationship curve of formazan standard (**Fig. 3.6** in the main text).

Table 1.3. Peak area used for formazan standard curve (Mean ± standard deviation).

Concentration (µg/mL)	7.8125	15.6250	31.2500	62.5000	125.0000
Formazan standard	8.0918±0.0254	16.4195±0.0644	33.7096±0.1295	67.5448±0.1590	134.6995±0.2426

Fig 1.3-1. Original HPLC data for formazan standard (7.8125 µg/mL).

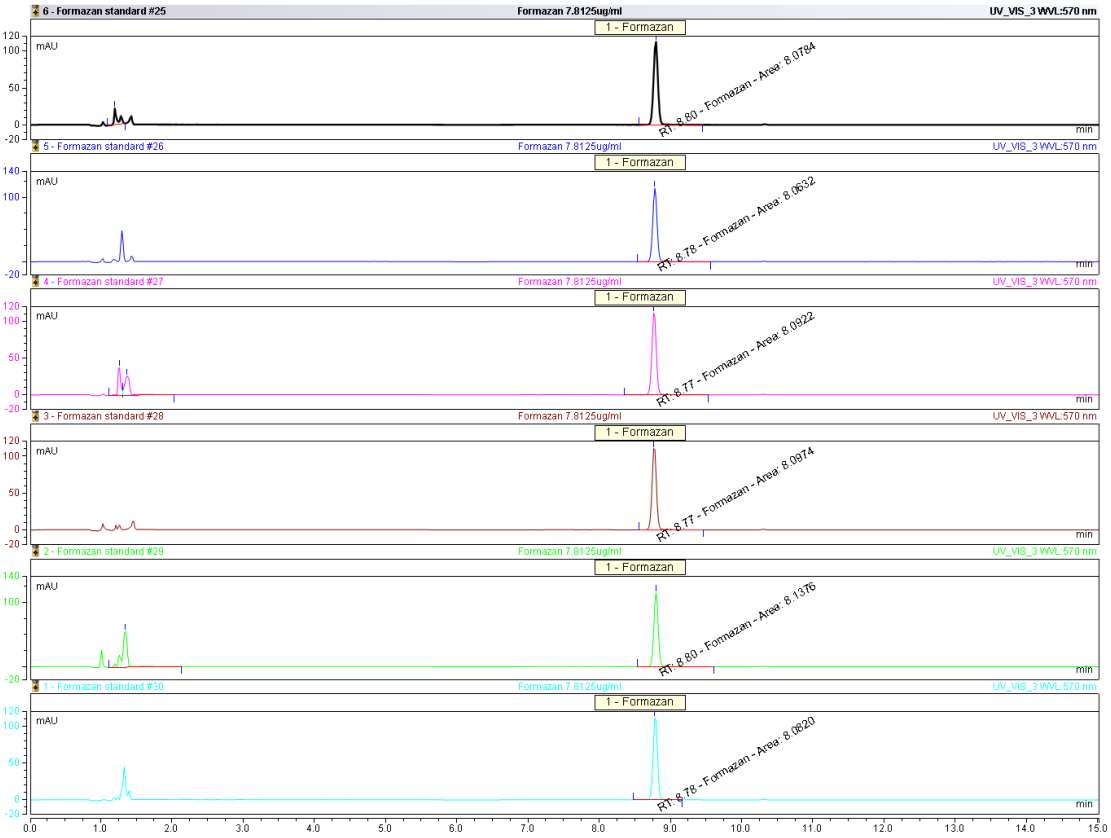

Fig 1.3-2. Original HPLC data for formazan standard (15.6250 µg/mL).

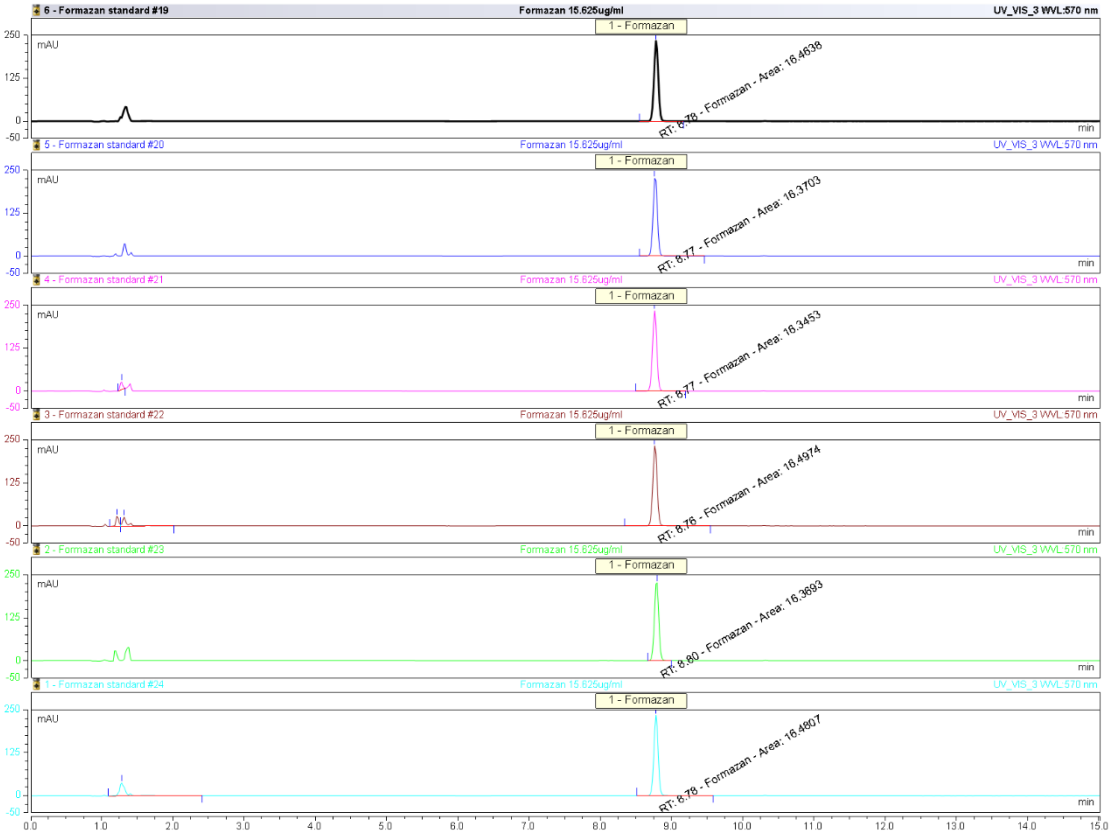

Fig 1.3-3. Original HPLC data for formazan standard (31.2500 µg/mL).

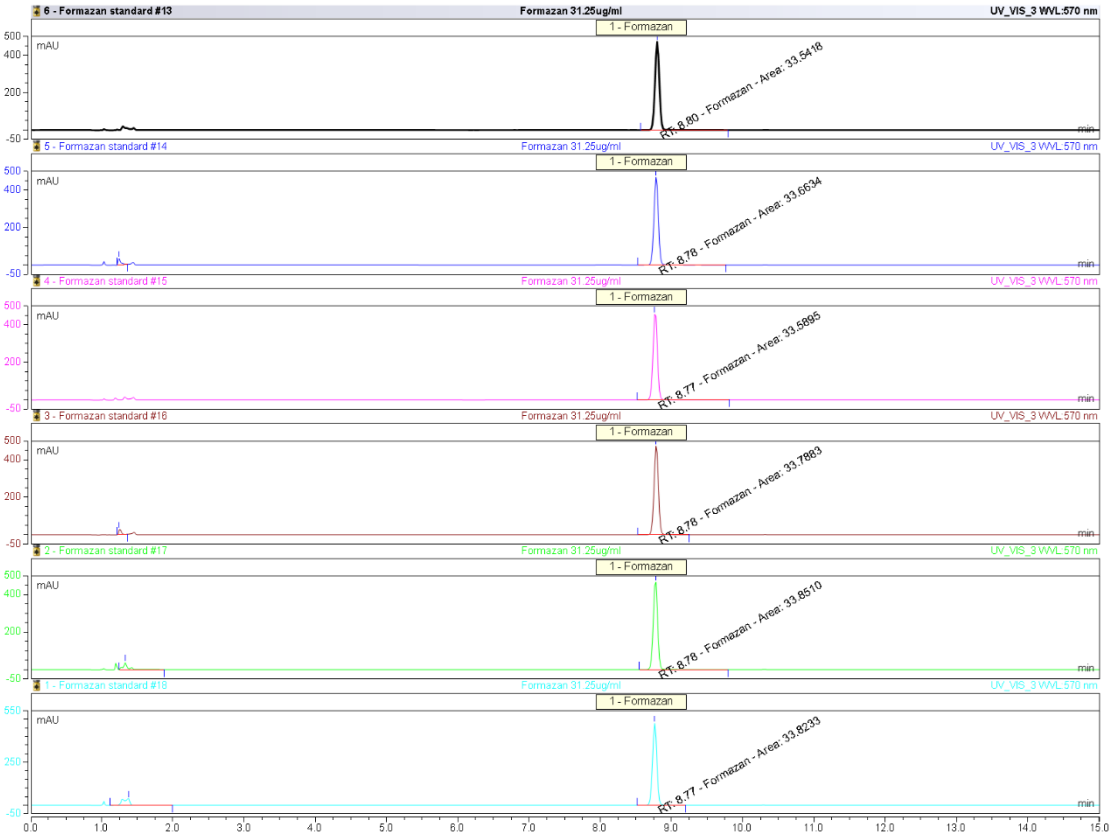

Fig 1.3-4. Original HPLC data for formazan standard (62.5000 µg/mL).

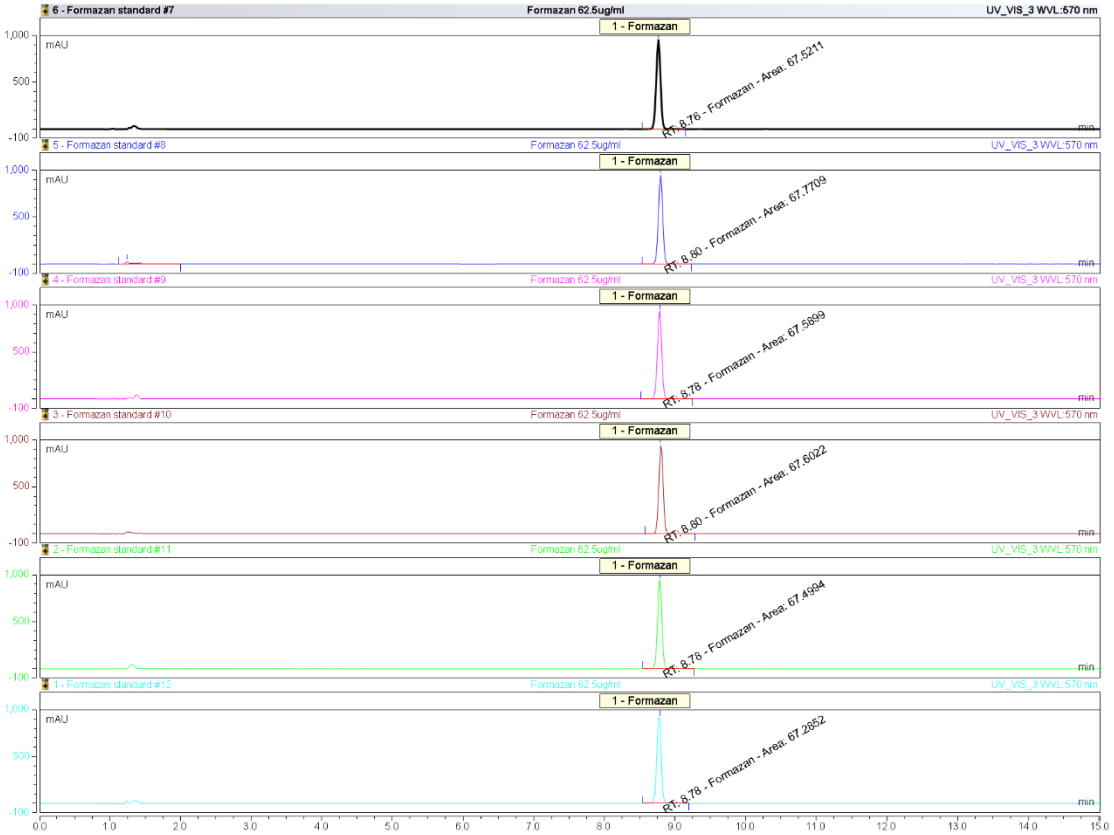

Fig 1.3-5. Original HPLC data for formazan standard (125.0000 µg/mL).

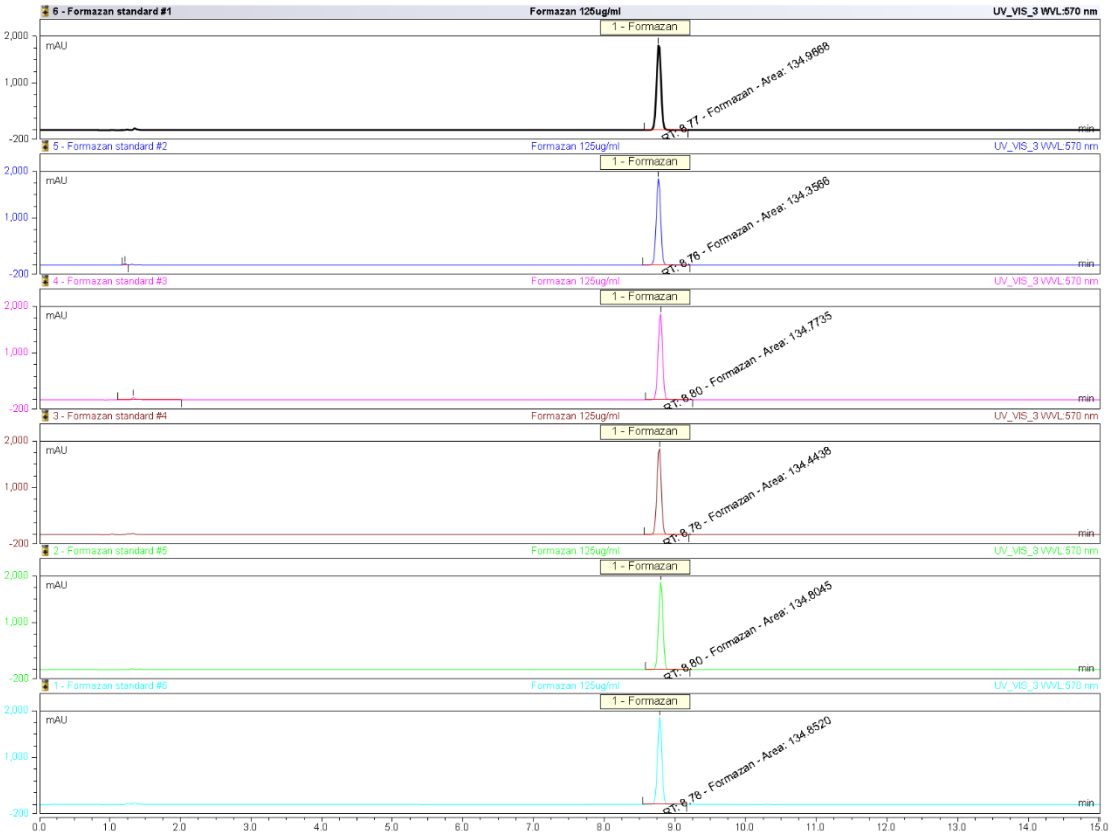

Fig 1.3-6. Original HPLC data for formazan standard (250.0000 µg/mL).

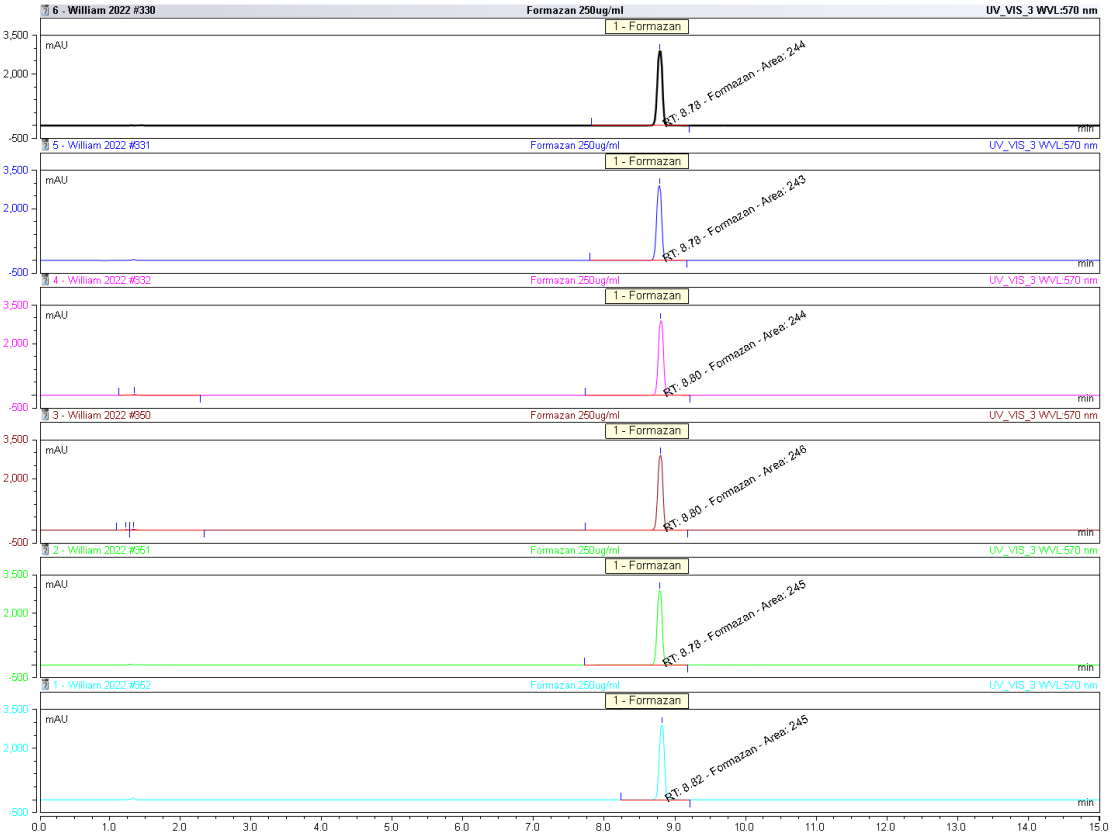

Fig 1.3-7. Original HPLC data for formazan standard (500.0000 µg/mL).

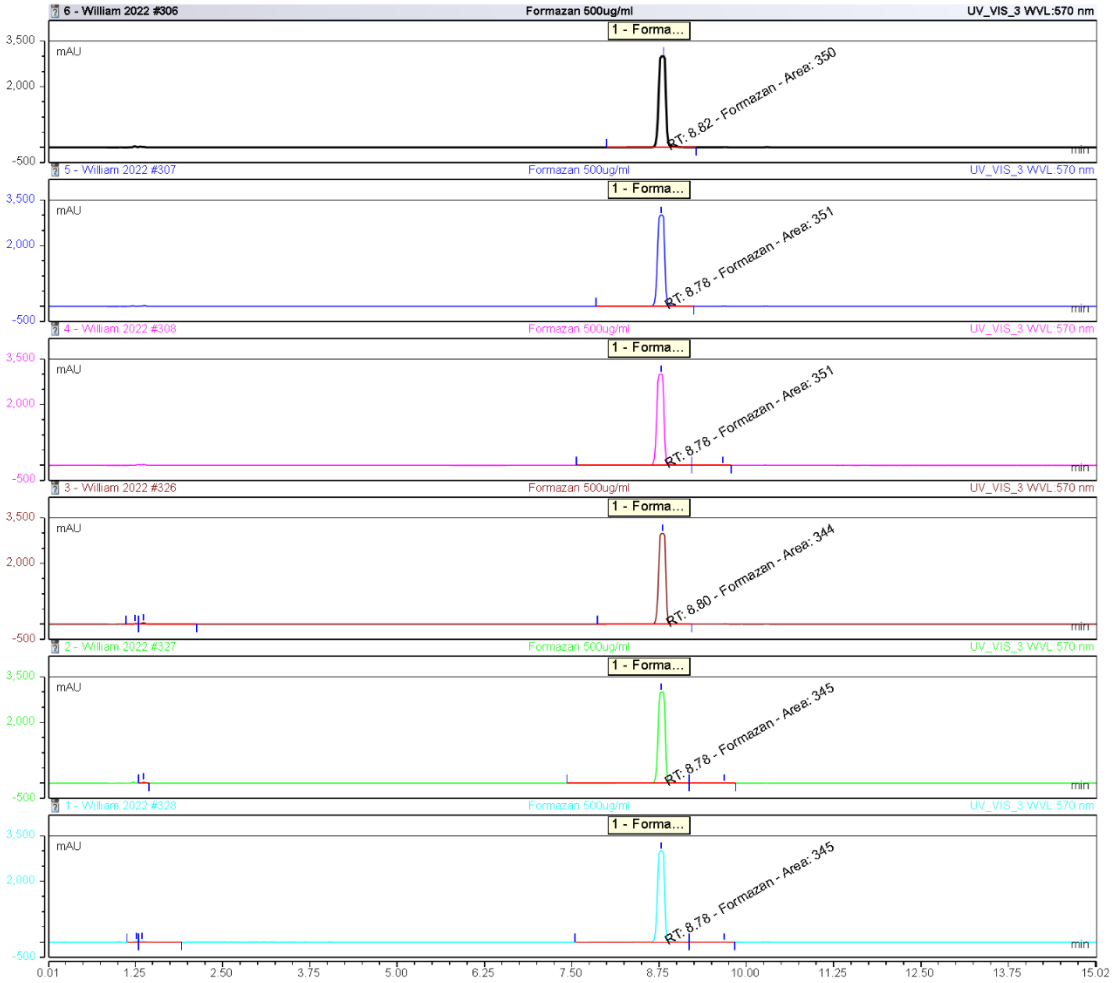

Fig 1.3-8. Original HPLC data for formazan standard (1000.0000 µg/mL).

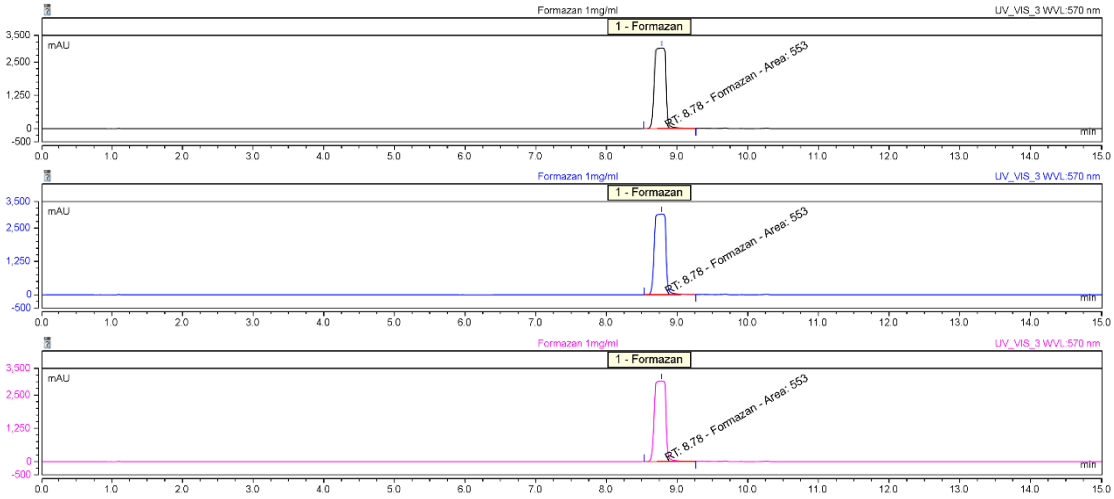

Appendix 2 Supplementary data of Chapter Four.

Appendix 2.1. Workflow used in Compound Discoverer 3.3.

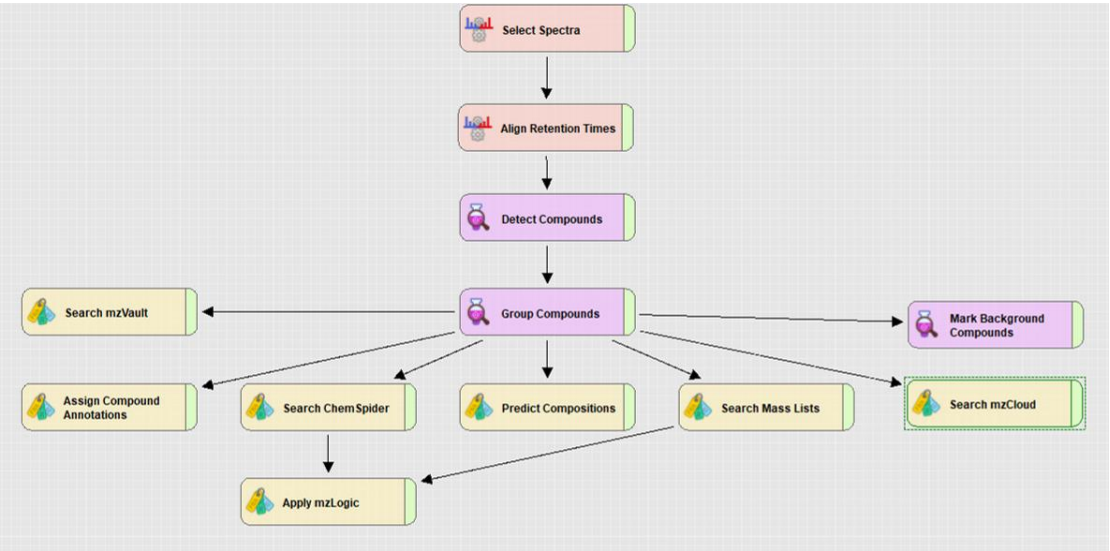

Appendix 2.2. Databases included in MassList:

1. Arita Lab 6549 Flavonoid Structure Database
2. EFS HRAM Compound Database
3. Endogenous Metabolites Database
4. Example Mass List
5. Extractables and Leachables HRAM Compound Database
6. Lipid Maps Structure Database
7. Natural Products Atlas 1
8. Natural Products Atlas 2

Appendix 2.3. HPLC raw data for obtained Flavone purity detection.

Fig 2.3-1. UV 255nm.

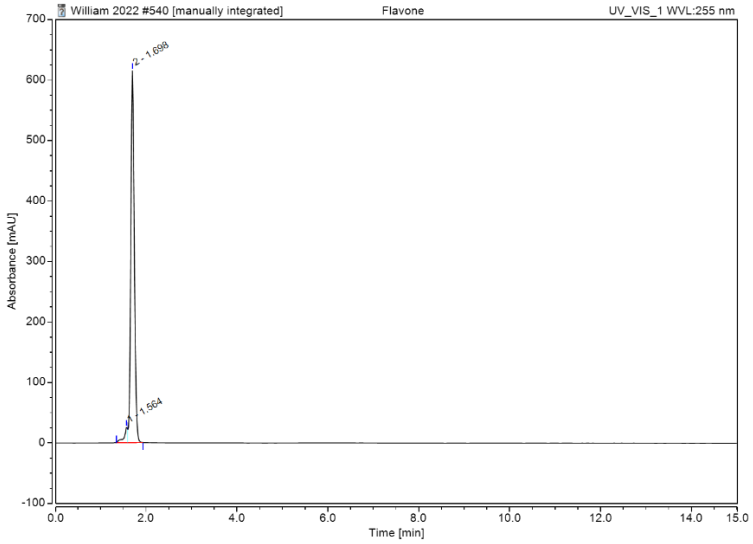

Table 2.3-1. Integration Results.

No.	Retention Time	Area	Area %	Height
1	1.564	2.273	3.94	25.241
2	1.698	54.697	96.06	615.076

Fig 2.3-2. UV 210nm.

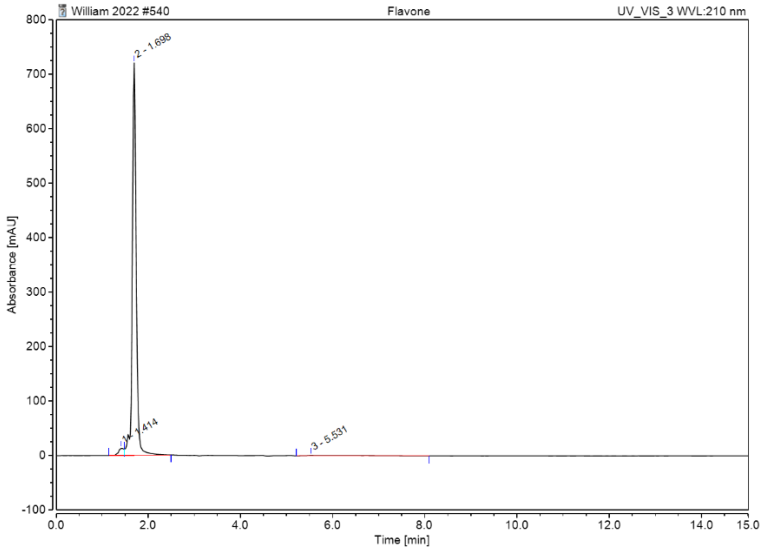

Table 2.3-2. Integration Results.

No.	Retention Time	Area	Area %	Height
1	1.414	1.60	1.77	12.993
2	1.698	70.795	98.10	720.476
3	5.531	1.224	0.13	0.950

Appendix 2.4. ^{1}H,^{13}C and DEPT NMR spectrum of obtained Flavone.

Fig 2.4-1. ^{1}H NMR original spectrum of flavone (500 MHz, Chloroform-d):

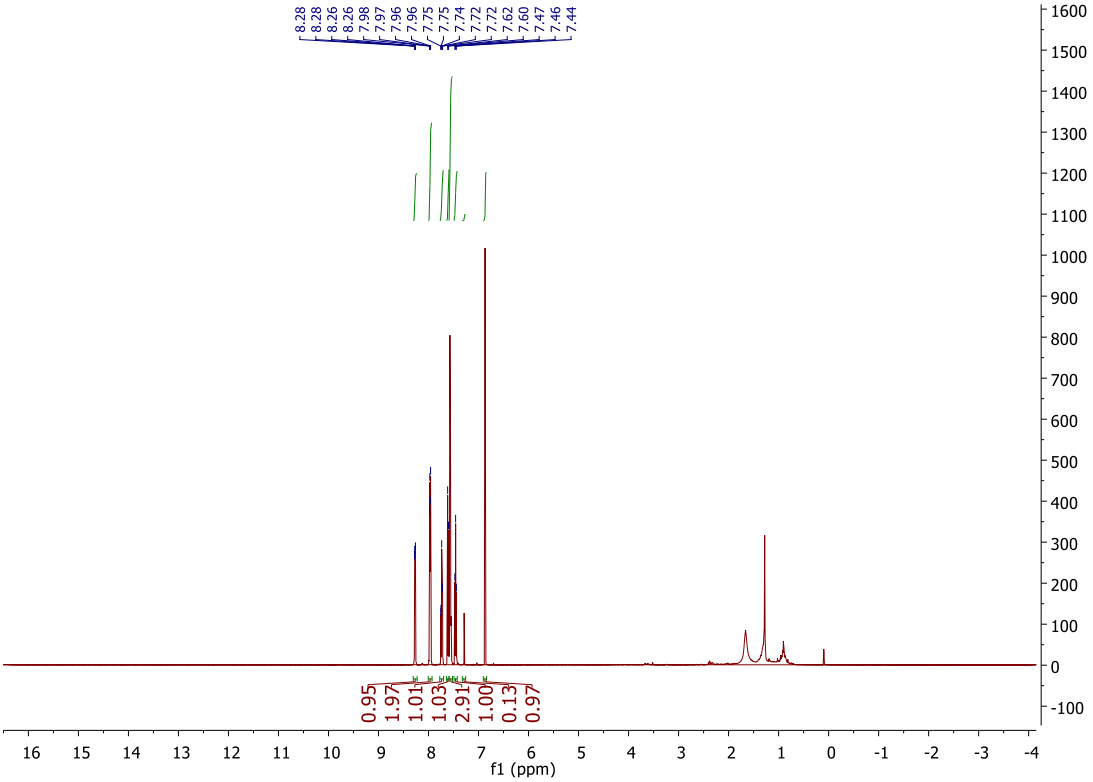

Fig 2.4-2. ^{1}H NMR partial magnified spectrum of flavone (500 MHz, Chloroform-d):

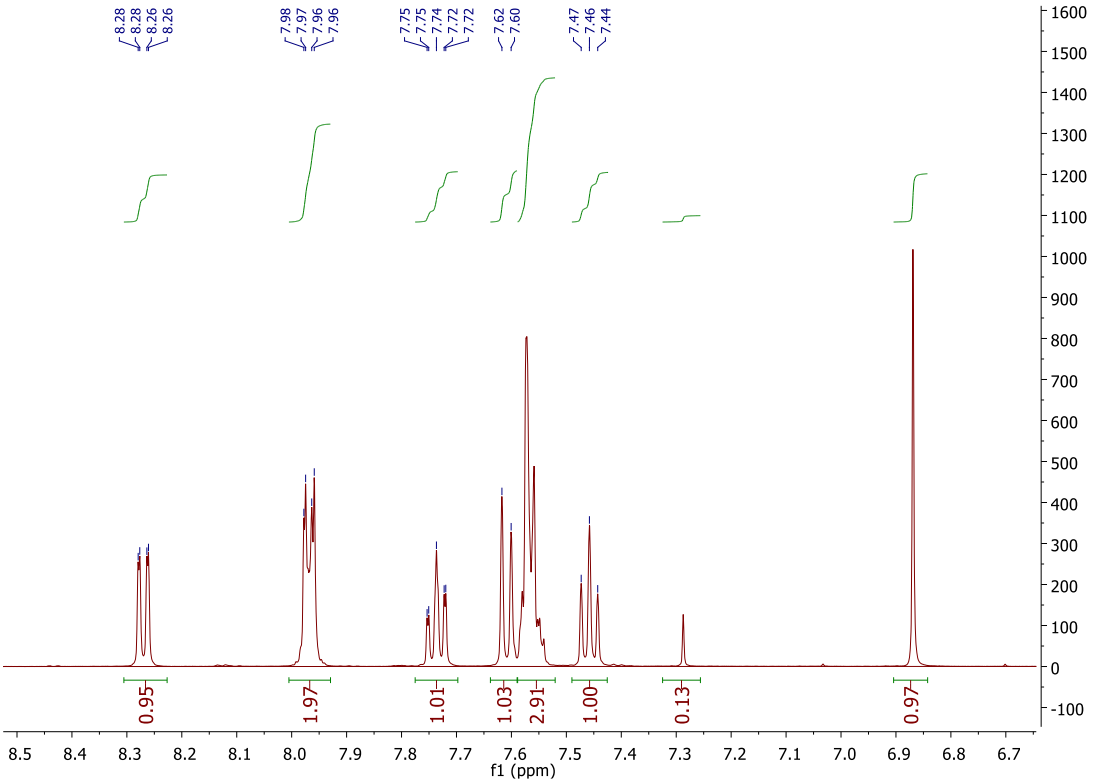

Fig 2.4-3. ^{13}C NMR original spectrum of flavone (125 MHz, Chloroform-d):

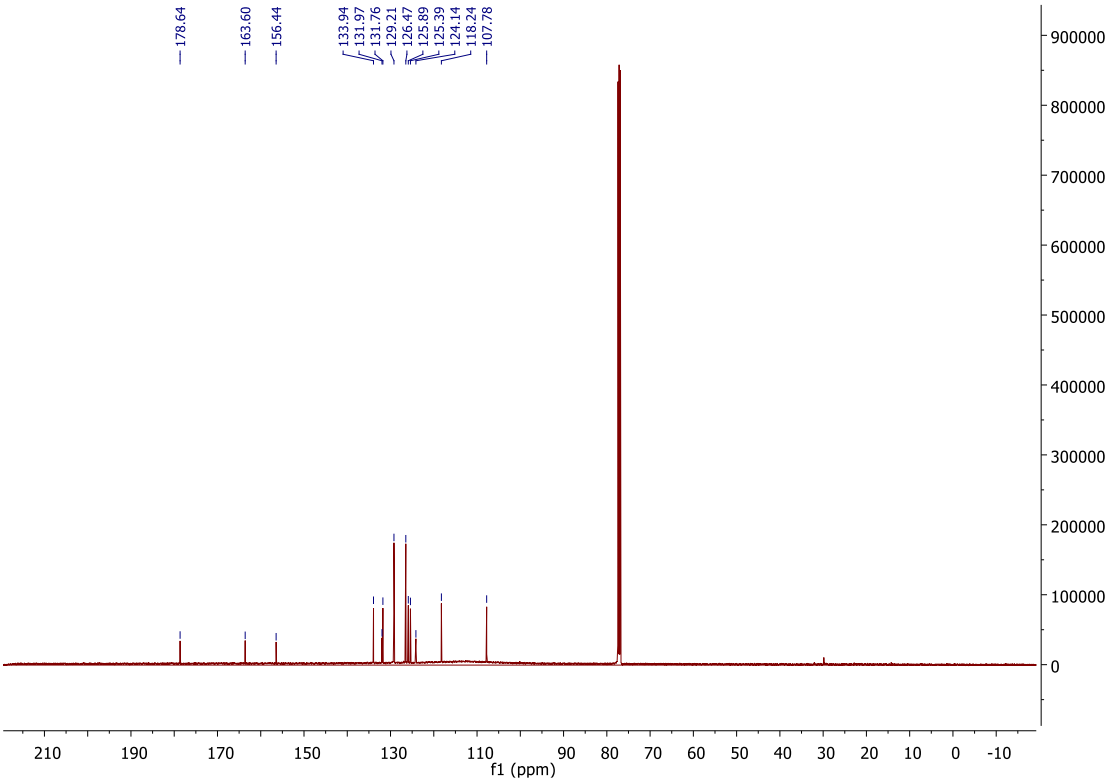

Fig 2.4-4. ^{13}C NMR partial spectrum of flavone (125 MHz, Chloroform-d):

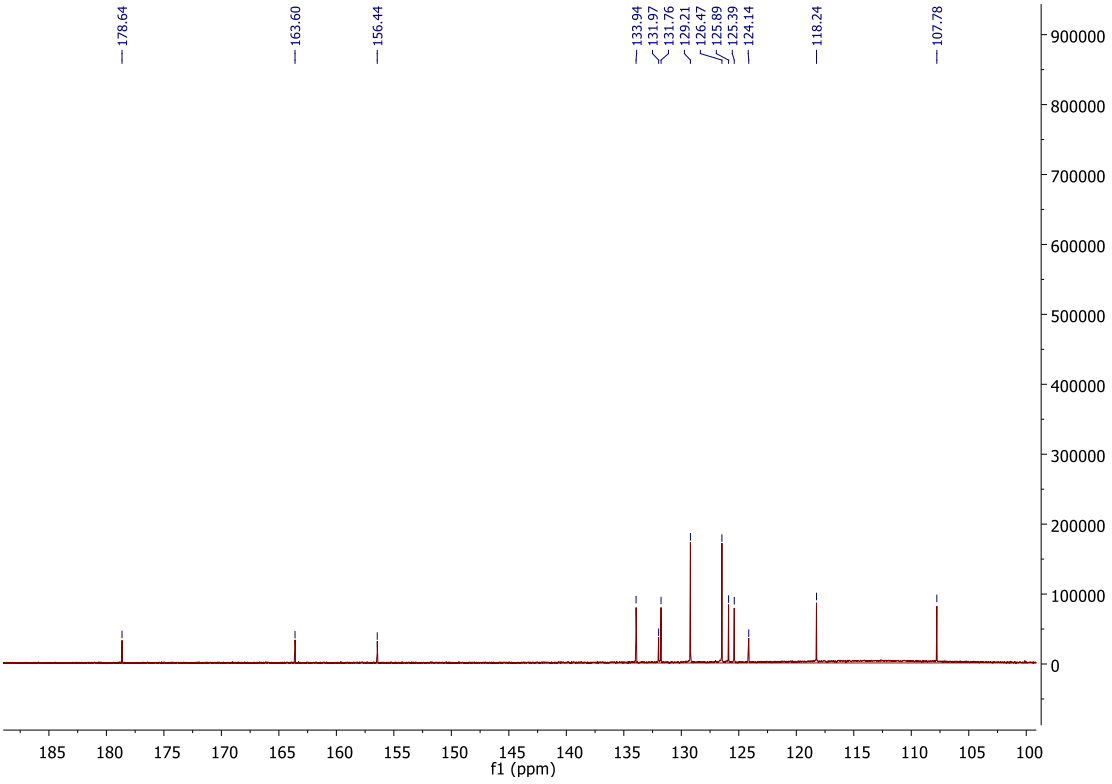

Fig 2.4-5. DEPT NMR original spectrum of flavone (125 MHz, Chloroform-d):

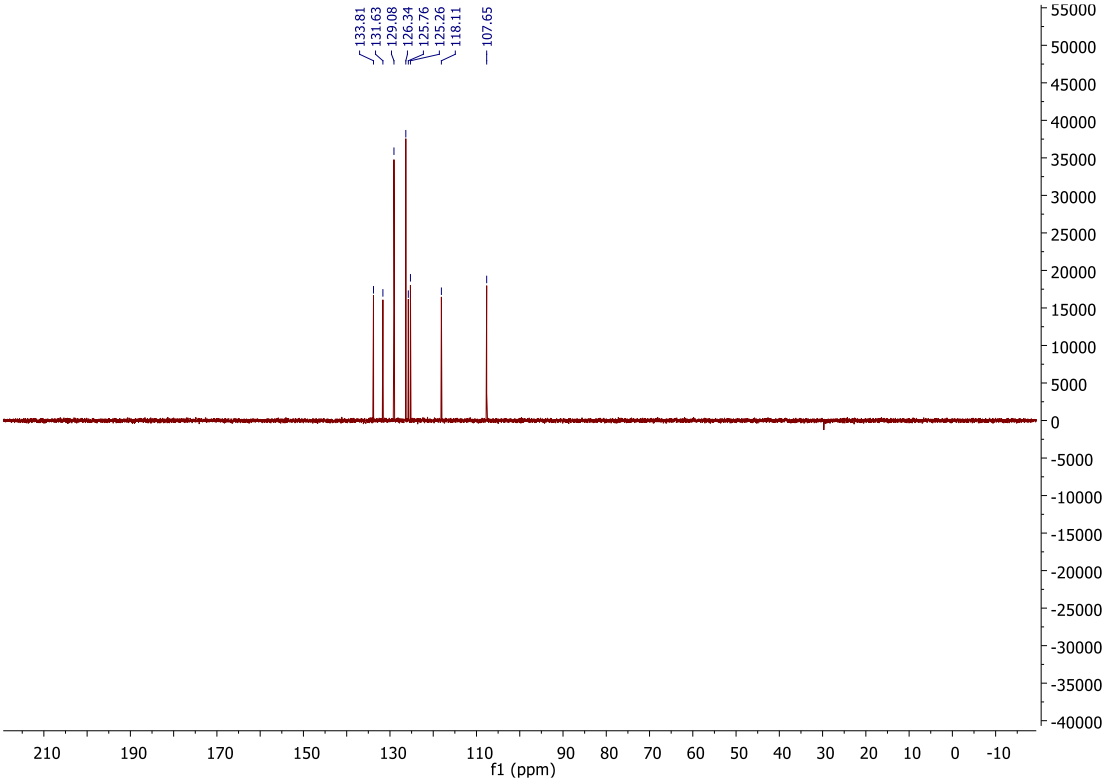

Fig 2.4-6. DEPT NMR partial magnified spectrum of flavone (125 MHz, Chloroform-d):

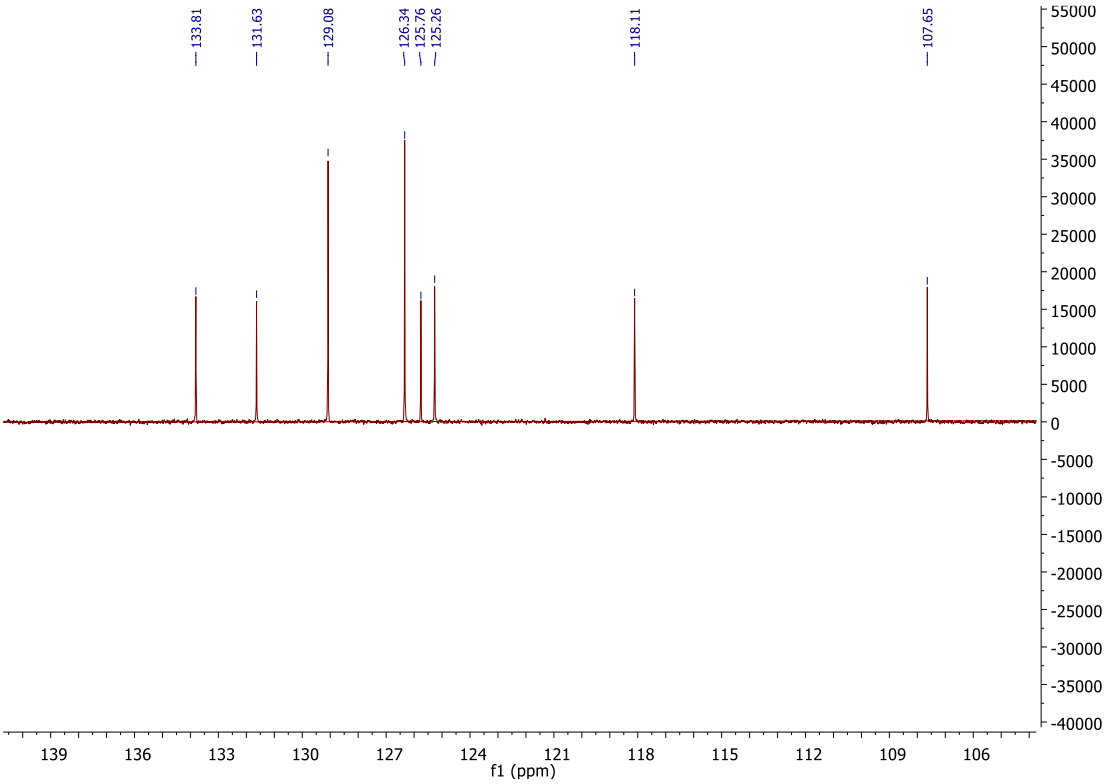

Appendix 3 Supplementary data of Chapter Five.

Appendix 3.1. Workflow used in Compound Discoverer 3.3.

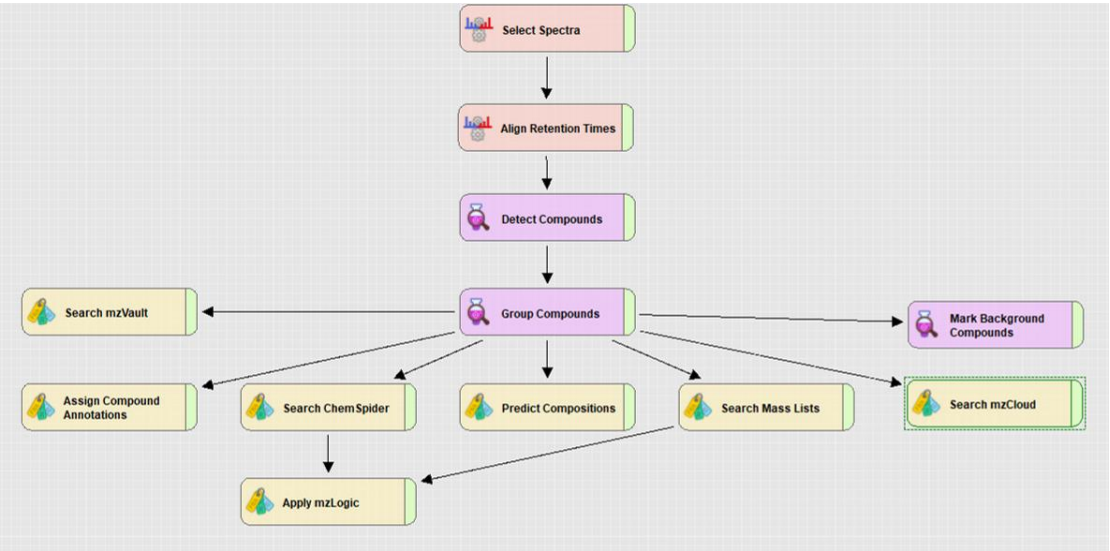

Appendix 3.2. Databases included in MassList:

1. Arita Lab 6549 Flavonoid Structure Database
2. EFS HRAM Compound Database
3. Endogenous Metabolites Database
4. Example Mass List
5. Extractables and Leachables HRAM Compound Database
6. Lipid Maps Structure Database
7. Natural Products Atlas 1
8. Natural Products Atlas 2

Appendix 3.3. LC-MS raw data of Mānuka hexane and dichloromethane extracts.

Fig 3.3-1: LC-MS analysis of Mānuka hexane extracts. (1) NZ untreated; (2) NZ steam-distilled; (3) CN untreated

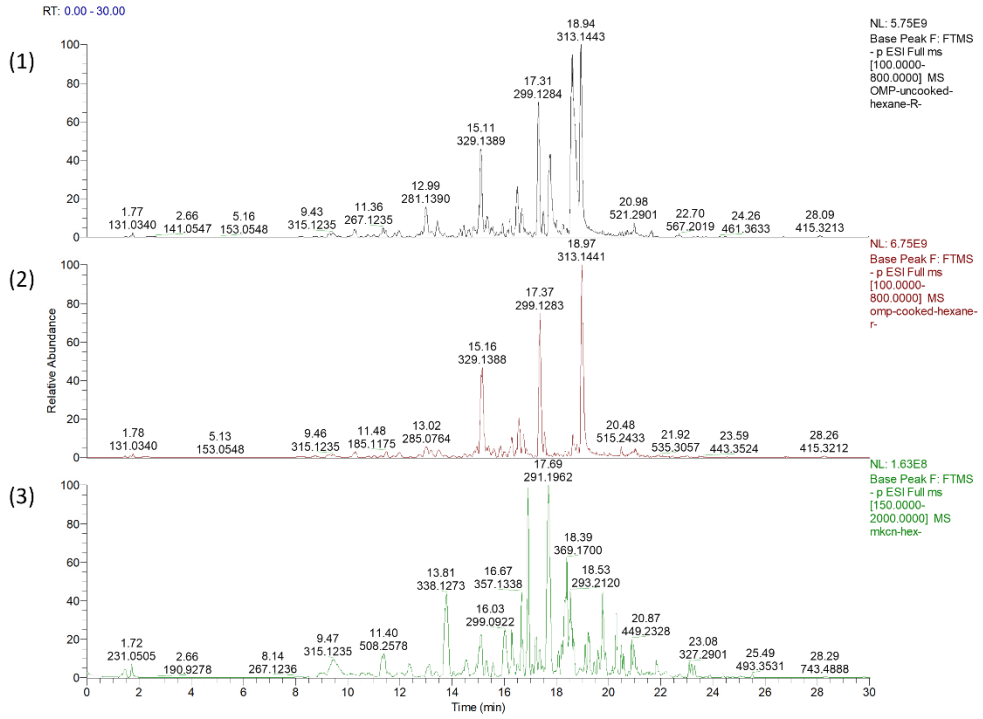

Fig 3.3-2: LC-MS analysis of Mānuka dichloromethane extracts. (1) NZ untreated (2) CN untreated

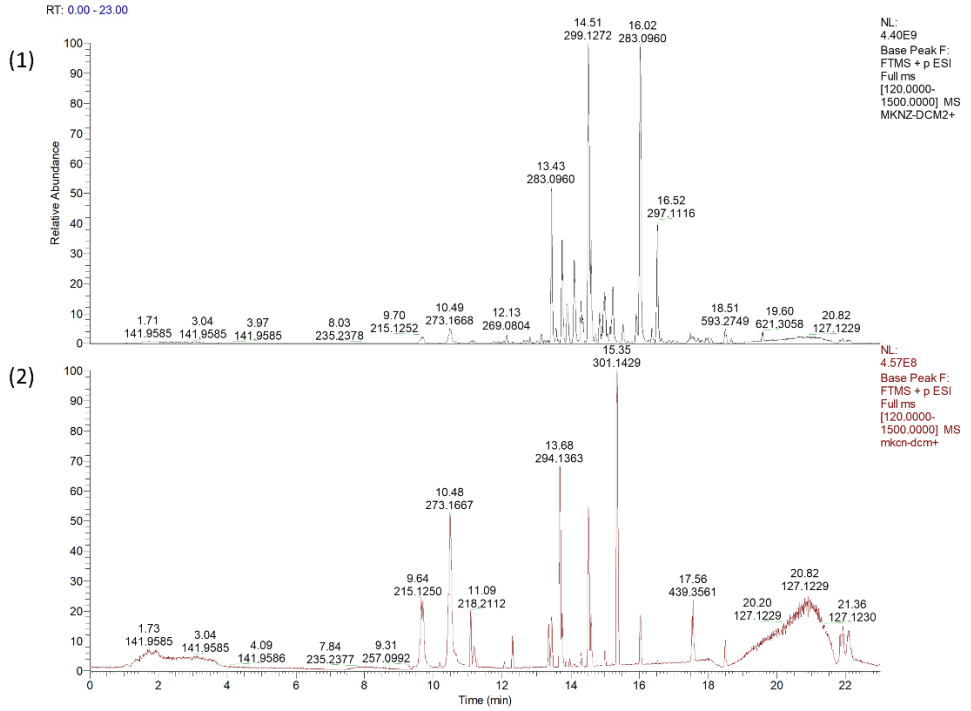

Appendix 3.4. 1H,13C and DEPT NMR spectrum of obtained Grandiflorone.

Fig 3.4-1. ^{1}H NMR original spectrum of Grandiflorone (500 MHz, Chloroform-d):

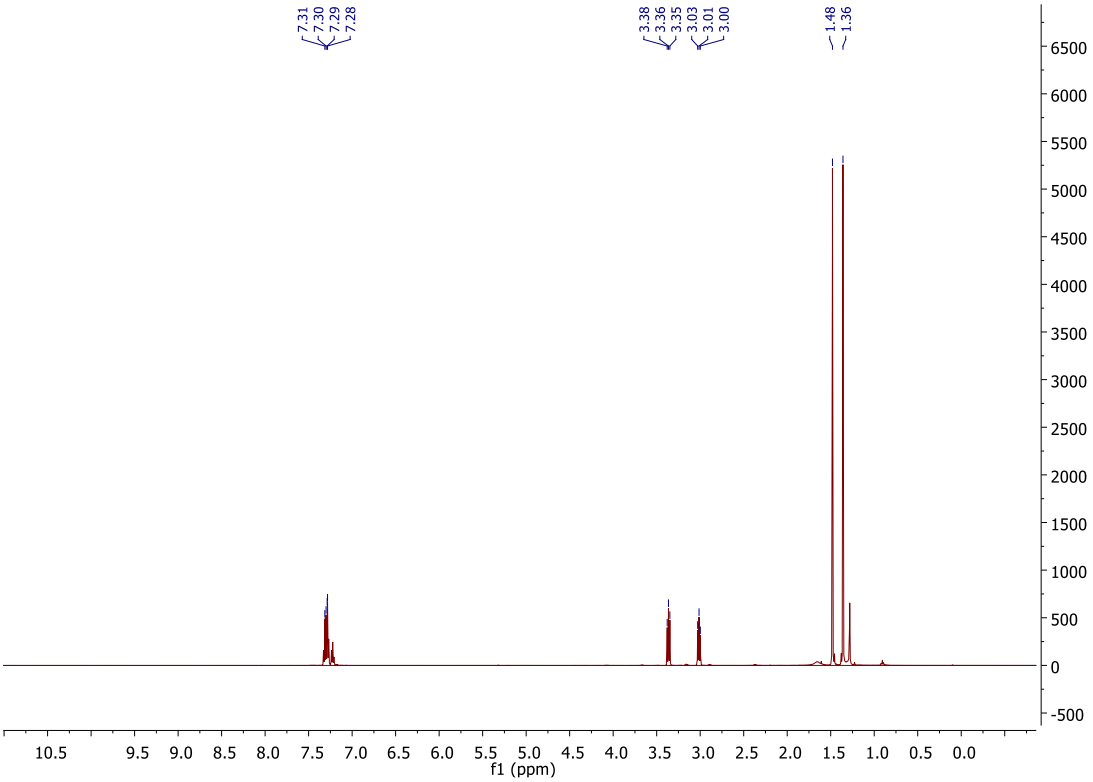

Fig 3.4-2. ^{1}H NMR partial magnified spectrum of Grandiflorone (500 MHz, Chloroform-d):

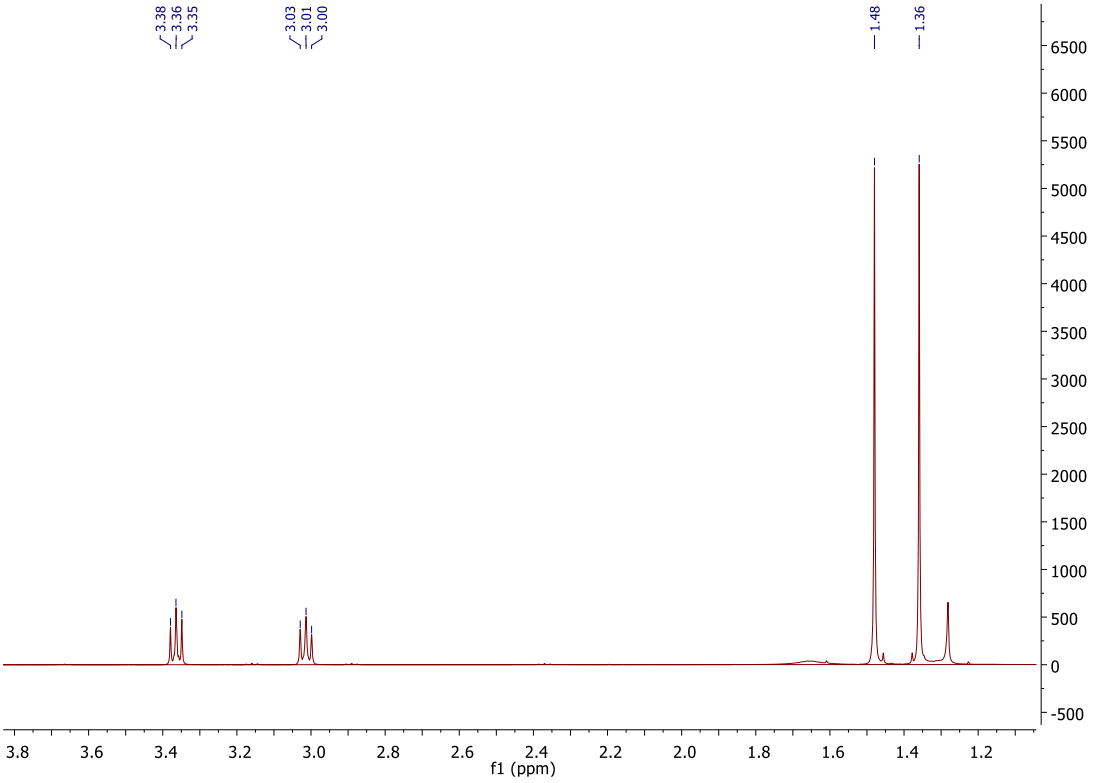

Fig 3.4-3. ^{13}C NMR original spectrum of Grandiflorone (125 MHz, Chloroform-d):

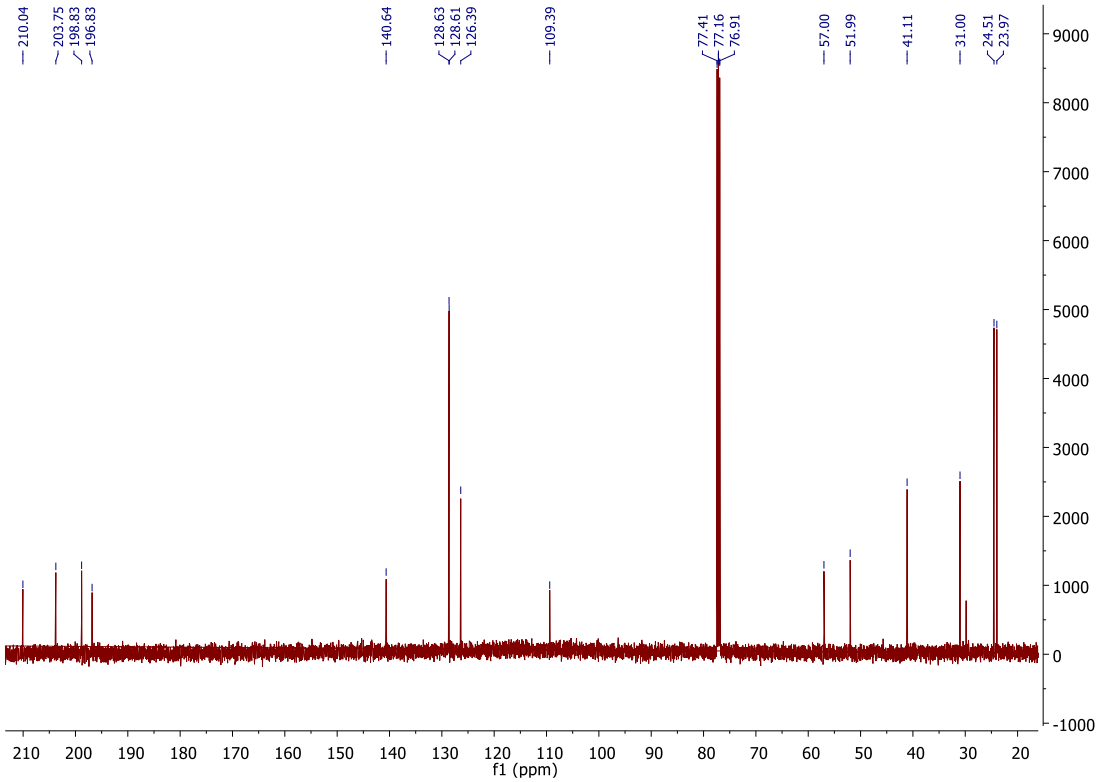

Fig 3.4-4. DEPT 135° NMR original spectrum of Grandiflorone (125 MHz, Chloroform-d):

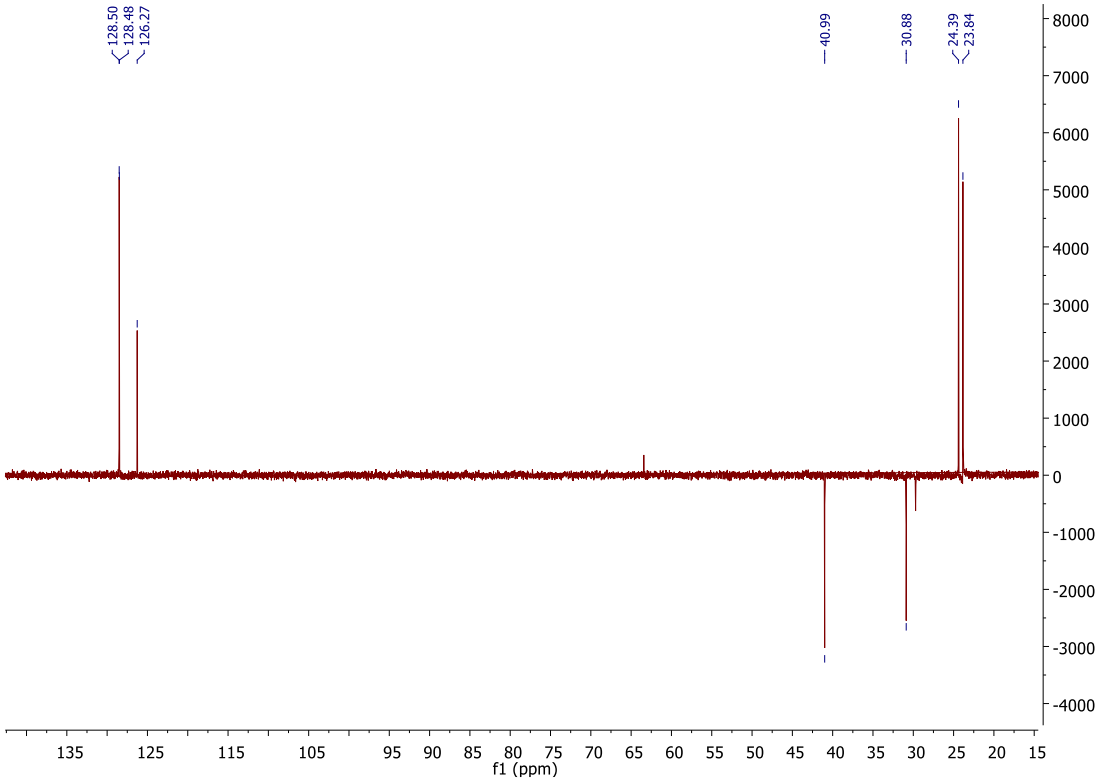

Appendix 4 A correction to the existing bacterial MTT assay protocol

The MTT assay, commonly employed as an indicator of cell viability, is also extensively utilized in bacterial studies. However, the inherent characteristics of bacteria, such as rapid proliferation, robust metabolic activity, and suspended growth in liquid culture, render the conventional MTT methodology, designed for mammalian cells, unsuitable for bacterial applications. The recently published experimental protocols have focused on optimizing the dissolution and quantification of formazan as key areas for improvement. Experimental results obtained while repeating and optimizing the existing MTT bacterial assay revealed discrepancies with some recently published protocols. Subsequent comparative verification experiments successfully identified errors in these articles. This study aimed to rectify those errors.

This rectification has been published in the following peer-reviewed publication:

Xu, W., & Popovich, D. (2023). NaOH as a solubilizer in bacterial MTT assay. *LWT*, *175*, 114506.

Statement of Contribution

<table>
<tr><td colspan="4">We, the student and the student's main supervisor, certify that all co-authors have consented to their work being included in the thesis and they have accepted the student's contribution as indicated below in the Statement of Originality.</td></tr>
<tr><td colspan="2">Student name:</td><td colspan="2">Wenliang Xu</td></tr>
<tr><td colspan="2">Name and title of main supervisor:</td><td colspan="2">Dr. David Popovich</td></tr>
<tr><td colspan="2">In which chapter is the manuscript/published work?</td><td colspan="2">Appendix Four</td></tr>
<tr><td colspan="2">What percentage of the manuscript/published work was contributed by the student?</td><td colspan="2">85%</td></tr>
<tr><td colspan="4">Describe the contribution that the student has made to the manuscript/published work:
Conceptualization; Data curation; Formal analysis; Visualization; Investigation; Methodology; Validation; Writing - original draft; Writing - review & editing.</td></tr>
<tr><td colspan="4">Please select one of the following three options:</td></tr>
<tr><td>✓</td><td colspan="3">The manuscript/published work is published or in press
Please provide the full reference of the research output:
Xu, W., & Popovich, D.W. (2023). Letter to the editor: NaOH as a solubilizer in bacterial MTT assay. LWT, 175, 114506.</td></tr>
<tr><td></td><td colspan="3">The manuscript is currently under review for publication Please provide the name of the journal:</td></tr>
<tr><td></td><td colspan="3">It is intended that the manuscript will be published, but it has not yet been submitted to a journal</td></tr>
<tr><td>Student's signature:</td><td>Wenliang Xu</td><td>Main supervisor's signature:</td><td> 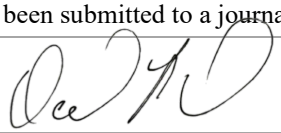 </td></tr>
</table>

Appendix 4.1 Letter to the editor: NaOH as a solubilizer in bacterial MTT assay.

Dear Editor,

With great interest, we tried to improve our bacterial 3-(4,5)-dimethylthiahiazo(-z-y1)-3,5-di-phenytetrazoliumromide (MTT) study with the method reported in the article entitled "Application of the MTT-based colorimetric method for evaluating bacterial growth using different solvent systems" published recently in your journal (Oh and Hong, 2022). This work has important implications for advancing the rapid detection of bacterial growth using the MTT assay.

However, I would like to point out some descriptions and conclusions in the article that were difficult to repeat. Hopefully, an adjustment can help other researchers exploring this field.

Oh and Hong (2022) described the process of the colorimetric assay several times in the text, but the concentration of the MTT solution used was different each time. For example: in 2.1. "a concentration of 5 mg/mL was prepared in phosphate-buffered saline (PBS; Sigma-Aldrich) and stored at 4 ℃ in the dark. A final concentration of 0.5 g/mL of MTT was used in the assay.", the final concentration here should be 0.5 mg/mL, due to the MTT stock solution was 10-fold diluted as described. In 2.3. "10 μL of 0.5 mg/mL MTT stock solution was added to each well" and in Fig.1. "Mix with MTT stock solution (0.1%)", while the MTT stock solution used was 5 mg/mL as described in 2.1.

Ignoring these descriptive errors, we reproduced the MTT assay cited in the text without using any living cells (Wang et al., 2010; Mosmann, 1983). After adding the solubilizer (NaOH at various concentrations) suggested in the article, we found that formazan was still formed in the absence of cells. As shown in **Fig. 4.1** below. In an aqueous solution, NaOH can convert MTT to formazan in a short time (Liu and Nair, 2010; Jambor, 1954) we show this conversion in 15 min and 30 min, and the amount of formazan produced increases with the increase in NaOH concentration and reaches the peak after 1N.

This result explains why the measured formazan absorbance is significantly higher than other solubilizers when using NaOH and explains why the measured formazan absorbance no longer increased after the NaOH concentration exceeds 1N. Besides, the correlation curve between the color responses of formazan and bacterial cell numbers displayed in the article showed an obvious intercept (the curve does not go through the origin), also caused by the additional formazan produced by NaOH. In conclusion, from the present results, NaOH is not a suitable solubilizer in the bacterial MTT assay as it causes a higher reading than the actual value.

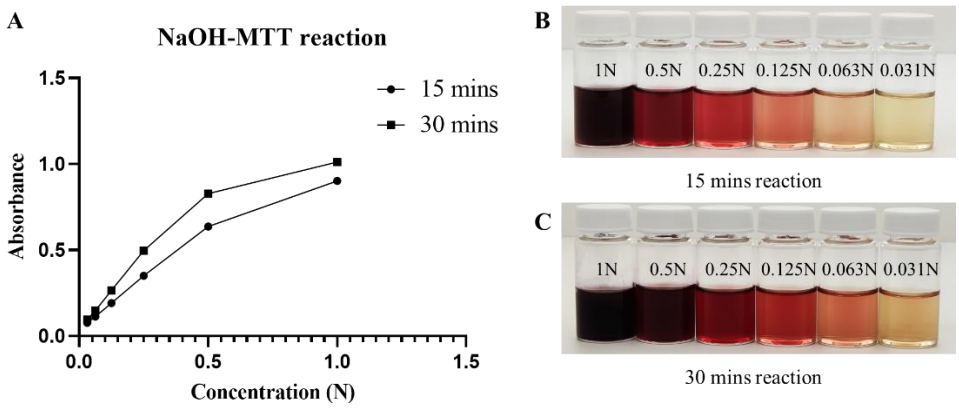

Fig. 4.1. Correlation between the formazan absorbance and NaOH concentration (A) and adding NaOH water solution into MTT water solution after 15 mins and 30 mins (B and C). Each vial contains a 5.5 mL mixture of MTT stock solution (0.5%) and sterile water (V: V=1:10) with no bacteria. Add 5mL of different concentrations of NaOH to each vial and make the final concentrations of NaOH approximately (0.03N-1N). Let stand up to 30 mins at room temperature (22 ℃) and measure the absorbance at 15 and 30 min.

Appendix 4.2 References

Jambor, B. 1954. Reduction of tetrazolium salt. *Nature*, 173, 774-775.

Liu, Y. & Nair, M. G. 2010. An efficient and economical MTT assay for determining the antioxidant activity of plant natural product extracts and pure compounds. *Journal of Natural Products*, 73, 1193-1195.

Mosmann, T. 1983. Rapid colorimetric assay for cellular growth and survival: application to proliferation and cytotoxicity assays. *Journal of Immunological Methods*, 65, 55-63.

Oh, Y. J. & Hong, J. 2022. Application of the MTT-based colorimetric method for evaluating bacterial growth using different solvent systems. *LWT*, 153, 112565.

Wang, H., Cheng, H., Wang, F., Wei, D. & Wang, X. 2010. An improved 3-(4, 5-dimethylthiazol-2-yl)-2, 5-diphenyl tetrazolium bromide (MTT) reduction assay for evaluating the viability of Escherichia coli cells. *Journal of Microbiological Methods*, 82, 330-333.